Universidade Federal de Minas Gerais

Instituto de Ciências Exatas

Departamento de Química

Isabel Alejandra Valero Antolínez

SYNTHESIS AND BIOLOGICAL POTENTIAL OF 1,2,4,5- TETRAOXANES AND γ−ALKYLIDENEBUTENOLIDES

.

Orientador: Luiz Cláudio de Almeida Barbosa

Belo Horizonte

2020

UFMG/ICEX/DQ 1408ª

T. 641ª

ISABEL ALEJANDRA VALERO ANTOLÍNEZ

SYNTHESIS AND BIOLOGICAL POTENTIAL OF 1,2,4,5- TETRAOXANES AND γ−ALKYLIDENEBUTENOLIDES

Tese apresentada ao Departamento de
Química do Instituto de Ciências Exatas
da Universidade Federal de Minas Gerais
como requisito parcial para obtenção do
grau de Doutor em Ciências - Química.

Orientador: Luiz Cláudio de Almeida Barbosa

Belo Horizonte

2020

Ficha Catalográfica

UNIVERSIDADE FEDERAL DE MINAS GERAIS

UF*m*G

Programa de Pós-Graduação em Química
Departamento de Química - ICEx

5Q anos
química
pós-graduação-ufmg

"Synthesis and biological potential of 1,2,4,5- tetraoxanes and γ-alkylidenebutenolides"

Isabel Alejandra Valero Antolinez

Tese aprovada pela banca examinadora constituída pelos Professores:

Prof. Luiz Cláudio de Almeida Barbosa - Orientador
UFMG

Prof. Denilson Ferreira de Oliveira
UFLA

Prof. Róbson Ricardo Teixeira
UFV

Profa. Rosemeire Brondi Alves
UFMG

Profa. Amanda Silva de Miranda
UFMG

Belo Horizonte, 24 de agosto de 2020.

To my loved grandmothers:

Isolina and Teresa

CHAPTER 3

SYNTHESIS OF PULCHELLALACTAM AND RELATED LACTONES AS POTENTIAL ANTI-QUORUM SENSING AGENTS

ABREVIATION LIST

ADM   Active compound derivatization method

AI-1   Atuoinducers type 1

AI-2   Atuoinducers type 2

CIM   Common intermediate Method

DIPEA   *N,N*-diisopropylethylamine

ESI   Electrospray ionization

GC   Gas chromatography

GLY   Glyphosate

Hz   Hertz

HPLC   High performance liquid chromatography

IMA   Imazethapyr

IR   Infrared

LA   Lewis Acid

MS   Mass spectrometry

m/z   Mass to charge ratio

mmol/L   Milimol/L

µmol/L   Micromol/L

M.p,   Melting point

NAA   2-(naphthalen-1-yl)acetic acid

QS   Quorum sensing

ROS   Reactive Oxygen Species

r.t.   Room temperature

t_r Retention time

TFA   Trifluoroacetic acid

T   Temperature

NMR symbols and abbreviations

b   Broad

δ Chemical shift

J   Coupling constant

d   Doublet

dd   Doublet of doublets

m   Multiplet

q   Quartet

t   Triplet

bs   Broad singlet

ABSTRACT

VALERO-ANTOLINEZ, Isabel Alejandra, PhD. Universidade Federal de Minas Gerais, May, 2020. **Synthesis and biological potential of 1,2,4,5-teraoxanes and γ−alkylidene-butenolides.** Supervisor: Luiz Cláudio de Almeida Barbosa

Heterocycles are compounds with at least one heteroatom in their ring structure. These types of scaffolds are present in both natural and synthetic compounds. In many natural products, this core is responsible for the biological activity of the compound. The present work shows the synthesis and biological potential of two different types of heterocycles tetraoxanes and γ−alkylidenebutenolides.

n chapter 1, is reported the synthesis and phytotoxic activity of a new tetraoxane derived from a commercial product. Tetraoxanes are compounds with a six-atom ring, that has oxygen at the 1, 2, 4, and 5 positions. These compounds studied due to its antimalarial activity own this potential to the peroxide bonds present in their structure. Since the herbicide potential of tetraoxanes has been recently reported, this work aimed to design a new tetraoxane derived from the commercial compound 2-(naphthalene-1-yl)acetic acid (NAA. The new compound, named 3-(naphthalene-1-ylmethyl)-1,2,4,5-tetraoxaspiro[5.5]undecane (37), was synthesized in gram scale with reliable methodologies in 23% yield. Greenhouse bioassays showed that this compound inhibited the growth of *I. acuminate*, *B. pilosa*, *A. ficoidea*, and *S. americanum*, all of them common weeds present in major crop cultures. Also, compound (**37**) caused chlorosis, necrosis, and leaf epinasty in the target species *C. sativa*. Such results suggest that this tetraoxane might act as ROS (Reactive oxygen species) stimulating compound and auxinic herbicides at the same time. Also, the degradation studies of compound **37** in the sand are presented. One of the hypotheses that emerged during the synthetic planning of tetraoxane **37**, was that the compound may degrade into its synthetic precursor NAA. Therefore, this work aimed to evaluate the degradation of tetraoxane in the sand under laboratory conditions. The experiment was carried out for 22 days and samples of sand were analyzed via high-pressure liquid chromatography (HPLC). The experiments revealed that, indeed, this compound degraded into its synthetic precursor: the commercial auxin NAA.

In chapter 2, the synthesis and antileishmanial activity of 12 tetraoxanes were studied. The synthesis of these compounds started with the obtention of different gem-dihydroperoxides. This was accomplished by reacting several aldehydes and ketones with hydrogen peroxide in presence of $SnCl_2$ (20 mol%) at room temperature. The desired intermediates were obtained in yields comprehended between 77 and 90%. Further reaction of these compounds with different aldehydes and ketone using H_2SO_4 as catalyst delivered

the desired tetraoxanes in moderate yields (11-50%), using common methodologies reported in the literature. Concerning the antileishmanial activity, five tetraoxanes (**12b**, **12c**, **12g**, and **12h**) were more active than the reference potassium antimonyl tartrate trihydrate. Moreover, the cytotoxicity of all compounds was evaluated against canine macrophages (DH82), human hepatoma (HepG2), and monkey renal cells (BGM). The results showed that all tetraoxanes were less cytotoxicity and more selective to the parasite. The compound 7,8,15,16-tetraoxadispiro[5.^{2}.5^9.2^6]hexadecane (**12b**) was the most active tetraoxane and presented an IC$_{50}$= 0.64 µM against *L. amazonesis*. Therefore, these results point out the tetraoxane scaffold as an excellent option to develop new compounds to treat leishmaniasis.

Finally, in chapter 3, the syntheses of Pulchellalactam and related butenolides as anti quorum sensing (QS) agents are reported. This natural product was isolated from the fungus *C. pulchella* in 1995. The proposed synthetic route uses the tandem Sonogashira *cross-coupling* lactonization as a key step. As a result, the natural product was synthesized in two steps starting from (*Z*)-iodobut-2-enoic acid, stereoselectively, with 64% of overall yield. On the other hand, it is widely established that the Sonogashira cross-coupling lactonization allows the stereoselective synthesis of (*Z*)-γ−alkylidenebutenolides. These types of compounds might have potential as quorum sensing agents due to their structural similarity with brominated furanones that have this type of activity. In doing so, 12 (*Z*)-γ−alkylidenebutenolides were synthesized using the cross-coupling reaction in yields between 23% and 69%. All compounds were tested as quorum sensing agents. Although Pulchellalactam was not active, several butenolides were able to interfere in the QS communication via AI-1 and AI-2 path. This type of communication is key for bacteria biofilm growth, and consequently, compounds able to interfere in it can be useful in the development of new treatments for chronic infections.

RESUMO

VALERO-ANTOLINEZ, Isabel Alejandra, PhD. Universidade Federal de Minas Gerais, maio, 2019. **Síntese e potencial biológico de 1,2,4,5-tetraoxanos e γ-alquildiene-butenolideos**. Orientador: Luiz Cláudio de Almeida Barbosa

Compostos heterocíclicos são substâncias com ao menos um heteroátomo na estrutura do anel. Esse tipo de unidade está presente em grande variedade de compostos naturais e sintéticos. Em muitos produtos naturais esse núcleo é responsável pela atividade biológica do composto. Visando contribuir no estudo deste tipo de moléculas, o presente trabalho tem por finalidade a síntese e avaliação do potencial biológico de dois tipos de heterociclos: 1,2,4,5-tetraoxanos e γ-alquildienelactonas.

No capítulo 1 é relatada a síntese e atividade fitotóxica de um novo tetraoxano derivado de um produto comercial. Os tetraoxanos são compostos com um anel de seis átomos, que possuem átomos de oxigênio nas posições 1, 2, 4 e 5. Esses compostos têm sido amplamente estudados devido à potente atividade antimalárica. Está amplamente estabelecido que esse potencial é relacionado à função peróxida presentes em sua estrutura. Recentemente, nosso grupo de pesquisa relatou o potencial herbicida de diversos tetraoxanos. Portanto, o objetivo deste trabalho foi projetar um novo tetraoxano derivado do composto comercial ácido 2-(naftalen-1-il)acético (NAA). O novo composto, denominado 3-(naftalen-1-ilmetil)-1,2,4,5-tetraoxaspiro[5.5]undecano (**37**), foi sintetizado em escala de grama com metodologias confiáveis com 23% de rendimento. Ensaios em casa de vegetação mostraram que este composto inibia o crescimento de *I. acuminate*, *B. pilosa*, *A. ficoidea* e *S. americanum*, todos elas plantas daninhas comumente encontradas em culturas de grande importância comercial. Além disso, observou-se que o novo composto (**37**) foi capaz de causar clorose, necrose e epinastía foliar na espécie alvo *C. sativa.* Tais resultados sugerem que esse tetraoxano pode atuar como composto estimulador de ROS (Espécies que reagem ao oxigênio) e herbicida auxínico ao mesmo tempo. Por outro lado, foram realizados estudos de degradação deste composto. Uma das hipóteses que surgiram quando o planejamento sintético do tetraoxano foi realizado, foi a possível decomposição do produto no seu precursor sintético NAA. Portanto, este trabalho também teve como objetivo avaliar a degradação do tetraoxano na areia em condições de laboratório. O experimento foi realizado durante 22 dias, durante os quais os extratos de amostras de areia foram analisados por cromatografia líquida de alta eficiência (CLAE). Esses estudos revelaram que, de fato, este composto é degradado em seu precursor sintético, a auxina comercial NAA

No capítulo 2, foi estudada a síntese e o potencial antileishmania de 12 tetraoxanos. A síntese desses compostos começou com a obtenção de diferentes *gem*-hidroperóxidos. Isso foi realizado reagindo vários aldeídos e cetonas com peróxido de hidrogênio na presença de $SnCl_2$ (20 mol%) à temperatura ambiente. Os intermediários desejados foram obtidos com rendimentos compreendidos entre 77 e 90%. Estes compostos reagiram com diferentes aldeídos e cetona usando H_2SO_4 (50 mol%) como catalisador. Como resultado, os tetraoxanos desejados foram obtidos com rendimentos moderados (11-50%), usando metodologias comuns relatadas na literatura. No que diz respeito à atividade antileshmania, cinco tetraoxanos (**12b**, **12c**, **12g**, **12g** e **12h**) foram mais ativos que areferência. Além disso, a citotoxicidade de todos os compostos foi avaliada contra macrófagos caninos (DH82), hepatoma humano (HepG2) e células renais de macaco (BGM). Os resultados mostraram que todos os tetraoxanos foram menos citotóxicos e mais seletivos ao parasita. O composto 7,8,15,16-tetraoxadispiro[5.^{2}.5^9.2^6]hexadecano (**12b**) foi o tetraoxano mais ativo e apresentou IC_{50} = 0,64 µmol/L contra *Leishmania amazonesis*. Portanto, esses resultados apontam tetraoxanos comoexcelentesopções para o desenvolvimento de novos compostos para o tratamento da leishmaniose.

Finalmente, no capítulo 3, é relatada a síntese da pulchellalactama e butenolídeos com potencial inibitório de comunicação via *quorum sensing* (QS). Este produto natural foi isolado do fungo *Corollospora pulchella*, em 1995. A rota sintética proposta utiliza a reação em cascata de acoplamento cruzado Sonogashira e lactonização como etapa principal. Como resultado, o produto natural foi sintetizado em duas etapas a partir do ácido *Z*-iodobut-2-enóico estereoseletivamente com 64% do rendimento global. Por outro lado, é amplamente estabelecido que a lactonização por acoplamento cruzado de Sonogashira permite a síntese estereosseletiva de *(Z)*-alquildienbutenolídeos. Esse tipo de composto pode ter potencial como inhibidor de comunicação QS devido à sua similaridade estrutural com furanonas bromadas que possuem esse tipo de atividade. Portanto, foram sintetizados 12 (*Z*)-γ−alquildienbutenolídeos usando a reação de acoplamento cruzado com rendimentos entre 23% e 69%. Todos os compostos foram testados como agentes de inibidores de QS. Embora a pulchellalactama não tenha sido ativa, vários butenolídeos foram capazes de interferir na comunicação QS via mecanismos AI-1 e AI-2. Esse tipo de comunicação é essencial para o crescimento do biofilme de bactérias, compostos capazes de interferir nele, podem ser úteis no desenvolvimento de novos tratamentos para infecções crônicas.

1. GENERAL INTRODUCTION

Natural products are an infinite source of inspiration to develop new molecules with the most diversity of biological activities. With the development of NMR spectroscopy in 1940, the identification and characterization of these substances became accessible to scientists. Since the discovery of penicillin, more than 23,000 of natural products with different biological activities have been isolated from diverse sources (Katz *et al.*, 2016).

Simultaneously, chemists have developed strategies and methodologies to obtain these compounds in the laboratory. As a result, many of these substances have been became important commercial drugs or agrochemicals. Some examples of these are erythromycin (**1**), one of the most important antibiotics of the past century, or the commercial herbicide glufosinate (**2**) (Newman, 2019; Loselieur, 2017).
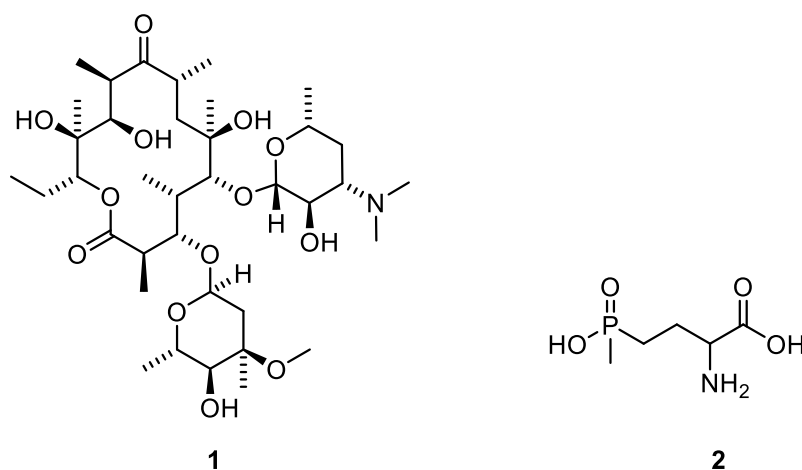
Figure 1. Structures of erythromycin (**1**) and glufosinate (**2**).

However, the use of natural products as commercial products is frequently hampered due to the complexity of their structure (Sparks *et al.*, 2017). Usually, the synthesis of a natural product requires the development and use of expensive strategies, not always guaranteeing the obtention of the target compound in economically viable yields. This is one of the main reasons why many scientists focus their attention on the synthesis of smaller structures (Kaschani and Van der Hoom, 2007).

In many cases, these small molecules may have a common scaffold with a natural product that allows them to replicate its biological activity (Barreiro *et al.*, 2015), as in others, they can be a natural product (Dayan et al, 2009). Herein, we explore the synthesis and biological potential of different types of small heterocycles that can have any of these characteristics.

1,2,4,5-Tetraoxanes are heterocycles traditionally studied due to their antimalarial potential (Kumar *et al.*, 2009). Such activity is related to the peroxide bonds in their structures. In fact, the same type of scaffold is present in the natural product artemisinin (Figure 2, 3) (Sen *et al.*, 2007). This natural product, isolated from the plant Artemisia annua L., has been widely studied due to its antimalarial activity (Terent´ev *et al.*, 2014). In 2015, Dr. Youyou Tou won the Nobel prize for the development of therapies using artemisinin as a treatment drug. (Su and Miller, 2015).
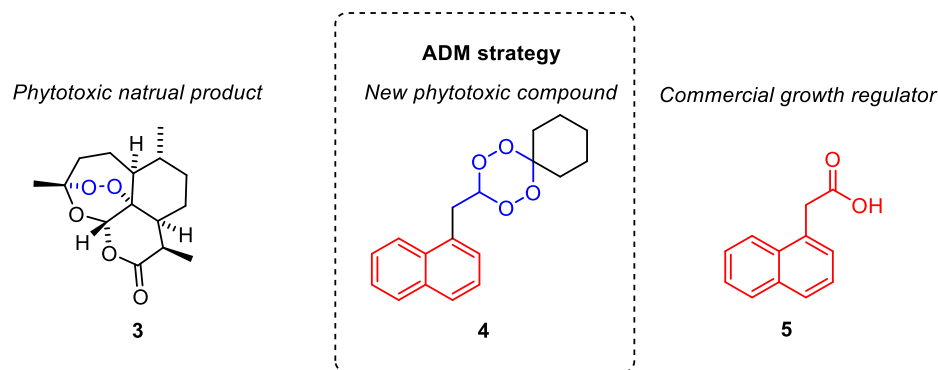
Figure 2. Compounds with phytotoxic activity (**3** and **5**) and tetraoxane planned *via* ADM strategy.

Also, artemisinin has been investigated in relation to its ecological role. Duke and co-workers reported in 2014 the phytotoxic activity of artemisinin against *Lactuca sativa* L. and *Raphanus sativa* L. (Knudsmark *et al.*, 2014). Based on this work, our research group started to study the herbicide potential of a diversity of compounds with peroxide bonds. In 2015, it was reported the phytotoxic activity of 1,2,4,5 tetraoxanes against the weed *Brachiaria brizantha* (Hosch A Rich) and *Bidens pilosa* L. (Cusati *et al.*, 2015).

To go further, the Active Derivatization Method (ADM) approach was used as a strategy to design tetraoxane **4** (Guan *et al.*, 2014). This compound is derived from the commercial auxin 2-(naphthalene-1-yl)acetic acid (**5**) and its effect over the species *Cucumis sativa* L. , *Sorghum bicolor* L., *Ipomoea acuminate* L., *Bidens pilosa* L., *Altherantera ficoidea* L. and *Solanum americanum* Mill. was tested under greenhouse conditions.

Subsequently, it was studied the degradation of tetraoxane **4** in sand, under laboratory conditions. Compound **4** was designed with the aim that its further degradation would deliver the commercial auxin **5** (Figure 3). If so, this compound might continue acting as an auxinic herbicide.
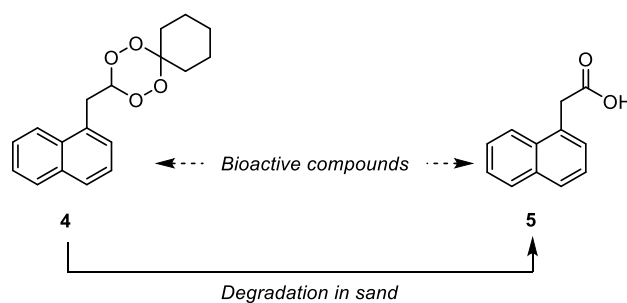
Figure 3. Transformation of tetraoxane **4** into compound **5.**

In chapter 2, a different biological potential of the 1,2,4,5-tetraoxanes is reported. Leishmaniosis is one of the most neglected diseases nowadays. According to the WHO, leishmaniosis causes 26,000 to 65,000 deaths per year around the world (World Health Organization, 2017). Some studies report that the activity of artemisinin derivatives against the *Leishmania donovani* (Laveran & Mesnill 1903) strain is related to the peroxide group in its structure (Avery *et al.*, 2003). Therefore, it was decided to explore the effect of different tetraoxanes against the parasite *Leishmania amazonesis* (Laison & Shaw, 1972) (Figure 4).
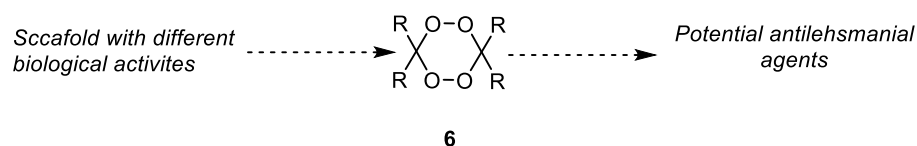
Figure 4. Tetraoxane as potential antileishmanial agents.

Finally, in chapter 3, it is reported a short and efficient synthesis of pulchellalactam and other butenolides. Pulchellalactam (Figure 4, **10**) is a natural product isolated from the marine fungus *Collolospora pullchella* (Kolhm, I. Schmidt & NB Nair, 1967) (Alvi *et al.*, 1995). Although there are several reported syntheses of this compound, many of them require the use of protection groups or afford the natural product with low stereoselectivity (Anselmi *et al.*, 2016).

Therefore, it was proposed to synthesize pulchellalactam stereoselectively in two steps, using the tandem Sonogashira cross-coupling lactonization as the key step in the synthetic route (Lu *et al.*, 1992). Furthermore, this reaction allowed easy access to a wide variety of butenolides (**9**) with Z-configuration (Figure 5).
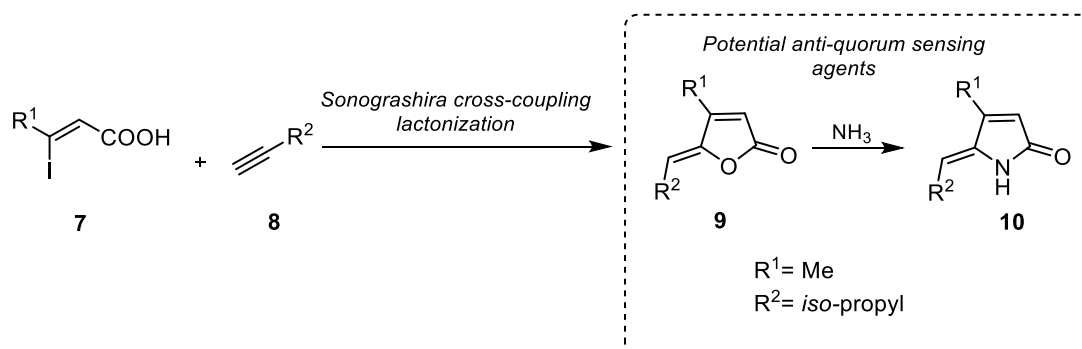
Figure 5 Synthetic route to prepare pulchellalactam and butenolides.

Then, it was explored the potential of the natural product and some butenolides as bacterial quorum sensing inhibitors. Quorum sensing is a form of bacterial communication. In this context, compounds that can interrupt it can lead to the development of alternative treatments for chronic infections (Saurav *et al*., 2017). This is a crucial concern nowadays,

due to the increasing resistance that many microorganisms are developing against traditional antibiotics (WHO, 2019).

Therefore, this work seeks to contribute to the study of the chemical and biological activities of small heterocycles. It is expected that the results reported here will help to reinforce the importance of small molecules and their role in the development of new scaffolds with biological potential.

2. REFERENCES

Anselmi, E., Cherry, K., Maaliki, C., Ngi, S.J. , Thibonnet, J., Abarbri, M., 2016. Two Novel and Simple Approaches to CD45 Protein Tyrosine Phosphatase Inhibitor (*Z*)-Pulchellalactam and Derivatives. Synthesis . 48, 1407–1413.

Alvi, K.A., Casey, A., Nair, B.G., 1998. Pulchellalactam: A CD45 Protein Tyrosine Phosphatase Inhibitor from the Marine Fungus *Corollospora pulchella*. J. Antibiot. 51, 3–5.

Avery, M. A., Muraleedharan, K. M., Desai, P. V., Bandyopadhyaya, A. K., Furtado, M. M., Tekwani, B. L., 2003. Structure-activity relationships of the antimalarial agent artemisinin Design, synthesis, and CoMFA studies toward the development of artemisinin-based drugs against leishmaniasis and malaria. J. Med. Chem. 46, 4244–4258.

Cusati, R., Barbosa, L. C. A., Maltha, C. R., Demuner, A. J., Oliveros-Bastidas, A., Silva, A. A., 2015. Tetraoxanes as a new class of efficient herbicides comparable with commercial products. Pest Manag. Sci. 71, 1037–1048.

Dayan, F. E., Cantrell, C. L., Duke S. O. 2009. Natural products in crop protection. Bioorg. Med. Chem. 17, 4022–4034.

Guan, A., Liu, C., Yang, X., Dekeyser, M., 2014. Application of the intermediate derivatization approach in agrochemical discovery. Chem. Rev. 114, 7079-7107.

Kaschani, F., Van der Horn., 2007. Small molecules approach in plants. Current Opinion in Chemical Biology. 11, 88-98.

Katz, L., Baltz, R.H. 2016. Natural product discovery: past, present, and future. J. Ind. Microbiol. Biotechnol. 43, 155–176.

Knudsmark, K., Jessing, K., Duke, S., Cedergreeen, N., 2014. Potential ecological roles of artemisinin produced by *Artemisia annua L.* J. Chem. Ecol. 40, 100–117.

Kumar, R. S., Nitin, D. R. S., 2009. Tetraoxanes: Synthetic and Medicinal Chemistry Perspective. Med. Res. Rev. 12,520–547.

Loiseleur, O., 2017. Natural Products in the Discovery of Agrochemicals. Chimia 12, 810-821.

Lu, X., Huang X., Shengming, M., 1993. A convenient synthesis of (*Z*)-alkylidene butenolides. Tetrahedron Lett. 34, 5963-5966.

Newman, D. J.,2019. Antibiotics from Natural Sources. Antibiotic Drug Resistance, 14,311–341. 1st Edition

Sen, R., Bandyopadhyay, S., Dutta, A., Mandal, G., Ganguly, S., Saha, P., Chatterjee, M., 2007. Artemisinin triggers induction of cell-cycle arrest and apoptosis in Leishmania donovani promastigotes. J. Med. Microbiol. 56, 1213–1218.

Sparks, T. C., Hahn, D. R., Garizi, N. V., 2017. Natural products, their derivatives, mimics and synthetic equivalents: role in agrochemical discovery. Pest. Manag. Sci. 73, 700–715.

Saurav, K., Costantino, V., Venturi, V., Steindler, L., 2018. Quorum Sensing Inhibitors from the Sea Discovered Using Bacterial N-acyl-homoserine Lactone-Based Biosensors. Mar. Drugs 15, 1-19.

Su, X. Z., Miller L. H., 2015. The discovery of artemisinin and the Nobel Prize in Physiology or Medicine. China Life Sci. 58, 1175- 1179.

Terent'ev, A. O., Borisov, D. A., Vil V. A., Dembitsky, V. M., 2014. Synthesis of five- and six-membered cyclic organic peroxides: Key transformations into peroxide ring-retaining products. Beilstein J. Org. Chem. 10, 34–114.

Word Heatlh Organization. 2019. Report We cannot wait: Secure the future against pharmacoresistent diseases.

CHAPTER 1

SYNTHESIS AND PHYTOTOXIC PROFILE OF A NEW TETRAOXANE DESIGNED FROM A COMMERCIAL AUXIN

1.1. INTRODUCTION

Pest management is one of the most important areas in agriculture. Among the different strategies applied on the field, nowadays, chemical control of weeds is the most used by farmers. However, there is a concern related with the increasing resistance presented by weeds against traditional herbicides. In 2019, the International Survey of Resistance Weeds registered more than 500 cases of herbicide resistance (Heap, 2019).

Herbicide resistance is caused mainly by the excessive use of the same herbicide on the field, the more frequent it is used, the greater the possibilities of weeds developing resistance mechanisms (Duke, 2012). Hence, it is necessary to develop new molecules that act through different modes of actions from traditional herbicides. In addition, these substances must also have affordable production as its application dose is in the range of grams per hectare (Duke, 2013). Moreover, the new candidates must have low toxicity and proper degradation in soil to avoid serious impacts on ecosystems (Peterson, 2017). Nature itself is one of the main sources of inspiration for the synthetic chemist to solve this issue. In this context, studying the herbicide potential of natural products enables the development of new compounds with those activities (Duke *et al.* 2019).

Artemisinin (Figure 1.1, **1**) is a natural product isolated in 1972 from the plant *Artemisia annua* L. and extensively used for the treatment of malaria (Kumari, 2019; O´Neil, 2004). Besides this activity, artemisinin plays a relevant role in the ecological interactions of *A. annua.* Previous studies detailed phytotoxic effects caused by this natural compound on *Lactuca sativa.* L. and *Raphanus sativa* L. (Knudsmark *et al.*, 2014). Artemisinin owes its biological activities largely to the peroxide bond in its structure. Still, further studies related to its potential as herbicide are hampered by the complexity of its

structure that requires expensive and complex synthetic strategies to be produced (Constantino *et al.*, 2014).
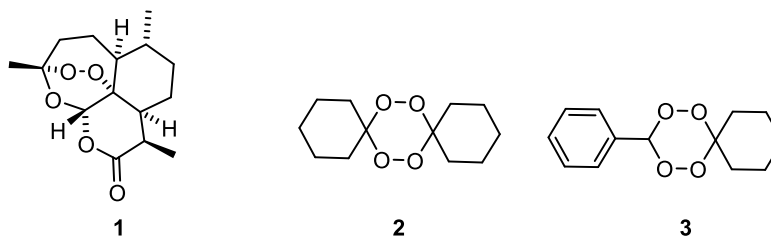
Figure 1.1. Artemisinin and tetraoxanes with phytotoxic activity.

Tetraoxanes (Figure 1.1, **2** and **3**) are compounds bearing six-member-ring with atoms of oxygen at positions 1, 2, 4 and 5 in their structure (Dong, 2002). Initially, these substances were prepared as precursors to produce lactones and macrocyclic hydrocarbons in industry (Story *et al.*, 1975). However, since the discover of artemisinin antimalarial activity, tetraoxanes became an attractive core to medicinal chemistry (Amewu *et al.*, 2006).

1.1.1. *Synthesis of 1,2,4,5-tetraoxanes*

The development of efficient methodologies for the synthesis of tetraoxanes has been a challenge since the reactions are highly dependent of pH, temperature or substrate (Dong, 2002). The mechanistic proposal for their formation from *gem*-hydroperoxides is showed in Scheme 1.1. The initial step is the activation of carbonyl compound (**4**) by a Lewis acid (LA). Thereafter, *gem*-hydroperoxide (**5**) attacks that electrophilic center. Once intermediate **8** is formed, an intramolecular reaction gives the tetraoxane core.
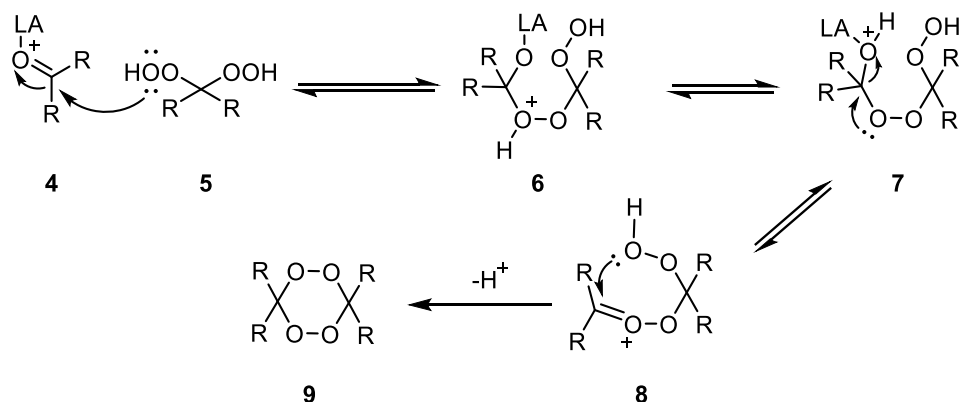
Scheme 1.1. Mechanistic proposal for tetraoxane formation (LA = Lewis Acid) (Dong, 2002).

The most common and economic methodology for the synthesis of tetraoxanes was developed in the early 1990s. It proposes the use of sulfuric acid as catalyst in the reaction between a *gem*-hydroperoxide and a carbonyl compound. That approach has been applied in the synthesis of tetraoxanes with the most variable structures (specially those ones derived from steroids), affording the products in moderate yields (Scheme 1.2) (Dong and Vennestrom, 2004; McCollough *et al.*, 2000).
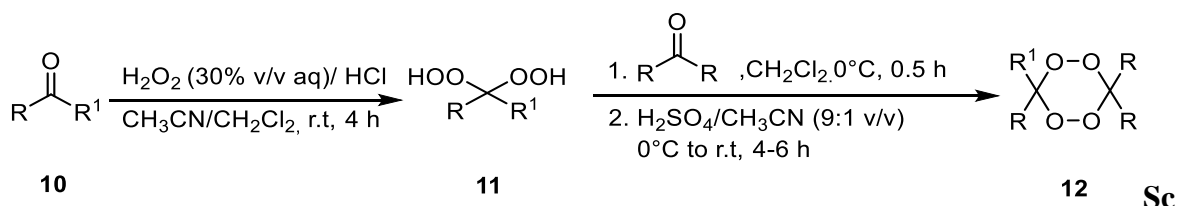
Scheme 1.2. General method for the synthesis of 1,2,4,5-tetraoxanes.

Also, the use of methyltrioxorhenium (MTO) as catalyst and fluorinated alcohols as reaction medium has been implemented to prepare the scaffold. The main advantage of that methodology is the generation of the *gem*-hydroperoxide *in situ* (one-pot reaction). It is possible since the reaction medium (fluorinated alcohols) activates the hydrogen peroxide, which becomes more reactive (Scheme 1.3). This approach is one of the most successful reported until now, once it made possible to synthetize non-symmetrical tetraoxanes in yields above 50% (Iskra *et al.*, 2010).
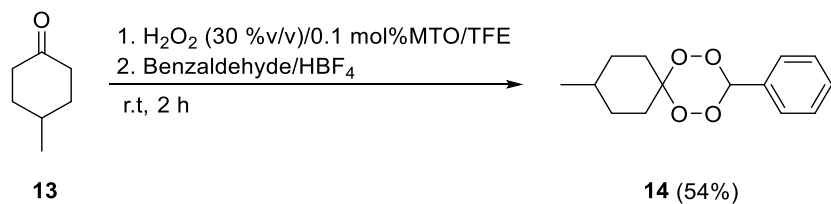
Scheme 1.3. Synthesis of 1,2,4,5-tetraoxanes using H_2O_2/MTO/fluorous alcohol system.

Another interesting method, published in 2011, yield tetraoxanes from the respective *gem*-hydroperoxides, and protected benzyl acetals or orthoesters, using $BF_3.OEt_2$ as catalyst. Such approach afforded non symmetric 1,2,4,5-tetraoxanes in yields between 50% and 70% (Scheme 1.4) (Hamann *et al.*, 2011).
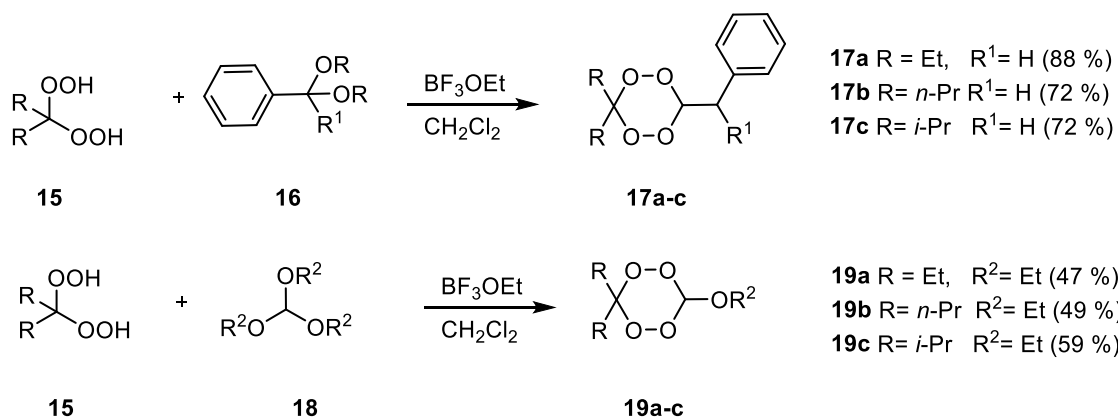
Scheme 1.4. Synthesis of 1,2,4,5-tetraoxanes starting from hemiacetals and orhtoesters (Hamman *et al.*, 2012).

1.1.2. Biological Activity of 1,2,4,5-tetraoxanes

In 2004, it was published the synthesis of compound OZ439 (Figure 1.2, **20**), a trioxolane that showed excellent activity and good biopharmaceutical profiles against *Plasmodium vivax* (Grassi & Fetti, 1890) and *Plasmodium falciparum* (Welch, 1897) in clinical trials (Charman *et al.*, 2011; O´Neil, 2004). Further structural optimizations led to the synthesis of tetraoxane RKA182 (**21**). The compound presented an excellent *in vivo* activity ($IC_{50} = 0.87$ nmol/ L against *P. falciparum.*) and higher stability than trioxolane **20** (Amewu *et al.*, 2006).

OZ439
20

RKA182
21
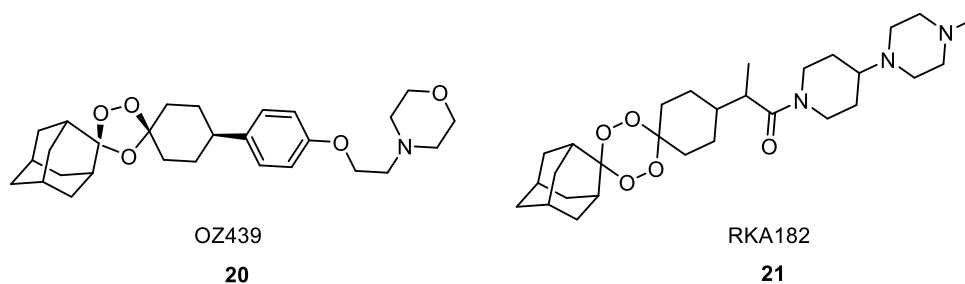
Figure 1.2. Peroxide compounds with antimalarial activity.

The antimalarial activity of tetraoxanes derived from steroids, was also explored, as this type of compounds are good carrier molecules. There are many studies addressing such issue (Terzić *et al*., 2007). For instance, tetraoxanes **22**, **23** and **24** (Figure 1.3) were tested against chloroquine resistant strains of *P. vivax.* Among them, compound **24** presented an $IC_{50}= 0,181$ µmol/L against the parasite (Opsenica *et al.*, 2008).
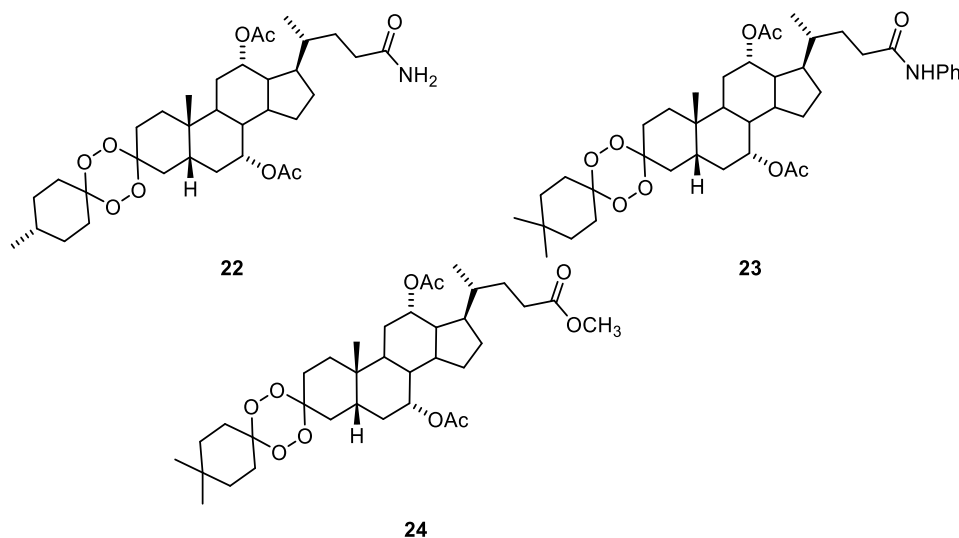
Figure 1.3.Tetraoxanes derived from steroids.

Regarding the phytotoxic activity of tetraoxanes, our research group has discovered their potential against different weeds. Pre-emergence bioassays demonstrated that compounds **25** and **27** (Figure 1.4) inhibited the shoot and root growth of the specie *Euphorbia heterophilla* L. around 76% at 1 mmol/L. Such value was comparable with the effect generated by commercial herbicide glyphosate at the same concentration (Cusati *et al.*, 2015).
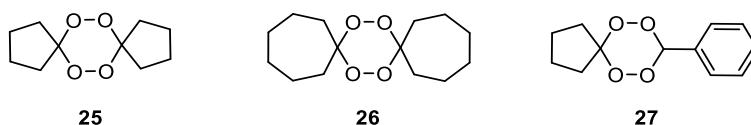
Figure 1.4. Tetraoxanes with herbicide activity.

Against the weed *Brachiaria brizantha* (Hosch. & A. Rish)*,* substance **26** inhibited root growth around 50% at concentrations of 0.25 mmol/L, while at higher concentrations, compound **25** regulated the shoot growth around 90%. In the case of *Bidens Pilosa* L.*,* tetraoxane **26** inhibited the growth of the root above 50% at 1 mmol/L on the other hand, compound **27** generated the same effect on the root in a range of 90% (Cusati *et al.*, 2015).

1.1.3. Synthetic planning in agrochemistry

As already outlined, the preparation of agrochemical must be simple and economic due to its application dose. The most common strategies to discover those compounds are random synthesis and screening, "me too chemistry" and rational design. Recently, Liu and coworkers provided a type of rational design named "Intermediate Derivatization Method" (Guan *et al.*, 2014). The strategy proposes the chemical modification of molecules with known activity for producing new candidates as agrochemicals. The authors stablished three different types of Intermediates Derivatization Methods (Scheme 1.5).

The Common Intermediate Method (CIM) uses key intermediates previously employed in the synthesis of known agrochemicals. For example, keratezam (**29**) is a growth regulator used in corn. That compound is synthesized from *β*-ketoester (**28**), a common starting material in synthesis of agrochemicals (Liu, 2002).
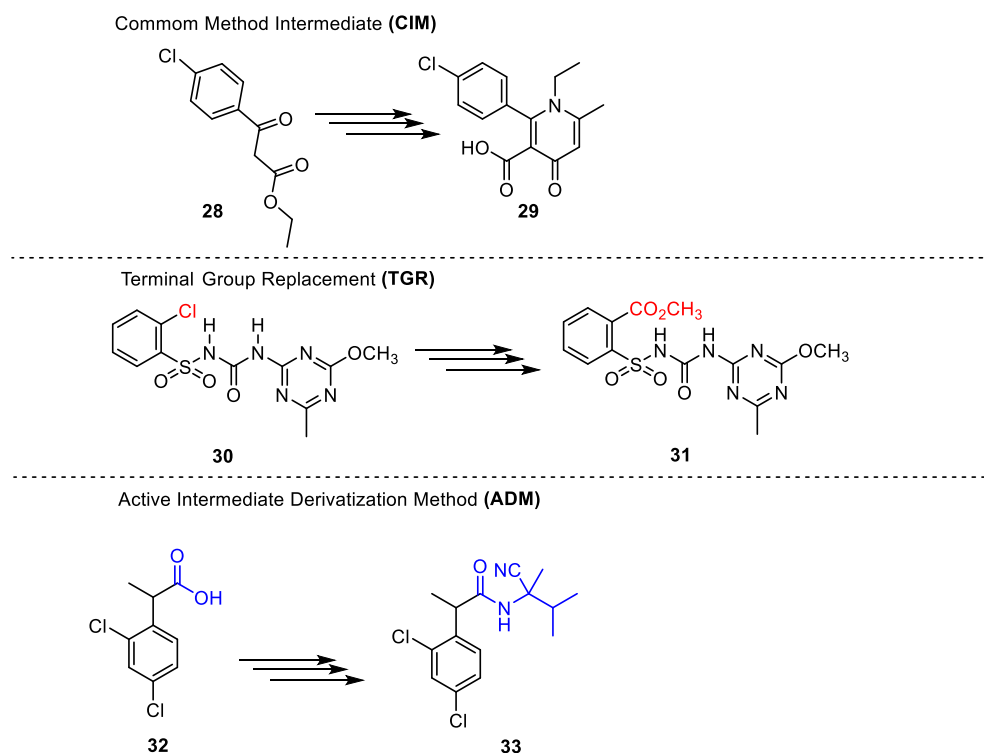
Scheme 1.5. Some examples of the different types of *"Intermediate Derivatization Method"* (IDM). Compounds: β-ketoester (**28**), keratezam (**29**), chlorosulfon (**30**), met-sulforonmet (**31**), dichloroprop (**32**), fenoxanil (**33**).

Concerning the Terminal Group Replacement (TGR), in this case, a new scaffold replaces the terminal group of an agrochemical or an active natural product. This approach has been broadly applied in the synthesis of sulfonyl-urea herbicides. Chlorsulfuron (**30**), was one of the first herbicides released to the market (Cremlyn, 1991). The replacement of chlorine by different types of functional groups made it able to prepare many other commercial herbicides. An example is the metsulforon-met (**31**) (Tomlyn, 1994).

The third strategy suggested by the authors is the Active Compound Derivatization Method (ADM), which consists in using a commercial product as synthetic intermediate to obtain a new molecule. An example is the fungicide fenoxanil (**33**). Its synthetic route was planned using the herbicides dichloroprop (**32**), as pivotal intermediate (Guan *et al.*, 2014).

1.1.4. Auxinic herbicides

Auxinic herbicides were the first family of agrochemicals classified as selective (Jugulam *et al.*, 2011). They are able to mimic natural auxins for entering the plant. Plant death due to auxinic herbicides is caused by supraoptimal concentrations of those substances in plant tissues. As consequence, there is an overstimulation in the production of ethylene and abcisic acid that causes senescence and stomatal closure in the plant (Kelley and Riecher, 2007).

Among the many auxinic herbicides, 1-naphthaleneacetic acid (NAA) (Compound **34,** Scheme 1.6) is one of the most common in the field (Grosmann, 2002). NAA was released to the market in 1960 (Coob and Reade 2010; Cremlyn, 1991) and, currently, it is used as an agent for thinning fruit sets in apples, pears, olives and some citrus (Bradbury *et al.*, 2014). In general, the compound has low toxicity against birds, fishes and mammals, besides unlikely bioaccumulation in marine organisms (Pohanis, 2015). Therefore, NAA is an excellent option to apply the ADM approach in order to develop new structures with herbicide potential.

1.1.5. Degradation of herbicides in soil

Herbicide persistence is defined as the time that a compound prevails in the soil before being degraded by microorganisms or other elements of the ecosystem (Curran, 2014). That parameter is important because it establishes the period of time that the compound has impacts and how it will affect other crops in the future (Fuscaldo *et al.*, 1999). Research on the degradation of herbicides in soil is a relevant factor that is directly related to the persistence of the agrochemical (Schreiber *et al.*, 2018).

The degradation of compounds in soil is quite complicated and depends of several variables. The main factors that influence it are: physicochemical properties of the soil, its pH or the activity and distribution of microorganisms, and environmental conditions (temperature of the soil, humidity, etc.) (Kah *et al.*, 2007). However, the path and the rate of degradation of an herbicide are closely related to its chemical structure (Wauchope *et al.*,

2002). Some herbicides will be more susceptible to be degraded by microorganism, while others will be degraded via photolysis or acid-base reactions (Schreiber *et al.*, 2018).

Furthermore, the products of degradation of the herbicide in soil are another aspect to be considered. In this context, it is not only necessary to consider the toxicity of the herbicide itself, but also the toxicity of its degradation products (Sheets, 1966). In addition, the biological activity of these products must be considered since they could act as agrochemicals as well.

Agrochemicals able to degrade in other active substances are known as pro-pesticides. The main advantage of those substances is that they can act via different path as they are degraded into metabolites. Such metabolites can be as active as or more active than the parent compound (Casia *et al.*, 2017). That is crucial in the specific case of herbicides considering the resistance that weeds are able to develop against agrochemicals. If a compound is able to inhibit the growth of a target plant via different mechanism, it is more complicate for the weed to develop resistance.

1.2. OBJECTIVES

As is possible to see from the discussion above, the development of a new substance that can be considered as herbicide candidate is a complex process. Aspects like phytotoxic effects and degradation of the compound must be considered. Therefore, the objective of this work was to synthesize a new herbicide candidate using the ADM strategy as rational planning to its design.

From the promising results obtained from the herbicides assays performed with several tetraoxanes, it was decided to synthesize a new molecule with herbicide potential. The ADM strategy was employed to design the new molecule. The commercial auxin 2-(naphthalen-1-yl)acetic acid (**34**, NAA) was chosen as starting material. As presented in

Scheme 1.6, compound **34** can be transformed into an aldehyde **35**. Once it is accomplished, obtention of tetraoxane **37** is furnished by reacting **35** with intermediate **36**.
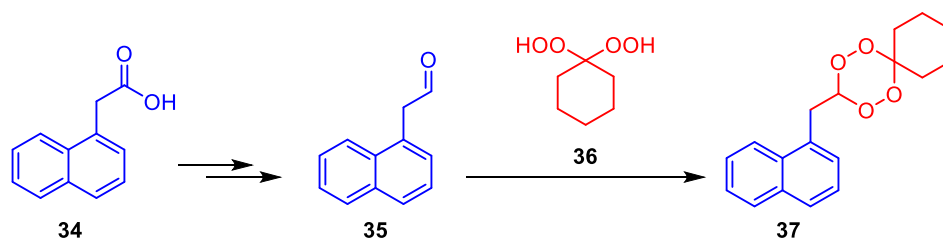
Scheme 1.6. Synthetic planning of tetraoxane **37** by applying the ADM approach.

As mentioned, tetraoxane **37** is designed via ADM strategy. The hypothesis is that this compound might act as auxinic herbicide since it is based on a synthetic compound with such type of activity. In addition, the previous studies carried out by our research group indicate that tetraoxanes might stimulate the reactive oxygen species (ROS) in plants (Cusati *et al.*, 2015). For this reason, it is expected that the new compound also causes the same symptoms as those caused by compounds that produces ROS. To corroborate such hypothesis, it was decided to investigate the phytotoxic profile of tetraoxane **37** by running greenhouse bioassays of the compound and its synthetic precursors.

As highlighted, tetraoxane **37** is a molecule designed via ADM in order to obtain a new substance with potential as an herbicide. One of the suppositions that emerged during its planning was that the compound might be able to degrade into its synthetic precursor, the commercial auxin NAA (Scheme 1.7). If so, the **NAA** could continuing acting as herbicide. To prove that assumption experiments to study the degradation pattern of **37** in sand were carried out.
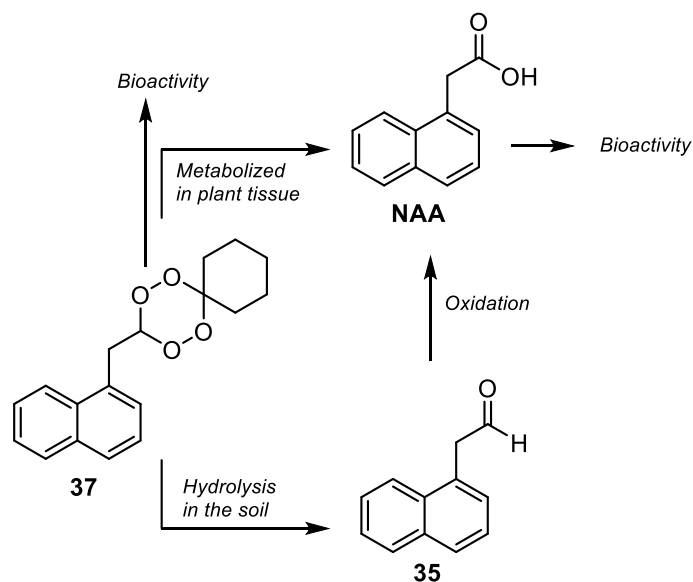
Scheme 1.7. Proposed degradation path of tetraoxane **37.**

1.3. RESULTS AND DISCUSSION

1.3.1. Synthesis of tetraoxane **37**

Synthesis of tetraoxane **37** is presented in Scheme 1.8. First, a sequential reduction oxidation was conducted to obtain aldehyde **35.** Treatment of carboxylic acid **34** with LiAlH$_4$ afforded the required alcohol in quantitative yield. Sequentially, different methodologies to oxidize the intermediate were used. Initial Swern oxidation resulted in total consumption of the alcohol, affording the required aldehyde in a consistent, but poor yield (9%) (Oshugui *et al.*, 2003). Such low yield could be due to degradation of the aldehyde, via initial aldol condensation in the presence of triethylamine in the reaction medium (Arimoto *et al.,* 1994; Pratt *et al.,* 1991). Further attempt to oxidize the alcohol involved the use of PDC at room temperature, but, under those conditions, the alcohol proved inert. Increasing the temperature to 45 ºC caused the decomposition of the starting material (Corey *et al.*, 1975).

Finally, the use of hypervalent iodine reagents was the most successful approach. Oxidation of substrate with Dess Martin periodinane (DMP) yield the desired product in 86% yield. Although it was a satisfactory result, the use of DMP in big amounts is not

recommended because of the difficulty to remove the side products from the reaction during the workup process.
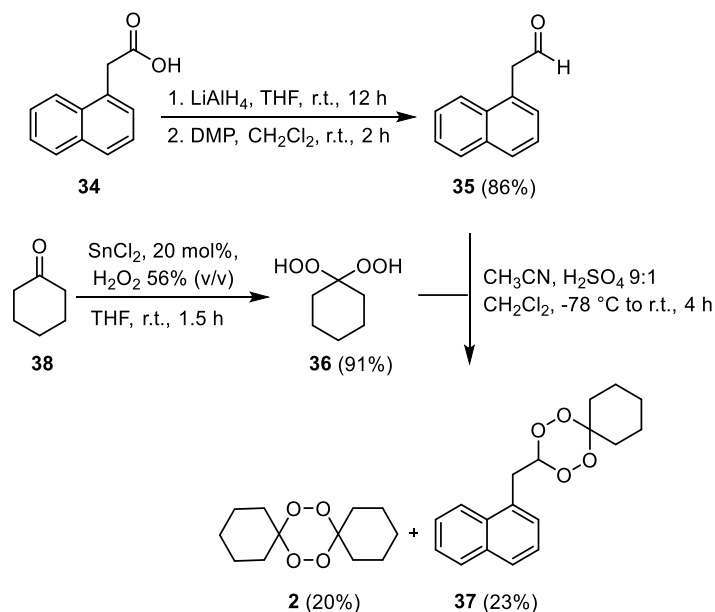
Scheme 1.8. Synthesis of compound **37**.

Therefore, an alternative to the alcohol oxidation was carried out using bis-acetoxyiodobenzene (BAIB) and 0.1 mol% of 2,2,6,6-tetramethylpiperidin-1-yl)oxyl (TEMPO) as oxidizing agents. With that methodology, the aldehyde **35** was synthesized in 63% yield (DeMico *et al.*, 1997). In addition, BAIB is a reagent that can be easily synthesized in gram-scale in laboratory. Thus, it was the methodology chosen to carry the oxidation with bigger amounts of substrate. It is important to highlight that the purification of aldehyde **35** by silica gel column fractionation was not efficient due to its instability under acid condition. It was found that the best way to purify **35** was by distillation at atmospheric pressure.

After obtaining aldehyde **35**, the intermediate **36** was synthesized. In this case, the use of a solution of hydrogen peroxide (aqueous H_2O_2 at 56% v/v) and $SnCl_2$ (20 mol%) as catalyst afforded **36** in a maximum reproducible yield of 91% (Baldaia, 2015). That compound was obtained as a low melting point solid, that was crystalized before use in the next reaction.

With compounds **35** and **36** in hand, synthesis of target tetraoxane **37** was carried out. The compound was obtained via acid catalysis in 9% of yield (Table 1.1, entry 1). Since the mechanism formation of tetraoxanes happens through a series of equilibriums, the formation of side products is a major issue (Dong, 2002). In the specific case of non-symmetric tetraoxanes, the formation of the symmetric tetraoxane, such as compound **2,** as *by*-product is another crucial problem (Šolaja *et al.*, 2002; Terzić*et al.*, 2007). In order to improve the result, the reaction conditions were optimized. First, it was decided to increase the amount of *gem*-hydroperoxides **36** in the reaction medium (Table 1.1, entry 2). This modification resulted in the reduction of the yield of both compounds **2** and **37**, similar results were obtained when the amount of aldehyde was increased (Table 1.1, entry 3).

As mentioned before compound **35** degraded under different reaction conditions of oxidation and during its purification with silica gel. The high reactivity of this compound was also a problem during the optimization of the synthesis of tetraoxane **37,** since the degradation of **35** was observed under several reaction conditions (Table 1.1, entries 4, 5 and 9). On the other hand, some reports of tetraoxane synthesis derived from steroids informed that decreasing the temperature of the reaction, can improve the product yield (Todorović *et al.*, 1996).

Considering these factors, it was decided to execute the reaction at -78 °C. As result, tetraoxane **37** was obtained in 23% yield, the higher value obtained during the optimization process (Table 1.1, entry 6). One possible explanation to this result is that, reduction of the temperature reaction has as consequence a decrease of the aldehyde **35** reactivity. Such reduction in the reactivity, might favor the reaction between the protonated aldehyde and the *gem*-hydroperoxide over other possible side-reactions. Finally, additional attempts to synthesize tetraoxane **37** with a more polar solvent, like acetonitrile, were not successful. Also, the reaction time was modified (Table 1.1, entries 7-11), and in none of the cases the non-symmetric tetraoxane was isolated. In counterpart, compound **2** was obtained in 20% yield.

Table 1.1. Optimization conditions for the synthesis of tetraoxane **37**
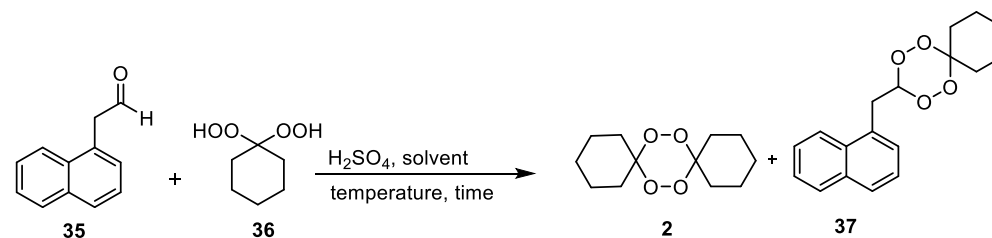
Entry	H$_2$SO$_4$ (mmol)	35 (mmol)	36 (mmol)	Time (h)	Temp (°C)	Solvent	37 (%)	2 (%)	Comment
1	13.3	1.8	2.7	24	0 to r.t	CH$_2$Cl$_2$	9	18	
2	13.3	1.8	3.2	24	0 to r.t	CH$_2$Cl$_2$	5	10	
3	13.3	2.7	1.8	4	0 to r.t.	CH$_2$Cl$_2$	7	19	
4	13.3	5.4	1.8	4	0 to r.t.	CH$_2$Cl$_2$	-	20	Degradation of **35**
5	13.3	1.8	2.7	-	r.t.	CH$_2$Cl$_2$	-	-	Degradation of **35**
6	13.3	1.8	2.7	4	-78 to r.t	CH$_2$Cl$_2$	23	20	
7	6.20	1.8	2.7	4	-78 to r.t	CH$_2$Cl$_2$	10	20	
8	0.9	1.8	2.7	4	-78 to r.t	CH$_2$Cl$_2$	-	-	No reaction
9	13.3	1.8	2.7	4	0 to r.t.	CH$_3$CN	-	20	Degradation of **35**
10	13.3	1.8	2.7	4	0	CH$_3$CN	-	18	
11	13.3	1.8	1.5	4	0 to r.t.	AcOEt	-	-	No reaction

Compound **37** was isolated as a white solid and had its structure confirmed by spectroscopic analysis. The infrared spectra show bands at 2935 and 2856 cm^{-1} related with the stretch of C-H vibration present in the structure. Furthermore, the band associated with C-O vibration is observed at 1445 cm^{-1} while the band related to the O-O stretching is observed at 1259 cm^{-1} (Barbosa, 2013) (Figure 1.5).
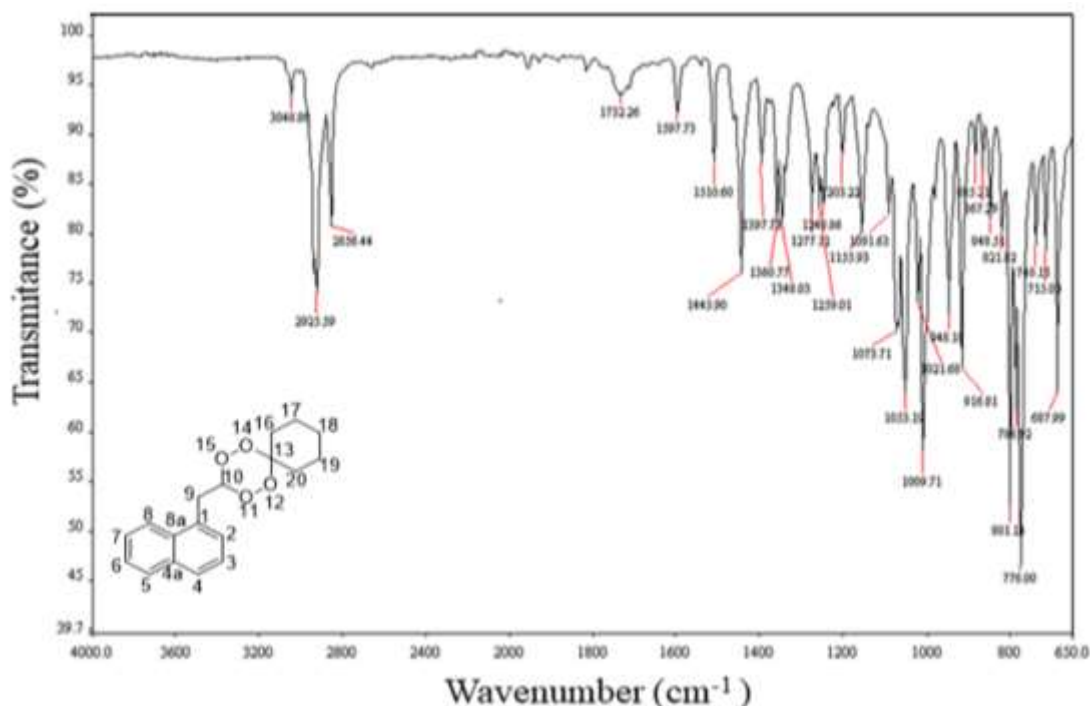
Figure1.5. IR (ATR/FTIR) spectra of tetraoxane **37.**

The ^{1}H-NMR spectrum is presented in Figure 1.6. The multiplet between 1.28-1.66 ppm, which integrates for 8 hydrogen atoms, is assigned to the cyclohexane ring hydrogens (from H-16 to H-19). A doublet at 3.33 ppm (J_{9-10}= 4.7 Hz) and a triplet at 6.14 ppm (J_{10-9}= 4.7 Hz) are assigned to the CH$_2$-CH side chain moiety (H-9 and H-10, respectively). Further signals related to the naphthalene core are observed between 7.26-8.01 ppm (H-2, H-3, H-4, H-5, H-6, H-7 and H-8).
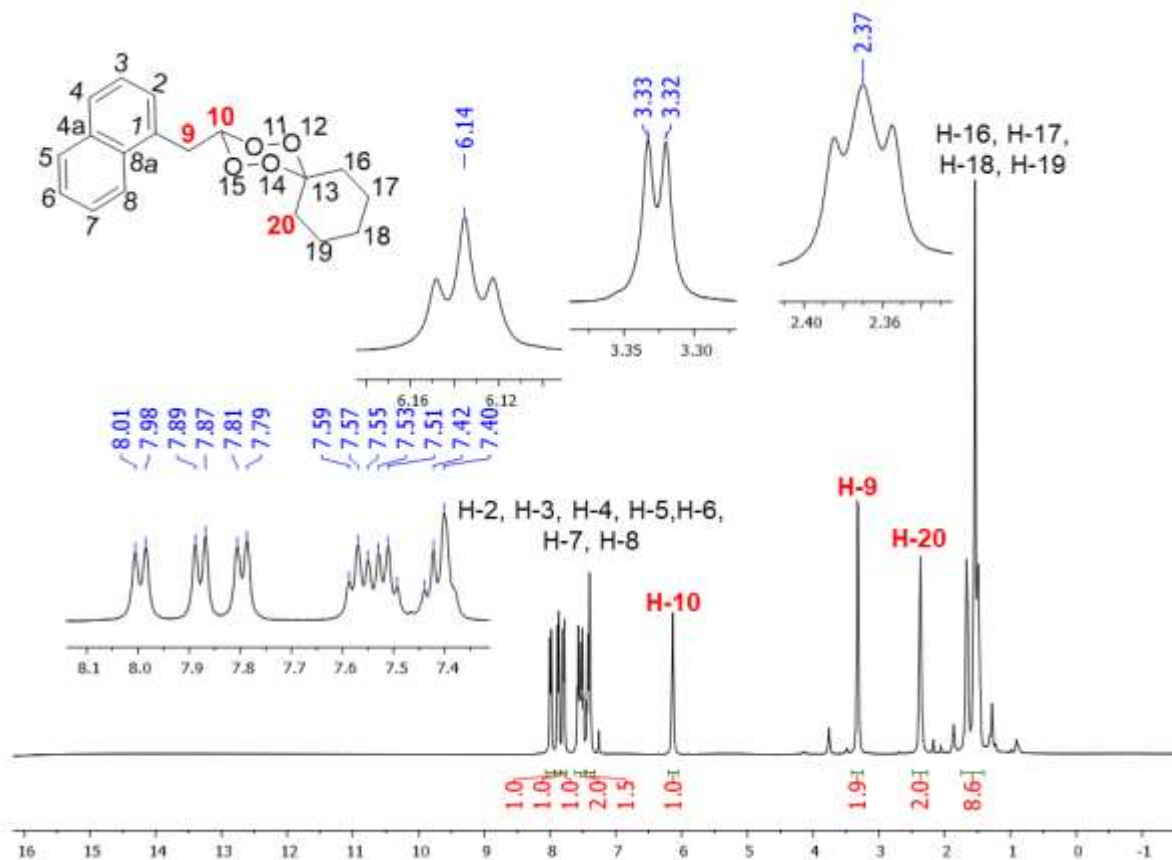
Figure 1.6. ^{1}H-NMR spectrum of (400 MHz, CDCl$_3$) of compound **37.**

Finally, the triplet at 2.37 ($J_{20,19}$ = 5.2 Hz) ppm must be related to a pair of more deshielded methylene hydrogens of the cycle. This affirmation was corroborated with the an HMQC experiment (Figure 1.7). As is possible to see, there are two different signals that are associated to the methylene at axial and equatorial position with respect to the tetraoxane core. Figure 1.7 shows a fragment of the HMQC spectrum of **37**, and as can be observed, there is a correlation between the signal the triplet at 2.37 ppm and one of the carbons of the cyclohexane ring. Therefore, the signal at 2.37 ppm must be associated with a methylene at the axial or equatorial position with respect to the tetraoxane ring.
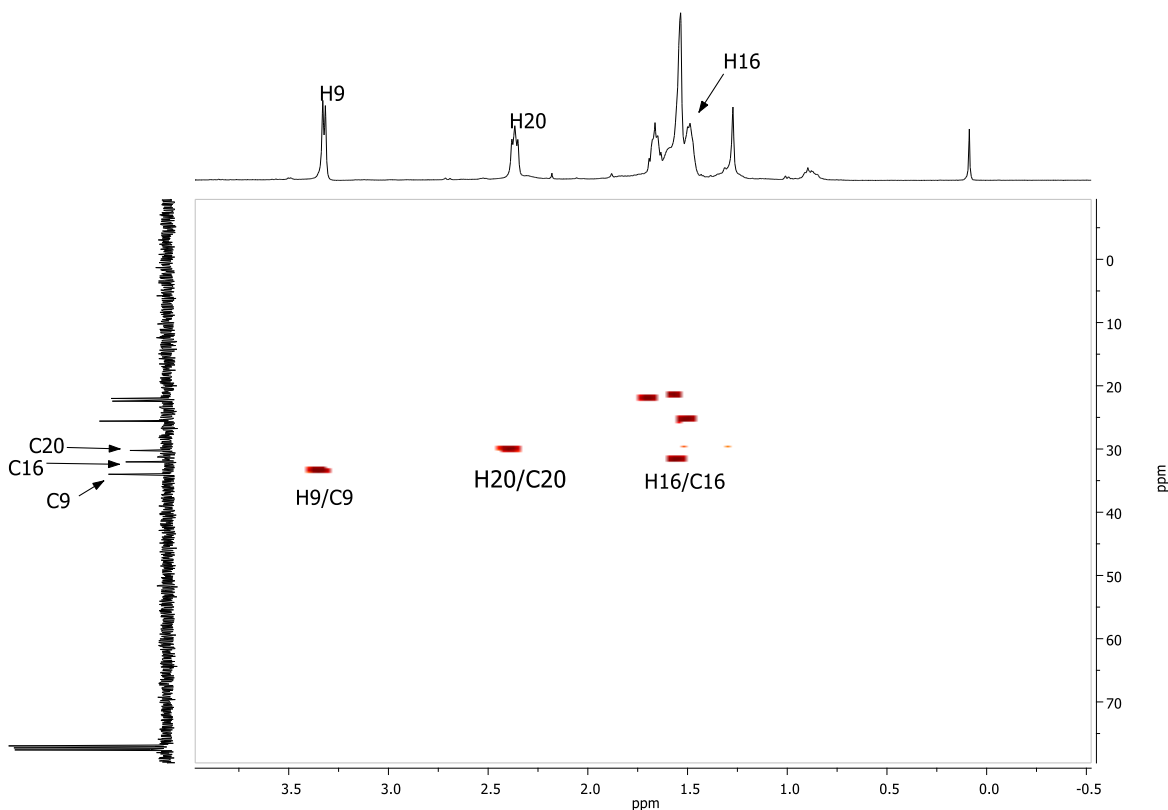
Figure 1. 7. Fragment of HSQC spectrum of tetraoxane **37.**

Previous studies about the pattern of tetraoxanes were carried out aiming to assign the signals of equatorial and axial positions in the ^{1}H-NMR spectrum. According to the authors, in the case of compound **38** (Figure 1.8), substituents at the equatorial position (1.80 ppm) are more deshielded than those of the axial position (1.36 ppm) (Murray *et al.*, 1965). They justified such assignment by making an analogy with cyclohexane (**39**) system, that has only carbon-carbon single bonds in its structure. In this case, it is known that axial substituents are more shielded than the equatorials due to the effect of the diamagnetic anisotropy of the carbon-carbon σ bond (Jackman, 1959). Those references were also used by Dong and Vennestrom to explain the ^{1}H-NMR signals of several tetraoxanes, including more than one cyclic system, such as compound **2** (Figure 1.8) (Dong and Vennestrom, 2001*).*
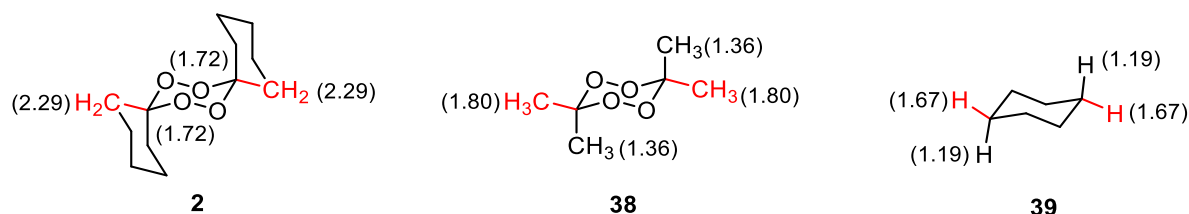
Figure 1.8. Structures previously studied to assign the ^{1}H-NMR pattern of tetraoxanes and cyclohexane. Moieties in red are the most deshielded according to the authors. Numbers in parenthesis are the chemical shifts (δ) of each hydrogen (Dong and Vennestrom, 2001).

To determinate if that assignment could be applied to the ^{1}H-NMR spectrum of tetraoxane **37**, computational studies of the compound were enforced. To start, the most stable conformations that the compound might adopt were calculated by Spartan'14 software, version 1.1.4. According to data, there are 14 possible conformers for the structure. The most stable is represented in Figure 1.9 and it corresponds to 20% of all conformers. The hydrogens of the methylene at axial position are numbered as H-20a and H-20b, while the hydrogens related to equatorial position are numbered as H-16a and H-16b.
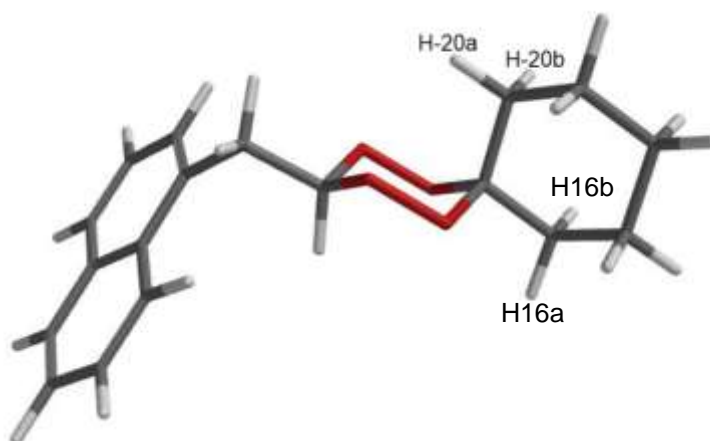
Figure 1. 9. Structure of the most stable conformer of tetraoxane **37**.

At Figure 1.9 one can see that there is a repulsive interaction between the electronic cloud of the hydrogens of methylene at position 20, and the electrons lone pair of the

oxygen atoms of the tetraoxane core. Such interaction has as consequence a displacement to the left of the signal in the ^{1}H-NMR spectrum. This result was corroborated when the experimental ^{1}H-NMR spectrum of **37** was compared with the theoretical prediction of ^{1}H-NMR (Figure 1.10). These results suggest that the assignment previously reported for other tetraoxanes can not be used to assign the ^{1}H-NMR of **37**. According to the computational experiments, in the case of **37**, hydrogens of the methylene at the axial substitution (H-20) in the tetraoxane ring are more deshielded than the equatorial (H-16). However more experiment must be carried in order to corroborate these results.
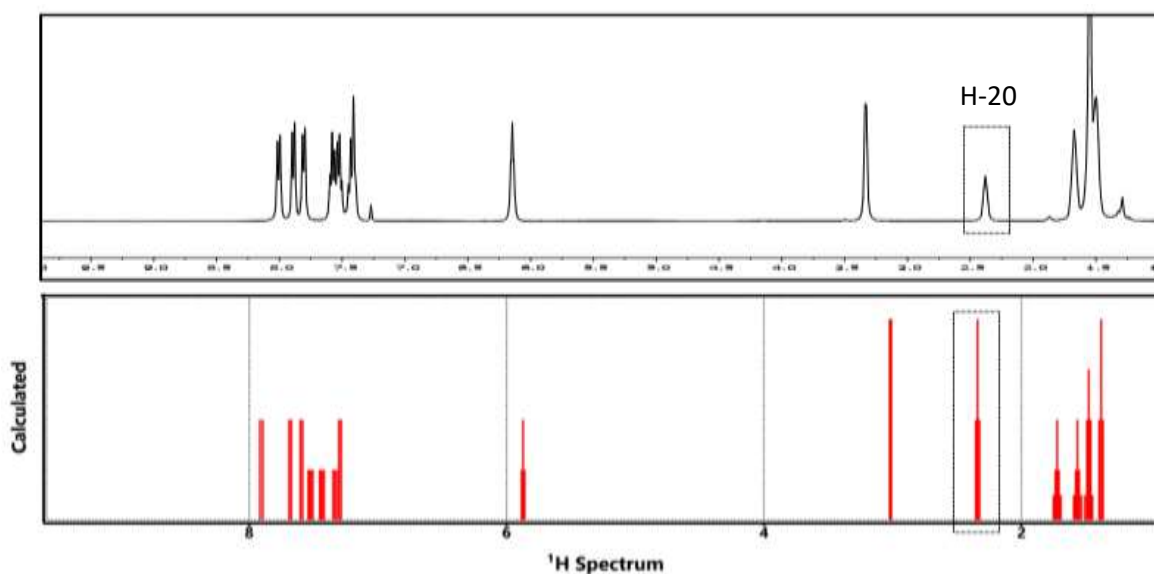
Figure 1.10. Experimental and theoretical ^{1}H-NMR spectrum of **37.**

Although the theoretical calculations corroborated the assignment of the signal at 2.37 ppm, when the structure of the most stable conformer of **37** is analyzed, it is possible to see that hydrogens H-20a and H-20b are not magnetically equivalents (Figure 1.8). Thus, the doubt if the signal at 2.37 ppm could be classified as a triplet emerged. Such question can be answered as the structure showed in Figure 1.9 is not the only conformer possible for the compound. As explained earlier, there are 14 possible conformers of tetraoxane **37.** Clearly, the most stable ones have the naphthyl substituent at the equatorial position (Table 1.10A pg. 144). Therefore, it is possible to infer that the mobility of the tetraoxane ring is restricted. Yet, the same affirmation does not apply to the case of the cyclohexane ring,

present in the structure of **37**. Because there are no substituents in any of the carbons that conform the cycle, it is expected the adoption of the two possible chair conformations.

Figure 1.11 shows the overlap of the conformers of **37** with the two chair conformations of the cyclohexane ring (Figure 1.11 A). From a different perspective (Figure 1.11, B and C), it is possible to see that both hydrogens H-20a and H-20b are susceptible to the same electronic effect, caused by the oxygen lone pair of the tetraoxane core. Then, both hydrogen atoms can be considered magnetically equivalent, and it is possible to affirm that the signal at 2.37 ppm is, in fact, a triplet. However, studies about the rate of the interconversion of the cyclohexane ring in the structure of **37** must be carried out in order to confirm this affirmation.
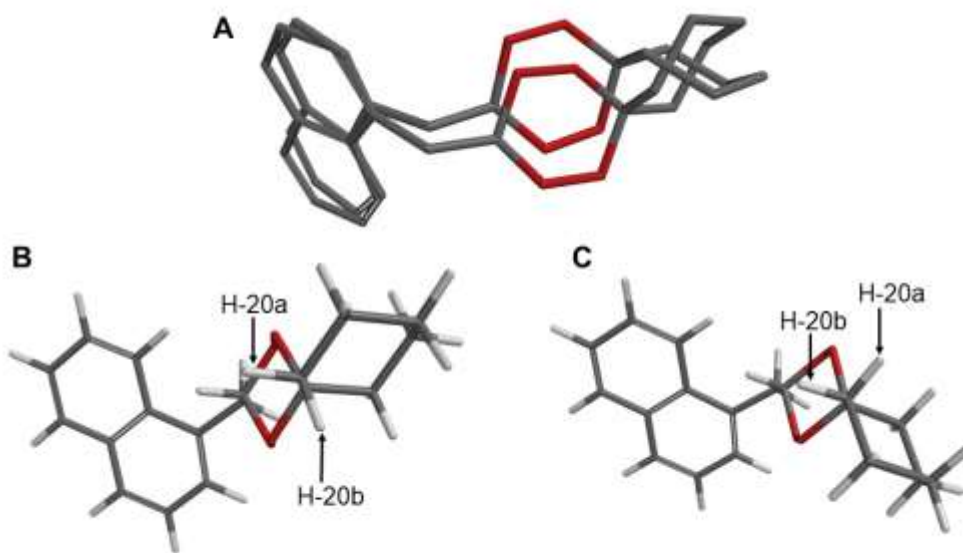
Figure 1. 11. Different perspective of conformers of tetraoxane **37.**

Figure 1.12 exposes the ^{13}C-NMR spectra of compound **37**. The spectrum shows a total of 18 signals. The signals between 22.0-34.0 ppm are associated with the cyclohexane ring and carbon C-9. Afterwards, the signals at 108.3 ppm and 109.1 ppm are assigned to

C-10 and C-13 of the tetraoxane core. Ultimately, the ten signals between 122.00-135.00 were observed for the naphthalene ring.
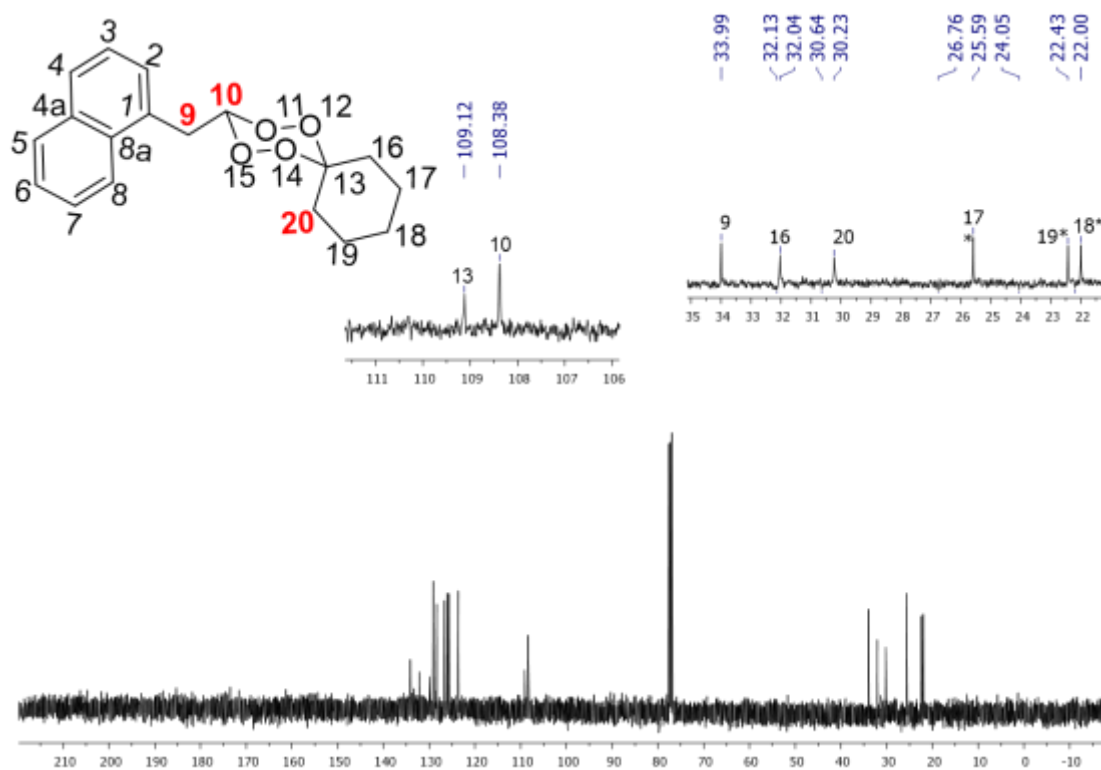
Figure 1.12. ^{13}C-NMR spectrum of (100 MHz, CDCl$_3$) of compound **37.**

Although the yield of the optimization was low, it is necessary to highlight that, in general, with that methodology, the yields for the synthesis of different tetraoxanes oscillate between 25-60% (Terent´ev *et al.*, 2014). Despite the limited overall yield for the preparation of tetraoxane **37**, the compound was produced in gram scale, which was sufficient for biological evaluation, as described in the next section.

1.3.2. Herbicidal activity

The pre-emergency herbicidal activity of compound **37**, along with the commercial herbicides 2-(naphtalen-1-il)acetic acid (NAA, **34**), glyphosate (GLY) and imazethapyr (IMA) was evaluated. Glyphosate is probably the most important herbicide developed in

modern agriculture. Until the current date, it is the main herbicide utilized on the field, especially since the introduction in the market of glyphosate genetically modified resistant crops (Duke *et al*., 2002). On the other hand, Imazethapyr is an imidazole that gives selective weed control over soybeans and legume crops (Jugulam, 2019). Although highly effective, there is a concern due to the increase of weeds that are presenting resistance to these products (Heap, 2019). In addition, many studies address that GLY might be a carcinogenic agent (Tarazona *et al*., 2017), while IMA is highly persistence in soil, which causes several environmental issues (Kraemer *et al*., 2009). Therefore, to find new compounds that can replace such commercial products is an important area of research. In addition, considering the possibility that, during the experiment, tetraoxane **37** could be degraded into its precursors **35** and **36**, these two compounds were also assayed.
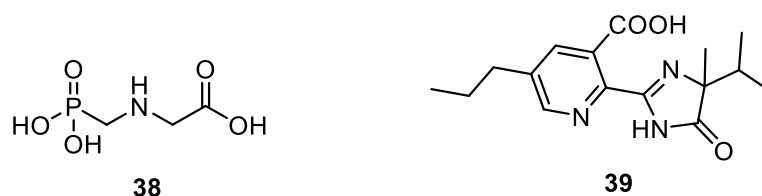
Figure 1. 13. Structure of Glyphosate (**38**) and Imazethapyr (**39**).

The initial greenhouse bioassays were carried out using *Cucumis sativa* L. and *Sorghum bicolor* L. as target species, due to their high sensitivity to herbicides (Pereira *et al.*, 2017). The compounds were tested at the dose of 8.3 x 10^{-6} mmol per gram of sand (a solution of 0.125 mmol/L was employed). All compounds reduced the germination on both species (Table 1.2). When tested on *C. sativa*, compound **37** was as active (40% of germination) as IMA, while all the others reduced the germination to 53-60%. The test against *S. bicolor* revealed that **37** caused 80% of germination, being less active than IMA and GLY, and as active as NAA. On the other hand, precursor **35** reduced the germination to 20%, being as active as IMA, while **36** (60% of germination) was more active than NAA.

Table 1.2. Percentage of germination of *Cucumis sativa* and *Sorghum bicolor* in the presence of compounds **35**, **36, 37** and 2-(naphthalen-1-yl)acetic acid, (NAA), glyphosate (GLY), imazethapyr (IMA) after five days of experiment.

Compound	*C. sativa*	*S. bicolor*
35	60 ± 0.0	20 ± 1.0
36	53 ± 0.7	60 ± 0.0
37	40 ± 0.6	80 ± 1.0
NAA	40 ± 0.6	80 ± 0.0
IMA	60 ± 1.0	20 ± 1.0
GLY	53 ± 0.6	66 ± 1.7

With respect to root inhibition, tetraoxane **37** caused little or no effect on both species, but inhibited the shoot growth of *C. sativus* and *S. bicolor,* by 44.2% and 61.1%, respectively. That level of activity is comparable to or higher than the reference NAA. The reference GLY is more active in comparison with the synthetic compounds **35**, **36** and **37** for *C. sativa*, at the same time, IMA is more potent against *S. bicolor* (Figure 1.14). In general, precursor **35** was not active for both species, although the peroxide **36** caused 67.3% inhibition on the root growth of *C. sativa*, being more active in comparison with NAA and IMA. Yet, it caused little effect (22.7%) on the roots of *S. bicolor*.
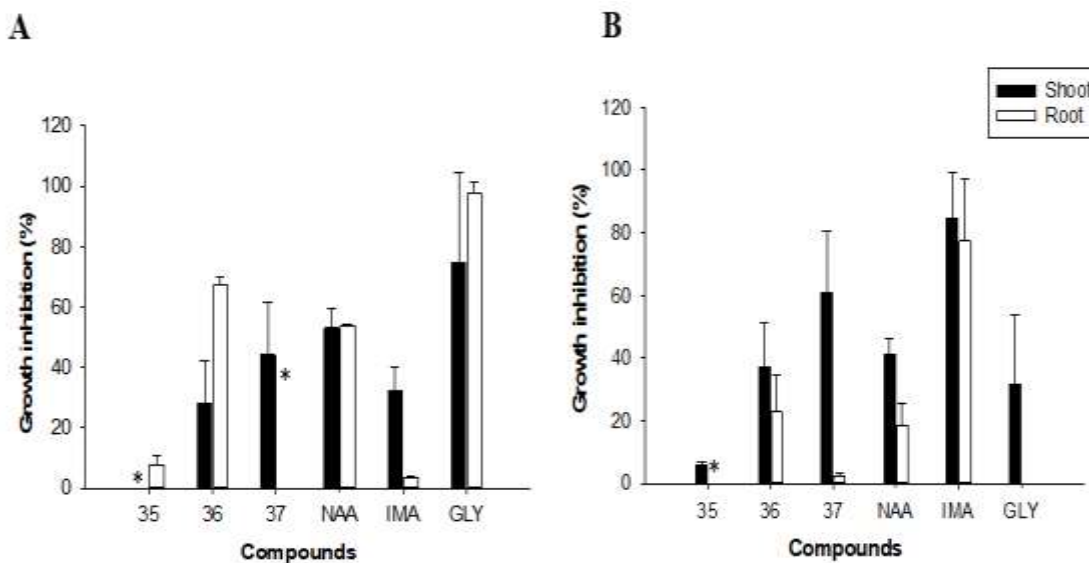
Figure 1.14. Effect of compounds **35**, **36** and **37** on the growth inhibition of shoot and roots of *Cucumis sativa* (A) and *Sorghum bicolor* (B). Values were calculated based on the dry weight of the control. Commercial herbicides used as positive control were: 2-(naphthalen-1-yl)acetic acid (NAA), imazethapyr (IMA), glyphosate (GLY). The compounds were tested at 0.125 mmol/L. *The presence of an asterisk (*) instead a bar indicates stimulation (see Tables 1.1A. and 1.2.A. for full data. Pg. 146-148).*

After demonstrating that the hybrid peroxide **37** provoked a significant inhibition on shoot formation in *C. sativa* and *S. bicolor*, the activities of all compounds against the weeds *Iponomea acuminate* L., *Bidens pilosa* L., *Solanum americanum* Mill and *Alternanthera ficoidea* L. were further investigated (Figure 1.15). The weeds are ubiquitous in different crops plantations, such as soybean, cotton and tomatoes. They are cultivated in large areas in Brazil and correspond to a high proportion of the national agricultural production (Freitas *et al.*, 2009; Pereira *et al.*, 2010; Storniolo *et al.*, 2017). For this reason, it is essential to control such species to guarantee a maximum profit from their crops.
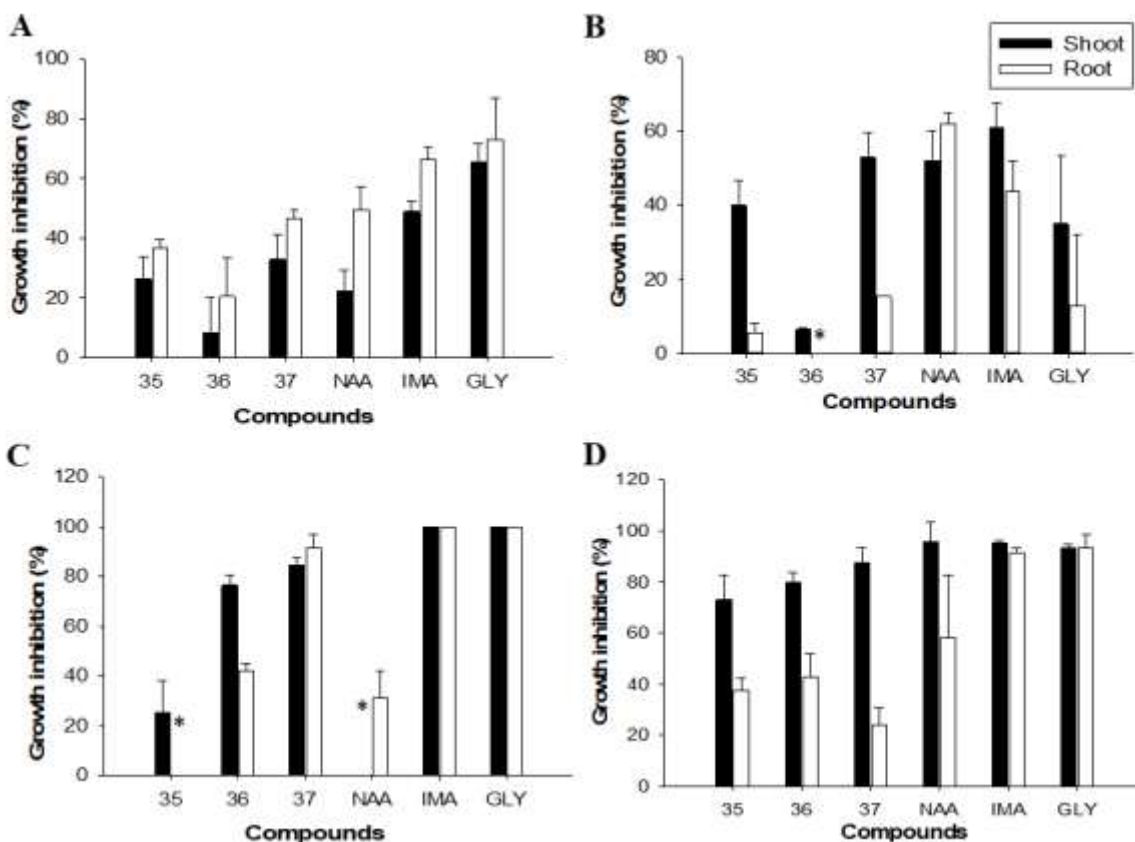
Figure 1.15. Effect of compounds **35**, **36** and **37** on the growth inhibition of shoot and roots of *Bidens pilosa* (A), *Iponomea acuminate* (B), *Solanum americanum* (C) and *Altenanthera ficoidea* (D). Values were calculated based on the dry weight of the control. Commercial herbicides used as positive control: 2-(naphthalen-1-yl)acetic acid (NAA), imazethapyr (IMA) and glyphosate (GLY). The compounds were tested at 0.125 mmol/L. *The presence of an asterisk (*) instead a bar indicates stimulation (see Tables 1.3A. 1.4A., 1.5A. and 1.6A. for full data. Pg. 146-148).*

With regard to *B. pilosa* (Figure 1.15, A), compound **37** was potent like NAA as root inhibitor (46.7% inhibition), but it had a greater effect on shoot, causing 32.7% inhibition, against 22.2% caused by NAA. It was found that **35** and **36** provoked some inhibition on both plant parts, but the impact was less pronounced in comparison with **37**. None of the compounds were as active as IMA and GLY, that generated more than 66% inhibition on roots and more than 48.9% inhibition on shoot.

In relation to *I. acuminate* (Figure 1.15, B), the commercial references NAA and IMA were the most potent against the weed, resulting in more than 40% inhibition on roots and shoots, while GLY caused only 35% inhibition on shoots and had little effect on roots. In comparison, tetraoxane **37** provoked 52.9% inhibition on shoot growth, equivalent to the activity of NAA. For **36,** only a small inhibitory effect on roots development was observed. The aldehyde **35** caused 40% inhibition on shoot growth, with no effect on roots. Differently, **36** caused unexpected root growth promotion and no significant effect on shoots. The root growth promotion is not easily explained, since the peroxide is expected to generate radicals that are toxic to plants and several other organisms (Forest and Norman, 1991). Despite the relatively small standard deviation (-53.9 ± 7.7 %, Table1.4 A), it should be further investigated to better understand the effect of hydroperoxyacetals on plant growth.

The *S. americanum* specie (Figure 1.15, C) proved to be very sensitive to IMA and GLY, because both herbicides generated 100% inhibition on the development of roots and shoot. Commercial herbicide NAA, at the dose of 8.3 x 10^{-6} mmol per gram of substrate (0.125 mmol/L solution employed), promoted the shoot growth by 141.2%. At the same time, it inhibited the roots by 31.1%. As it is well known, the low concentration of auxin in plants stimulates their growth, because auxin participates in ethylene biosynthesis and abscisic acid synthesis (Grossmann *et al.*, 2000). In contrast to NAA, compound **37** was very effective on controlling *S. americanum* by inhibiting shoot and roots by more than 84.5%. Aldehyde **35** caused a small effect on shoot development (25% inhibition), but promoted root growth by 63%, a similar effect observed for NAA on shoot. Nevertheless, hydroperoxide **36** also caused a pronounced inhibition on the whole plant. Finally, when tested against *A. ficoidea* (Figure 1.15, D), all compounds inhibited shoot growth by at least 72.9%, with special attention to **37**, that caused 87.5% inhibition at 0.125 mmol/L. Opposing to IMA and GLY, the effects of **35**, **36** and **37** on root inhibition were less pronounced.

Besides the quantitative inhibitory effects reported for all compounds, a qualitative visual evaluation was carried out by three trained experts on weed science (Sant´Ana,

2015). For such evaluation, the observed phytotoxic effect was analyzed and rated on a scale from zero (no effect) to 100 (plant death). In order to have a better evaluation of the changes, the assay was made using a solution of 1 mmol/L. The averages of three independent evaluations are presented on Table 1.3. All plant species were very sensitive to IMA ($\geq$ 95% intoxication), although, some species were less affected by GLY ($\geq$ 80% inhibition). The major reference NAA also caused $\geq$ 80% intoxication on most species, except for *S. bilocor*, which was also resistant to peroxides **36, 37** and aldehyde **35**. In general, peroxide **37** was as active as NAA, but **36** had a pronounced effect only against *S. americanum* and *C. sativa*. The *gem*-hydroperoxide **35** was very effective only against *S. americanum*.

Table 1.3. Percentage of intoxication of the target species treated with 1 mmol solution of the compounds after 22 days of experiment. Values are disclosed according to the ALAM scale (1974)

Compound	*C. sativa*	*S. bicolor*	*B. pilosa*	*I. acuminate*	*S. Americanum*	*A. Ficoidea*
35	77	0	37	0	95	33
36	80	0	0	0	95	60
37	90	0	90	80	100	86
NAA	90	0	90	80	100	93
IMA	100	100	95	100	100	100
GLY	80	90	95	80	100	100

Among all the evaluated species, *C. sativa* exhibited the most pronounced visual changes. The reference NAA caused leaf epinasty and root nodulation, both typical effects of auxinic herbicides (Figure 1.16B). In the case of **37,** the leaf epinasty was also observed.

In addition, that compound also urged chlorosis and necrosis in the aerial parts, that were also observed in plants treated with peroxide **36** (Figure 1.16 C and D).
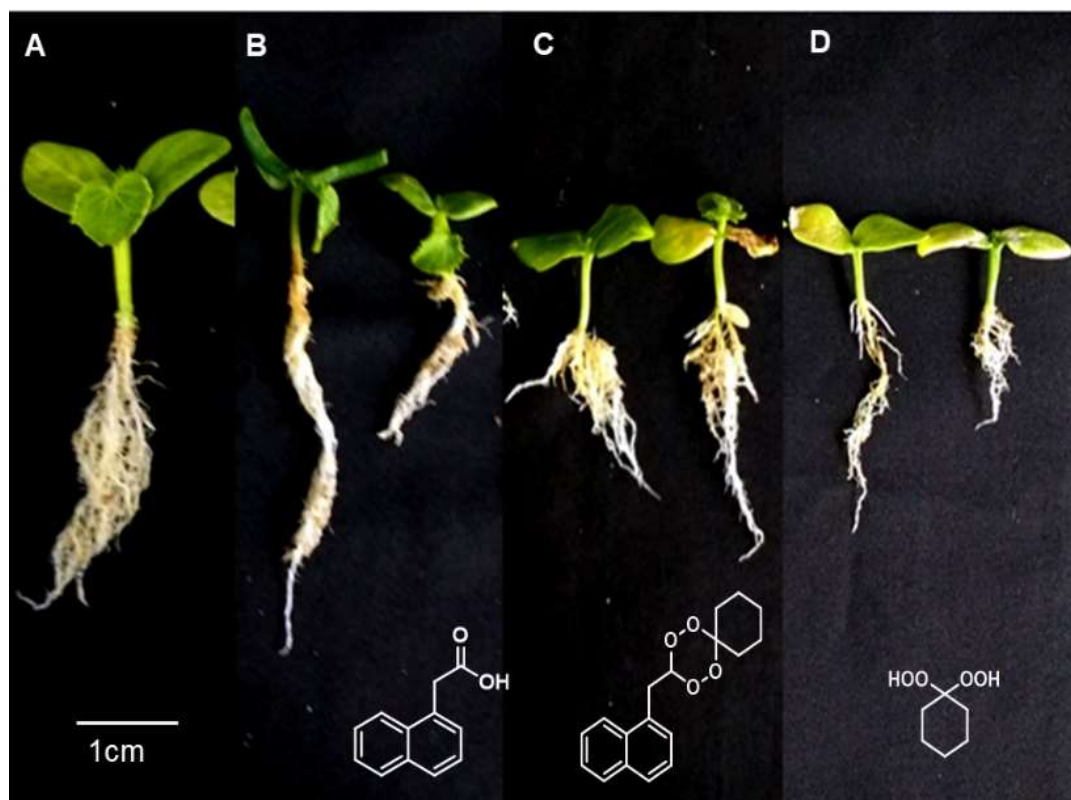
Figure 1. 16. Visual changes or effects caused by compounds **36**, **37** and NAA (at 1 mmol/L) on *Cucumis sativa* under greenhouse conditions, after 22 days. Control (A), plants treated with NAA (B), plants treated with **36** (C) and plants treated with **37** (D).

Chlorosis of the leaf is a symptom provoked by compounds that interfere, at some level in the photosynthesis of the plant (Coob and Reade, 2012). These types of symptom were also observed in plants treated with artemisinin (Corral *et al.,* 2017; Dayan *et al.*, 1999). From these observations several research groups studied the mode of action of artemisinin. The results suggested that the peroxide bond in the artemisinin structure is responsible for the overproduction of reactive oxygen species (ROS) (Yan *et al.*, 2015). High concentration of ROS can generate, among others, lipid peroxidation and cell division. In the matter of artemisinin, it can affect photosystem II by reducing the formation of plastoquinone pool, which affects the electron transfer in photosynthesis (Bharati *et al.*, 2012). Considering the similarities on the visual changes caused by compounds **36**, **37** and

artemisinin, we have the hypothesis that some of the phytotoxic effect caused by **36** and **37** might be related to the peroxide group present in their structures.

1.3.3. Study of the degradation of tetraoxane

*1.3.3.1. Method development for detection of tetraoxane **37***

Initially, solutions of compounds **35**, **37** and NAA were prepared at 2 mmol/L concentration. Then, each solution was injected using acetonitrile-water (95:5) as eluent mixture with an injection flow of 1mL/min and a running time of 40 min. In those conditions, commercial auxin NAA was not detected during the analysis, therefore, it was decided to repeat the analysis with different mobile phase mixture (Table 1.7A. entry 2). In the second experiment, it was employed a mixture of an aqueous solution of trifluoracetic acid 0.1 % v/v and acetonitrile. With that condition, the three analytes were detected during the analysis.

Then, several separation conditions were tested for developing the best condition to study the biodegradation of tetraoxane **37**. For that, a solution with **35**, **37** and NAA was prepared and injected using different proportions of solvents and running times. The best condition was accomplished using a mixture of water/acetonitrile (95:5) as mobile phase, with an injection flux of 0.4 mL/min in a period of 102 min (Table 1.7A, entry 12). Further attempts to reduce the running time by modifying the solvent mixture were not successful.

Figure 1.17 shows the HPLC chromatogram of compounds **37**, **35** and NAA injected separately, with the optimized conditions previously established. As it is demonstrated, tetraoxane **37** have the biggest retention time (82 min) of the three compounds. On the other hand, compounds **35** and NAA have close retention times: 70 min and 71.5 min, respectively.
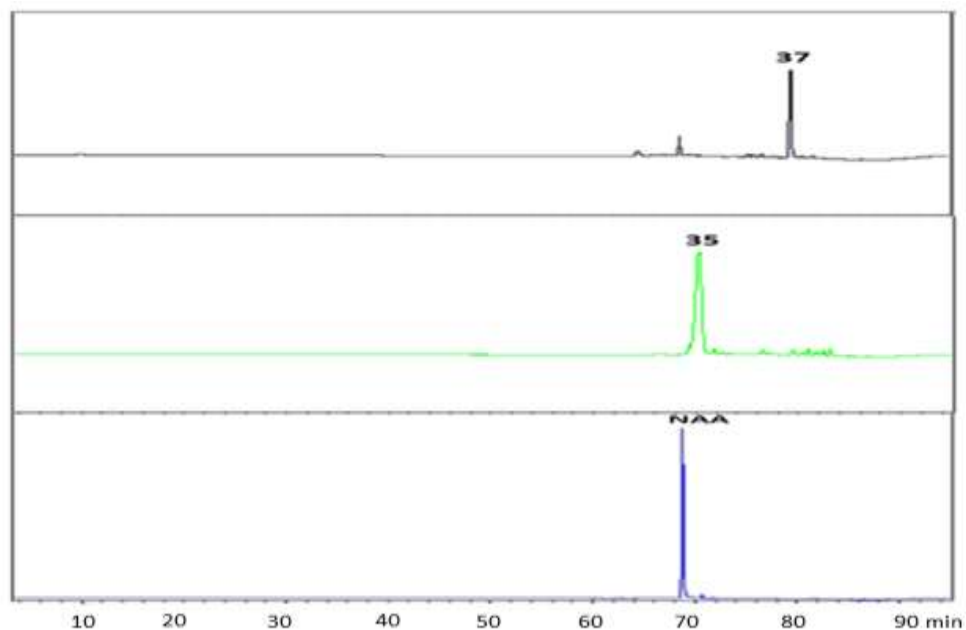
Figure 1. 17. HPLC chromatogram of compounds **35**, **37** and NAA at 2 mmol/L**.** The separations were implemented utilising a Phenomenex C18 column (2.6 μm size particles, length 100 mm, i.d. 3 mm) and a mixture of acetonitrile/water 95:5 as eluent.

Yet the retention time of NAA and aldehyde **35** are quite similar, both peaks did not overlap when the solution with the three compounds was injected. Chromatogram of that mixture is presented in Figure 1.18. It is possible to see that the signals related to both compounds are easily differentiated in the chromatogram.
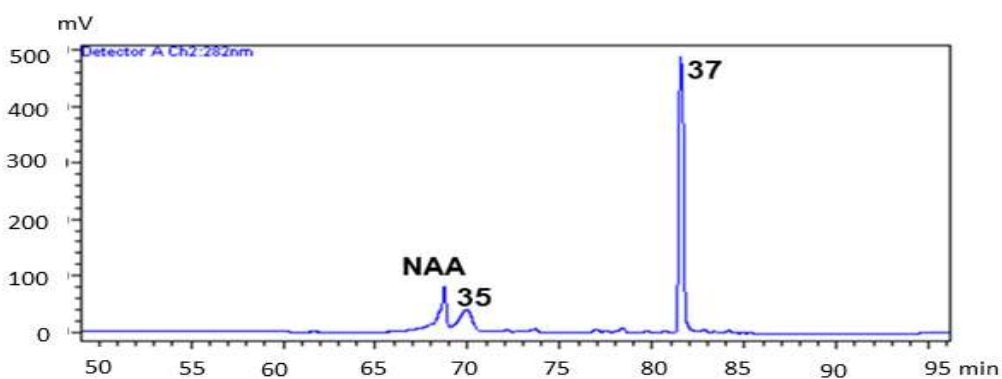
Figure 1. 18. HPLC Chromatogram of the compounds **35** (t_r=70 min), **37** (t_r= 82 min) and NAA (t_r= 71.5 min). The separations were made with a Phenomenex C18 column (2.6 μm size particles, length 100 mm, i.d. 3 mm), using a mixture of water/acetonitrile 95:5 as eluent

After establishing the best conditions for the separation of the analytes, optimizing the extraction methodology of compounds **37** in sand became the focus. First, a calibration curve of the compound was obtained. For its standard, solutions of compound **37** were injected in increasing concentration (from 0.10 to 0.75 mmol/L). The calibration curve is shown on Figure 1.19, which shows that the R^2 value for the curve is 0.9991. This value is an evidence of an ideal data fit for the regression line (Assis *et al.*, 2011).

$$y = 835679x - 1474.6$$
$$R^2 = 0.9991$$
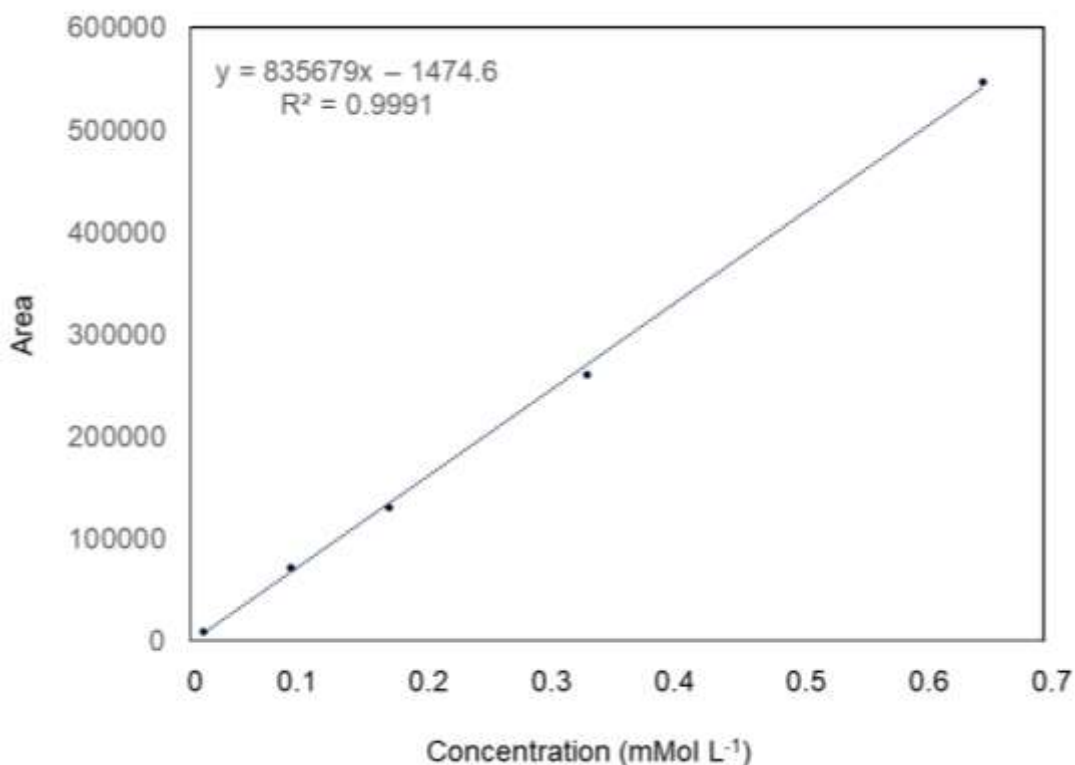
Figure1.19. Standard curve of tetraoxane **37**. The curve was obtained by injecting solution at concentrations from 0.65 to 0.01 mmol/L, considering the effect of the matrix caused by the surfactant Tween 80.

Then, a test to evaluate the extraction conditions for the experiment was executed. For that, it was mixed 1 mL of solution of tetraoxane 34 at 2 mmol/L with 1g of sand. After that, the sample was centrifuged and the full volume of the liquid phase was taken. A second extraction of the organic material present in the sand was carried out. Next, the liquid phases were filtered over a SPE cartridge. All fractions were combined and an aliquot of this resulting dilution was used for HPLC analysis (For detail of the methodology see section 1.5.5.4). An aliquot of the resulting solution was injected with the conditions

previously optimized. The experiment was carried out in triplicate. The result of the experiment showed that the extraction methodology was reliable as the analyte was recovered in 90% ± 0.08. After the parameters of separation and extraction methodologies optimized, the experiment was executed.

*1.3.3.2. Study of tetraoxane **37** degradation in sand*

The experiment was conducted for 22 days, under similar conditions employed in the greenhouse bioassay. The quantification of **37** was performed by HPLC, using the analytical conditions previously established and described.

As observed from Figure 1.20, during the first day of experiment, the concentration of **37** decreased by approximately 20%. Between days 3 and 14, the concentration of **37** remained constant at approximately 58 %. After 14 days of experiment, the concentration of compound **37** decreased sharply, resulting in its total degradation after 22 days.

Figure 1. 20. Percentage of tetraoxane **37** in contact with sand, at room temperature, during 22 days (see Appendix Table 2.1A).

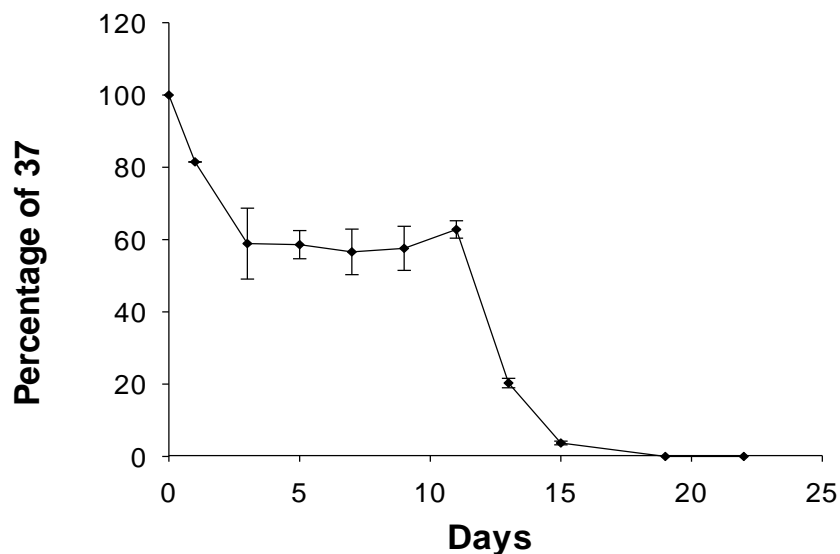As already explained, one of the objectives of this study was to investigate if **37** could be hydrolyzed into aldehyde **35**, that, subsequently, would be naturally oxidized into NAA. There different explanation about how this transformation might happen. The first proposal is that such transformation could occur via the aldehyde **35** that would be naturally oxidized. The other possibility would be a direct transformation of tetraoxane **37** into NAA via radical mechanisms.

Although the chromatogram did not show any trace of **35** during the 22 days of experiment, an amount of NAA was observed from days 13 to 15. This result confirms the initial hypothesis of the transformation of **37** into NAA. Since the substrate used in the experiment (sand) is inert, the detection of NAA suggest that **37** might be hydrolyzed into aldehyde **35**, which is rapidly could be oxidized as proposed in Scheme 1.7.

The other possibility, is the direct transformation of **37** into **35** *via* radical mechanism. Previous studies about the thermal degradation of tetraoxanes revealed that this type of scaffold can produce a biradical intermediate (Cafferata *et al.*, 1983). The formation of this specie is related with the lability of the O-O bond, the ΔH of the homolytic cleavage of O-O bond at 150 °C isabout 35.7 Kcal mol^{-1}(Fernandez and Robert, 2011). However, more detailed experiments need to be done in order to determinate if in fact, which pathway enables the transformation of tetraoxane **37** into NAA.

Once tetraoxane **37** is degraded, but the expected product NAA is not accumulated during the 22 days of experiment, it was concluded that NAA is degraded faster under the experimental conditions. Since sand is inert, the degradation must be caused by some photo-induced process, in agreement with the literature that revealed the photolysis of NAA resulting in four products (Bradbury *et al.*, 2007; EFSA, 2011). Concerning the degradation of NAA when applied in soil, the studies are very restricted. For instance, it has been shown that NAA is converted, under aerobic conditions, by microorganisms into catechol and naphthol in less than 72 hours (Proctor, 1963).

1.4 CONCLUSION

In summary, it was developed a synthetic procedure to convert commercial NAA into a new tetraoxane **37** (23% overall yield). In a pre-emergency bioassay, the new tetraoxane is effective in inhibiting the growth of several important weeds. The compound caused effects that suggest that it may act *via* auxinic path and also as a photosystem inhibitor. Moreover, some synthetic precursors of **37** also have high phytotoxic activity, suggesting that, if it is degraded, it could provide other non-toxic substances that may act as herbicides.

1.5. MATERIALS AND METHODS

1.5.1. Chemicals, instruments and experimental procedures

All reagents and solvents used for the experiments were purchased from commercial sources (Sigma-Aldrich, Milwaukee, Wisconsin, USA). The ^{1}H and ^{13}C NMR spectra were recorded on a *Bruker NMR* spectrometer (400 MHz and 100 MHz, respectively). All samples were dissolved in deuterated chloroform, using *tetramethylsilane (TMS)* as internal standard *(δ= 0).* The IR spectra were obtained using an Aminco Bowmen Adrid Zone infrared spectrometer (Thermofischer, Waltham, MA, USA). High-resolution mass spectra were obtained in a LC/MS–TOF (Agilent 6210, Santa Clara, CA, USA), using electrospray ionization (ESI). Melting points are uncorrected and were measured in a digital melting point apparatus (MQAPF-302, Microquímica Equipamentos, Rio de Janeiro, Brazil). Analytical thin layer chromatography analyses were made using aluminum packed pre-coated silica gel plates Polygram-UV254. All compounds purifications were carried out by column chromatography, using silica gel (70-230 mesh) as stationary phase.

1.5.2.1 Synthesis of 1,1-dihydroperoxyciclohexane (**36**)
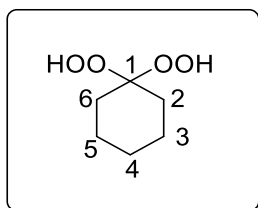
Cyclohexanone (0.5 g, 5.1 mmol) and acetonitrile (8 mL) were placed in a round bottom flask. Then, an aqueous solution of hydrogen peroxide (56% v/v, 2.9 g, 51 mmol) was incorporated and the catalyst tin chloride (0.05 g, 20 mol%) was slowly added to the mixture. The reaction remained under magnetic stirring at room temperature for 1.5 h. Next, the reaction was quenched by the addition of 25 mL of saturated solution of sodium bicarbonate ($NaHCO_3$) and extracted with dichloromethane (3 x 25 mL). The organic layers were combined and dried over anhydrous $MgSO_4$. After filtration, the solvent was removed under reduced pressure at 40 °C. The compound was obtained as a white solid that was crystallized with hexane (600 mg, 4.3 mmol, 85%). (Terentév et al. 2008) M.p.: 40-42°C. IR (KBr, cm^{-1}): 3422, 2940, 2862, 2676, 1710, 1449, 1353, 1051. ^{1}H-NMR (400 MHz, CDCl$_3$) δ: 1.40-1.80 (m, 10H, H-2, H-3, H-4, H-5, H-6), 9.5 (s, 2H, OH).^{13}C-RMN (1000 MHz, CDCl$_3$) δ: 22.6 (C-3, C-5); 25.5 (C-4); 29.9 (C-2, C-6), 111.3 (C-1).

1.5.2.2 Synthesis of 2-(naphthalen-1-yl) ethan-1-ol.
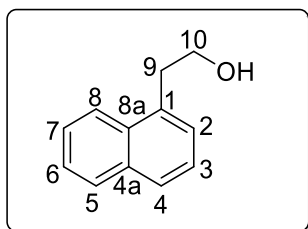
Compound **34** (1.0 g, 5.3 mmol), lithium aluminum hydride (0.4 g, 10.7 mmol) and dry THF (10 mL) were allocated in a round bottom flask - conserved at 0 °C. The cold bath

was removed and the system was kept stirring under argon atmosphere and room temperature for 12 h. Afterward, the mixture was diluted with diethyl ether (40 mL) and cooled at 0 °C. Subsequently, 1.8 mL of water were slowly added, followed by 1.8 mL of aqueous solution of NaOH (15% v/v). The ice bath was removed and the mixture was maintained under magnetic stirring until it reached room temperature. In the last place, the mixture was dried and filtered over anhydrous $MgSO_4$ and concentrated under reduced pressure to afford the required product as yellow oil (900 mg, 5.5 mmol, 95%) that was used without further purification. (Toyao et al. 2017): IR (KBr, cm^{-1}): 3369, 3049, 2947, 2878, 1596, 1510. ^{1}H-NMR (400 MHz, CDCl$_3$) δ: 1.92 (s, 1H); 3.35 (t, 2H, $J_{9,10}$ = 6.7 Hz, H-9); 3.98 (t, 2H, $J_{10,9}$ = 6.7 Hz, H-10); 7.39-7.46 (m, 2H, H-2, H-3); 7.49-7.57 (m, 2H, H-6, H-7); 7.65 (bd, 1H, J = 8.0 Hz, H-4); 7.77 (m, 1H, H-5); 8.06 (bd, 1H, J = 8.0 Hz, H-8).^{13}C-NMR (100 MHz, CDCl$_3$) δ: 36.4 (C-9); 63.3 (C-10); 123.9 (C-8); 125.7 (C-6); 125.9 (C-3); 126.3 (C-7); 127.4 (C-2); 127.5 (C-5); 129.1 (C-4); 132.3 (C-1); 134.2 (C-8a); 134.5 (C-4a).

*1.5.2.3. Synthesis of 2-(naphthalen-1-yl)acetaldehyde (**35**).*
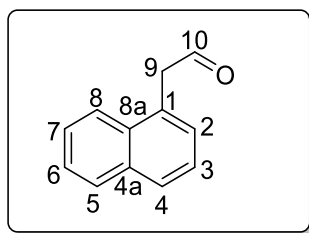
*Synthesis of 2-(naphthalen-1-yl)acetaldehyde (**35**) using the Dess-Martin methodology.* To a round bottom flask were added 2-(naphthalen-1-yl)ethan-1-ol (0.1 g, 0.9 mmol) and dichloromethane (5 mL). The mixture was cooled at 0 °C and stirred for 5 min. Then the Dess-Martin periodinane (0.57 g, 1.4 mmol) was added and the temperature was raised to 25 °C. The mixture was stirred during 1.5 h and then diluted with dichloromethane (10 mL). This reaction mixture was quenched with a saturated solution of NaHCO$_3$ (10 mL). The aqueous solution was extracted with dichloromethane (3 x 10 mL), and then the organic layers were collected and filtered over anhydrous Na$_2$SO$_4$. The solvent was removed by distillation under reduced pressure. Purification of the product was carried out

by filtering the mixture over a plug of neutralized silica gel (previously treated with a 10% aqueous solution of NH_4OH). The product was obtained as a yellow oil (131 mg, 0.77 mmol, 86%).

Synthesis of **35** *using BAIB and TEMPO.* It was set in a 50 mL round bottom flask: 2- (naphthalen-1-yl) ethan-1-ol (0.5 g, 2.9 mmol), bis-acetoxyiodobenzene (BAIB) (1.3 g, 3.9 mmol) and *(2,2,6,6-tetramethylpiperidin-1-yl)oxyl* (TEMPO) (4.5 mg, 0,29 mmol) in dichloromethane (10 mL). The reaction mixture was kept under stirring for 12 h, and then diluted with dichloromethane (10 mL), and quenched by addition of a saturated solution of Na_2SO_3 (10 mL). The organic layer was separated and washed with a saturated solution of $NaHCO_3$, then dried over anhydrous Na_2SO_4. The solvent was removed by distillation under reduced pressure. Purification was conducted by distillation (160ºC, 1 atm), affording the required product as yellow oil (310 mg, 1.82 mmol, 63%).

Data for 2-(naphthalen-1-yl)acetaldehyde (**35**). (Li *et al.* 2013): IR (ATR, cm^{-1}): 3361, 3055, 2947, 2873, 1610, 1515. ^{1}H-NMR (400 MHz, CDCl$_3$) δ: 3.87 (d, 2H, $J_{9,10}$ = 2.4 Hz, H-9); 7.29-7.44 (m, 4H, H-2, H-3, H-6, H-7); 7.71-7.78 (m, 3H, H-4, H-5, H-8); 9.65 (t, 1H, $J_{10,9}$= 2.4 Hz, H-10). ^{13}C-NMR (100 MHz, CDCl$_3$) δ: 48.5 (C-9); 123.7(C-8); 125.8 (C-6); 126.3 (C-3); 126.9 (C-7); 128.6 (C-2, C-5); 129.1 (C-4); 132.1 (C-1); 132.5 (C-8a); 134.1 (C-4a); 199.9 (C-10).

1.5.2.4 Synthesis of 3-(naphthalen-1-ylmethyl)-1,2,4,5-tetraoxaspiro[5.5]undecane (**37**)
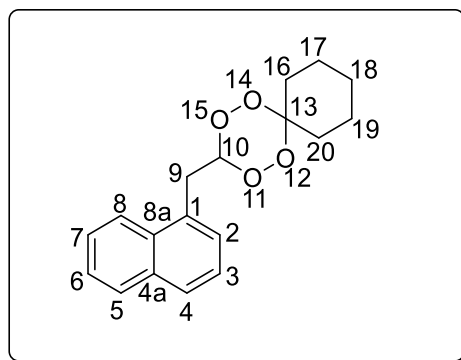
Compounds **35** (0.3 g, 1.8 mmol), **36** (0.4 g, 2.7 mmol) and 10 mL of dichloromethane were deposited in a 50 mL round bottom flask. The mixture was cooled to -78 °C and stirred for 30 min. Then, a solution of H_2SO_4-Acetonitrle 9:1 (6.5 mL, 13.3 mmol) was included drop by drop. The reaction was kept under magnetic stirring for 2 hours at -78 °C, before being quenched by the addition of a saturated solution of $NaHCO_3$ (15 mL). The aqueous phase was extracted with dichloromethane (3 x 10 mL). After that, the organic phases were combined, dried over anhydrous $MgSO_4$ and concentrated under reduced pressure to provide the crude product as a white solid. Further fractionation of such crude mixture by silica gel column chromatography, eluting with a mixture of hexane: chloroform (7:3 v/v), resulted in the required compound **5** as a white solid (124.3 mg, 0.41 mmol, 23%) and the tetraoxane **3** also as a white solid (123.4 mg, 0.54 mmol, 20%).

*Data for (**37**):* White solid. M.p.*:* 162.0-163.1°C. IR (ATR, cm^{-1}): 3048, 2926, 2856, 1510, 1445. ^{1}H-NMR (400 MHz, $CDCl_3$) *δ:* 1.28-1.66 (m, 8H, H-16, H-17, H-18, H-19); 2.37 (t, 2H, $J_{20\text{-}19}$= 5.2 Hz, H-20); 3.33 (d, 2H, $J_{10,9}$ = 4.7 Hz, H-9); 6.14 (t, 1H, $J_{9.10}$ = 4.7 Hz; H-10); 7.26-8.01 (m, 7H, H-2, H-3, H-4, H-5, H-6, H-7, H-8). ^{13}C-NMR (100 MHz, $CDCl_3$) *δ*: 22.0 (C-18)*; 22.4 (C-19)*; 25.6 (C-17)*; 30.2 (C-16); 32.1 (C-20); 33.9 (C-9); 108.4 (C-10); 109.1 (C-13), 123.6 (C-8); 125.6 (C-6); 126.0 (C-3); 126.7 (C-7); 128.3 (C-2, C-5); 129.1 (C-4); 129.9 (C-1); 132.2 (C-8a); 134.1 (C-4a). HRMS (ESI-TOF) *m/z* [M+H] $^+$: Calculated for $C_{18}H_{21}O_4^+$: 301.1434; found: 301.1407. * Signal can be exchanged.
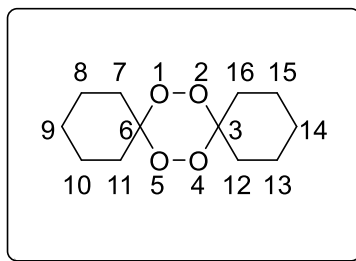
*Data for (**2**):* White solid. M.p.: 129.2-130.2 °C. Lit. (Cusati *et al.* 2015): 129.2-130.1°C. ^{1}H (400 MHz, $CDCl_3$) *δ*: 1.40-2.80 (m, 18H, H-7b, H-8, H-9, H-10, H-11b, H-12b, H-13, H-14, H-15, H-16b) 2.10- 2.50 (m, 4H, H-7a, H-11a, H-12a, H-16a). ^{13}C (100

MHz, CDCl$_3$) δ: 22.3 (C-9, C-14), 25.6 (C-8, C-10, C-13, C-15), 30.9 (C-11, C-16), 31.8 (C-7, C-12), 108.4 (C-3, C-6).

1.5.3. Calculation of conformation stability of isomers of tetraoxane (**37**)

In the first step of the theoretical calculation, a conformational search using the Spartan 14 program (wavefunction Inc) was performed for the structure of **37.** For this, level B3LYP / 6-31G (d, p) was used, specifying the maximum number of examined conformers equal to 1000. Secondly, the resulting conformers were subjected to calculation of shield tensor at level B3LYP / 6-31G (d, p) using Spartan 14 (wavefunction Inc). The resulting set of tensor values, weighted by Boltzmann distribution, were converted into chemical shift by subtracting the tetramethylsilane (TMS) computer shielded tensors.

1.5.4. Greenhouse herbicide Assay

Greenhouse bioassays of compounds **35**, **36** and **37** were carried out at the Departamento de Ciencias Agricola of the Universidade Federal de Viçosa, under the supervision of Professor Antonio Alberto Silva and the support of Dr. Gustavo Mendes Pereira.

The stock solutions of the compound to be tested and the references (1 mmol/L) were prepared by dissolving the samples in a mixture of penta-3-one (50 μL), the surfactant Tween 80® (100 μL) and distilled water (50 mL). That suspension was shaken for 1 min, then transferred to a 250 mL volumetric flask, whose volume was completed with distilled water. The mixture was diluted in water to the final concentration of 0.125 mmol/L. Assays were conducted using *Cucumis sativa*, *Sorghum bicolo*r, *Iponomea acuminate*, *Bidens pilosa*, *Solanum americanum* and *Alternanthera ficoidea* as target species. Plastics pots (0.25 mL) were filled with washed sand (140 g), then approximately 5 seeds of each specie were put and covered with more sand. Next, 5 mL solution of each active ingredient (a.i.) solution was added. The experiment was carried out in triplicate, under greenhouse conditions. Each pot was irrigated three times per day. Micro and macronutrients were provided by adding Hoagland solution every 5 days (Hoagland &

Arnon, 1950). After 22 days, plants were finally harvested. The roots and shoots were separated and dried at 70 °C until constant weight. So, both roots and shoots dry weight was obtained using an analytical scale. The percentage of growth inhibition was calculated with respect to the mass of the control. To every control, 5 mL of a solution of penta-3-one (1 μL/mL) and surfactant Tween 80® (2 μL/L) were added. The data were analyzed using the Sigma Plot 12.5 software.

1.5.5. Degradation experiment of tetraoxane 37

1.5.5.1. Chemicals, Instruments and experimental procedures

Compounds **35** and **37** were prepared as previously described while NAA was purchased from Sigma-Aldrich (Milwaukee, Wisconsin, USA). In regard with its store conditions compound **35** and **37** were kept at 0 °C whereas NAA was stored at room temperature. HPLC solvents acetonitrile and methanol and trifluoracetic acid were procured from Sigma-Aldrich (Milwaukee, Wisconsin, USA). Purified water was generated by a Millipore Direct-Q ultrapure water system.

1.5.5.2. Equipment

All the HPLC analyses were performed in a Shimadzu LC-20A series equipment. The HPLC system was equipped with Shimadzu UV diode array detector (SPD-20A), a vacuum degasser, a binary pump (LC-20AT) and an autoinjector (SIL-10AF). The separations were carried out using a Phenomenex C18 column (2.6 μm size particles, length 100 mm, i.d. 3 mm). All data were processed with the LC solution software 1.23 SPI.

1.5.5.3. Standard solutions

Stock solutions of compounds **35**, **37** and NAA (2 mmol/L concentration) were prepared by dissolving 5-10 mg of each compound in 10 mL of water, and 30 μL of Tween 80. Once the solutions were prepared, they were kept in an ultrasound baths from 3 to 5

minutes. Furthermore, standard solutions of compound **37** were prepared for calibration curves in 6 concentrations (0.0625, 0.125, 0.250, 0.500, 1.00, 2.000 mmol/L).

1.5.5.4. Experiment conditions and extraction methodology

In a falcon tube with 50 mL od capacity were added 1g of sand and 1 mL of the compound standard solution (2 mmol/L). The resulting mixture of **37** was homogenized for 2-3 min. A total of 33 tubes were prepared and stored at room temperature and with light exposition. The experiment was maintained during 22 days, and the samples for analysis were taken every 2 days.

To extract the compounds, the full volume of the aqueous phase was taken from the falcon tube, centrifuged and collected. Then, 1 mL of acetonitrile was added to the remained sand. This new mixture was kept in an ultrasound bath for 1 minute. After that, the sample was centrifuged and the full volume of the liquid phase was taken. This solution was combined with the water phase previously collected. The new mixture was filtered over a SPE cartridge, then 3 mL of acetonitrile were eluted through the cartridge. All fractions were combined and an aliquot of this resulting dilution was used for HPLC analysis. The samples were injected using a mixture of acetonitrile/water 95:5 as eluent. Compound **37** was detected at 81 min while NAA was detected at 70.1 min.

1.6.   REFERENCES

Amewu, R., Stachulski A.V., Ward, S., Berry, N.G., Bray, P.G., Davies, J., Labat, G., Vivas, L., M. O'Neill, P., 2006. Design and synthesis of orally active dispiro 1,2,4,5-tetraoxanes; synthetic antimalarials with superior activity to artemisinin. Org. Biomol. Chem. 4, 4431–4436.

Arimoto, H., Ohba, S., Nishiyama, S., Yamamura, S., 1994. Chemical properties of β-triketones: Re-examination of Albizati's tandem aldol process. Tetrahedron Lett. 26, 4581-4584.

Assis, E. C., Silva, A. A., Barbosa, L. C., Queiroz, M. E. L. R., D´Antonino, L., Goncalves, V. A., 2011. Optimization and validation of the solid-liquid extraction technique for

determination of Picloram in soils by high performance liquid chromatography. Planta Daninha 29, 683-696.

Baldaia, A., 2015. Conversão catalítica de cetonas em 1,1-diidroperóxidos e tentativas de obtenção de 1,2,4,5-tetraoxanos potencialmente herbicidas. Dissertação de Mestrado, Universidade Federal de Minas Gerais.

Barbosa, L. C. A., 2013 Espectroscopia no infravermelho na caracterização de compostos orgânicos. Primeira ed. Editora UFV, Brasil.

Bharati, A., Kar, M., Sabat, S., 2012. Artemisinin inhibits chloroplast electron transport activity: Mode of action. Plos One. 7,1-10.

Bradbury, S., Daiss, B., Otakie, G., Khasawinah, A., Melendez, J., Young, D., Vaughn, A., Heflin, J., Zinn, N., Bazuin, J., Kish, T., Howard, M., Anderson, N., Dutch, V., 2007. Environmental US Agency Protection. Reregistration Eligibility Decision (RED) Naphthaleneacetic Acid its Salts, Ester and Acetamide.

Cafferata, L. F. R., Eyler, G. N., Mirifico, V., 1985. Kinetics and Mechanism of Acetone Cyclic Diperoxide (3,3,6,6-Tetramethyl-l,2,4,5-tetraoxane) Thermal Decomposition in Benzene Solution. J. Org. Chem. 49, 2107-2111.

Casida, J. E., 2017. Why Prodrugs and Propesticides Succeed. Chem. Res. Toxicol. 30, 1117−1126

Castro, M. A., 2014. Estudo comparativo de duas formas farmacêuticas de cloridrato de diltiazem. aplicação de método análitico desenvolvido e validado visando o controle de qualidade. Dissertação de Mestrado, Universidade Federal de Minas Gerais

Charman, S., Arbe-Barnes, S., Bathurst, I.C., Brun, R., Campbell, M., Charman, W.N., Chiu, F. C. K., Chollet, J.,Craft, J.C., Creek, D. J., Dong, Y., Matile, H., Maurer, M., Morizzi, J., Nguyen, T., Papastogiannidis, P., Scheurer, C., Shackleford, D. M., Sriraghavan, K., Stingelin, L., Tang, Y., Urwyler, H., Wang,X., White, K. L., Wittlin, S., Zhou, L., Vennerstrom, J. L., 2011. Synthetic ozonide drug candidate OZ439 offers new hope for a single-dose cure of uncomplicated malaria. Proc. Natl. Acad. Sci. U. S. A. 108, 4400–4405.

Constantino, M., Beltrame, M., Gil-Valdo, J., Zuckerman, J., 1996. A novel asymmetric total synthesis of (+)-Artemisinin. Synth. Commun. 26, 321-329.

Coob, A. H., Reade, J. P. H., 2010. Herbicides and plant physiology, second ed. Wiley-Blackwell, Oxford, UK.

Corey, E. J., Williams, J., 1975. Pyridinium Chlorochromate. An efficient reagent for oxidation of primary and secondary alcohols to carbonyl compounds. Tetrahedron Lett. 16, 2647.

Corral, M. G., Leroux, J., Stubbs, K. A., Mylne J.S., 2017, Herbicidal properties of antimalarial drugs. Scientific Report 7, 31-38.

Cremlyn, R. J., 1991. Agrochemicals: Preparation and mode of action. John Wiley, Surrey, UK.

Curran, W. S., 2014. Persistence of herbicides in soil. Crops & Soils 49, 16-21

Cusati, R., Barbosa, L. C. A., Maltha, C. R., Demuner, A. J., Oliveros-Bastidas, A., Silva, A. A., 2015. Tetraoxanes as a new class of efficient herbicides comparable with commercial products. Pest Manag. Sci. 71, 1037–1048.

Dayan, F., Hernández, A., Allen, S. N., Moares, R. M., Vroman, J., Avery, M. A., Duke, S. O., 1999. Comparative phytotoxicity of artemisinin and several sesquiterpene analogues. Phytochemistry, 50, 607-614.

De Mico, A., Margarita, R., Parlanti, L., Vescovi, A., Piancatelli, G., 1997. A versatile and highly celective hypervalent iodine (III)/2,2,6,6-tetramethyl-1-piperidinyloxyl-mediated oxidation of alcohols to carbonyl compounds. J. Org. Chem. 62, 6974–6977.

Dong, Y., 2002. Synthesis and Antimalarial Activity of 1, 2, 4, 5-Tetraoxanes. Mini Rev. Med. Chem. 2,113–123.

Dong, Y., Vennestrom, J.L., 2001. Differentiation between 1, 2, 4, 5-Tetraoxanes and 1, 2, 4, 5, 7, 8-Hexaoxonanes Using ^{1}H and ^{13}C NMR Analyses. J. Heterocyclic Chem. 38, 463-466.

Duke, S. O., 2013. The history and current status of glyphosate. Pest. Manag. Sci. 70. 1027-1034.

Duke, S. O., 2012. Why have no new herbicide modes of action appeared in recent years?. Pest. Manag. Sci. 68, 505–512.

Duke, S. O., Evidente, A., Vurro, M., 2019. Natural products in pest management: Innovative approaches for increasing their use. Pest. Manag. Sci. 75, 2299-2300.

European Food Safety Authority, 2011. Conclusion on the peer review of the pesticide risk assessment of the active substance 1-naphthylacetic acid. EFSA Journal. https://ec.europa.eu/food/plant/pesticides/eu-pesticidesdatabase/public/?event=activesubstance.detail&language=EN&selectedID=85. (accessed 11 December 2019)

Fernández, I., Robert, A., 2011. Peroxide bond strength of antimalarial drugs containing an endoperoxide cycle. Relation with biological activity. Org. Biomol. Chem., 2011, 9, 4098-4107.

Fuscaldo, F., Bedmar, F., Monterubbianes, G., 1999. Persistence of atrazine, metribuzin and simazine herbicides in two soils. Pesq. Agropec. Bras. 34, 2037-2044.

Forest, P., Norman, M., 1991. Inetractions of herbicides with photosynthetic electron transport. Weed Science. 39, 458-464.

Freitas, R., Berger, P. G., Ferreira, L. R., Silva, A. C., Cecon, P. R., Silva, M. P., 2009. Manejo de plantas daninhas na cultura do algodoneiro em sistema de plantio direto. Planta daninha. 24, 339-346.

Grossmann, K., 2000. Mode of action of auxin herbicides: A new ending to a long drawn out story. Trends. Plant. Sci. 5, 506–508.

Guan, A., Liu, C., Yang, X., Dekeyser, M., 2014. Application of the intermediate derivatization approach in agrochemical discovery. Chem. Rev. 114, 7079-7107.

Heap, I., 2019. Global Increase in Unique Resistance Cases. http://www.weedscience.com/Graphs/ChronologicalIncrease.aspx (accessed 11 December 2019

Hamann, H. J., Hecht, M., Bunge, A., Gogol, M., Liebscher, J., 2011. Synthesis and antimalarial activity of new 1,2,4,5-tetroxanes and novel alkoxy-substituted 1,2,4,5-tetroxanes derived from primary gem-dihydroperoxides. Tetrahedron Lett. 52, 107–111.

Hoagland, D.A. and D.I. Arnon. 1950. The Water Culture Method for Growing Plants Without Soil. Circular 347. California Agricultural Experimental Station, Berkeley, CA

Iskra, H., Bonnet-Delpon, D., Bégué, J. P., 2003. One-pot synthesis of non-symmetric tetraoxanes with the H_2O_2/ MTO/ fluorous alcohol system. Tetrahedron Lett. 44, 6309–6312.

Jugulam, M., Hall J. C., Johnson W.G., Kelley, B., Riechers, D. E., 2011. Evolution of Resistance to Auxinic Herbicides: Historical Perspectives, Mechanisms of Resistance, and Implications for Broadleaf Weed Management in Agronomic Crops. Weed Sci. 59, 445–457.

Jugulam, M., Shyam, C., 2019. Non-target-site resistance to herbicides: Recent developments. Plants 8, 417- 445.

Kah., M., Beukle, S., Brown, C. D., 2007. Factors that influencing degradation of pesticides in soil. J. Agric. Food Chem. 55, 4487-4492.

Kelley K., Riechers, D., 2007. Recent developments in auxin biology and new opportunities for auxinic herbicide research. Pestic. Biochem. Physiol. 89, 1–11.

Knudsmark, K., Jessing, K., Duke, S., Cedergreeen, N., 2014. Potential ecological roles of artemisinin produced by *Artemisia annua L.* J. Chem. Ecol. 40, 100–117.

Kumari. A, 2019. Current Scenario of artemisinins and its analogues for anitmalrial activity. European Journal of Medicinal Chemistry,163, 804-829.

Kraemer, A. F., Marchesan, E., Avila, L. A., Machado, S. L. O., Grohs, M., Massoni, P. F. S., Sartori, G. M. S., 2009, Persistência dos herbicidas imazethapyr e imazapic em solo de várzea sob diferentes sistemas de manejo. Planta Daninha, 27, 58.

Li, H., Misal Castro, L., Zheng, J., Roisnel, T., Dorcet, V., Sortais, J.B., Darcel, C., 2013. Selective Reduction of Esters to Aldehydes under the Catalysis of Well Defined NHC– Iron Complexes. Angew. Chem. Int. Ed. 52, 8045 –8049.

Liu, C. L., 2002. Proceedings of Research and Development of New Pesticides. Chemical Industry Press Publishers, Beijing, China.

McCullough K. J., Wood, J. K., Bhattacharjee, A. K., Dong, Y., Kyle, D. E., Milhous, W. K., Vennerstrom, J. L., 2000. Methyl-substituted dispiro-1,2,4,5-tetraoxanes: Correlations of structural studies with antimalarial activity. J. Med. Chem., 43, 1246–1249.

Meyer, V. M., 2010. Practical High-Performance Liquid Chromatography, 5th ed. Wiley and Sons, Sussex, UK.

Murray, R. W., Story, P.R., Kaplan, M. L., 1965. Nuclear magnetic resonance study of conformational isomerization in acetone diperoxide. J. Am. Chem. Soc. 88, 526-529.

Nutman, P. S., Thorton, H. G., 1945. Inhibition of plant growth by 2,4 Dichlorophenoxyacetic acid and other plant growth inhibitors. Nature. 155, 498-500.

O'Neill, P. M., 2004. Medicinal chemistry: a worthy adversary for malaria. Nature, 430, 838–839.

Opsenica, D. M., Terzić, N., Smith, P. L., Yang, Y., Anova, L., Smith, K. S., Šolaja, B. A., 2008. Mixed tetraoxanes containing the acetone subunit as antimalarials. Bioorg. Med. Chem. 16, 7039–7045.

Ohsugi, S., Nishide, K., Oono, K., Okuyama, K., Fudesaka, M., Kodamaa, S., Node, M., 2003. New odorless method for the Corey–Kim and Swern oxidations utilizing dodecyl methyl sulfide (Dod-S-Me) Tetrahedron 59, 8393-8398.

Pereira, M., Hernández, D., Giancotti, P., Alves, P., 2010. Efetito da densidade e do espaçamento de maria pretinha (*Solanum americanum Mill.*) sobre a cultura do tomate. Rev. Bras. Ciên. Agrár. Recife 5, 474-478.

Peterson, M., 2017. The challenge of herbicide resistance around the world: A current summary. Pest. Manag. Sci. 74, 2246-2259.

Proctor, M., 1963. Some steps in the degradation of naphtalene acetic acid. Plant and soil 3, 338-345.

Sant´ana, G. L., 2015. Sintomas de intoxicação de culturas por herbicidas. Dissertação de Mestrado, Universidade Federal de Viçosa.

Schreiber, F., Scherner, A., Andres, A., Concenço, G., Christofari, W. C., Martins, M., 2018. Experimental methods to evaluate herbicides behavior in soil. Rev. Bras. Herb. 17, 71-85.

Sheets, T. J., Shaw, W. C., 1963. Herbicidal properties and persistence in soil of s-triazines. Weed Science 11, 15-21.

Snyder, L. R.; Kirkland, J. J.; Glajch, J. L., 1997. Practical HPLC method development. 2th ed. John Wiley & Sons, New York.

Storniolo, F., Vargas, L., Pisa, D., Karam, D., 2017. Impacto econômico da resistência de plantas daninhas a herbicidas no Brasil" EMBRAPA Circular Tecnica 132.https://ainfo.cnptia.embrapa.br/digital/bitstream/item/162704/1/CT132-OL.pdf (accessed 11 December 2019).

Tarzona, J. V., Court-Marques, D., Titimani, M., Reich, H., Pfeil, R., Istace, F., Crivellente, F., 2017. Glyphosate toxicity and carcinogenicity: a review of the scientific basis of the European Union assessment and its differences with IARC. Arch Toxicol., 91, 2723-2744.

Tang, Y., Dong, Y., Vennerstrom, J. L., 2004. Synthetic peroxides as antimalarials. Beilstein J. Org. Chem. 24, 425–448.

Terent'ev, O., Platonov, M. M., Tursina, A. I., Chernyshev, V. V., Nikishin, G. I., 2008, Synthesis of Cyclic Peroxides Containing the Si-*gem*-bisperoxide Fragment. 1,2,4,5,7,8-Hexaoxa-3-silonanes as a New Class of Peroxides. J. Org. Chem., 73, 3169.

Terent'ev, A. O., Borisov, D., Vil, V., Dembitsky, V. M., 2014. Synthesis of five- and six-membered cyclic organic peroxides: Key transformations into peroxide ring-retaining products. Beilstein J. Org. Chem. 10, 34–114.

Terzić, N., Opsenica, D., Milić, D., Tinant, B., Smith, K. S., Milhous, W. K., Šolaja, B., 2007. Deoxycholic acid-derived tetraoxane antimalarials and antiproliferatives. J. Med. Chem. 50, 5118–5127.

Todorović, N. M., Stefanović, M., Tinant, B., Declercq, J. P., Makler, M. T., Šolaja, B.A., 1996. Steroidal geminal dihydroperoxides and 1,2,4,5-tetraoxanes: Structure determination and their antimalarial activity. Steroids. 61, 688–696.

Tomlin, C., 1994. The Pesticide Manual, 10th ed. RSC, Surrey, UK.

Toyao, T., Hakim Siddiki S. M. A., Touchy, A. S., Onodera, W., Kon, K., Morita, Y., Kamachi, T., Yoshizawa, K., Shimizu, K., 2017. TiO_2-Supported Re as a General and Chemoselective Heterogeneous Catalyst for Hydrogenation of Carboxylic Acids to Alcohols. Chem. Eur. J., 23, 1001**.**

Wauchope, R.D., Yeh, S., Linders, J.B., Kloskowski, R., Tanaka, K., Rubin, B., 2002.Pesticide soil sorption parameters: theory, measurement, uses, limitations and reliability. Pest. Manag. Sci. 58, 5, 419-445

Yan, Z., Wang, D., Ding, L., Cui, H., Jin, H., Yang, X., Yang, J., Qin, B., 2015. Mechanism of artemisinin phytotoxicity action: Induction of reactive oxygen species and cell death in lettuce seedlings. Plant Physiol. Biochem. 88, 53–5.

CHAPTER 2

TETRAOXANES AS NEW AGENTS AGAINST *Leishmania amazonensis*

2.1. INTRODUCTION

Leishmaniasis is a neglected disease transmitted by the bite of infected female sandflies (Okwor *et al.*, 2016). The disease is widespread in the tropical and subtropical areas of the world and 90% of new cases are concentrated in 13 countries: Afghanistan, Algeria, Bangladesh, Bolivia, Brazil, Colombia, Ethiopia, India, Iran, Peru, South Sudan, Sudan and Syria (Anversa *et al.*, 2016). According to the World Health Organization (WHO), about 700,000 to 1 million of new cases and 26,000 to 65,000 deaths occur annually around the planet (World Health Organization, 2017). Leishmaniasis mainly affects people who are living in the most impoverished parts of developing countries, because the poor house conditions, inadequate sanitation and irregular garbage collection provide sandflies breeding grounds (Okwor *et al.* 2016).

This disease is caused by different species of parasite *Leishmania*. The different types of microorganisms provoke two main clinical forms: cutaneous leishmaniasis (CL) and visceral leishmaniasis (VL) (Cotton, 2017; Sverding, 2017). CL happens when the parasites infect macrophages resident in the skin. If the disease spreads to the mucous membranes of the nose, mouth and throat, it is characterized as mucocutaneous leishmaniasis (MCL). VL occurs when parasites are spread by the blood circulation and infect cells of the mononuclear phagocyte system of the liver, spleen, bone marrow, lymph nodes and intestine. If not treated, it is fatal (Sverding, 2017).

1.1.1. *Leishmania amazonesis* L. S.

As previously outlined, there are differente species of *Leishmania* parasites. Among them, *L. amazonensis* is a dermotropic species, very common in Brazil, manly in the Amazon region (Ayres *et al.,* 2007). This species is associated with cutaneous leishmaniosis, and is able to cause chronic cutaneous lessons (Bittencourt *et al.*, 1989).

One of the main problems in the treatment of Leishmaniosis, is the absence of low toxic compounds able to combat this microorganism (Rocha *et al.*, 2015;). In addition, the outcome of CL is highly dependent of the of the host immune response to the parasite (Wanase *et al.*, 2008). These problems joined with the fact that leishmaniosis is disease that mainly affect the most vulnerable population in Brazil are the most concerning issues related with this disease.

2.1.2. Treatments for leishmaniosis

The main drugs in current use to treat leishmania are pentavalent antimonial drugs, amphotericin B, pentamidine, and multitone (Figure 2.1) (Cotton, 2017). Despite the effectiveness of those drugs to combat the parasite, they have severe side effects on the cardiac, kidney and liver systems, and also teratogenicity (Uline *et al.*, 2018). Besides that, other drawbacks include their high cost, long therapies and necessity of performing the treatment in a hospital environment (Simon *et al.*, 2006). In addition, the emergence of parasite resistance to drugs has limited the use of those medicines in many places (Simon *et al.*, 2016). Thus, the development of new drugs for the treatment of leishmaniasis is urgent. Such new compounds must have minimal side effects and desirably be administered orally and at low cost.
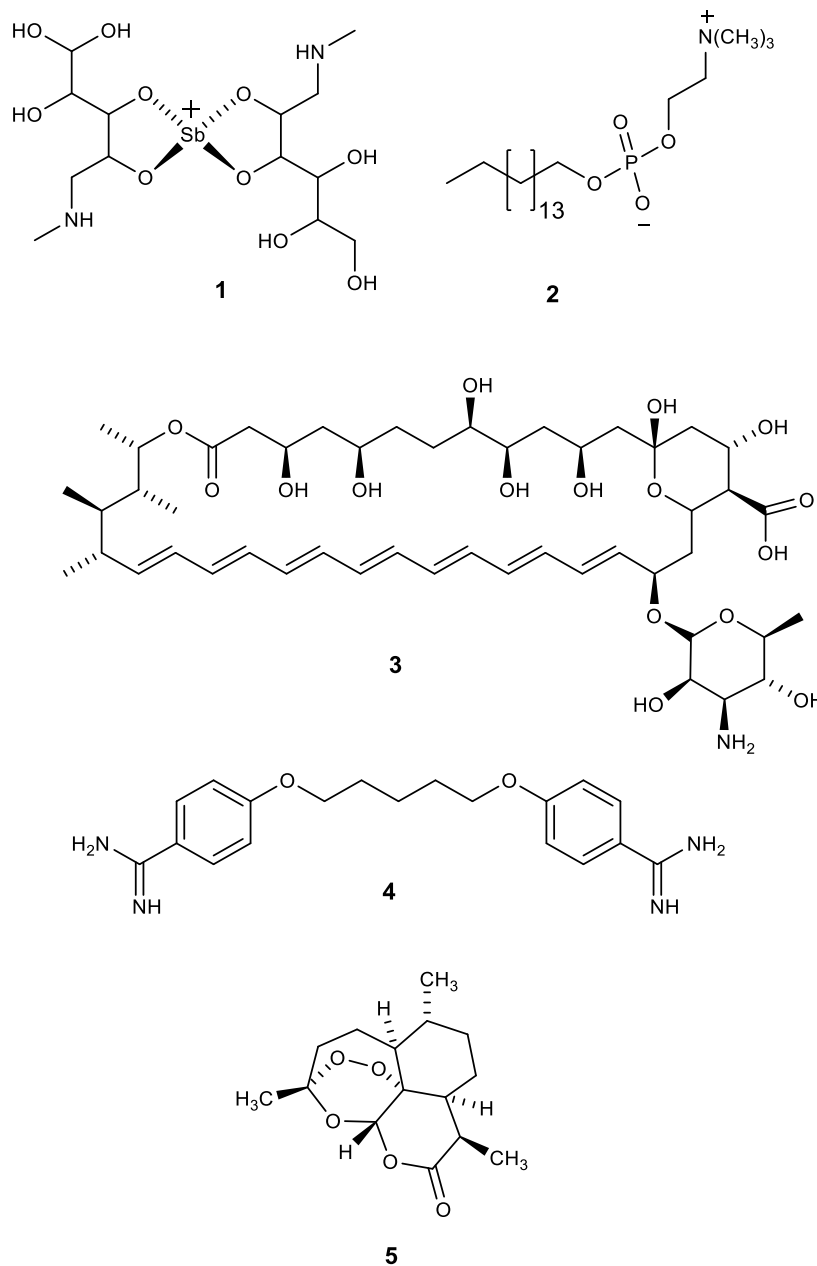
Figure 2.1. Structures of glucantime ® (**1**), miltefosine (**2**) amphotericin B (**3**), pentamidine (**4**) and artemisinin (**5**).

2.1.3.Peroxide compounds with antileismanial activity

As explained in Chapter 1, artemisinin is a natural product with several biological activities and all of them are related to the peroxide bonds present in its structure. In the specific case of malaria, its mechanism of action has been widely studied. It is believed that the toxic effect of artemisinin against *Plasmodium falciparum* (Welch, 1897) involves free radical intermediates, generated in a reaction activated by heme group (Pal and Purandare, 2001). In this sense, *Leishmania* parasite is also known for utilizing heme and free iron- (II) for its survival. Therefore, is possible that artemisinin has similar mode of action against leishmaniosis (Nitin and Kumar, 2009)

In 2003, Avery and co-workers detailed the activities of artemisinin derivatives against *Leishmania donovani* (Laveran & Mesnill, 1903) strain. Biological assays showed that these analogues were active at nM concentrations. In addition, studies about the structure-activity relationship of this compounds were carried out. The obtained results showed that bulky substituents at the. C-9β of the scaffold increased the biological activity of the derivatives. Even more relevant, the study highlighted the importance of peroxide function in the structure, since it is key to maintain the antileishmanial potential of the analogues. (Avery *et al.*, 2003). Considering this, it is expected that other peroxides compounds like 1,2,4,5-tetraoxanes also have toxic effects over the parasites that cause leishmania.
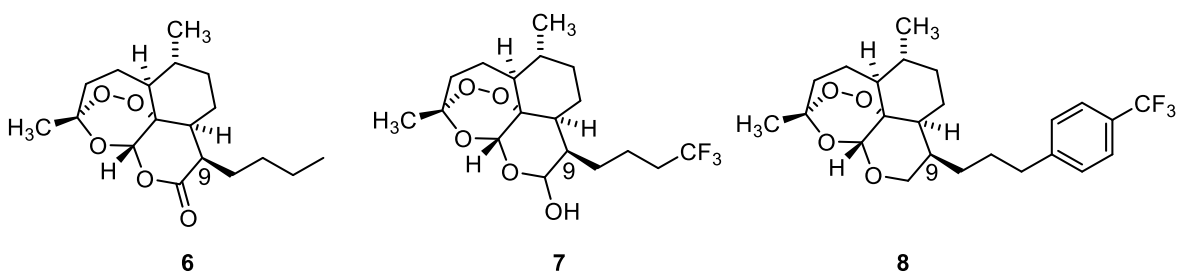
Figure 2. 2. Artemisinin derivatives with leishmanicide activity.

Recently, the anti-leishmanial activity from tetraoxanes against intramacrophage forms of *L. donovani* was communicated (Cabral *et al.*, 2020). In this study 15 tetraoxanes were evaluated in range of concentration from 2 to 45 µmol/L. Among them, compound **9**

and **10** turned to be the most active presenting an IC_{50} value of 7.75 µmol/L and 2.52 µmol/L respectively (Figure 2.3). In addition, *in vivo* tests of compound **10** revealed that it reduced the liver parasite burden in mice in 33%.
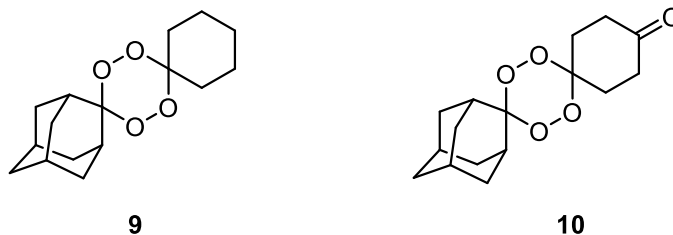

9 **10**

Figure 2. 3. Tetraoxanes with anti-leishmanial potential.

2.2. OBJECTIVE

From all that has been discussed, it is clear that there is a need to find new compounds with anti-leishmanial potential. In this sense, peroxide compounds have proven to be effective in previous studies. Hence, the objective of this work was to evaluate the antileishmanial activity of different tetraoxanes against *L. amazonesis*.

The synthesis of the tetraoxanes was carried out by using the optimized conditions developed in chapter 1. In addition, previous studies about the anti-leishmania activity of tetraoxanes were focus in their effect over the specie *L. donovani*. Considering that in Brazil the main parasite responsible of CL is *L. amazonesis*, the aim of this work was to evaluate the antileishmanial activity of 1,2,4,5-tetraoxanes against this specie. In addition, the cytotoxicity of all tetraoxanes was also a focus of this study as the high toxicity of compounds with anti-leishmanial activity against human is a constant concern.

2.3. RESULTS AND DISCUSSION

2.3.1. Synthesis of 1,2,5,4-tetraoxanes

In order to determinate the scope of the methodology described in chapter 1, the synthesis of tetraoxanes was executed using the same reaction conditions. For this step of the research, the required compounds were obtained from cyclic ketones and also aromatic aldehydes. These compounds were previously synthesized and its antimalarial and herbicide activity are reported in literature (Cusati *et al.*, 2015; Atheaya *et al.*, 2008; Zmitek *et al.*, 2006; Iskra *et al.*, 2003). The dihydroperoxide precursors **11a-d** were obtained from cyclic ketones, using an aqueous solution of H_2O_2 (56% v/v), $SnCl_2$ as catalyst and THF as solvent (Baldaia, 2015). The compounds were isolated in good yields (77-90%) (Scheme 2.1).
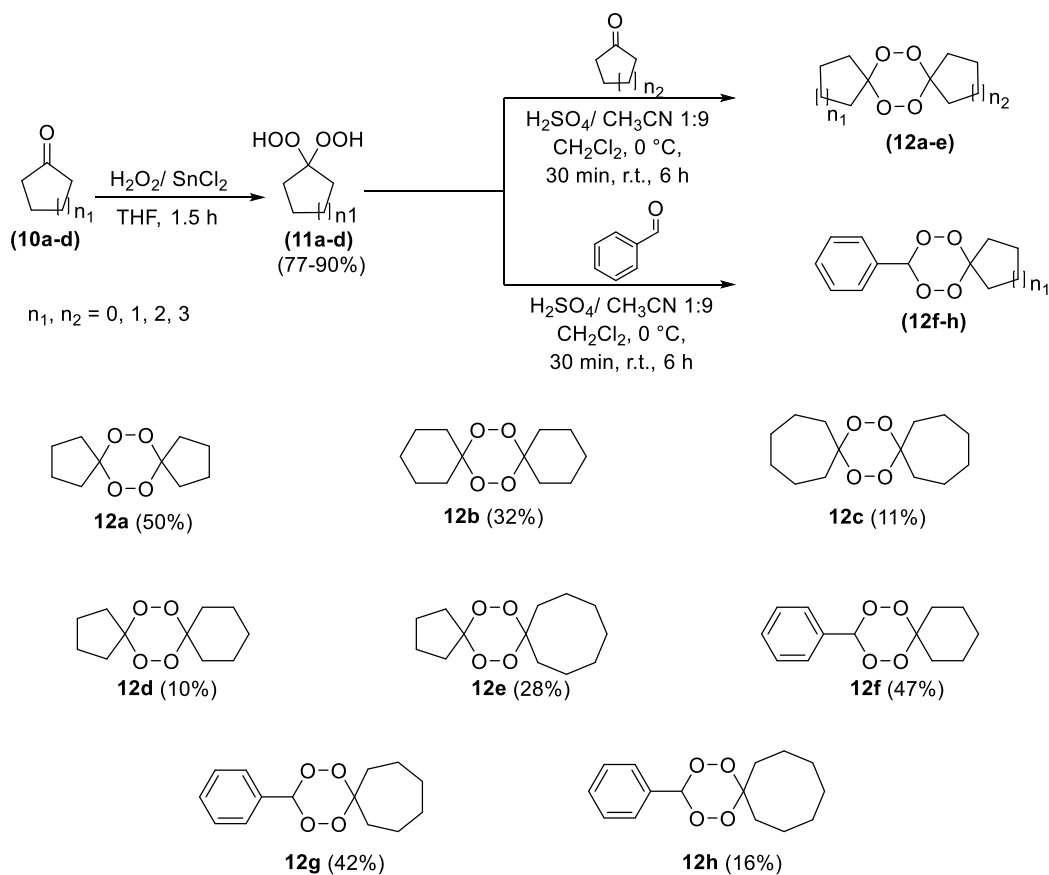
Scheme 2.1. Synthesis of 1,1-dihydroperoxicycloalkanes derived from ketones and their conversion into symmetric and asymmetric tetraoxanes.

With a reliable source of **11a-d**, these compounds were reacted with cyclic ketones and benzaldehyde, under catalysis of H_2SO_4 (50 mol%), affording the tetraoxanes **12a-h** in the range of 10 to 50% yields. In general, the yields were higher than those previously presented for the same compounds (Cusati *et al.*, 2015). It was also found that, in the case of asymmetric tetraoxanes **12d-f**, lowering the temperature to -78 ℃ resulted in better yields.

The tetraoxanes **12i** and **12j** were obtained from benzaldehyde and 4-ethylbenzaldehyde, respectively. In opposition to the good yields obtained from cyclic ketones, the use of benzyl aldehydes as substrates delivered the target peroxide in lower yields (Scheme 2.2). In those cases, the formation of the carboxylic form of both aldehydes was observed from the crude mixture (Valero-Antolínez, 2015). Such side product could be formed via direct oxidation of the aldehyde, by a Baeyer-Villiger oxidation (Baeyer & Villiger,1996). Other plausible path involves a Kornblum-DeLaMare rearrangement of the 1,1-dihydroperoxide, resulting in the perbenzoic acid, which reacts more with another benzaldehyde (Kornblum and De La Mare, 1951).
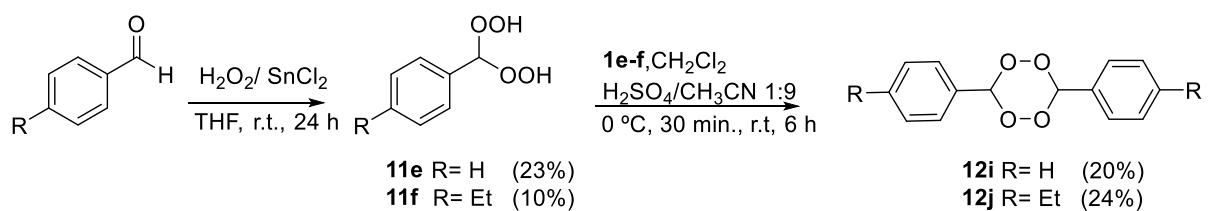
Scheme 2.2. Synthesis of dihydroperoxides derived from aldehydes and their conversion into corresponding symmetric tetraoxanes.

Another plausible path involves a Kornblum-DeLaMare rearrangement of the 1,1-dihydroperoxide (**11e**), resulting in the perbenzoic acid (**13**), which reacts more with another benzaldehyde (Kornblum and De La Mare, 1951). In this case, intermediate **13** reacts with a molecule of the protonated aldehyde (**14**) delivering peroxy acid **15**, then this molecule collapses to deliver the corresponding benzoic acid (**16**) (Scheme 2.3).
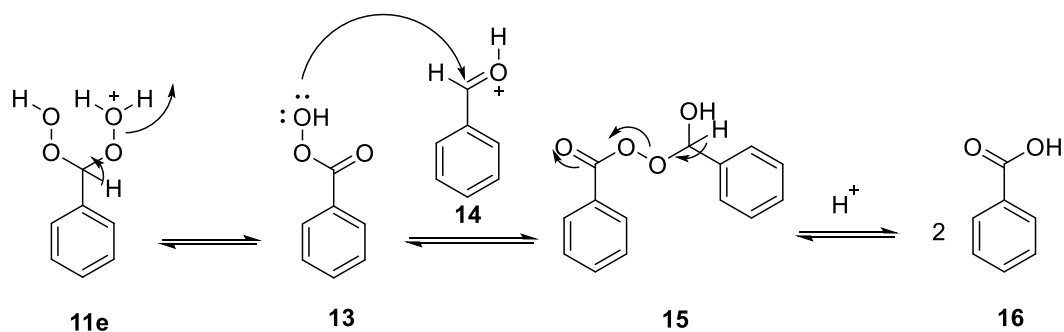
Scheme 2. 3. Mechanistic proposal for the formation of benzoic acid via Kornblum-DeLaMare rearrangement.

Finally, with compound **11e** and **11f** in hands, the synthesis of target products **12i** and **12j** was implemented. The required tetraoxanes **12i** and **12j** were obtained in 20% and 24%, respectively, which correspond approximately to the same result previously described (Cusati *et al.*, 2015).

2.3.2. Biological Activity

The leishmanicidal activities of compounds **12a-j** were evaluated by *in vitro* ELISA assay employing intracellular amastigotes of *L. amazonensis* parasite of canine macrophages DH82. In a preliminary experiment, the percentage of parasite growth inhibition was determined for each compound at 1000 µmol/L, in order to select those with some potential activity for further evaluation. As observed at the data on Table 2.1, from the ten compounds evaluated, six (**12b**, **12c**, **12d**, **12g**, **12h** and **12j**) caused parasitemia reduction greater than 50%.

Table 2.1. Percentages of *Leishmania amozonensis* parasitemia reduction at 1000 µmol/L.

Compound	% Inhibition
12a	49
12b	50
12c	52
12d	55
12e	17
12f	39
12g	58
12h	55
12i	25
12j	58

At this stage, it was not attempted to correlate the structure with activity. Anyhow, it is possible to notice that, for the most active compounds, the percentage of *L. amazonensis* reduction varied from 50% to 58%, which is a very narrow interval. From those initial results, the six most active compounds were subjected to the same assay at concentrations varying from 0.1 to 1000 µmol/L. The objective was to prepare a dose-response curves log (substance concentration) versus percentage inhibition of intracellular amastigote forms of *L. amazonensis* - as illustrated for compound **12g** (Figure 2.4) - and to calculate the IC_{50} values - as displayed in Table 2.2.
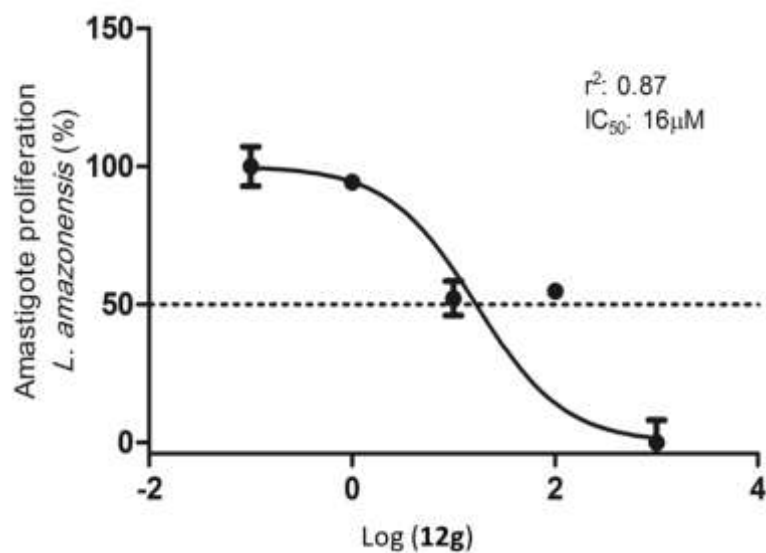
Figure 2.4. Inhibition of intracellular amastigote forms of *Leishmania amazonensis* caused by **12g**. The dose-response curve log (concentration of **12g**) versus inhibition of *Leishmania amazonensis* was performed in four replicates and the results are represented by the mean $\pm$ SD.

Despite potassium antimonyl tartrate pentahydrate (glucantime ®) being the first-line drug in the treatment of leishmaniasis, potassium antimonyl tartrate trihydrate was used as positive control of the test. It is suggested that pentavalent antimony may be a pro-drug, which undergoes a bio-reduction of Sb^{5+} to its trivalent form, and that Sb^{3+} is responsible for the toxicity and therapeutic activity of the drug (Rath *et al.*, 2005).

Table 2. 2. Antileishmanial activity of some tetraoxanes against the intracellular amastigotes of *Leishmania amazonensis* parasite of canine macrophages DH82.

Compound	$IC_{50} \pm SD$ (µmol/L) [a]	$CC_{50} \pm SD$ (µmol/L) [b]	SI [c]
		Toxicity DH82	
	Amastigotes		Intracellular
		Canine macrophages	amastigotes forms
12b	0.64 ± 0.14	221.00 ± 0.17	345.3
12c	19.70 ± 0.19	>1000	>50.8
12d	99.50 ± 0.10	$268.00 \pm. 0.17$	2.7
12g	16.00 ± 0.17	150.00 ± 0.09	9.4
12h	22.60 ± 0.13	141.00 ± 0.11	6.2
12j	18.00 ± 0.13	175.00 ± 0.15	10.0
Control [d]	80.00 ± 1.15	3.20 ± 0.11	0.04

[a] IC_{50} – concentration of active ingredient able to inhibit by 50% the in vitro growth of *L. amazonensis*; SD – standard deviation.

[b] CC_{50} – concentration that kills 50% of canine macrophages DH82.

[c] SI – selectivity index corresponding to the ratio CC_{50}/IC_{50}.

[d] Potassium antimonyl tartrate trihydrate, used as positive control.

As observed on Table 2.2, the positive control presented IC_{50} of 80 µmol/L and the tetraoxanes had IC_{50} values in the range of 0.64 to 99.50 µmol/L. Only **12d** was slightly less active (IC_{50} = 99.5 µmol/L) than the positive control. It is interesting to note that all

tetraoxanes derived from cyclopentanone (**12a**, **12d** and **12e**) were amongst the less potent ones. On the other hand, **12b** was the most active (IC_{50} = 0.64 µmol/L), being 125 more potent in comparison to the positive control. Tetraoxanes **12c**, **12g**, **12h** and **12j** have IC_{50} in the range of 16 to 22.6 µmol/L, being 3.5-5 times more potent when comparing them to the positive control. It should be noted note that **12c** - a symmetric tetraoxane derived from a seven-membered ring ketone - was 31 times less potent than **12b**, derived from cyclohexanone

After demonstrating that the tetraoxanes are active against *L. amazonensis* parasite, their toxicity (CC_{50}) and selectivity index (SI) towards canine macrophages DH82 were also determined (Table 2.2). Conforming to Weninger and co-works, the biological activity of the tested compounds is not attributable to cytotoxicity when SI ≥ 10 (Weginer *et al.*, 2001). It can be observed on Table 2.2 that the commercial standard drug has the lowest selectivity index (SI = 0.04) when compared to all six tetraoxanes. Even **12d,** that has the highest IC_{50} (99.5 µmol/L), is approximately 68 times (SI = 2.7) more selective than the positive control, presenting the lowest toxicity towards the canine macrophages. Compound **12b** not only has the lowest IC_{50}, but also has the highest SI (345.5), it is 8,638 times more selective, comparing to the positive control. The other tetraoxanes have SI in the range of 6.2 to 50.8, being much less toxic than the positive control.

Once the investigation indicated that the tetraoxanes are promising candidates for the development of a new therapeutic agent for *L. amazonensis* and considering that the main side effect of drugs on the treatment of leishmaniasis are nephrotoxicity and hepatotoxicity, the compounds were tested on two strains of human hepatoma (HepG2) and monkey renal (BGM) cells. The goal was to evaluate their impacts on liver and kidney. All results, including the corresponding SI values, are depicted in Table 2.3 (De Menezes *et al.*, 2015).

As expected, data on Table 2.3 confirms that the antimony positive control is very toxic towards the human hepatoma (HepG2) and the monkey renal (BGM) cells, with selectivity index of 0.4 and 0.02, respectively. In line with data presented on Table 2.2, all tetraoxanes are less toxic in correlation to positive control for both cell lines. In relation to

the HepG2 cells, the CC_{50} values are in the range of 57 µmol/L (**12h**) to >1000 µmol/L (**12c** and **12j**). All tetraoxanes were more selective than the positive control, with the lowest SI = 1.0 for **12d** and the best result for **12b** (SI = 268.8). This last compound is 672 times more selective in comparison to the antimony reference.

Table 2.3. Cytotoxic concentration (CC_{50}) of some tetraoxanes and a standard antimonial drug against HepG2 and BGM cells and their corresponding selectivity index (SI).

Compound	$CC_{50} \pm SD$ (µmol/L) [a]HepG2	SI [b]HepG2	$CC_{50} \pm SD$ (µmol/L) [c]BGM	SI [c]BGM
12b	172.00 ± 0.13	268.8	101.00 ± 0.43	157.8
12c	>1000	>50.8	>1000	>50.8
12d	98.00 ± 0.45	1.0	39.00 ± 0.20	0.4
12g	89.00 ± 0.12	5.6	82.00 ± 0.31	5.1
12h	57.00 ± 0.07	2.5	10.00 ± 0.08	0.4
12j	>1000	>55.6	>1000	>55.6
Control [d]	32.00 ± 0.05	0.4	2.00 ± 0.12	0.02

[a] CC_{50} – concentration of active ingredient that inhibits 50% of human hepatoma cells HepG2; SD – standard deviation.

[b] SI – selectivity index corresponding to the ratio between CC_{50} and the IC_{50} values presented on Table 2.

[c CC_{50} – concentration that kills 50% of monkey renal cells BGM.

[d Potassium antimonyl tartrate trihydrate, used as positive control.

For the renal monkey cells, the CC_{50} values are in the range of 10 µmol/L (**12h**) to >1000 µmol/L (**12c** and **12j**). Compounds **12d** and **12h** are the most toxic, showing SI = 0.4, but they are still much less toxic than the reference. For the same cell line, compounds

12b, **12c** and **12j** presented SI > 50, with **12b** being the one with the highest selective index (SI = 157.8, corresponding to 7,890 times more selective than the antimony compound). A possible explanation for the high selectivity of tetraoxanes is the endoperoxide bridge, which can be cleaved and activated in the presence of heme iron or free Fe^{2+} (Kwofie *et al.*, 2009). *Leishmania* gets iron from host macrophages for survival and growth, and the accumulation of iron within the parasite can be generated by oxyradicals (Das *et al.*, 2009; Gosh *et al.*, 2003). Fenton reaction degradation of the oxyradical intermediates can produce hydroxyl radicals. They are very reactive against a wide variety of molecules, such as enzyme, protein and nucleic acids, and also take the parasite to death (Kwofie *et al.*, 2009).

Based on all data presented on Tables 2.1 to 2.3, the most active and less toxic compound was **12b**. Nevertheless, compounds **12c**, **12g** and **12j** were also more potent and more selective towards the canine macrophage (DH82), human hepatoma (HepG2) and monkey renal (BGM) cell lines. Tetraoxanes showed greater SI values than the SI of positive control potassium antimonyl tartrate trihydrate. Because of that, the study tetraoxanes as antileishmanial agents can be considered a good strategy to discover new candidates to combat *L. amazonensis* (Regina *et al.*, 2019).

2.4. CONCLUSIONS

The anti-leishmanial activity of tetraoxanes were evaluated against the intracellular amastigotes of *L. amazonensis* parasitized macrophages (DH82). Five compounds (**12b**, **12c**, **12g**, **12h** and **12j**, with IC_{50} ranged from 0.64 µmol/L to 22.6 µmol/L) were more active than potassium antimonyl tartrate trihydrate (IC_{50} = 88.0 µmol/L) - the positive control of the test. The cytotoxicity and selectivity index were also screened using DH82, BGM and HepG2 line cells. In comparison to the positive drug control, all tetraoxanes were less cytotoxic and more selective to parasite. In summary the results revealed good leishmanicide activity for some tetraoxanes and pointed that class of compounds as a possible strategy for the treatment of leishmaniasis. It should be highlighted compound **12b**, which was not only the most active for leishmania (IC_{50} = 0.64 µmol/L), but was also

the least toxic and most selective (SI), when compared to a positive drug control and other tetraoxanes evaluated. Therefore, tetraoxane **12b** can be considered a new candidate for the development of new drug to treat leishmaniasis.

2.5. MATERIALS AND METHODS

2.5.1. Chemicals, instruments and experimental procedures.

All reagents and equipment utilized for this work are described in Chapter 1, item 1.5.1.

2.5.2. Synthetic procedures.

Compounds **11a-d** and **12a-f** were synthesized by the same methodology described in Chapter 1, item 1.5.2. All reactions were monitored by TLC. The spectrometric data of the compounds was compared to the data previously reported (Cusati *et al.*, 2015; Altheaya *et al.*, 2008; Iskra *et al.*, 2003).

2.5.2 .1. Data for 6,7,13,14-tetraoxadispiro[4.2.4^8.2^5]tetradecane **(12a)**
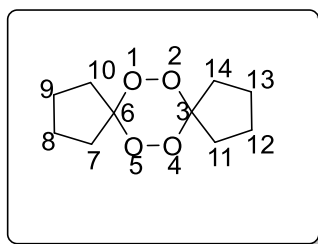
White solid (20 mg, 0.11 mmol, 50%). Lit. (Iskra *et al.*, 2003). ^{1}H-NMR (400 MHz, CDCl$_3$) δ: 1.68-1.77 (m, 12H, H-7, H-8, H-9, H-12, H-13, H-14); 2.39-2.42, m, 4H, H-10, H-11). ^{13}C-NMR (100 MHz, CDCl$_3$) δ: 24.1 (C-9, C-13); 25.3 (C-8, C-12); 34.6 (C-10, C-14); 35.5 (C-7, C-11); 120.0 (C-3, C-6). HRMS *m/z* (M+): Calculated for C$_{10}$H$_{16}$O$_4$: 200.1049; found: 200.0983.

2.5.2 .2. Data for 7,8,15,16-tetraoxadispiro[5.2.5^9.2^6]hexadecane **(12b)**
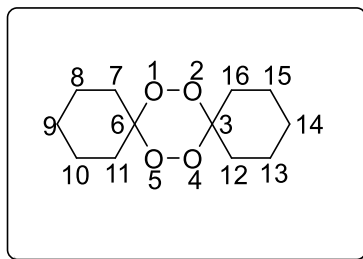
White solid (129 mg, 0.64 mmol, 32%). Lit. (Iskra *et al.*, 2003). M.p.: 129.2-130.2 °C. ^{1}H-NMR (400 MHz, CDCl$_3$)δ:1.40-2.80 (m, 18H, H-7, H-8, H-9, H-10, H-11b, H-12, H-13, H-14, H-15); 2.10- 2.50 (m, 4H, H-11, H-16).^{13}C (100 MHz, CDCl$_3$) δ: 22.3 (C-9, C-14); 25.6 (C-8, C-10, C-13, C-15); 30.9 (C-11, C-16); 31.8 (C-7, C-12); 108.4 (C-3,C-6).HRMS *m/z* (M$^+$Na$^+$): Calculated for: C$_{12}$H$_{19}$NaO$_4$, 250.1181; found: 250.1221.

2.5.2 .3. Data for 8,9,17,18-tetraoxadispiro[6.2.6^{10}.2^7]octadecane **(12c).**
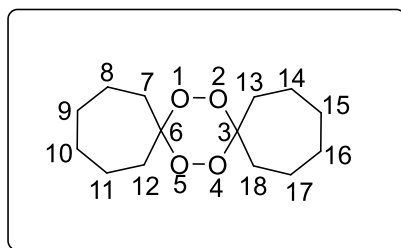
White solid (57 mg, 0.20 mmol, 11%). Lit. (Altheaya *et al,* 2008). M.p.: 145.5-145.9 °C. ^{1}H-NMR (400 MHz, CDCl$_3$)δ: 1.50-1.80 (m, 16H, H-7, H-8, H-9, H-10, H-11, H-14, H-15, H-16, H-17, H-18); 2.41 (m, 4H, H-12, H-13). ^{13}C-NMR (100 MHz, CDCl$_3$) δ: 22.6 (C-10, C-16, C-9, C-15); 29.7 (C-11. C-17); 30.4 (C-8, C-14); 31.2 (C-12, C-18); 36.2 (C-7, C-13); 112.7 (C-3, C-6). HRMS *m/z* (M$^+$Na$^+$): Calculated for C$_{16}$H$_{27}$NaO$_4$:278.1594; found: 278.1627.

2.5.2 .3. Data for 6,7,14,15-tetraoxadispiro[4.2.5^8.2^5]pentadecane **(12d).**
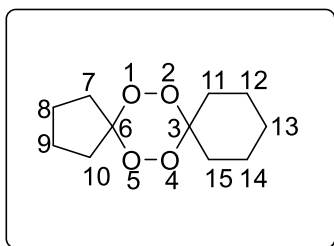
White solid (43 mg, 0.2 mmol,10%). Lit. (Cusati *et al.*, 2015) M.p.: 122.3-123.5°C.
^{1}H-NMR (400 MHz, CDCl$_3$) *δ:* 1.47-149 (m, 6H, H-12, H-13, H-14); 1.57-1.59 (m, 8H, H-7, H-8, H-9, H-11, H-12, H-13, H-14); 2.28 (m, 4H, H-10, H-15,). ^{13}C-NMR (100 MHz, CDCl3)*δ:* 22.1 (C-9); 22.4 (C-8); 25.6 (C-12, C-13, C-14); 29.8 (C-15); 31.9 (C-11); 34.6 (C-10); 35.6 (C-7); 108.40 (C-3); 119.9 (C-6). HRMS *m/z* (M$^+$Na$^+$): Calculated for C$_{11}$H$_{17}$NaO$_4$: 236.1025; found; 236.1035.

2.5.2 .4. Data for 6,7,16,17-tetraoxadispiro[4.2.7^8.2^5]heptadecane **(12e).**
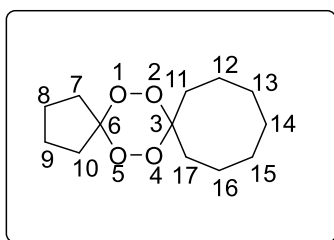
White solid (137.1 mg, 0.56 mmol, 28%). Lit. (Cusati *et al.*, 2015).^{1}H-NMR (400 MHz, CDCl$_3$) *δ:* 1.54-1.78 (m, 18H, H-7, H-8, H-9, H-12, H-13, H-14, H-15, H-16,H-18); 2.39- 2.46 (m, 4H, H-10, H-11). ^{13}C-NMR (100 MHz, CDCl$_3$) *δ:* 22.6 (C-15); 22.9 (C-13); 24.1 (C-9); 24.7 (C-14); 24.7 (C-8); 25.2 (C-16, C-12); 29.7 (C-17); 32.9 (C-11); 33.5 (C-10); 35.4 (C-7); 112.1 (C-3); 119.4 (C-6). HRMS *m/z* (M$^+$): Calculated. for C$_{13}$H$_{22}$O$_4$: 242.1318; found: 242.1289.

2.5.2 .5. Data for 3-phenyl-1,2,4,5-tetraoxaspiro[5.5]undecane **(12f).**
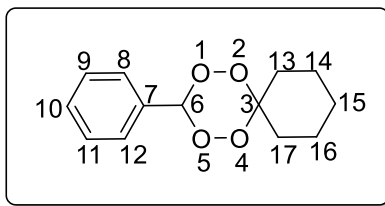
White solid (224.1 mg, 0.11mmol, 47%). Lit. (Iskra *et al.*, 2003). ^{1}H-NMR (400 MHz, CDCl$_3$) *δ:* 1.62-1.74 (m, 10H, H-13, H-14, H-15, H-16); 1.79- 1.81 (m, 2H, H-13); 6.69 (s, 1H, H6); 7.43 - 7.4 (m, 5H, H-8, H-9, H-10, H-11, H-12). ^{13}C-NMR (100 MHz, CDCl$_3$) *δ:* 22.5 (C-15); 22.8 (C-14); 29.6 (C-16); 30.3 (C-13); 36.1 (C-17); 107.6 (C-3); 113.6 (C-6); 127.6 (C-9, C-11); 128.7 (C-8, C-12); 131.0 (C-10); 131.6 (C-7). HRMS *m/z* (M$^+$): Calculated for C$_{13}$H$_{16}$O$_4$: 236.1049; found: 236.1007.

2.5.2 .6. Data for 3-phenyl-1,2,4,5-tetraoxaspiro[5.6]dodecane **(12g)**
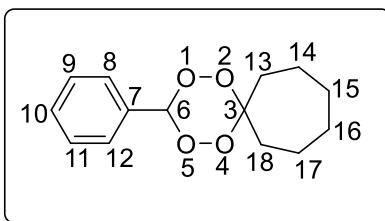
White solid (211.2 mg, 0.16 mmol, 42%). Lit. (Cusati *et al.*, 2015). M.p.: 182.3-183.0 °C. ^{1}H-NMR (400 MHz, CDCl$_3$) *δ:* 1.61-1.80 (m, 10H, H-13, H-14, H-15, H-16, H-17); 2.63-2.65 (m, 2H, H-18); 6.67 (s, 1H, H-6); 7.37-7.44 (m, 5H, H-8, H-9, H-10, H-11, H-12). ^{13}C-NMR (100 MHz, CDCl$_3$) *δ:* 22.5 (C-16); 22.8 (C-15); 29.6 (C-14); 30.3 (C-17); 31.8 (C-18); 36.1 (C-13); 107.6 (C-3); 113.6 (C-6); 127.6 (C-9, C-11); 128.7 (C-8, C-12); 131.0 (C-10); 131.6 (C-7). HRMS *m/z* (M$^+$): Calculated for C$_{14}$H$_{18}$O$_4$: 250.1205; found: 250.1187.

*2.5.2 .7. Data for 3-phenyl-1,2,4,5-tetraoxaspiro[5.7]tridecane (**12h**).*
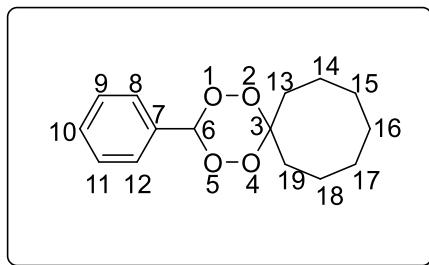
White solid (85 mg, 0.08 mmol, 16%). Lit. (Cusati *et al.*, 2015). M.p.: 190.1-190.8 °C. ^{1}H-NMR (400 MHz, CDCl$_3$) *δ:* 1.61-1.79 (m, 12H, H-13, H-14, H-15, H-16, H-17, H-18, H-19); 2.62-2.64 (m, 2H, H-19a); 6.65 (s, 1H, H-6); 7.37-7.47 (m, 5H, H-8, H-9, H-10, H11, H-12). ^{13}C-NMR (100 MHz, CDCl$_3$) *δ:* 21.4 (C-17); 22.3 (C15); 25.1 (C-16); 26.8 (C-18); 27.0 (C-14); 29.0 (C-19); 32.9 (C-13); 107.9 (C-6); 112.6 (C-3); 127.6 (C-9, C-11); 128.7 (C-8, C-12); 131.0 (C-10); 131.5(C-7). HRMS *m/z* (M$^+$): Calculated for C$_{15}$H$_{20}$O$_4$: 264.1362; found: 264.1322.$^]$

*2.5.2 .8. Data for 3,6-diphenyl-1,2,4,5-tetraoxane (**12i**).*
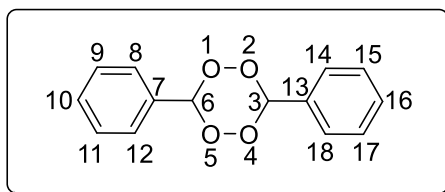
White solid (98.6mg, 0.44 mmol, 20%). Lit. (Cusati *et al.*, 2015). M.p.: 201.0-202.0 °C. ^{1}H-NMR (400 MHz, CDCl$_3$) *δ:* 6.94 (s, 2H, H-3 e H-6); 7.35-7.52 (m, 10H, H8, H-9, H-10, H-11, H-12, H-14, H-15, H-16, H-17,H-18). ^{13}C-NMR (100 MHz, CDCl$_3$) *δ:* 109.1(C-3, C-6); 128.1 (C-9, C-11, C-15, C-17); 129.1 (C-8, C-12, C-14, C-18); 131.1 (C-10, C-16); 131.7 (C-7, C-13). HRMS *m/z* (M$^+$): Calculated for C$_{14}$H$_{12}$O$_4$: 244.0736; found: 244.0623.
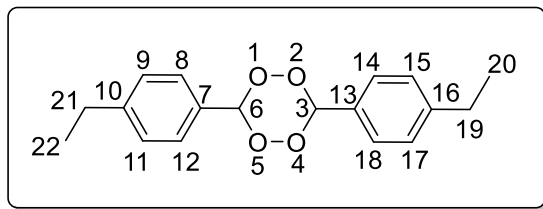
White solid (145.6 mg, 0.48 mmol, 24%). Lit. (Cusati *et al.*, 2015). M.p.: 230.7–231.2 °C. ^{1}H-NMR (400 MHz, CDCl$_3$) δ: 1.28 (t, 6H, $J_{20,19} = J_{22,21} = 7.6$, H-20, H-22); 2.71 (q, 4H, $J_{19,20} = J_{21,22} = 7.6$, H-19, H-21); 6.94 (s, 2H, H-3,H-6); 7.30 (*d*, 4H, $J_{9,8} = J_{11,12} = J_{15,14} = 8.1$, H-9, H-11, H-15, H-17); 7.48 (dd, 4H, ; $J_{12,11} = J_{8,9} = J_{14,15} = J_{18,17} = 6.6$, H-8, H-12, H-14, H-18). ^{13}C-NMR (100 MHz, CDCl$_3$) δ: 15.5 (C-20, C-22); 29.1 (C-19, C-21); 108.4 (C-3, C-6); 128.1 (C-9, C-11, C-15, C-17); 128.5 (C-8, C-10,C-12, C-14, C-16, C-18); 148.1 (C-7, C-13). HRMS *m/z* (M$^+$Na$^+$): Calculated for C$_{16}$H$_{16}$NaO$_6$: 323.0839; found: 323.0832.

2.5.3. Biological assay.

Biological assays of compounds **12a-12h** were executed at the Instituto de Ciências Biológicas of the Universidade Federal de Minas Gerais, under the supervision of Professor Ricardo T. Fujiwara and with the support of Dr. Sebastião R. Ferreira.

2.5.3.1. Anti-leishmanial assay.

The leishmanicidal activities of compounds **12a-h** were assessed *in vitro* against amastigote forms of *L. amazonensis* by ELISA assay, with canine macrophages (DH82), and based on previous work found in literature (Rodriguez-Hernádez *et al.,* 2016). About 5×10^4 macrophages/well were distributed in 96-well culture plates and incubated at 37 ºC in 5% CO$_2$. After 24 h, the adherent macrophages were infected with *L. amazonensis* amastigotes at 50:1 (parasite: cell host ratio). Four hours after the infection, cultures were washed three times with ice-cold PBS (phosphate-buffered saline) and compound solutions

in RPMI (growth medium) were added at the wells. Forty-eight hours later, the cultures were fixed in ice cold methanol, washed three times with 100 μL PBS, containing 5% v/v BSA (bovine serum albumin), and incubated for 1 hour at 37 ℃. After that period, the plates were washed four times with PBS-Tween-20 (pH 7.4) and incubated with serum of a dog infected with Leishmania parasite, cell host ratio at 1: 300 (promastigotes form) for 1 h at 37 ℃. The plates were washed four times and 100 μL of HPR-conjugated anti-human IgG (1: 2000) were added. The plates were incubated for 1 h at 37 ℃ and, then, washed four times with PBS containing 0.05% v/v Tween-20 (pH 7.4). The reaction proceeded by adding 100 μL of substrate solution (10 mL citrate buffer, 10 mg of ortho-phenylenediamine and 2.0 mL H_2O_2) to each well. After 15 min, the reaction was stopped by the addition of 30 μL of H_2SO_4 (2 mol/L). Optical density reading was measured at 492 nm in an ELISA reader (Molecular Devices, USA).

In the first time, all compounds were tested at the concentration of 1000 μmol/L. Those ones that inhibited 50% of *in vitro* parasites growths were tested at 0.1, 1, 10, 100 and 1000 μmol/L. The experiment was performed in quadruplicate. Potassium antimonyl tartrate trihydrate was used as positive drug control at the same concentrations that the compounds 0.1 – 1000 μmol/L. The results were evaluated by the GraphPad Prism 5.0 software to determine the dose – response curves plotted with sigmoidal fit. The concentration of the compound capable of reducing in 50% of parasite growth (IC_{50}) was determined using statistical software GraphPad Prism 5.0.

2.5.3.2. Cytotoxicity assay.

Cytotoxicity determination was implemented in monkey renal cell (BGM), human hepatoma (HepG2) and dog macrophage cell lines (DH82), by MTT (3- (4,5-dimethylthiazol-2-yl) -2,5-diphenyltetrazolium bromide) assay. The cells were grown in RPMI (growth medium), containing penicillin (100 U/mL), streptomycin (100 μg/mL^{-1}) and inactivated fetal bovine serum (10% v/v). BGM and HepG2 cells were plated at $1x10^4$ cells per well and DH82 were plated at $5x10^4$ cells per well. Then, 100 μL of solution of compounds 10a-j in RPMI were set in each well and incubated for 48 h at 37 ℃ in a 5%

CO$_2$. Compounds were tested in the following concentrations: 1000, 100, 10, 1 and 0.1 µmol/L. After the incubation period, the amount of 10 µL of MTT solution (5 mg/mL) was added to the wells and incubated again for 4h. Then, the supernatant was removed and 50 µL of DMSO were placed in each well. The experiments were performed in quadruplicate. The culture plates were read by a spectrophotometer with a 560 nm. While the concentration values were inhibiting 50% of the cell metabolism, the cytotoxic concentration (CC$_{50}$) was determined using statistical software GraphPad Prism 5.0 and the selective indexes (SI= CC$_{50}$/IC$_{50}$) were calculated for each compound.

2.6. REFERENCES

Anversa, L. S., Tiburcio, M. G. S., Richini-Pereira, V. B., Ramirez, L. E., Human leishmaniasis in Brazil: A general review, 2018. Rev. Assoc. Med. Bras. 64, 281–289.

Avery, M. A., Muraleedharan, K. M., Desai, P. V., Bandyopadhyaya, A. K., Furtado, M. M., Tekwani, B. L., 2003. Structure-activity relationships of the antimalarial agent artemisinin: Design, synthesis, and CoMFA studies toward the development of artemisinin-based drugs against leishmaniasis and malaria. J. Med. Chem. 46, 4244–4258.

Baeyer A, Villiger V. 1902. Ueber die Einwirkung des Caro'schen Reagens auf Ketone. Zeitschrift. Anal Chemie. 41, 765–766.

Baldaia, A., 2015. Conversão catalítica de cetonas em 1,1-diidroperóxidos e tentativas de obtenção de 1,2,4,5-tetraoxanos potencialmente herbicidas. Dissertação de Mestrado, Universidade Federal de Minas Gerais.

Bittencourt, A., Barral, A., de Jesus, A. R., de Almeida, R. P., Grimaldi Júnior, G. 1989. In situ identification of *Leishmania amazonensis* associated with diffuse cutaneous leishmaniasis in Bahia, Brazil. Mem. Inst. Oswaldo Cruz, 84, 585–586.

Brasil, Manual De Vigilância Da Leishmaniose Tegumentar, 2017.

Cotton, J. A., 2017. The Expanding World of Human Leishmaniosis. Trends Parasitol. 33, 341–344.

Cabral, M. L., Pmel, L. I. L., Cojean, S., Amado, S., Loiseau, P. S. M., Cristiano, P. M., 2020. Synthesis and Antileishmanial Activity of *L. donovani*. Molecules, 25, 1-9.

Cusati, R. C., Barbosa, L. C. A., Maltha, C. R. A., Demuner, A. J., Oliveros-Bastidas, A., Silva, A. A., 2015.Tetraoxanes as a new class of efficient herbicides comparable with commercial products. Pest Manag. Sci. 71, 1037–1048.

Das, N. K., Biswas, S., Solanki, S., Mukhopadhyay, C. K., 2009. *Leishmania donovani* depletes labile iron pool to exploit iron uptake capacity of macrophage for its intracellular growth. Cell. Microbiol. 11, 83–94.

De Menezes, J. P. B., Guedes C. E. S., De Oliveira Almeida Petersen, A. L., Fraga, D. M. B., Veras, P. S. T., 2015. Advances in development of new treatment for leishmaniasis. Biomed Res. Int. 15–18.

Ghosh, S., Goswami, S., Adhya, S., 2003. Role of superoxide dismutase in survival of Leishmania within the macrophage Biochem. J. 369, 447–452.

Iskra, J., Bonnet-Delpon, D., Begue., J. P., 2003. One-pot synthesis of non-symmetric tetraoxanes with the H_2O_2/MTO/fluorous alcohol system. Tetrahed. Lett., 44, 6309-6312

Kornblum, N., De LaMare, H. E., 1951. The base catalyzed decomposition of a dialkyl peroxide. J. Am. Chem. Soc. 73, 880–881.

Kwofie, K. D., Sato, K., Sanjoba, C., Hino, A., Shimogawara, R., Amoa-Bosompem, M., Ayi, I., Boakye, D. A., Anang, A. N., Chang, K. N., Ohashi, M., Kim, H. S., Ohta, N., Matsumoto, Y., Iwanaga, S., 2018. Oral activity of the antimalarial endoperoxide 6-(1,2,6,7-tetraoxaspiro[7.11]nonadec-4-yl)hexan-1-ol (N-251) against *Leishmania donovani* complex. PLoS Negl. Trop. Dis.*13*, 1–15.

Nitin, R. S., Kumar, D. S. R., 2009. Tetraoxanes: Synthetic and Medicinal Chemistry Perspective. Med. Res. Rev.520–547.

Okwor I., Uzonna J., 2016. Social and economic burden of human leishmaniasis. Am. J. Trop. Med. Hyg. 94, 489–493.

Pal, J. K., Joshi-Purandare, M., 2001. Dose-dependent differential effect of hemin on protein synthesis and cell proliferation in *Leishmania donovani* promastigotes cultured in vitro, J. Biosci. 26, 225–231.

Rath, S., Augusto Trivelin, L., Imbrunito, T. R., Tomazela, D. M., De Jesús, M. N., Calvo Marzal, P., De Andrade, H. F., Gustavo Tempone, A., 2003. Antimoniais empregados no tratamento da leishmaniose: Estado da arte. Quim. Nova, 26, 550–555.

Regina, R., Moreira, D., Gonzaga, A., Carvalho, A., Perego, C. H., Crevelin, E. J., Eduardo, A., Crotti, M., Cogo, J., Lane, M., Cardoso, C., 2019. Antileishmanial activity of *Melampodium divaricatum* and *Casearia sylvestris* essential oils on *Leishmania amazonensis*. Rev. Inst. Med. Trop. Sao Paulo, 1–7

Rocha, M. N., Nogueira, P. M., Demicheli, C., De Oliveira, L. G., Da Silva, M. M., Frézard, F., Melo, M. N., Soares, R. P., 2013. Cytotoxicity and in vitro antileishmanial activity of antimony (V), bismuth (V), and tin (IV) complexes of Lapachol. Bioinorg. Chem. Appl. 2013, 1-7.

Rodríguez-Hernández, D., Barbosa, L. C. A., Demuner, A. J., de Almeida, R. M., Fujiwara, R. T., Ferreira, S. R., 2016. Highly potent anti-leishmanial derivatives of hederagenin, a triperpenoid from Sapindus saponaria L. Eur. J. Med. Chem. 124, 153–159.

Sen, R., Bandyopadhyay S., Dutta, A., Mandal, G., Ganguly, S., Saha, P., Chatterjee, M., 2007. Artemisinin triggers induction of cell-cycle arrest and apoptosis in *Leishmania donovani* promastigotes. J. Med. Microbiol. 56, 1213–1218.

Simon A. H. F., Croft, L., Sundar, S., 2006. Drug Resistance In Leishmaniasis. Clin. Microbiol. Rev. 19, 111–126

Steverding, D., 2017. The history of leishmaniasis, Parasites and Vectors 10, 1–10.

Terent'ev, A. O., Borisov, D. A., Yaremenko, I. A., 2012. General methods for the preparation of 1,2,4,5-tetraoxanes - Key structures for the development of peroxidic antimalarial agents. Chem. Heterocycl. Compd. 48, 55–58.

Uliana, S. R. B., Trinconi C. T., Coelho A. C., 2018. Chemotherapy of leishmaniasis: Present challenges. Parasitol. 145, 464–480.

Valero Antolínez, I., 2015. Otimização da Síntese de 1,2,4,5-tetraoxanos Assimétricos Visando à Obtenção de Derivados do Ácido α-naftalenoacético. Dissertação de Mestrado, Universidade Federal de Minas Gerais

Vennerstrom, J. L., Fu, H. L., Ellis, W. Y., Andersen, S. L., Gerena, L., Ager, A. L., Wood, J. K., 1992. Dispiro-1,2,4,5-tetraoxanes: A New Class of Antimalarial Peroxides. J. Med. Chem. 35, 3023–3027.

Weniger, B., Robledo, S., Arango, J. G., Deharo, E., Aragón, R., Muñoz, V., Callapa, J., Lobstein, A., Anton, R., 2001. Antiprotozoal activities of Colombian plants. J. Ethnopharmacol. 78, 193–200.

Zmitek, K., Stavber, S., Zupan, M., Bonnet-Delpon, D., Iskra, J., 2005. Fluorinated alcohol directed formation of dispiro-1,2,4,5-tetraoxanes by hydrogen peroxide under acid conditions. Tetrahedron. 62, 1479.

CHAPTER 3

SYNTHESIS OF PULCHELLALACTAM AND RELATED LACTONES AS POTENTIAL ANTI-QUORUM SENSING AGENTS

3.1. INTRODUCTION

γ-Lactams are cyclic amides with five atoms rings (Figure 3.1). They are also known as γ-butyrolactams, pyrrolidin-2-ones, azolydin-2-ones or 2-oxopyrrolydines (Nay *et al.*, 2009). The interest on those substances emerged due to the increasing resistance that many bacteria have shown against traditional β-lactams antibiotics (Baldwin *et al.*, 1990). Some studies revealed that the biological potential of those compounds is related to π-delocalization of the nitrogen lone pair, which facilitates their reactivity. In the same way that β-lactams, γ-lactams inhibit the enzymes that build the network of carbohydrate and proteins chains, that brace the bacterial cell walls (Baldwin *et al.*, 1990).

a R^3 = OH
b R^3 = H, alkyl
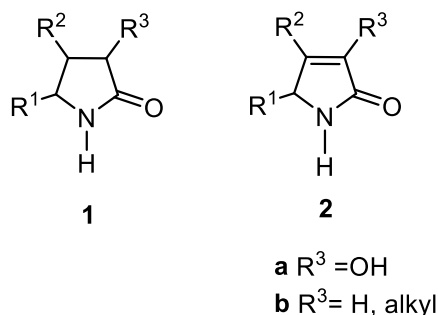
Figure 3.1. General structures of γ-lactams.

Alkylidenes lactams (Scheme 3.1, **4**) - mostly present in fungal metabolites - have a wide range of biological activities. Those ones derived from tetronic acid have a hydroxyl group bonded at the third position of the ring (Figure 3.1, **2a**). Moreover, such scaffold has direct relation to 5-hydroxy-5-alkyldiene lactam core (**3**), as **4** is the dehydrated form of **3** (Scheme 3.1) (Nay *et al.*, 2009).
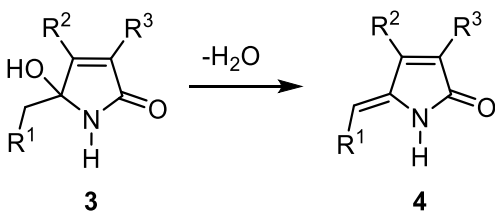
Scheme 3.1. Chemical relation between 5-hydiroxy-5alkyl-2-ones (**3**) and 5-alkylidene-pyrrolin-2-ones (**4**) (Nay *et al.*, 2009).

3.1.1. Pulchellalactam

In 1995, it was announced the isolation of pulchellalactam ($C_9H_{13}NO$) **5** (Figure 3.2) from the fungus *Corollospora pulchella* (Kolhm, I. Scmidt & N. B. Nair, 1967) (Alvi *et al.*, 1998). The microorganism is a marine fungus, especially detected in sand-buried driftwoods of tropical water. The interest in the biological potential of pulchellalactam (**5**) resides in its capacity to inhibit the CD45 protein tyrosine phosphatase. The natural product exhibited a dose response pattern in the inhibition of CD45 enzyme. Its value of IC_{50} was 124 µg/mL, comparable to sodium orthovanadate reference (91.9 µg/mL) (Alvi *et al.*, 1998).
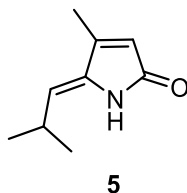
Figure 3. 2. Chemical structure of (*Z*)-pulchellalactam.

3.1.2. Reported Synthesis of Pulchellalactam

Although it is a small molecule, pulchellalactam (**5**) has been a synthetic target of interest for several research groups. Until this date, nine syntheses of it have been communicated. Scheme 3.2 shows the key intermediates employed in those disclosed routes. Among them, Boc-protected lactam (**6**) is the most common. Other intermediates like haloenamide **7,** haloester **8,** dienoic acid **9** and protected lactam **10** have been also

implemented. Such a variety of intermediates gives an idea about the high number of strategies developed to synthesize that natural product.
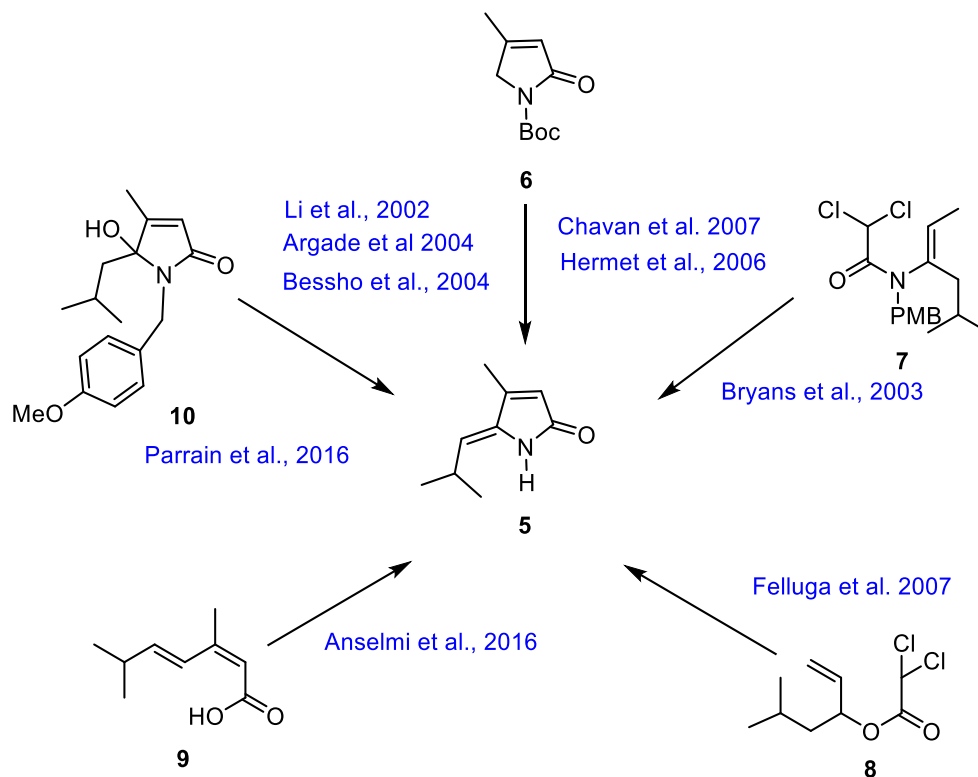
Scheme 3.2. Key intermediates in the reported syntheses of pulchellalactam (**5**).

The first total synthesis of pulchellalactam was announced in 2002. The compound was synthetized in six steps, with 32% overall yield. The key step in that synthetic route was the preparation of intermediate **6,** by coupling Boc-protected glycine (**11**) with Meldrum acid (**12**). The addition of the isopropyl unit was made by the condensation between isobutyraldehyde and the lactam core, in presence of sodium hydride. Migration of the Boc-group in the intermediate (**15**) afforded an adequate substrate for an E_{1CB} elimination, which lead to the final product **5** (Scheme 3.3) (Li *et al.*, 2002).
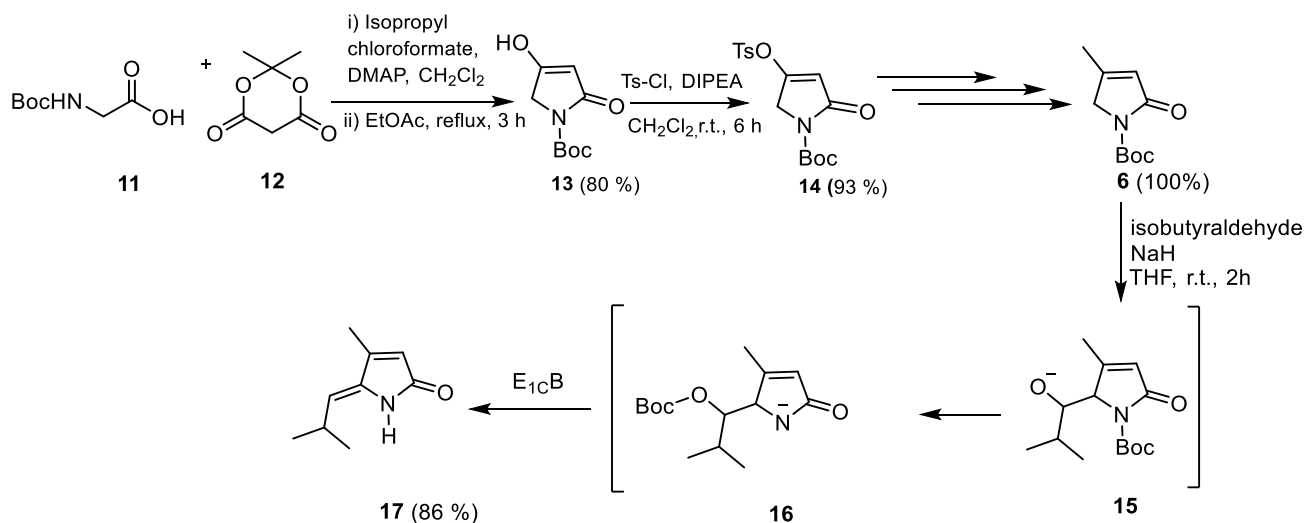
Scheme 3.3. Total synthesis of pulchellalactam (**5**), starting from Boc-protected glycine (**11**) and Meldrum´s acid (**12**) (Li *et al.*, 2002).

A year later, the natural product was synthesized using an atom transfer radical cyclisation as main strategy. In that case, haloenamide **19** was the precursor of cyclic intermediate **21** (Scheme 3.4). The overall yield of the synthetic route was only 10%, so it presented a low selectivity to the formation of the *Z*-isomer (Bryans *et al.,* 2003).
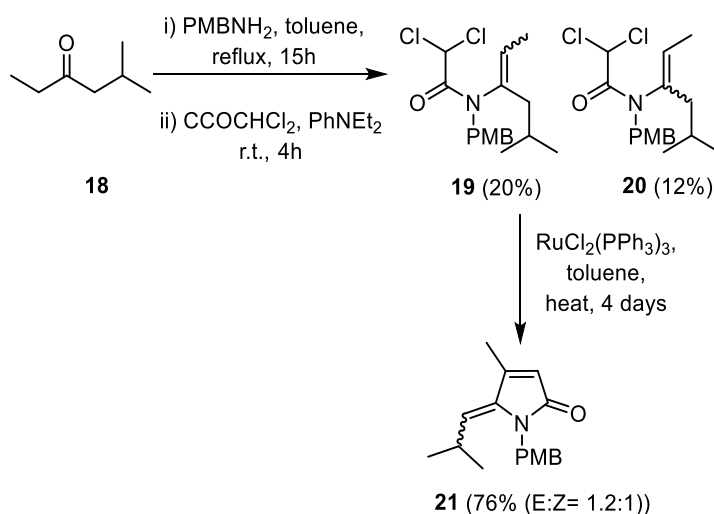
Scheme 3.4. Synthetic route of pulchellalactam utilising an atom transfer radical cyclisation reaction (Bryans *et al.*, 2003).

In 2004, pulchellalactam was synthetized in six steps, starting from the citraconic intermediate **22** in a 32% overall yield (Scheme 3.5). The approach took advantage of regioselective reduction of maleimide **23** to yield the hydroxylactam **24** when $NaBH_4$ is used as reducing agent. Studies about the stability of the *Z* and *E* isomer revealed that the first one is stable for at least six months, while *E* isomerize to *Z* relatively fast (Mangaleswar and Argade, 2004.).
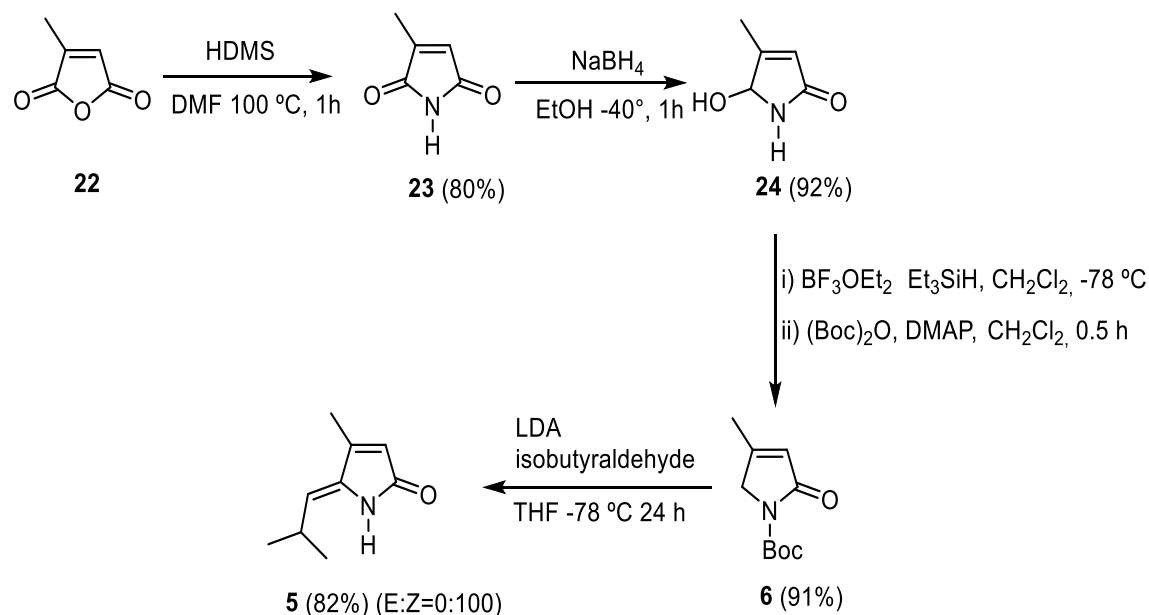
Scheme 3.5. Synthesis of pulchellalactam using regioselective reduction of maleimide **23** (Mangaleswar and Argade, 2004).

Another route, reported in the same year, afford the natural product in 5 steps, with 64% overall yield starting form non-commercial citraconimide **23** (Bessho *et al.*, 2004). That strategy was also based in the regioselective reduction of maleimides with $NaBH_4$ (Scheme 3.6).
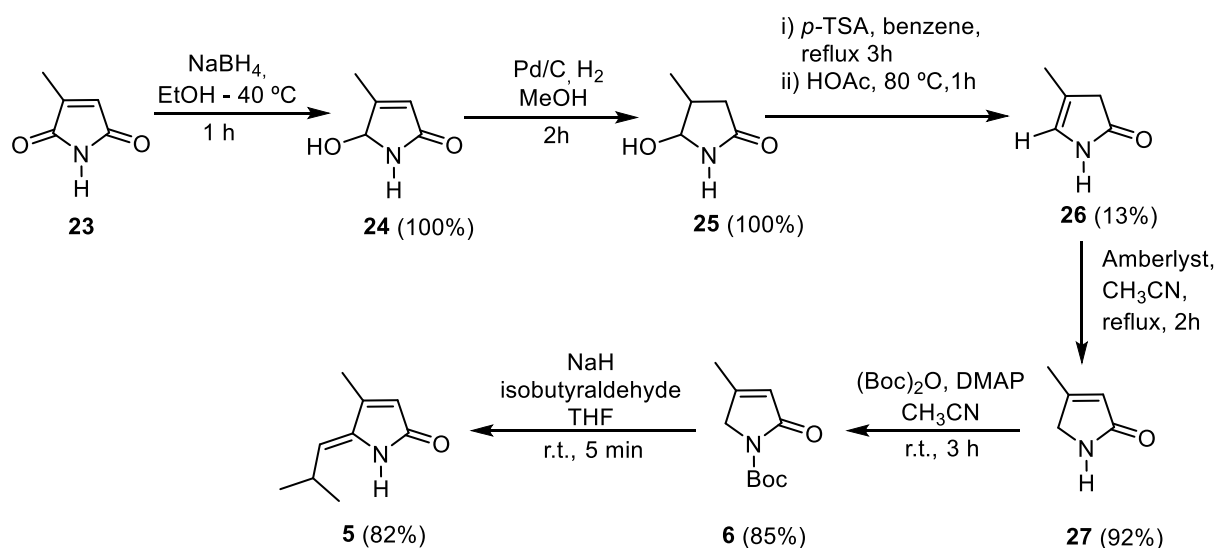
Scheme 3.6. Synthesis of pulchellalactam starting from citraconimide **23** (Bessho *et al.*, 2004).

Furthermore, cycloaddition reactions have been used as a key step for the synthesis of pulchellalactam. In that case, the product was obtained in three steps, with 48% overall yield starting from the protected lactam **28**. A 1,3-dipolar cycloaddition reaction between that intermediate and diazomethane afforded compound **29**. Further thermolysis of **29**, gave compound **6**. The natural product was synthesized by aldolic condensation of **6** with isobutyraldehyde, in presence of LDA (Scheme 3.7) (Hermet *et al.*, 2006).
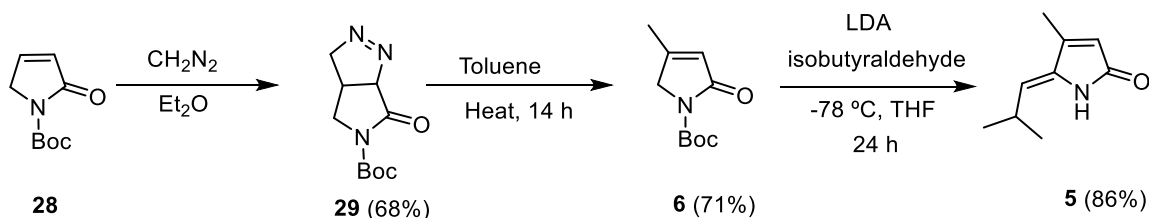
Scheme 3.7. Total synthesis of pulchellalactam utilising cycloaddition as the main strategy (Hermet *et al.*, 2006).

In 2007, a transitioning metal radical cyclization reaction was employed again to afford the natural product. Copper (I) chloride–bipyridyl was the catalyst choses for the cyclisation reaction of the compound **30**. The resulting dichlorolactone (**31**) suffered a dehydrochlorination and a rearrangement that yielded compound **31**. Finally, under

aminolysis conditions, pulchellalactam (**5**) was obtained in overall yield of 54% (Scheme 3.8) (Felluga *et al.*, 2007).
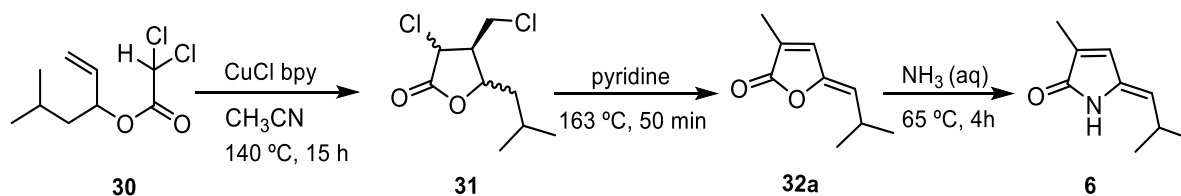
Scheme 3.8. Synthesis of pulchellalactam by the metal radical cyclisation key step (Felluga *et al.*, 2007).

Also, in that year, another synthesis of pulchellalactam was reported. The key intermediated **6** was obtained via ring closure metathesis of compound **35.** Further aldol condensation of protected lactam **6** with isobutyraldehyde afforded the natural product in an overall yield of 34 % (Scheme 3.9.) (Chavan *et al.*, 2007).
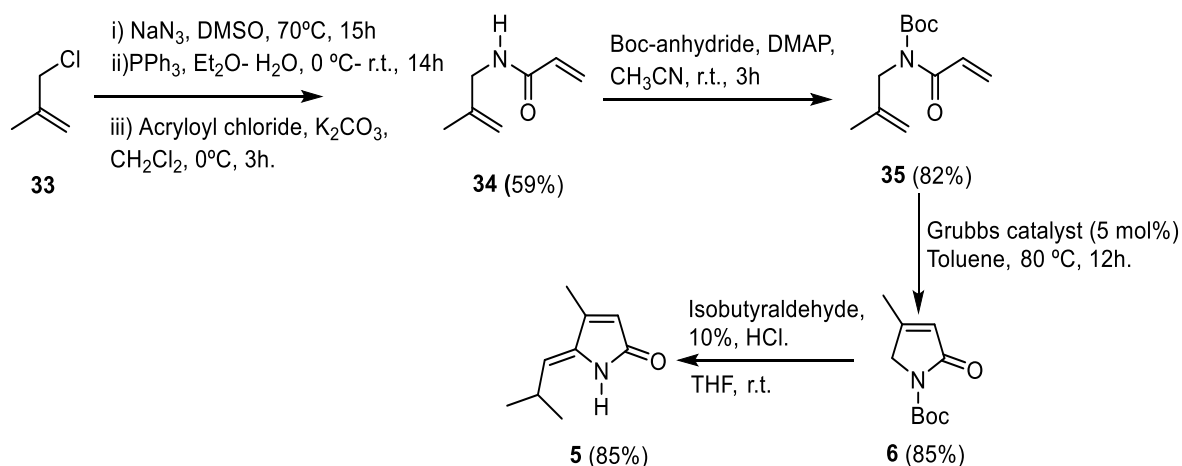
Scheme 3.9. Total synthesis of pulchellalactam via ring closure metathesis of olefins (Chavan *et al.*, 2007).

The two-last synthesis of pulchellalactam were described in 2016. One of them involved a multicomponent reaction. In that case, lactam **39** was obtained in 41% yield, by reacting alkenoic acid **36** with 3-methylbutine (**37**) and amine **38,** in the presence of CuI

and K_2CO_3 (Scheme 3.10). Further deprotection of **39** with TFA afforded the natural product in overall yield of 31% (Mardjam *et al.*, 2016).
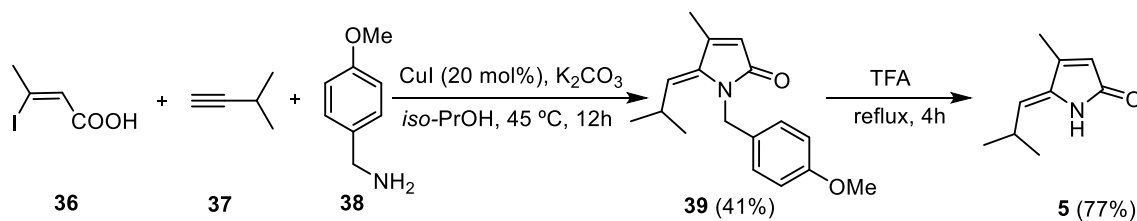
Scheme 3.10. Synthesis of **5** by multicomponent reaction (Mardjam *et al.*, 2016).

With respect to the other route, pivotal intermediate **32a** was obtained via cyclization of dienoic acid **40.** Further aminolysis of the butenolide yielded the desired natural product with an overall yield of 22% (Scheme 3.11) (Anselmi *et al.*, 2016).
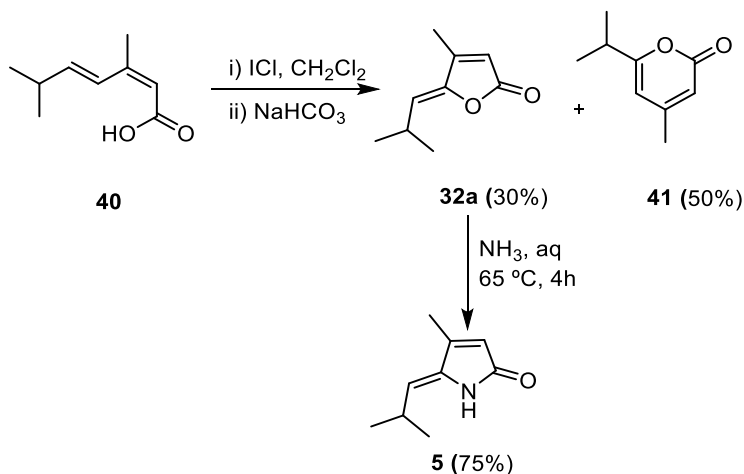
Scheme 3.11. Total synthesis of pulchellalactam via iodocyclization of dienoic acid **40** (Anselmi *et al*., 2016).

As already mentioned, pulchellalactam (**5**) is a small molecule that have attracted the attention of many research groups. As shown above, a wide variety of reactions and elegant strategies has been applied in order to synthesize that natural product. However, low overall yields and side products are problems that hinder the easy access to **5,** which would make possible to explore the biological activities of such compound.

3.1.3. Sonogashira coupling: synthetic relevance and mechanistic aspects

The Sonogashira cross-coupling is an important reaction to carbon-carbon bond formation in organic synthesis. Since its report in 1975, the reaction has been extensively studied for different research groups and several variations of its methodology has been divulged (Scheme 3.12) (Sonogashira, 1975).

$$R_1\text{—}X \quad R_2\text{—}\!\!\equiv\!\!\text{—}H \xrightarrow[\text{Et}_3\text{N, r.t.}]{\text{Pd(PPh}_3)_2\text{Cl}_2,\ \text{CuI}} R_1\text{—}\!\!\equiv\!\!\text{—}R_2$$

$$\textbf{42} \qquad\qquad \textbf{43} \qquad\qquad\qquad\qquad\qquad\qquad \textbf{44}$$
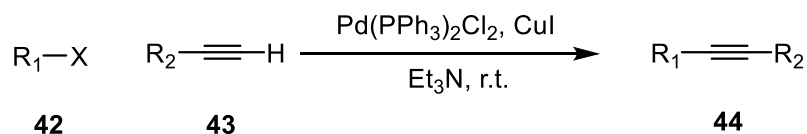
Scheme 3.12. Sonogashira Cross-coupling reaction.

The mechanism of the Sonogashira reaction is a catalyst cycle that starts with the oxidative addition of the alkyl halide to the palladium catalyst, which results in a tetrahedral complex **47.** Further transmetallation of acetylide nucleophile from copper intermediate **53** lead to the formation of palladium complex **54**. The new intermediate suffers an isomerization that finally motivates the reductive elimination that produce the desired alkyne **56** (Scheme 3.13) (Chichilla and Nájera 2011). The complexity of the mechanism of Sonogashira reaction is related to the different catalytic cycles involved in the reaction. The transmetallation step is only possible because of the formation of the copper acetylide (**53**). It may happen via catalytic cycles, as presented on Scheme 3.1.

Although the mechanism is not completely elucidated, the most plausible proposal involves the formation of π complex **50** (Chichilla and Nájera 2011). In that complex, the acidity of terminal hydrogen increases. As consequence, the base (normally an amine) can effortlessly extract the proton. In addition, the insertion of the copper in the alkyne structure allows the formation of key intermediate **53** (Karak *et al.*, 20014).
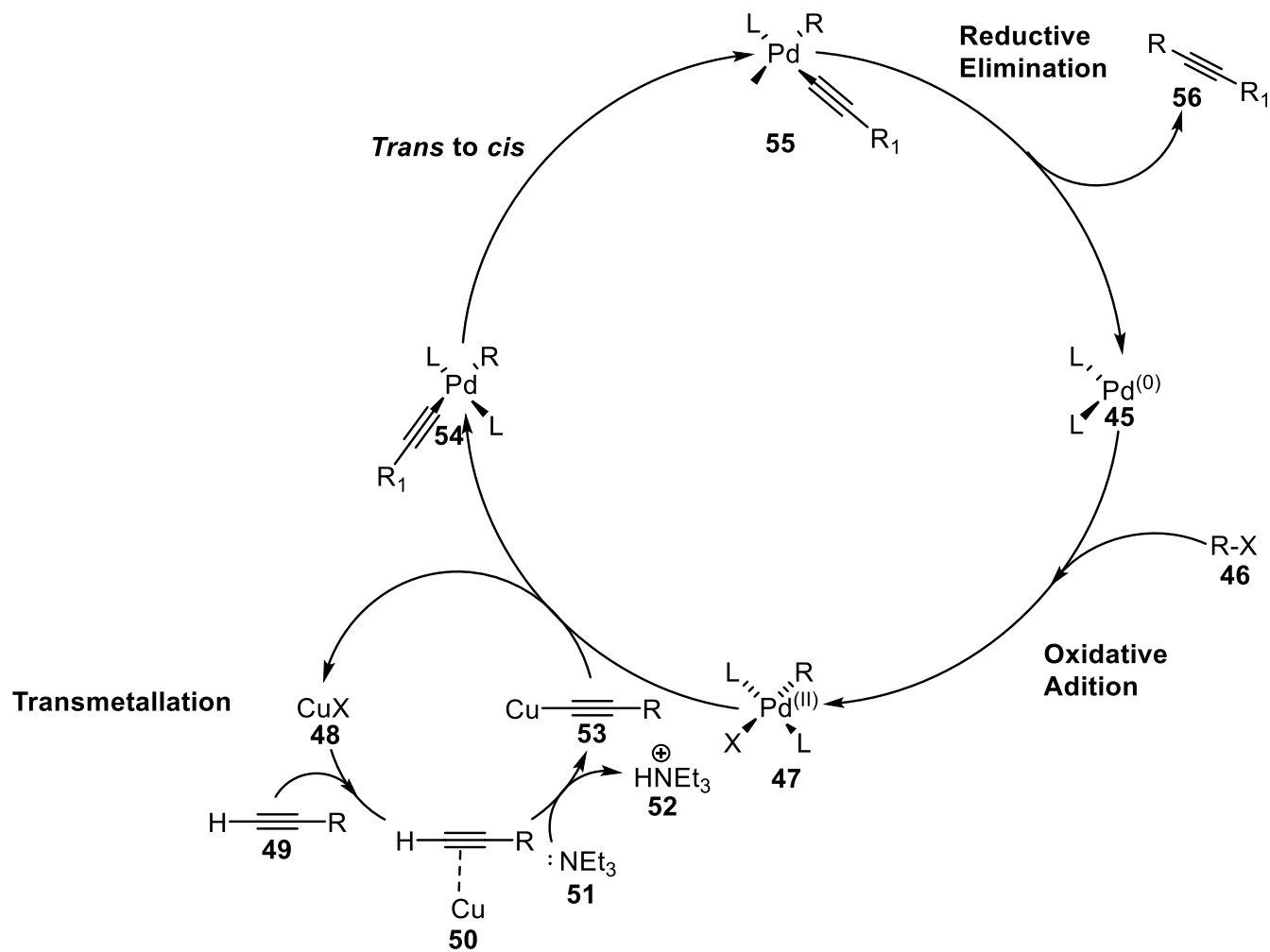
Scheme 3.13. Catalytic cycle for the Sonogashira cross-coupling reaction (Karak *et al*., 2014).

3.1.4. Tandem Sonogashira cross-coupling lactonization

In 1990, Lu and co-workers discovered, by serendipity, the selective formation of (*Z*)-*γ*-alkylidenebutenolides. They delineated the synthesis of diverse lactones, by reacting a halogenated alkenoic acid with a terminal alky under Sonogashira reaction conditions. Further investigations about the reaction's mechanism concluded that, besides the expected Sonogashira cross-coupling reaction, a lactonization (catalyzed by palladium) of the Sonogashira product **57** takes place (Scheme 3.14). With that methodology, *γ*–alkylidenebutenolides (**60**) were obtained regioselectively with the *Z* configuration, in yields above to 50% (Lu *et al*., 1990).
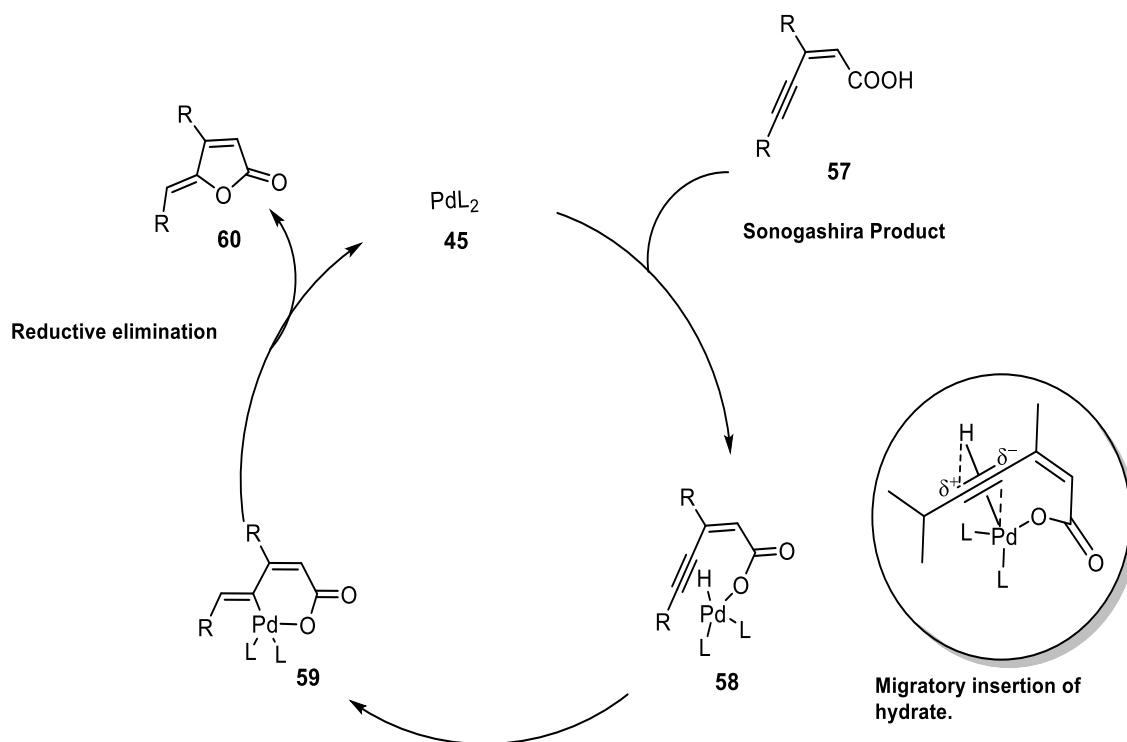
Scheme 3.14. Catalytic cycle for the tandem lactonization catalyzed by palladium.

The proposed mechanism of the lactone cyclization starts with the coordination of the Sonogashira product (intermediate **57**) with the palladium center. Next, a migratory insertion of the hydrate to the triple bond deliver the intermediate **59** (Negishi and Kotora, 1997). That is the key step of the catalytic cycle, the *Z* configuration of the butenolide core resulted from the *trans* addition of the hydrate to the triple bond related to the palladium,

for forming **59** (Scheme 3.14) (Lu *et al.* 1990). Since it was discovered, the tandem Sonogashira cross-coupling lactonization turned to be a useful reaction in organic synthesis. It enables the synthesis of variety of lactones with a selective configuration and good yields (Neguishi and Kotora, 1997).

3.1.5. Bacterial Biofilm

Bacterial resistance is an issue of great concern nowadays. In 2019, the WHO (2019) reported the death of 700.000 people caused by pharmacoresistant diseases. That issue does not only affect the human health, but also impacts various areas of agriculture (FAO, 2018). Biofilm is defined as a community of microorganism adhering to a surface (Sadekuzzaman *et al.*, 2015). Once the bacteria are associated and organized, they are able to produce a matrix comprised of polysaccharides, proteins and nucleic acids that protect them in an adverse environment (Leon *et al.*, 2015).

Biofilm structures are ubiquitous, which means that they can be formed in a variety of surfaces, such as medical implants, foods or plants. It is estimated that around 80% of bacteria exist in biofilm form (Bassak *et al.*, 2015). In addition to those concerns, it is stated that bacteria associated in biofilm formation are 1000 times less susceptible to antibiotics than their planktonic counterpart (Leon *et al.*, 2015). That resistance is directly related to a change of gene expression that happens when they switch from the planktonic to the sessile form. According to Wen and colleagues, the cycle of biofilm formation can be described in the following steps: i) initial reversible attachment of planktonic cells; ii) transition from reversible to irreversible attachment; iii) early development of biofilm architecture; iv) development of microcolonies into mature biofilms; v) dispersion of cells from the biofilm to return to the planktonic state (Wen *et al.* 2014).

3.1.6. Quorum sensing

Biofilm formation is a process that depends of the chemical communication process among bacteria known as quorum sensing. Such communication is possible thanks to the ability of the pathogens to release and detect a specific type of compounds, known as autoinducers. Many investigations have proved that, once the concentration of those autoinducers reach certain level, the bacteria can detect each other and switch their gene transcription (Figure 3.3). The changes on the gene transcription let those microorganisms organize themselves as a colon. Besides biofilm formation, quorum sensing communication regulates other processes in bacteria, such as virulence factor and bioluminescence (Bassler *et al.*, 1990).
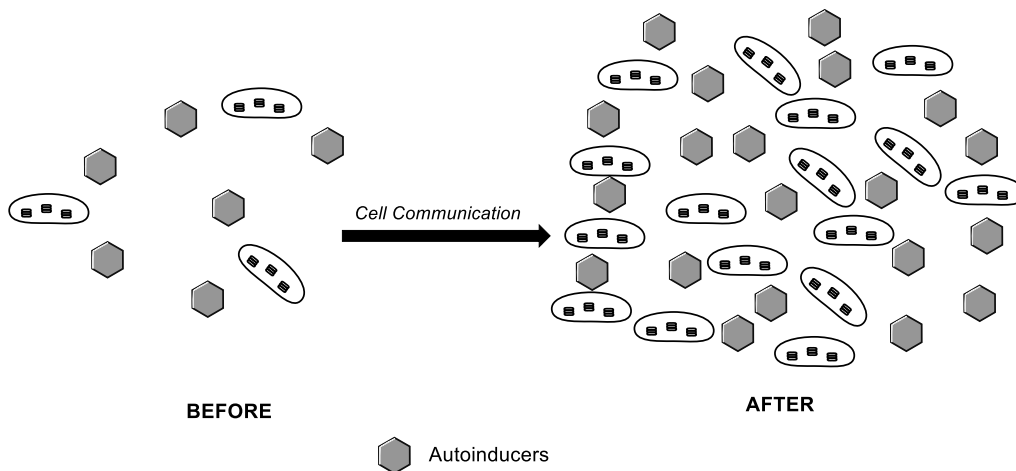
Figure 3.3. Quorum sensing communication in bacteria.

Researches in the recent years have focused on how quorum signaling system works. As discussed before, those pathways are mediated by autoinducers. Galloway and colleagues define them as "small diffusible molecules that are synthesized intracellularly and released into the surrounding milieu" (Galloway *et al.*, 2008). There are several systems that regulate the quorum sensing signaling, but, until now, two of them are well understood. Those systems are regulated by *N*-acylated-L-homoserine lactones derivatives (AI-1) and furanosyl borate diesters (AI-2) (Figure 3.4) (Pen and Ren, 2009).

X= O, OH or O
R= alkyl chain

61

62
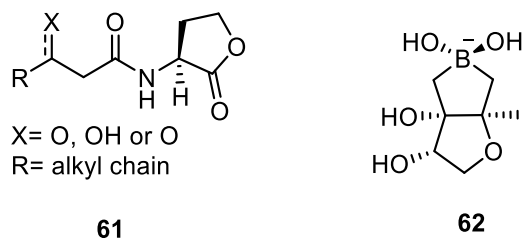
Figure 3.4. Some examples of autoinducers. *N*-acylated-L-homoserine lactone derivatives and AI-1 mediators in *Vibrio fischeri* (**61**). S-THMF-Borate AI-2 regulator in *Vibrio harveyi* (**62**).

Quorum sensing regulated by AI-1 is found in Gram-negative bacteria and plays a key role in intra specie communication. The AI-1 is produced by LuxS enzyme and the autoinducers are synthesized from S-adenosyl methionine and the proper charged acyl carrier protein (Manefield et al., 1999). At the moment that the compound is released to the environment, it can be detected by LuxR type receptor protein (Figure 3.5).
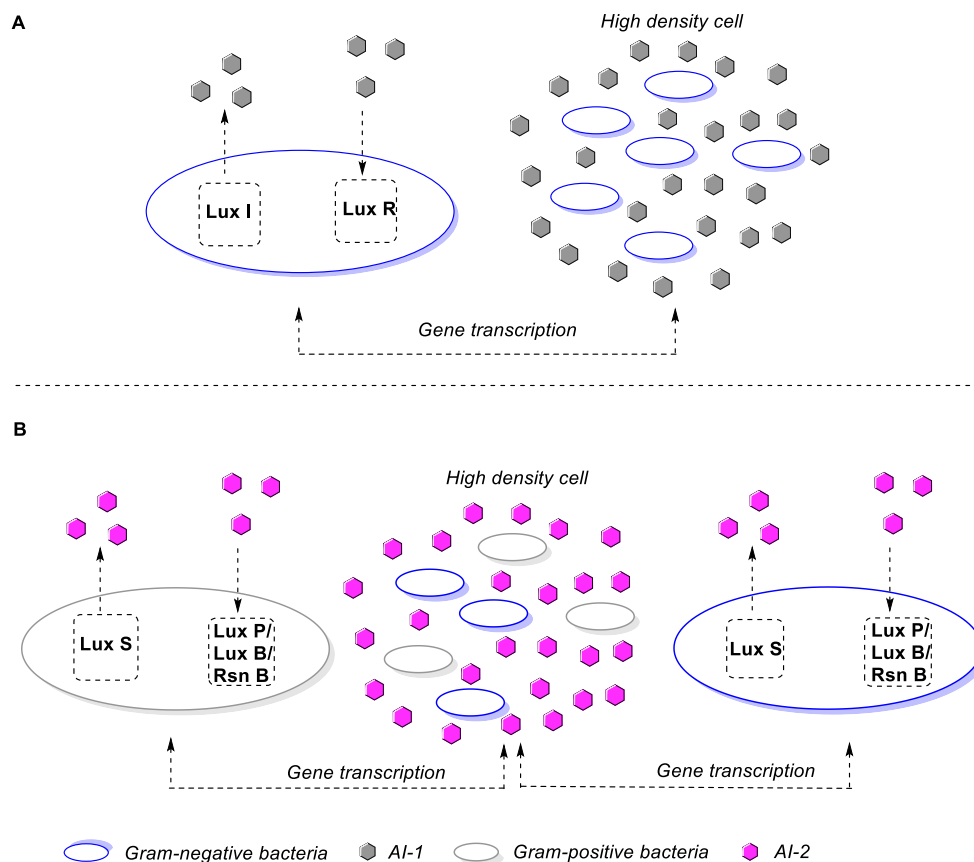
Figure 3.5. Quorum sensing communication via AI-1 path (**A**). Quorum sensing communication via AI-2 path (**B**).

The main difference between A-I and AI-2 systems is that the last one is found in both Gram-positive and Gram-negative bacteria. Hence, the AI-2 system is responsible for interspecies communication via quorum sensing (Kaur *et al.*, 2019). Towards its biosynthesis, AI-2 compounds are produced by the enzyme LuxS. That metalloenzyme synthesizes 4,5-dihydroxypentene-2,3-dione (DPD), that, via spontaneous rearrangement, is transformed in derivatives of DPD, which co-exists in an equilibrium known as AI-2 pool (Geske *et al.*, 2008). Concerning their signaling, there are three characterized proteins that bind with AI-2 autoinducers: LuxP, LuxB and RsnB (Figure 3.5)

Since its discovery, the interception of quorum sensing communication has raised as an alternative strategy to develop new therapies for treating chronic infections (Bassak *et al.*, 2015). Several studies address that quorum sensing inhibitors are capable to slow the virulence factor and to reduce the biofilm formation (Sadekuzzaman *et al.*, 2015). Therefore, the host could be treated with lower doses of antibiotics or it's immune system could clear the infection (Geske *et al.*, 2008).

3.2. OBJECTIVE

Nine different methodologies have been published for the synthesis of pulchellalactam (**5**). However, its synthesis is still a challenge due to different problems like large number of steps in the synthetic routes or undesired products. For that reason, this work aims to develop a short, efficient and stereoselective route to synthesize pulchellalactam (**5**). In addition, the activity of pulchellalactam and its analogues as QS inhibitors is also evaluated.

The retrosynthetic analysis of **5** is outlined Figure 3.6, pulchellalactam (**5**) could be lightly reached via aminolysis of lactone **32a**, a common methodology for the synthesis of lactams (Pereira *et al.*, 2014). Furthermore, that butenolide could be stereoselectively synthesized *via* tandem Sonogashira cross-coupling lactonization, by reacting alkenoic acid **36a** with terminal alkyne **37a**. Such strategy has been used in the synthesis of other natural products, like xerulin (Negishi *et al.* 2000) and auricin B (Ribaucourt and Hodgson, 2016).
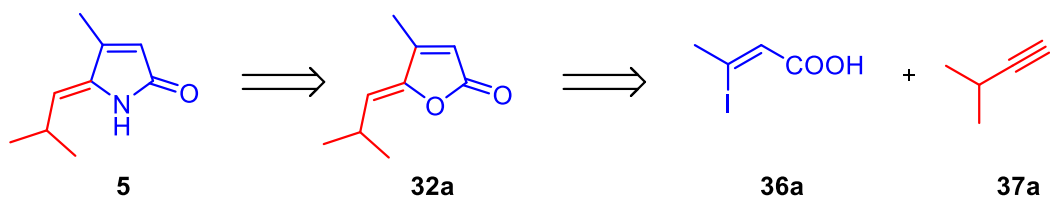
Figure 3.6. Retrosynthetic analysis of pulchellalactam.

In contrast with the many researches on synthetic routes to synthesize pulchellalactam, its biological potential is still barely studied. Until now, only pulchellalactam's activity as CD45 enzyme inhibitor is narrated in the literature (Alvi *et al.*, 1995). In this context, our research group has been studying the antibiofilm potential of different scaffolds over the years (Pereira *et al.*, 2014; Sordi *et al.*, 2018; Mayrink *et al.*, 2019). Among them, analogue lactones of rubrolides proved to be an attractive core to develop new antibiofilm inhibitors (Pereira *et al*., 2014).

Thereupon, it was decided to investigate the biofilm and quorum sensing inhibition potential of pulchellalactam. Beyond that, the tandem Sonogashira cross-coupling lactonization reaction enables the easy access to a variety of butenolides, which are also analysed as antibiofilm and quorum sensing inhibitors in this research.

3.3. RESULTS AND DISCUSSION

3.3.1. Synthesis of (Z)-3-Iodobut-2-enoic acid (**36a**)

Although it is commercially available, (*Z*)-3-Iodobut-2-enoic (**36a**) was easily synthesized by hydroiodination of but-2-ynoic acid (**63a**). Moreover, with that methodology, two other *Z*-iodoalkenoic acids were prepared for the synthesis of further butenolides. The *Z* configuration of the alkenes was fundamental for such approach, as it made possible the lactonization that leaded to the butenolide intermediate with the desired configuration (Scheme 3.15).

63a R= CH$_3$
63b R= CH$_2$CH$_3$
63c R= CH$_2$CH$_2$CH$_3$

36a R= CH$_3$, 83%
36b R= CH$_2$CH$_3$, 65%
36c R= CH$_2$CH$_2$CH$_3$, 55%
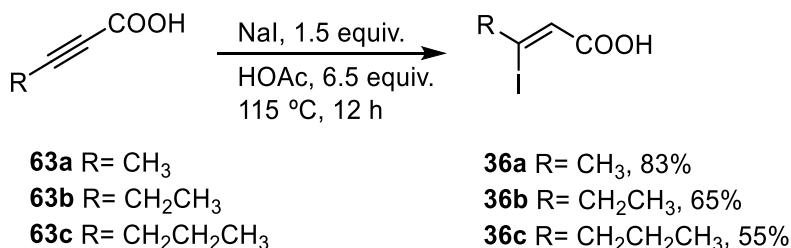
Scheme 3.15. Hydroiodination of alkynoic acids (**63a-c**).

Hydroiodination of alkynoic acids with NaI, in presence of acetic acid, is a common methodology for the selective synthesis of the *Z* isomer (Piers *et al.*, 1990). Such selectivity can be explained because of the *trans*-addition of H-X to the triple bond (Figure 3.7). Several studies about the kinetic of that reaction confirmed the nucleophilic attack of the halide ion as the rate limiting step of the mechanism (Bowden and Price, 1970). That attack lead to the formation of a vinylic carbanion intermediate. In the case of the carbanion that afford *E* isomer, the intermediate is destabilized in reason to the electronic repulsion between the lone pair of electrons of the carbon and the electronic cloud of iodine (Figure 3.7). As expected, the formation of a more stable intermediate during the *trans* addition explains the stereoselectivity to the *Z*-isomer of that reaction (Ma *et al.*, 1990).
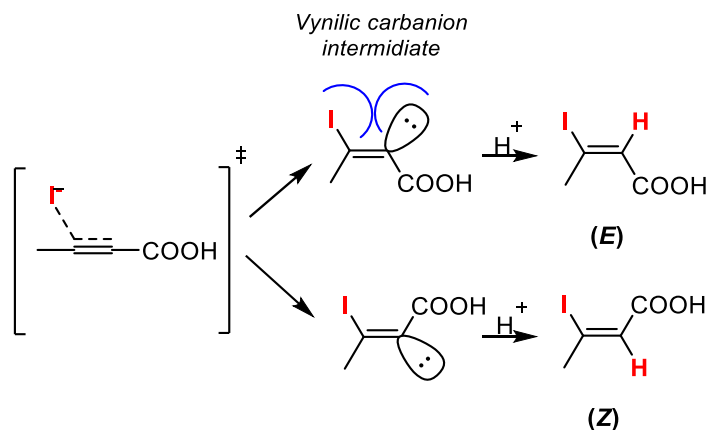
Figure 3.7. Nucleophilic addition of iodine to but-2-ynoic acid.

The product was obtained after 12 h of reaction as a white solid (83% yield) and its structure was corroborated by spectroscopic techniques. The obtained results were compared with the previous data reported in literature (Arbarbi *et al*., 2002). In the ^{1}H-NMR spectrum, two signals are observed: a singlet at 2.78 ppm, related to the hydrogens of

94

the methyl group, and the other a doublet at 6.37 ppm ($J_{4\text{-}2}$= 1.0 Hz), associated with the hydrogen of the position 2 (Figure 3.8). Meantime, the ^{13}C-NMR spectrum showed the signal associated with the carboxylic carbon at 168.31 ppm (Figure 3.9). The presence of the carboxylic group was also confirmed by the broad band between 2500-3500 cm^{-1} observed through the infrared spectra (See appendix related to chapter 3, Figure 3.1.A.)
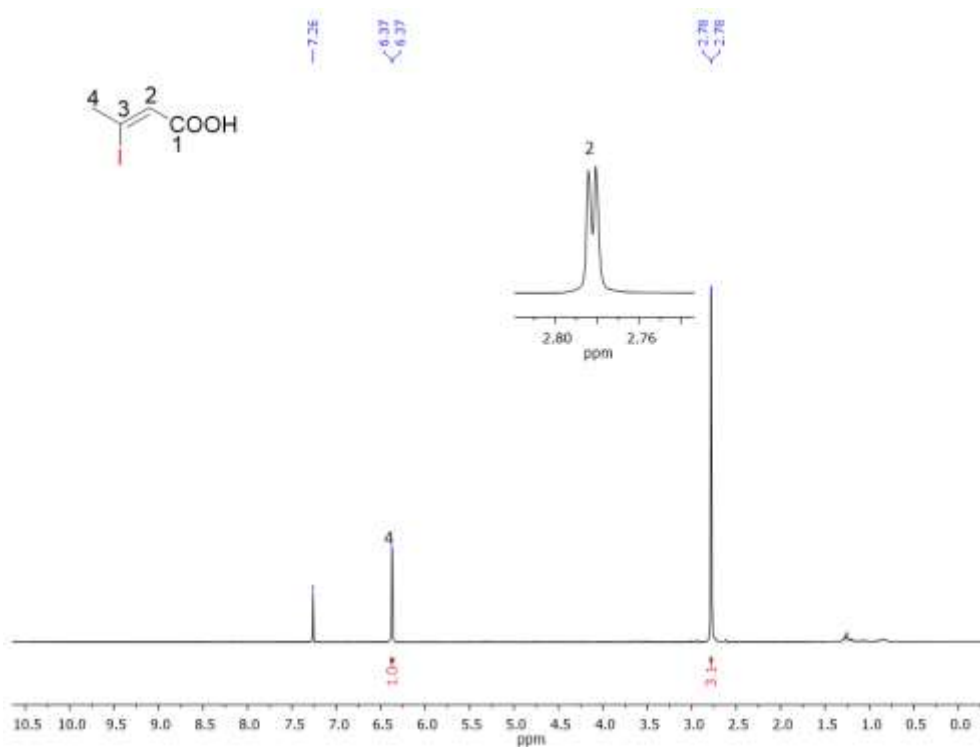
Figure 3.8. ^{1}H-NMR (400 MHz, CDCl$_3$) of (*Z*)-3-iodobut-2-enoic acid **(36a).**
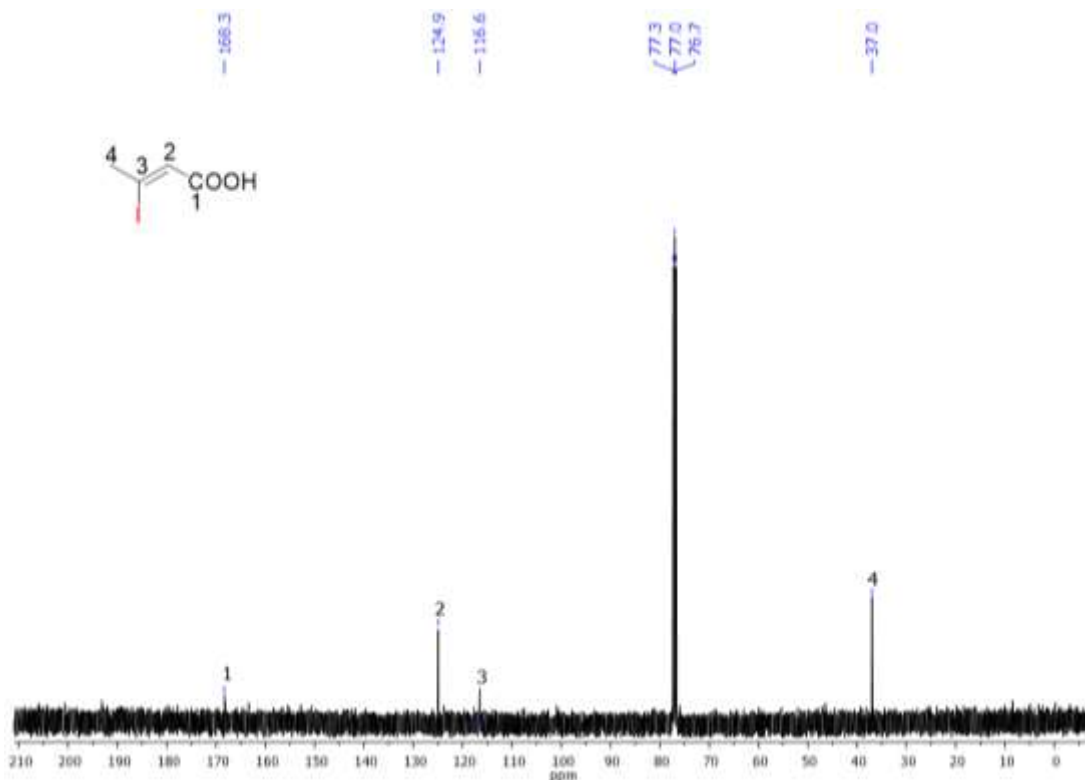
Figure 3.9. ^{13}C-NMR (100 MHz, CDCl$_3$) of (*Z*)-3-iodobut-2-enoic acid **(63a).**

As mentioned above, compounds **36b** and **36c** were synthesized using the same methodology implemented to prepare **36a.** A comparative analysis of the ^{1}H-NMR spectra of the three compounds proved that chemical shift of the hydrogen at position 2 was similar in the three cases (Figure 3.10). In the specific case of compound **36c**, it was previously synthesized by Abarbri and co-workers, the spectroscopic data obtained in this work matched with the results obtained bay these researchers (Arbarbi *et al.*, 2002). These observations corroborated the *Z* configuration of the three iodo-alkenoic acids.
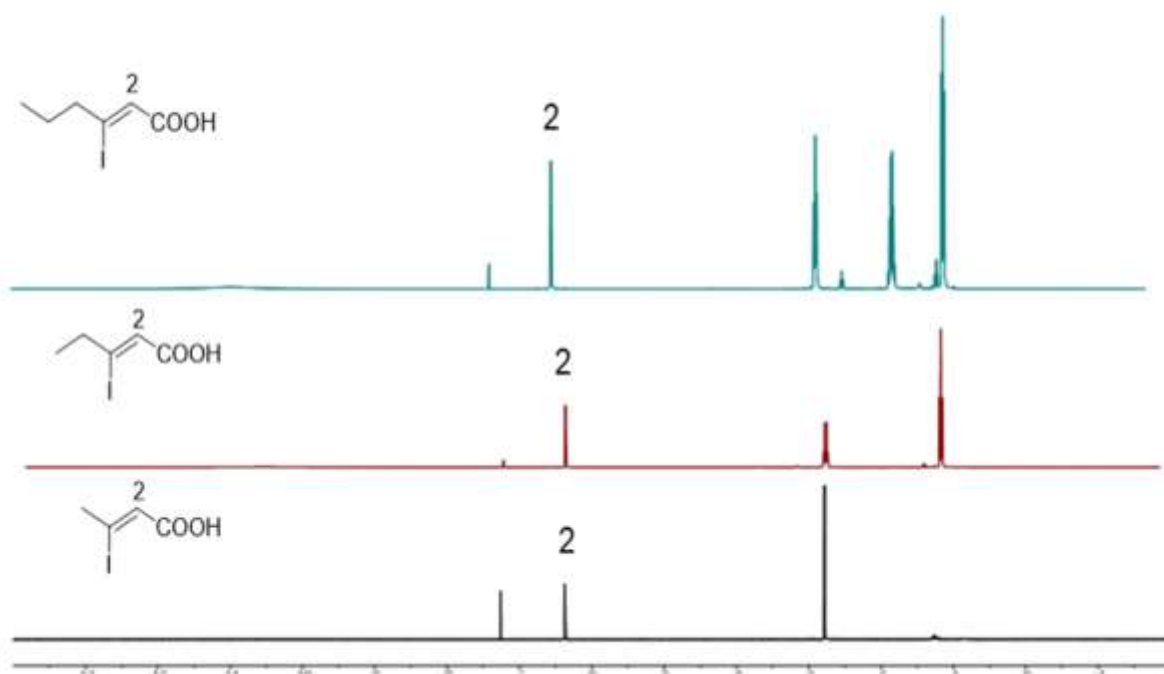
Figure 3.10. Comparison between ^{1}H-NMR spectra of compounds **36a**, **36b** and **36c.**

The three intermediates were obtained in yields above 50%. Besides that, no traces of the *E*-isomer were isolated and the products were purified by recrystallization. Thus, hydroidoination of alkenoic acid is a useful reaction to be used in synthetic planning strategies. That simple reaction facilitates an easy access to synthetic intermediates with a selective Z configuration and different functional groups in its structure.

3.3.2. Synthesis of (Z)-4-methyl-5-(2-methylpropylidene)furan-2(5H)-one (**32a**)

With intermediate **36a** in hand, the synthesis of butenolide **32a** was carried out. As explained in the synthetic proposal, Sonogashira cross-coupling lactonization for the synthesis of pivotal intermediate **36a** is the key step for the synthetic route. That strategy provided, selectively, the desired intermediate with *Z* configuration of the required lactone, without the utilization of any protecting group.

Initially, the synthesis of butenolide **32a** was executed under the conditions reported in the total synthesis of auricin B. In that case, initial Sonogashira reaction of **36a** with **37a** was made using 1 mol% of PdCl$_2$(PPh$_3$)$_2$ and 2 mol% of CuI as catalyst, at room temperature (Ribaucourt and Hodgson, 2016). Unexpectedly, those conditions did not result

in the required product. Therefore, it was decided to increase the amounts of catalyst in the reaction (5 mol% of PdCl$_2$(Ph$_3$)$_2$ and 10 mol% of CuI). Under those conditions, compound **32a** was obtained in 27% of yield (Figure 3.11).
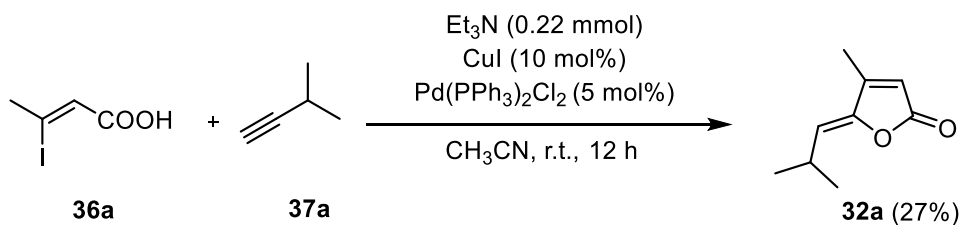
Figure 3.11. Initial conditions for the synthesis of lactone **32a.**

The structure of **32a** was corroborated by spectroscopic technics. In the infrared spectrum presented in Figure 3.12, two bands 1772 cm^{-1} and 1752 cm^{-1} are observed. The first one is related to the C=O vibration, while the second is consequence of the Fermi resonance (Pavia *et al.*, 2009). The presence of that band is common for lactones with substituents at the β-position (Barbosa, 2013).
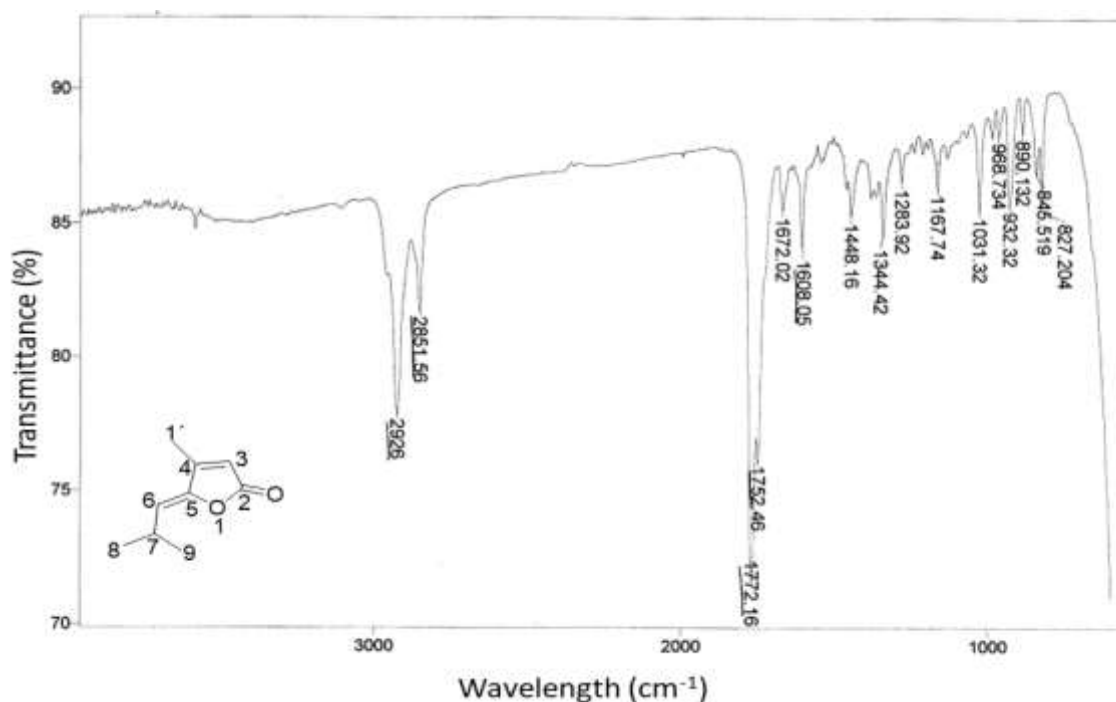
Figure 3.12. IR spectrum (NaCl film) of butenolide **32a.**

The ^{1}H-NMR spectrum of butenolide **32a** is presented on Figure 3.13**.** At 1.08 ppm, it is observed a doublet that integrates to 6 hydrogens. That signal is associated to the methyl hydrogens of the positions 8 and 9. The next signal, a singlet at 2.11 ppm, is related to the hydrogens of methyl of the position 1´, while at 2.99 ppm is found a double of septept assigned to the hydrogen methyne of position 7. Lastly, at 5.15 (d, $J_{6,7}$ = 9.6 Hz) ppm there is a doublet related to hydrogen 6 and, at 5.88 ppm, it is found a singlet associated to hydrogen of position 3.
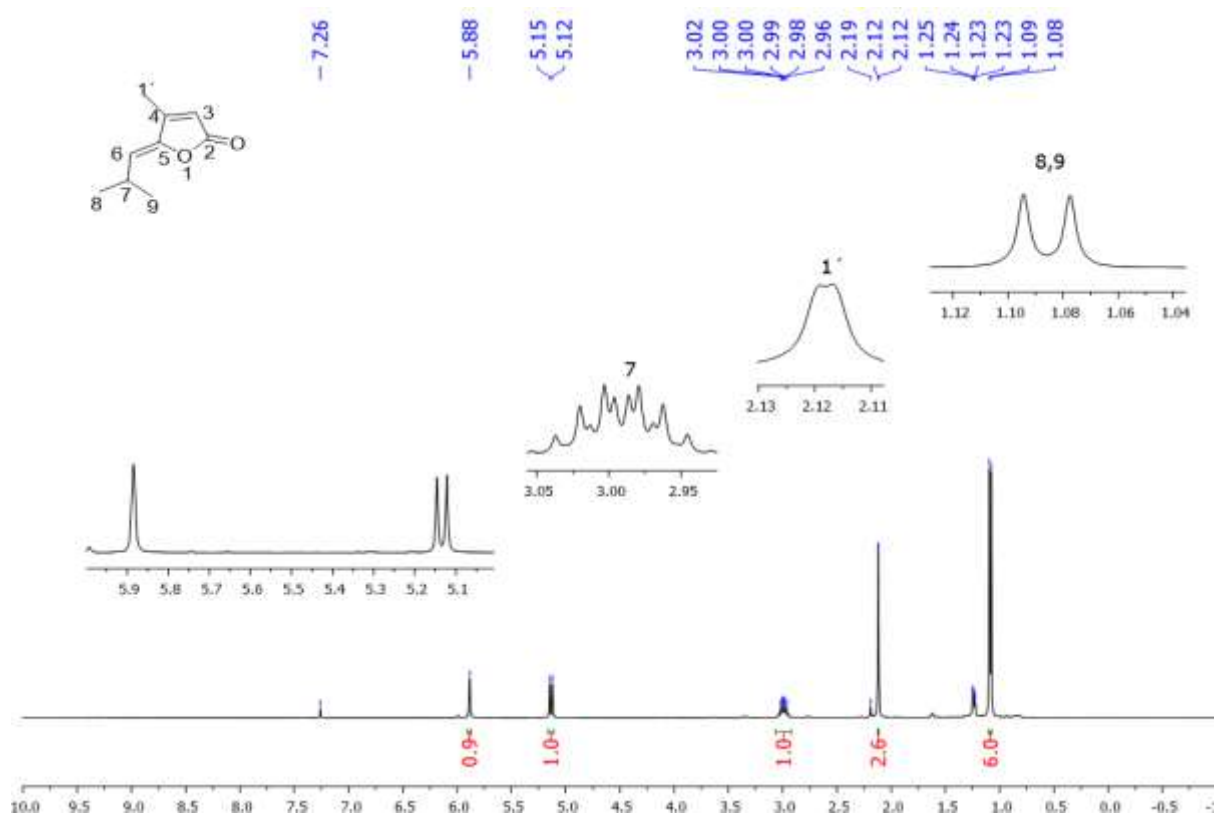
Figure 3.13. ^{1}H-NMR (400 MHz, CDCl$_3$) of (*Z*)-4-methyl-5-(2-methylpropylidene)furan-2(5*H*)-one (**32a**).
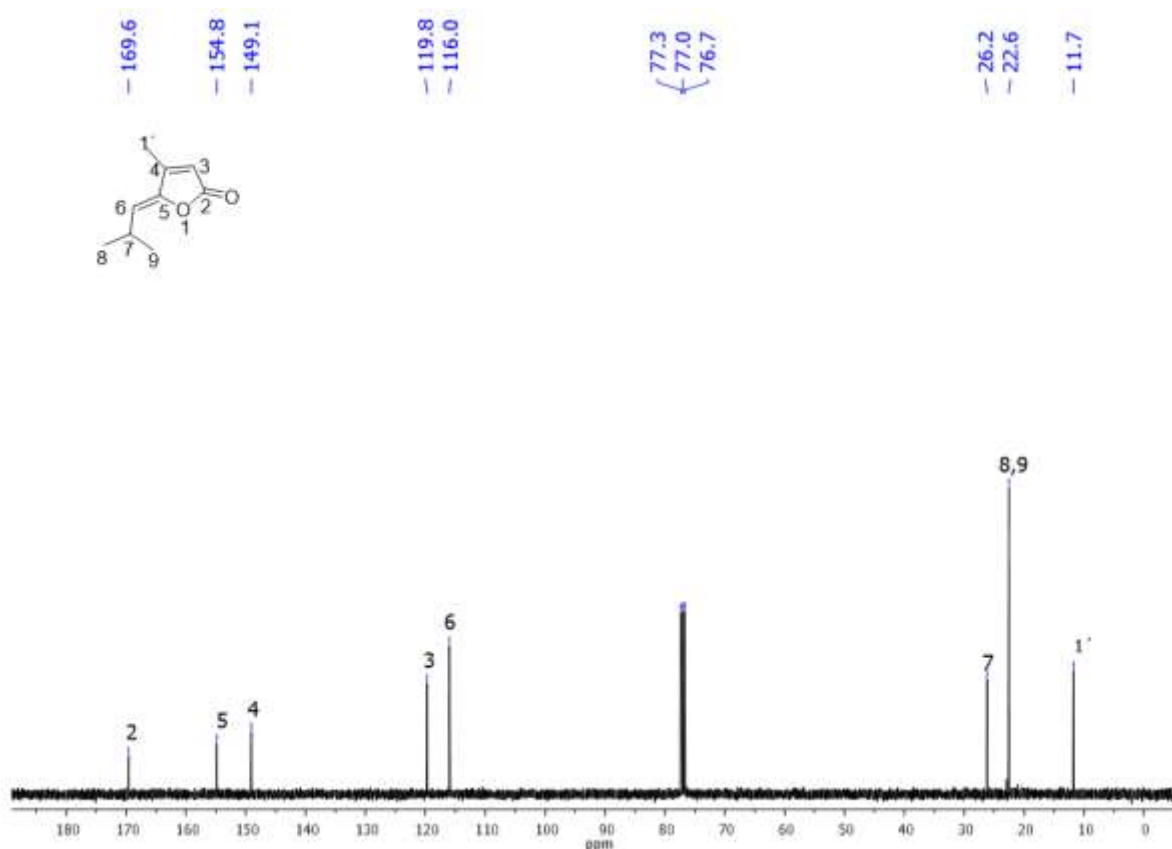
Figure 3.14. ^{13}C-NMR (100 MHz, CDCl$_3$) of (*Z*)-4-methyl-5-(2-methylpropylidene)furan-2(5*H*)-one (**32a**).

Through the spectrum of ^{13}C-NMR (Figure 3.14), a total of 8 signals is observed. The first one, at 11.7 ppm, is assigned to the methyl of the position 1´. After that, at 22.6 ppm, the signal is related to the methyl groups at positions 8 and 9. At 26.2 ppm it is located the signal associated to carbon 7. The carbon signals of positions 6 and 3 are observed at 116.0 and 119.7 ppm, respectively. At 149.1 ppm and 154.8 ppm, there are located the signals assigned to carbons 4 and 5, accordingly. Ultimately, the signal of the carbonyl carbon of the lactone core is found at 169.5 ppm. This compound was previously synthesized by Felluga and co-workers, comparison between their results and the data reported in this work is found in Table 3.1A (pg. 182)

As mentioned, in the first attempt to synthesize butenolide **32a,** the compound was obtained in only 27% of yield (Table 3.1, entry1). In order to improve that result, an optimization of the reaction conditions was performed. Table 3.1 presents the results obtained in those experiments.

Table 3.1. Optimization conditions for the synthesis of **32a**[a].

Entry	Catalyst	Solvent	37a (mmol)	Base (mmol)	Yield (%)
1	A	CH_3CN	1.1	Et_3N (0.22)	27
2	A	CH_3CN	1.1	Et_3N (0.66)	63
3	A	CH_3CN	1.1	DIPEA (0.66)	42
4	A	CH_3CN	1.1	DIPEA (0.22)	
5	A	CH_3CN	1.1	$i\text{-}Pr_2NH$ (0.66)	57
6	A	CH_3CN	0.66	Et_3N (0.66)	13
7	A	CH_3CN	2.2	Et_3N (0.66)	42
8	A	1,4-Dioxane	1.1	Et_3N (0.66)	40
9	A	DMF	1.1	Et_3N (0.66)	48
10	A	THF	1.1	Et_3N (0.66)	67
11	B	THF	1.1	Et_3N (0.66)	36
12	C	THF	1.1	Et_3N (0.66)	-
13	D	THF	1.1	Et_3N (0.66)	42
14	E	THF	1.1	Et_3N (0.66)	10
15	F	THF	1.1	Et_3N (0.66)	5

[a] All reactions were conducted at 25-28 °, employing 0.22 mmol of **36a** in 1.5 mL of solvent, for 12 hours. [b] Catalyst A: 5 mol% $PdCl_2(PPh_3)_2$ and 10 mol% CuI. as catalysts; catalyst B: 5 mol% $Pd(PPh_3)_4$ and 10 mol% CuI; catalyst C: 5 mol% $PdCl_2(PPh_3)_2$; catalyst D: 20 mol% CuI; catalyst E: 10 mol% CuI; catalyst F: 5 mol% CuI.

The quantity of base used during the reaction had an important effect in the yield. Increasing the amount of base from 0.22 to 0.66 equivalent resulted in a significant improvement of the reaction yield (Table 3.2, 63% entry 2 and 57% entry 5). On the other hand, the structure of each amine must also be considered to analyze these results.

Basicity of triethylamine is favored due to the inductive effects caused by alkyl groups of its structure. Alkyl substituents, are electron releasing groups, therefore, they are able to donate negative density charge the nitrogen lone pair through the σ-bonds (Clayden *et al.*, 2006). In contrast, the good yield obtained with *i*-Pr₂NH can be connected to the stability of its conjugated acid in the reaction medium. Considering that acetonitrile have an high dielectric constants (38.8) is plausible that this solvent is able to easily stabilize charged species.(Reichard and Welton, 2008). Finally, the decrease of the yield observed when DIPEA was used as base might be related to steric effects associated with the bulky substituents present in its structure (Clayden *et al.*, 2006).

Further experiments (Table 3.1) disclosed that reducing the amount of alkyne (from 1.10 mmol to 0.66 mmol) or increasing it (to 2.20 mmol) was detrimental for the reaction (Table 3.1, entries 6 and 7, respectively). This last result could be connected to the formation of dimeric diacetylene as a side product (Karak *et al.*, 2014; Sonogashira, 2002). The dimer **67** is formed via Glasser coupling, a common side reaction in Sonogashira reaction (Kurti*et al.*, 2005). The proposed mechanism for the Glasser reaction starts with the formation of several copper complexes, which leads to the dimeric copper acetylide **74** (Scheme 3.16). The formation of that intermediate is the rate limiting step of the reaction, that responds to a second order kinetics (Hen *et al.*, 2008). Although it was not possible to isolate or characterize the dimeric form of acetylene **37a**, the side product of others substituted acetylenes were isolated and characterized in yields between 5% and 20%, in the synthesis of analogues of butenolide **32a**.
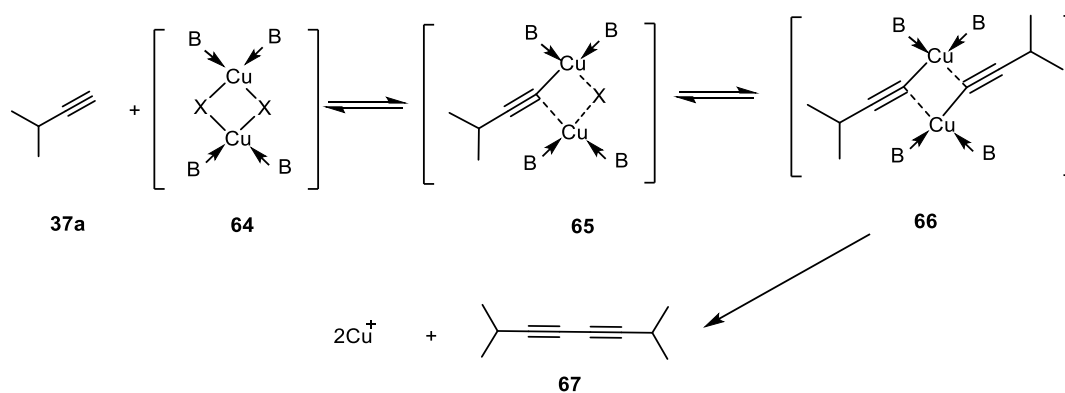
Scheme 3.16. Mechanistic proposal for the Glasser coupling reaction.

The effect of the solvent in the reaction was another parameter evaluated during the optimization. Acetonitrile, 1,4-dioxane, tetrahydrofuran and *N,N*-dimethylformamide were the selected items for the screening. Neither dioxane nor *N,N*-dimethylformamide provoked improvement in the reaction yield (Table 3.1 entries 8 and 9). In the specific case o *N,N*-dimethylformamide the low yield was related with the low solubility of the reagents in the reaction medium. In the contrary, acetonitrile (Table 3.1, entry 2) and tetrahydrofuran (Table 3.1, entry 10) were the best choices to synthesize compound **32a.** The reaction with acetonitrile afforded the butenolide **32a** in a yield of 63%, but, with THF, the yield was slightly improved to 67%.

After establishing the best conditions in terms of base, substrate and solvent (entry 10, Table 3.1), the effect of the catalyst was the last parameter evaluated. It is a key factor for the tandem Sonogashira cross-coupling lactonization, as all mechanisms depend on the coordination of the alkyne with the metallic center. By the results displayed on Table 3.1, it is possible to infer that, indeed, the catalyst is the most relevant effect for the reaction.

For that optimization, the complexes $Pd(PPh_3)_2Cl_2$ and $Pd(PPh_3)_4$ were selected as palladium source. In both cases, the concentration of the catalyst precursor was 5 mol% and the co-catalyst concentration (CuI) was 10 mol%. In the best results, it was accomplished 67%, using $Pd(PPh_3)_2Cl_2$. On the other hand, the utilization of $Pd(PPh_3)_4$ decreased drastically the yield to 36% (Table 3.2, entries 10 and 11).

The several difference between those results might be linked to the formation of the catalytically active species in the reaction medium. In the case of $Pd(PPh_3)_2Cl_2$, the specie is formed via reductive elimination of the complex. Some authors propose a catalytic cycle with participation of the copper and the terminal acetylene, as showed on the Scheme 3.17. A transmetallation process between copper and palladium lead to the formation of intermediate **74.** Additional reductive elimination of that complex delivers the desired Pd (0), which starts the Sonogashira cross coupling (Negishi, 2002).
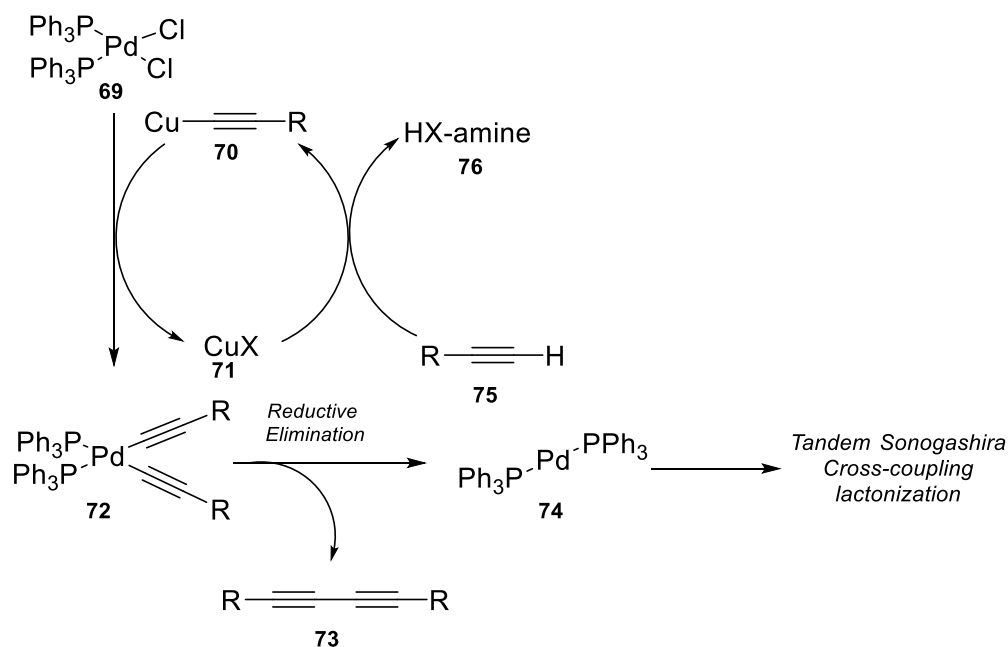
Scheme 3.17. Mechanistic proposal for the formation of the catalytically active specie from the reductive elimination of $PdCl_2(PPh_3)_2$ (Negishi, 2002).

Nevertheless, when $Pd(PPh_3)_4$ is used as pre-catalyst, the catalytically active specie is formed by dissociation of the complex, as presented on Scheme 3.18. Fauvarque and Pelluger implemented studies about the kinetic reaction of the oxidative addition of aryl bromides to $Pd(Ph_3)_4$. They found that dissociation of $Pd(Ph_3)_4$ is the faster step in the mechanism. As well, the preequilibrium is dislocated to the left, as complex **78** is a more stable specie that meet the 16-electron rule (Fauvarque and Pelluger, 1981*).*
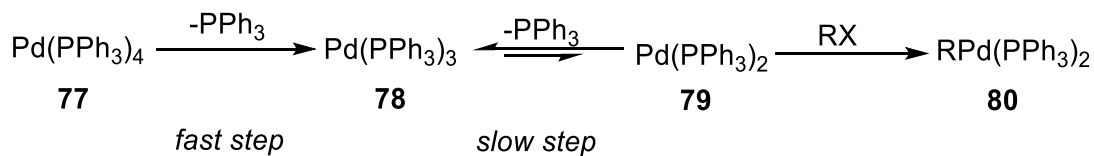
Scheme 3.18. Mechanistic proposal for the formation of the catalytically active specie from the dissociation of $Pd(PPh_3)_4$ (Fauvarque and Pelluger, 1981).

As already elucidated, this last mechanistic proposal explains the results obtained in the optimization. The good reaction yield, 67%, obtained when Pd(PPh$_3$)$_2$Cl$_2$ is employed as pre-catalyst, may due to the formation of the Pd(0), by the reductive elimination of the catalytic cycle (Scheme 3.17). However, the low yield (36%), obtained when the reaction was accomplished with Pd(PPh$_3$)$_4$, could be explained by the unfavorable equilibrium in the dissociation of Pd(PPh$_3$)$_3$ into the catalytically active specie.

Other important factor studied in that optimization was the effect of the co-catalyst on the reaction. Even though the presence of copper is very important for such reactions, there are several reports of successful Sonogashira cross-couplings using only Palladium in the reaction (Anastasia *et al.*, 2002). Based on that, it was decided to attempt the reaction without the presence of CuI. Unfortunately, under those conditions, the product was not formed.

One explanation of why copper iodide is so important in that reaction is the nucleophilicity of acetylide specie (Scheme 3.13). Without its complexation with Cu, the specie is not nucleophilic enough to coordinate with the palladium center. Consequently, the formation of the copper acetylide affords a more powerful nucleophile, that enables such coordination via transmetallation process. In fact, kinetic investigations about the Sonogashira cross-coupling have demonstrated that transmetallation is the rate-limiting step for that type of cross coupling reactions (He *et al.*, 2013).

Finally, the other approach studied in the screening was the utilization of CuI as the only catalyst in the reaction medium (Inack-ngi *et al.*, 2009). The compound was employed at three different concentrations: 5 mol%, 10 mol% and 20 mol%. Among them, the use of 20 mol% of CuI affords the desired product in the highest yield: 42% (Table 3.2, entry 13).

Scheme 3.19 shows the mechanistic proposal for that reaction (Idham *et al.*, 2016). The cycle starts with the oxidative addition of copper iodide by the insertion of (*Z*)-3-Iodobut-2-enoic acid to obtain intermediate **83.** After that, the alkyne is added to the coordination sphere of the metallic center. Reductive elimination yields the intermediate **85** that cyclizes to form the compound **86**. The final step is a protodemetallation that affords butenolide **32a**.
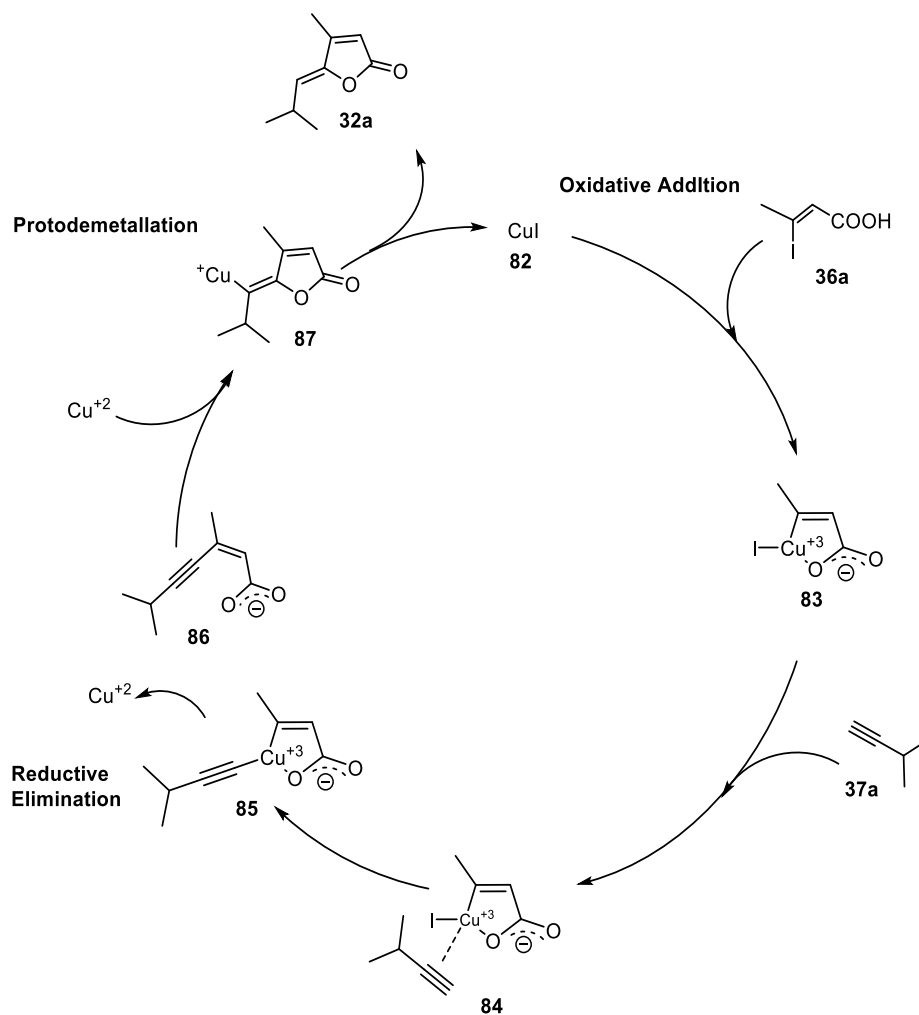
Scheme 3.19. Catalytic cycle for the tandem Sonogashira-lactonization catalyzed by Copper (Idham *et al.*, 2016).

As result of that optimization, pivotal intermediate **32a** was successfully synthesized in 67% yield. Such accomplishment was based on employing the conditions of entry 10 (Table 3.2). Among all parameters studied, the effect of the catalyst seems to be the most preponderant factor for the reaction.

3.3.4. Aminolysis of (Z)-4-methyl-5-(2-methylpropylidene)furan-2(5H)-one (**32a**)

The last step for the synthesis of pulchellalactam was the aminolysis of lactone **32a**. To reach the natural product, butenolide **32a** was treated with an aqueous solution of NH_3 (33% v/v) for 6 h, at 65 °C. The mechanism presented on Scheme 3.20 begins with the attack of a molecule of ammonia to the carbonyl carbon of the butenolide ring, to form intermediate **89.** Further collapse and rearrangement of that specie delivers the intermediate **91,** which closes again to form hydroxyl lactam **93**. In the end, dehydration of that intermediate lead to the formation of Pulchellalactam (**5**).
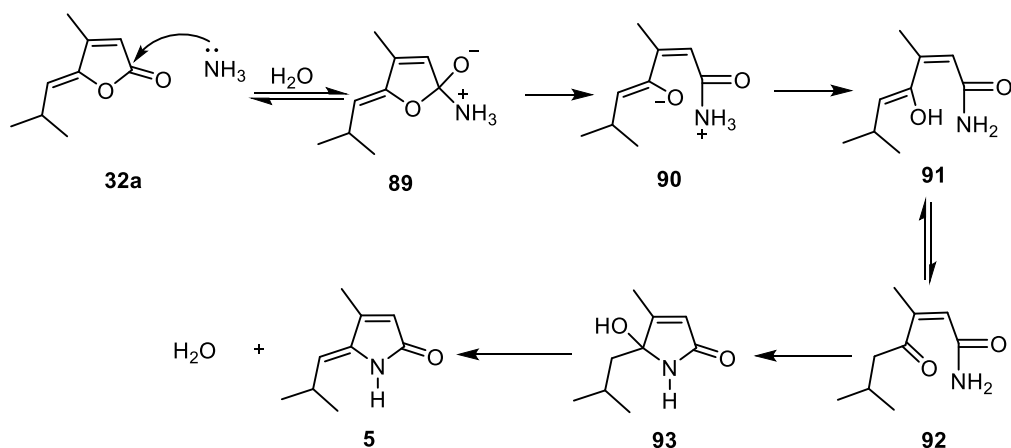
Scheme 3.20. Mechanistic proposal for the aminolysis of **32a.**

The dehydration of intermediate **93** defines the selectivity to the *Z* configuration of the natural product. That type of elimination happens via an E_2 mechanism in basic conditions. It is widely known that the reaction success requires an angle of 180 ºC between the hydroxyl and the acidic proton (*anti*-elimination) (Clayden *et al.*, 2005).

Figure 3.15 illustrates the anti-periplanar conformation that brings the formation of isomer *E* and *Z* of pulchellalactam. In the case of conformer (I), which affords the *E* isomer of the natural product, there is repulsive interaction between the isopropyl group and the methyl at the position 3 of the lactam core. In opposition, the interactions among the substituents of the lactam ring are less destabilizing in the conformer II. That my might be the explanation for the complete selectivity to the *Z* isomer formation of pulchellalactam.
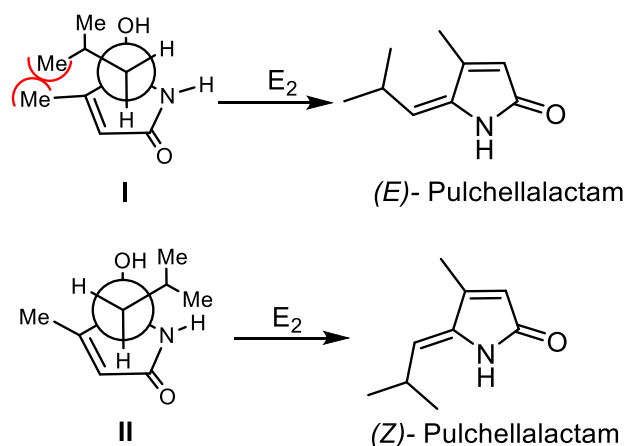
Figure 3.15. Anti-periplanar conformations that lead to the *Z* and *E* isomers of pulchellalactam (**5**).

Pulchellalactam was obtained as a colorless oil in 89% yield. Figure 3.16 presents the infrared spectrum of the natural compound. Between 3155 and 2666 cm^{-1} are found the bands characteristic of Csp^3 and N-H stretch. Still, the band associated to the C=O vibration is located at 1673 cm^{-1}.
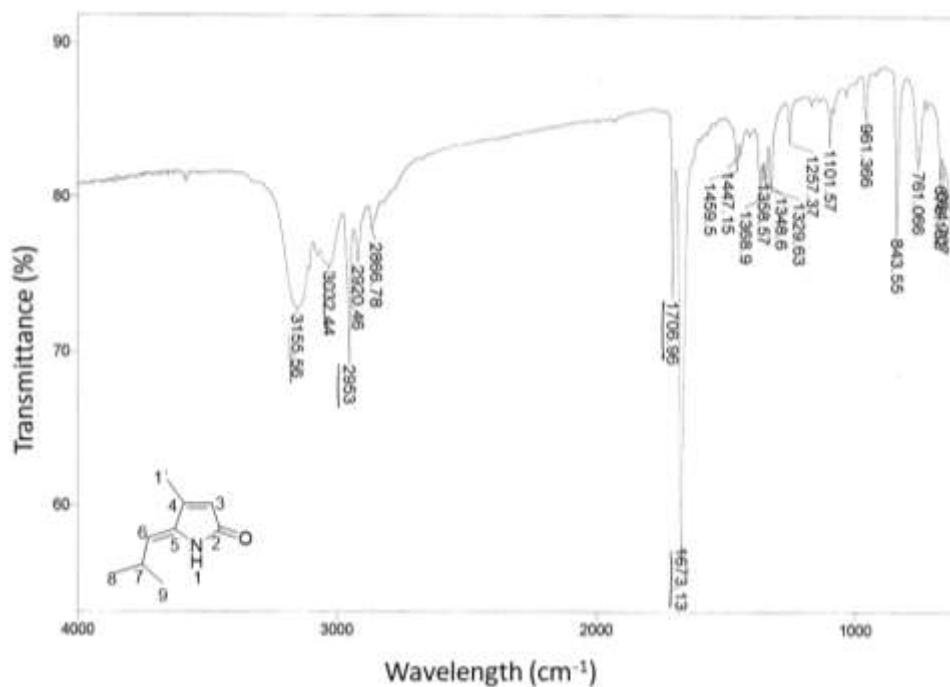
Figure 3.16. IR spectrum (NaCl film) of pulchellalactam.

Figure 3.17 shows the spectrum of ^{1}H-NMR of the natural product. A doublet at 1.09 ppm integrates for six hydrogens and is related to the methyl groups at position 8 and 9. In a row, a singlet 2.07 ppm is associated to methyl of position 3, while the multiple at 2.64 ppm is connected to the hydrogen of position 7. The signals at 5.12 ppm ($J_{6-7}= 9.7Hz$) and 5.86 correspond to the hydrogens at the positions 3 and 6. Then, the singlet at 8.39 ppm is linked to the of the lactam group (position 1).
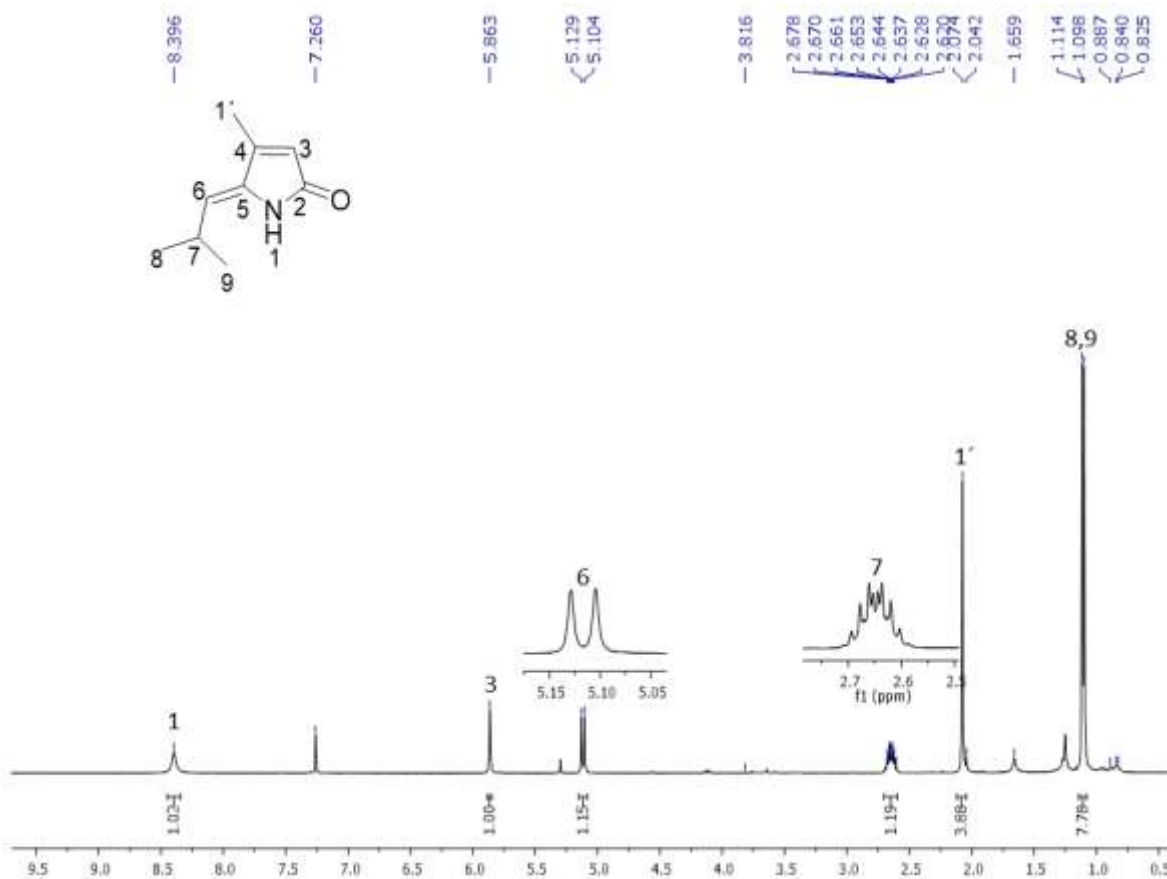
Figure 3.17. ^{1}H NMR (400 MHz, CDCl$_3$) of pulchellalactam (**5.**)

The ^{13}C-NMR presents a total of 8 signals (Figure 3.18). The two first, at 11.9 and 22.9 ppm, are associated to the methyl gropus of the structure. The signal at 27.5 ppm is related to the CH of the positon 7. Meanwhile, signals at 119.8 and 120.8 are asigned to the

carbons of position 3 and 6 respectively. Signals at 137.4 ppm and 148.7 ppm are linked to the carbons at positons 4 and 5. Ultimately, the signal associated to the carbonilyc carbon of the lactam core is found at 172.2 ppm.
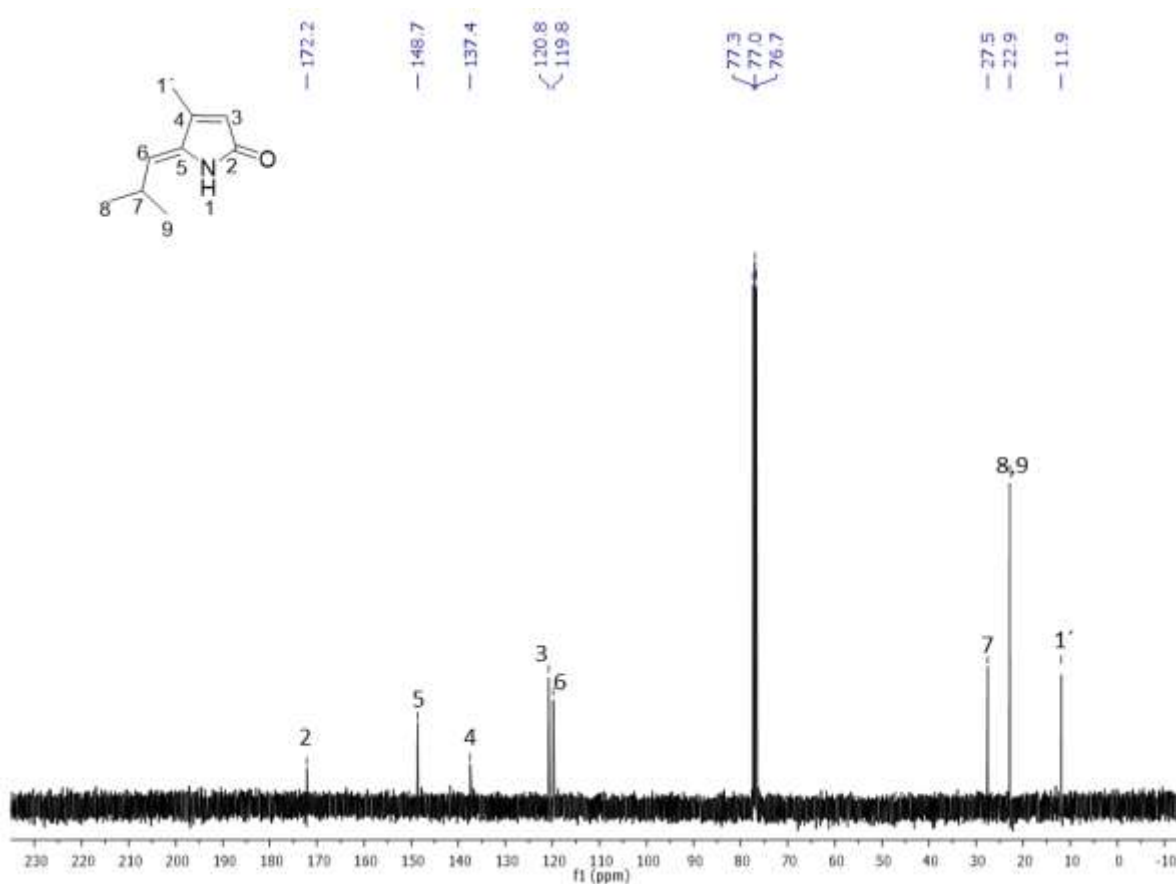
Figure 3.18. ^{13}C-NMR (100 MHz, CDCl$_3$) of Pulchellalactam (**5**).

The spectroscopy data obtained in this work for pulchellalactam was compared with the ones reported by Li and co-workers (2002) (Table 3.2A pg.183). Both data results match with the data reported in here, confirming the structure of the compound synthesized in this study. Hence, pulchellalactam (**5**) was synthesized in two steps, starting from commercially available materials with an overall yield of 64%, the best result accomplished until now. The applied strategy allowed the obtention of the natural product stereoselectively without the use of protecting group.

The tandem Sonogashira cross-coupling lactonization is a useful reaction to obtain γ-alkylidenebutenolides with a selective *Z-* configuration. Several studies address that *Z-*configuration might be important for the biological activity of brominated lactams (Pan and Ren, 2009). With that in mind, it was resolved that the study would synthesize different analogues of butenolide **32a,** utilising the reaction conditions previously optimized. As result, twelve butenolides were achieved in yield between 22% and 69%. The results are presented on Table 3.2.

Table 3.2. Synthesis of new butenolides analogues of pulchellalactone (**32a**).
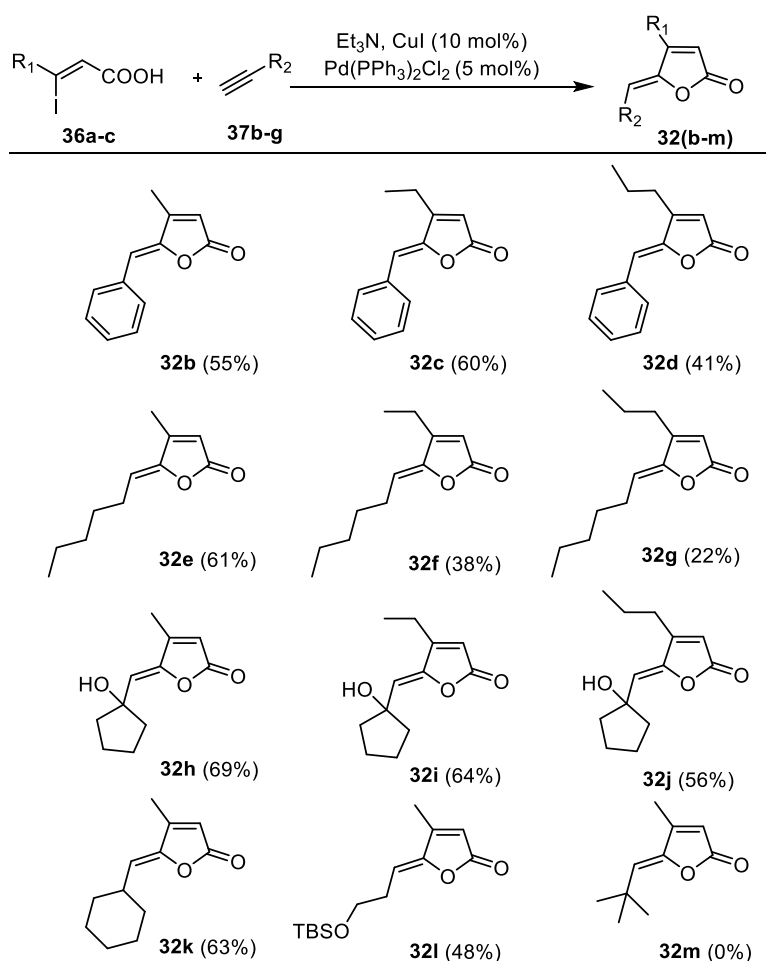
Reaction conditions: Alkenoic acid **36a-c** (0.23 mmol), alkyne **37b-g**(1.18 mmol), PdCl$_2$(PPh$_3$)$_2$ (0.012 mmol), CuI (0.02 mmol), Et$_3$N (0.71 mmol), THF (1.5 mL), r.t, 12 h. .

Initially, the aromatic butenolides **32b-d** were prepared in variable yields (41-60%) (Table 3.2). The procedure also afforded long alkyl-chain analogues **32e**-**g** (22-61%). It is clear, from the data, that the use of aliphatic long-chain alkynes as hept-1-yne afforded the required lactone **32** in good yield (61%). Yet, increasing the size of the alkyl group at β position resulted in reduced efficiency for the tandem coupling-lactonization process (**32f**, 38% and **32g**, 22%). The similar trend was observed in the case of **32b-d**, with a lowest yield communicated for **32d**, bearing a β-propyl group. Other aliphatic alkynes, bearing a cyclic moiety and an additional OH functionality, were also good substrates for the reaction, affording **32h-j** (56-69%). A simple cyclic derivative **32k** (63%) and the protected alcohol **32l** (49%) were also easily formed, but the attempted reaction of a highly hindered alkyne failed to produce **32m**.

Due to the complexity of the mechanism of the tandem Sonogashira cross- coupling lactonization, is hard to explain the difference between the yields obtained in the synthesis of the analogues. However, the presence of bulky substituents at positions 3 and 6 reduced the yield of the reaction, therefore it seems that steric factors could be important in this reaction. It is important to remember that the mechanistic preproposal for this reaction suggest the formation of different cyclic intermediates. In this context, the presence of bulky groups in the structure might difficult the formation of this intermediates due to repulsive interactions. However, more studies related with the stability and kinetic of formation of this intermediates must be carried in order to confirm this proposal.

All compounds were characterized by spectroscopy techniques. Compound **32b** was chosen to exemplify the characterization of the analogues. In regard to the IR spectrum, bands at 2928 cm^{-1} and 2851 cm^{-1} are associated to the C-H vibration in the structure, while, at 1773 cm^{-1} and 1754 cm^{-1}, the bands associated wit the C=O vibration are detected (Figure 3.19).
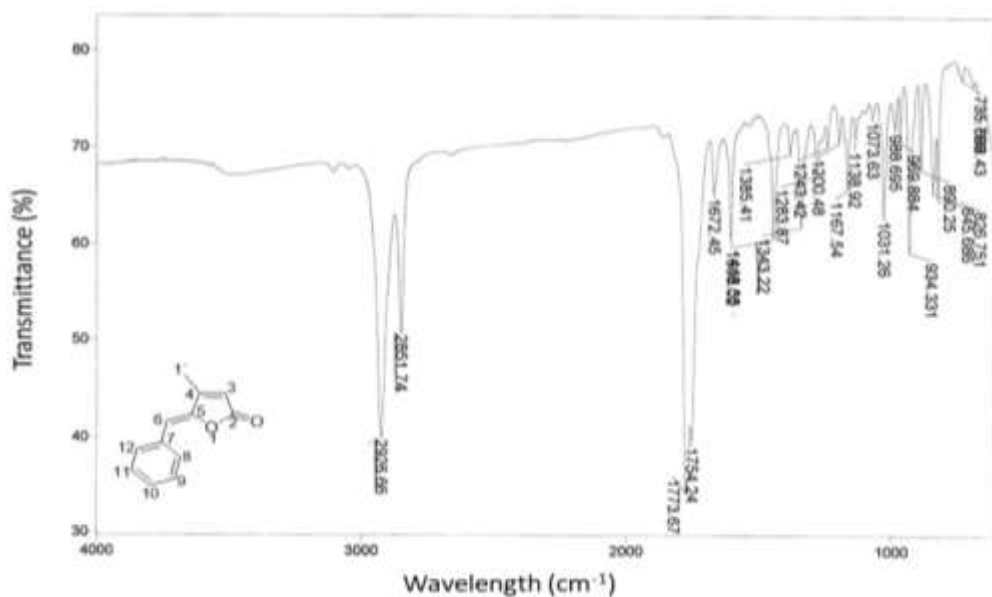
Figure 3.19. IR spectrum (NaCl film) of compound **32b.**

The spectrum of ^{1}H-NMR shows a total of six signals (Figure 3.20). The first signal, at 2.26 ppm, is linked to the methyl group of position 1´. The two singlets at 5.98 ppm and 6.05 ppm are related to the CH groups at the positions 3 and 6, in that order. Then, the multiplets located between 7.30 and 7.82 ppm are assigned to the hydrogens of the aromatic ring.
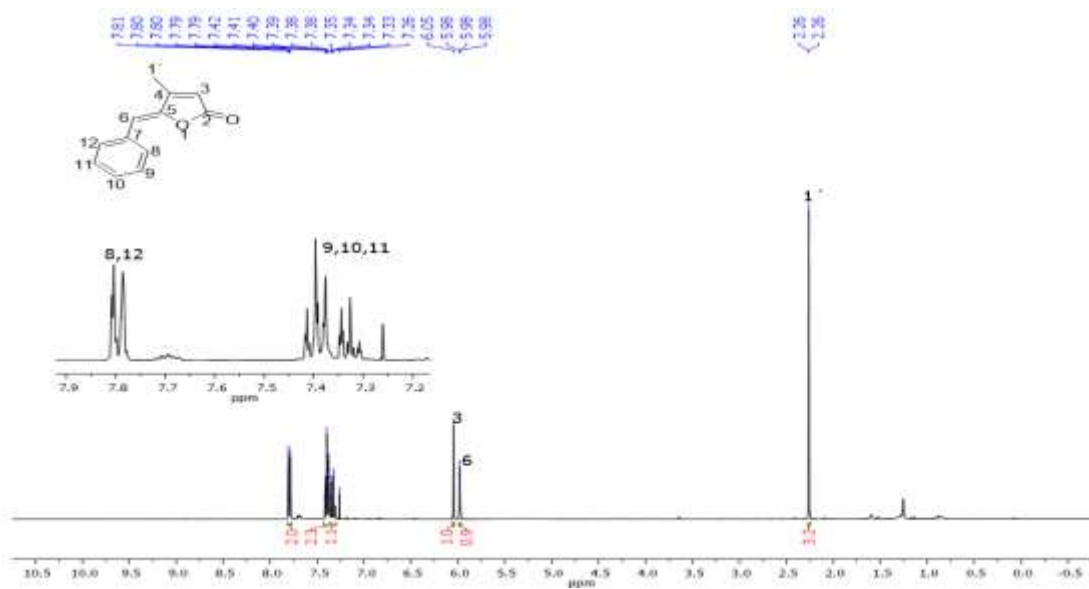
Figure 3.20. ^{1}H NMR (400 MHz, CDCl$_3$) of (*Z*)-5-benzylidene-4-methylfuran-2(5*H*)-one (**5b**).

Considering the spectrum of ^{13}C-NMR, it has a total of nine signals (Figure 3.21). The signal methyl of the position 1´ is found at 12.0 ppm. Signal at 109.9 ppm is associated to the methyne of the position 3, while the next one at 115.5 ppm is assigned to the methyne of the position 6. The for signals between 128.0 ppm and 132 ppm are related to the carbons of the aromatic ring. Currently, the signals of carbons 4 and 5 are found at 149.4 and 156.0, respectively, and the signal carbonyl carbon is located at 169.5. Compound **32b** was previously synthesized by Sekine and co-worker, the results obtained in tis work matched with the data reported by these authors (2015) (Table 3.3A pg. 184)
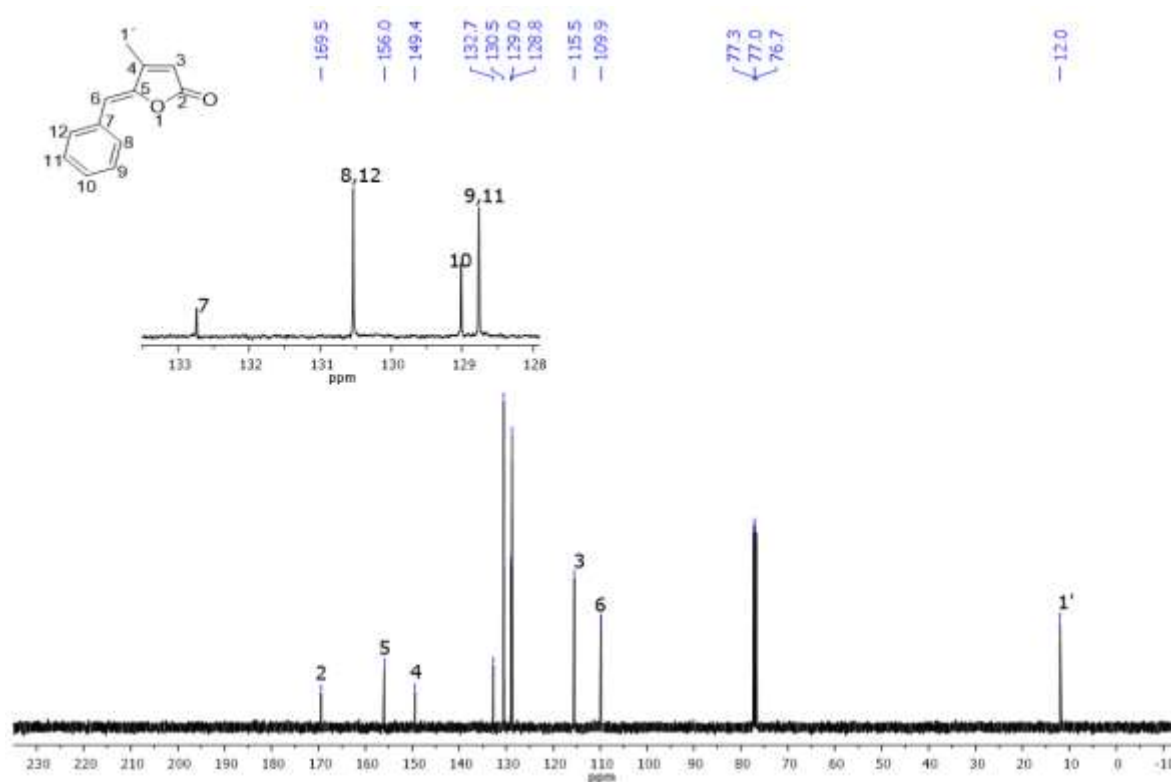
Figure 3.21. ^{13}C-NMR (100 MHz, CDCl$_3$) of (*Z*)-5-benzylidene-4-methylfuran-2(5*H*)-one (**32b**).

The reaction conditions optimized for the synthesis of butenolide **32a** made possible the simple access to an extensive variety of *Z*-lactones. To act of increasing the long chain of the alkenoic acid reduced the yield of the reaction. That result was also attained when size of long chain, in the terminal alkyne, was increased (Table 3.2**,** analogues **32f** and

32g). In the contrary, the reaction of the yields was maintained when all of terminal alkynes with cyclic moiety were utilized.

3.3.6 Biological assays

Pulchellalactam, synthetic butenolides **32a-l** and their synthetic precursors **36a-c** were evaluated as biofilm and quorum sensing inhibitors. The biofilm formation was evaluated against two pathogenic Gram-negative strains: *Escherichia coli* (T. Escheri, 1985) and *Pseudomona aeruginosa* (Schroeter, 1872) (*E. coli* RP437 and *P. aeruginosa* PAO1). *E. coli* is Gram negative bacteria that is usually found in the intestine of warmblood organism. In that circumstance, the microorganism and the host have a beneficial interaction, because *E. coli* prevents the colonization of the host by pathogenic bacteria (Sharma *et al.* 2016). Nonetheless, strains of *E. coli* also colonize anaerobic surfaces of medical devices, such as urethral or intravascular catheters. When it happens, the bacterium is able to form biofilms that cause several infectious diseases (Fang *et al.*, 2018). In contrast, *P. aeruginosa* is a pathogenic opportunistic organism found in different environments, like soil, water, plants or animals (Mangal *et al.*, 2019). Lung infection, acute septicemia and bloodstream dissemination are some of the diseases caused by that bacterium (Wu *et al.* 2004).

All compounds were tested at a concentration of 50 µg/mL, using the microtiter crystal violet assay. The cultures without the addition of the chemical compounds were utilized as controls. After 24 hours of growth, the reading of optical density at 600 nm (OD_{600}) was taken for evaluating the planktonic growth. Figure 3.22 displays the effect of the compounds over the planktonic cells of both strains of *E. coli* RP437 and *P. aeruginosa* PAO101. About *E. coli,* only compound **32a** generated inhibition by 20.1% (p < 0.05) (Figure 3.22, A). Compared to *E. coli* RP437, *P. aeruginosa* PAO1 was more sensitive to the chemical compounds during planktonic growth. Twelve compounds exhibited moderate, but significant reduction of its growth (Figure 3.22, B). For example, **36c** was able to reduce PAO1 planktonic growth by 33.7% (p<0.05).
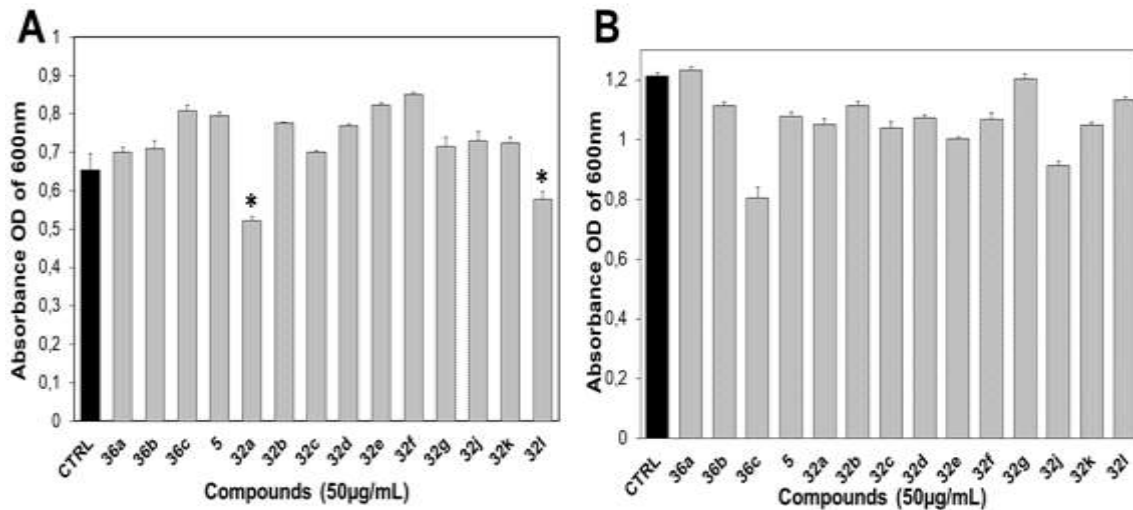
Figure 3.22. Effects of chemical compounds on *E. coli* RP437 and *P. aeruginosa* PAO1 over planktonic cell growth. (The control is the growth of the bacteria without any compound is the black bar of each graphic). Crystal violet microtiter biofilm assay was used to evaluate the biofilm formation, when exposed to the various chemical compounds and compared to E. coli RP437 and *P. aeruginosa PAO101* biofilm without any compound as a control (black bar). The results were normalized by its corresponding medium (either in LB or LB with 50 μg/mL of the compounds). (**A**) The total OD_{600} of *E. coli* RP437 before removing planktonic cells was measured to evaluate the effects of candidate compounds**.** (**B**) The total OD_{600} of *P. aeruginosa* PAO1 before removing planktonic cells was measured to evaluate the effects of candidate compounds**.** Means ± SE are presented (n=4). (*p-value <0.05 from one-way ANOVA followed by Tukey test).

Potential biofilm inhibitors should have minimal impact on the growth of planktonic cells. The utilization of that type of compounds for the treatment of infections implies a different strategy for the more classical approach of attacking the microorganisms. In that instance, the destruction of biofilm structures slows the bacterial virulence in the host. As consequence, the microorganism returns to their planktonic form and it is more susceptible to lower doses of antibiotics or elimination by the host's immune system (Geske *et al.*, 2008).

After establishing that pulchellalactam and butenolides **32a-32l** had minimal effect on planktonic cells of *E. coli* and *P. aeruginosa* strains, their impact over biofilm formation

was evaluated. Figure 3.23 illustrates the results of the compound over the biofilm formation of E. *coli* RP437 101 and *P. aeruginosa* PAO101.
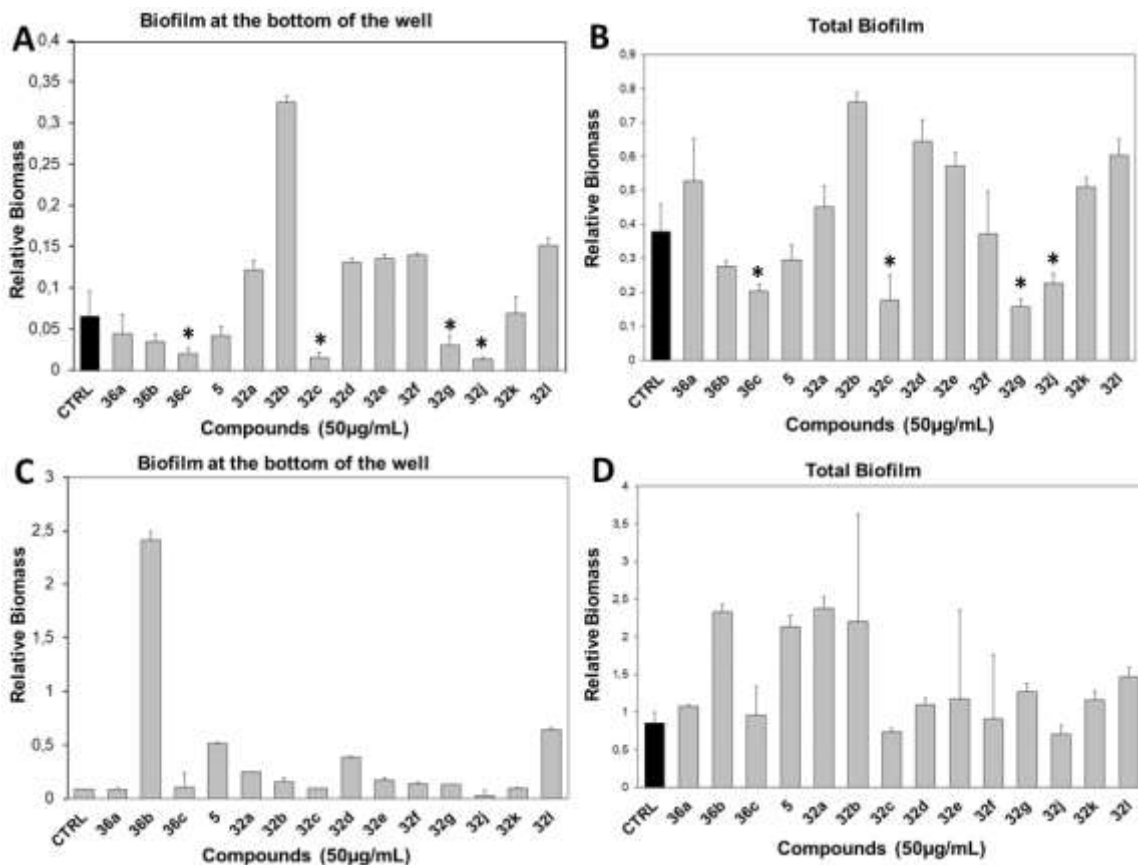
Figure 3.23. Effects of chemical compounds on *E. coli* RP437 and *P. aeruginosa* PAO 101 biofilm formation. Crystal violet microtiter biofilm assay was utilized to evaluate the biofilm formation when exposed to the various chemical compounds and compared to *E. coli* RP437 biofilm, without any compounds as a control (black bar). The results were normalized by its corresponding medium (either in LB or LB with 50 μg/mL of the compounds). (**A**) Effects of the chemical compounds on *E. coli RP437* biofilm formation at the liquid-surface interface (biofilm at the bottom of the well). (**B**) Effects of the chemical compounds on biofilm formation on *E. coli RP437* after addition of 95% ethanol (total biofilm). (**C**) Effects of the chemical compounds on *P. aeruginosa* PAO1 biofilm formation at the liquid-surface interface (biofilm at the bottom of the well). (**D**) Effects of the chemical compounds on biofilm formation on *P. aeruginosa* PAO1 after addition of 95% ethanol (total biofilm). Means ± SE are presented (n=4). (*p-value <0.05 from one-way ANOVA followed by Tukey test).

Pulchellalactam (**5**) did not exhibit significant biofilm inhibition against either of those two Gram-negative strains. Out of the 13 compounds, five of them showed inhibition of *E. coli* RP437 biofilm formation. Specifically, three compounds (**36c**, **32c** and **32g**) had significant reduction of total biomass to 46.3% ($p < 0.05$), 53.2% ($p < 0.01$) and 58.7% ($p < 0.01$), in that order (Figure 3.23B). Four out of the five compounds showed significant inhibition of biofilm formation at the bottom of the well, including **32c** (68.9%, $p < 0.05$), **32c** (77.4%, $p < 0.05$), **32g** (54.0%, $p < 0.05$) and **32h** (78.9%, $p < 0.01$) (Figure 4.23 A). However, none of the tested compounds inhibited the biofilm formation of *P. aeruginosa* PAO1 (Figure 3.23, C and D).

As explained in the introduction, interrupting the bacterial communication is a promising strategy to develop new therapies for the treatment of infections. Quorum sensing plays a pivotal role in bacterial communication, thus, controlling that system may help to reduce bacterial virulence (Ren *et al.*,2001). In order to determinate if any of the compounds interfere on that mechanism, assay with two different strains of *Vibrio harveyi* (Johnson & Shunk, 1936) were executed. Results are presented on Figure 3.24. QS systems regulate different process in bacteria, one of them is bioluminescence. As the reduction of bioluminescence is directly related to QS communication, it is a good parameter to determinate the potential of a compound as QS inhibitors. There are several bacteria employed for such task and *Vibrio harveyi* strain is one of the most used. It is a marine Gram-negative bacterium, which is part of microflora bacterial when associated to eukaryotes. The bioluminescence emitted by that microorganism is regulated by the both QS system, AI-1 and AI-2. Such characteristic made *V. harveyi* an excellent strain to study QS inhibitors and its mode of action.

To evaluate if any of the compounds inhibits AI-1 production, the *V. harveyi* BB886 (AI-1 sensor+, AI-2 sensor-) was used to measure relative bioluminescence and to compare to the untreated control (Ren *et al.*, 2001).The results identified four compounds (**36a**, **32b**, **32g**, and **32l**) that caused more than ten-fold decrease in bioluminescence correlated to the control (Figure 3.24, A).
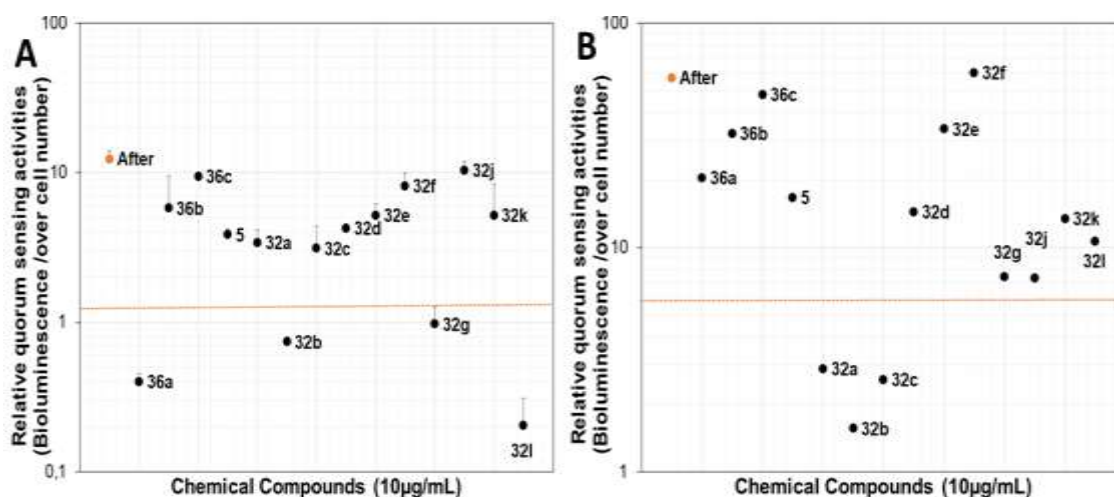
Figure 3.24. (**A**) Bioluminescence of *V. harveyi* BB886, in response to the addition of candidate compounds (10 µg/mL) to measure AI-1 based quorum sensing. *V. harveyi* BB886 without added compound, was used as control. (**B**) Bioluminescence of *V. harveyi* BB170, in response to the addition of candidate compounds (10 µg/mL) to measure AI-2 based quorum sensing. Orange dotted line indicates ten-fold inhibition compared to the control. Compounds below the dotted line are candidates for further studies. Means ± SE are presented (n = 2).

Similarly, *V. harveyi* BB170 (AI-1 sensor-, AI-2 sensor+) was utilized to analyse the effects on AI-2 signaling. The results demonstrated that **32a**, **32b** and **32c** inhibit AI-2 production by more than ten-folds (Figure 3.24, B). Inhibitors AI-2 are important for many reasons. Its production does not only regulate the same process that AI-1, but makes possible the communication between Gram-positive and Gram-negative bacteria (Galloway *et al.*, 2011). Based on those results, it was found that compound **32b** was the only substance that inhibits both AI-1 and AI-2 based quorum sensing. Differently, analogue **32c** inhibited the quorum sensing via AI-2 and reduced the biofilm formation of *E. coli.* Finally, butenolide **32g** inhibited the quorum sensing via AI-1 and the biofilm formation of *E. coli* RP437.

3.4. CONCLUSION

In this work we have developed a most efficient (63.7% overall yield) protecting-group-free strategy for the synthesis of pulchellalactam (**5**), involving 2 steps from commercially available starting materials. In addition, the optimized conditions for the tandem Sonogashira cross-coupling lactonization enabled the production of a variety of butenolides in good yield (45-67%). In regard to the biofilm tests, we concluded that compound **32b** inhibited quorum sensing via both AI-1 and AI-2. Furthermore, two new butenolides (**32c** and **32g)** inhibited the quorum sensing via AI-1 and AI-2 production, respectively, and also reduced the biofilm formation of *E. coli* RP437 by more than 50%.

These results showed that the tandem Sonogashira cross-coupling lactonization is an efficient methodology to obtain alkylidenebutenolides with structural diversity. In addition, some of the synthesized lactones were active as biofilm inhibitor via QS pathway. Therefore, this type of compounds can be considered as new candidates to develop new drugs for the treatment of chronic infections.

3.5.   MATERIAL AND METHODS

3.5.1. Chemical Instruments and experimental procedures

All reagents and equipment employed in this work are described in item chapter 1, item 1.5.1.

Part of this work was carried out at the Laval University under the supervision of Professor John Boukouvalas. Therefore, characterization of some compounds was carried out with the equipment described below. IR spectra were recorded Aminco-bowman-FIT-IR equipment using NaCl plates film as matrix. The ^{1}H-NMR and ^{13}C-NMR spectra were recorded in 500 and 400 Bruker spectrometers. Finally, high resolution mass spectra were obtained from a Varian (ESI-TOF) equipment.

3.5.2. Synthetic procedures: Preparation of alkenoic acids 8a-c

3.5.2.1. Synthesis of (Z)-3-Iodobut-2-enoic acid (36a)
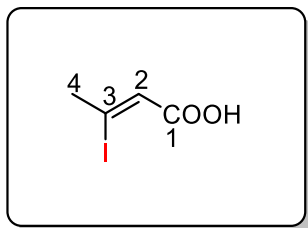
In a round bottom flask were combined but-2-ynoic acid (0.50 g, 5.95 mmol), NaI (1.42 g, 9.5 mmol) and glacial acetic acid (2.18 mL, 38 mmol). The flask was immersed in an oil bath at 115 °C and stirred for 6 h. The reaction mixture was diluted with diethyl ether (10 mL) and washed with a saturated solution of $Na_2S_2O_3$ (10 mL). The aqueous phase was extracted with diethyl ether (3 x 10 mL). After that, the combined organic fractions were dried over anhydrous $MgSO_4$ and the solvent evaporated under reduce pressure to yield *(Z)-*3-iodobut-2-enoic acid (**37a**) as a white solid (1.60 g, 7.5 mmol, 83%). M.p.: 112-115 ºC. (Arbarbi *et al.*, 2002). IR (NaCl film, cm^{-1}): 3200-2400, 1691, 1617. ^{1}H-NMR (400 MHz, CDCl$_3$) δ: 2.78 (d, 3H, J_{4-2} =1.0 Hz, H-4), 6.37 (d, 1H, J_{2-4} =1.0 Hz H-2). ^{13}C-NMR (100 MHz, CDCl$_3$) δ: 36.9 (C-4), 116.6 (C-2), 124.9 (C-3), 168.3 (C-1).

3.5.2.2. Synthesis of (Z)-3-iodopent-2-enoic acid (36b)
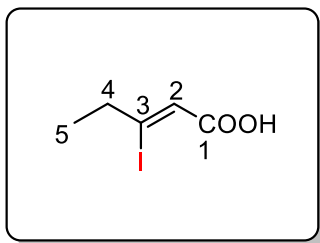
The same procedure mentioned above was used for the synthesis of **36b**, but instead of but-2-ynoic acid, pent-2-ynoic acid was used as starting material. In this case the desired product **36b** was obtained as a white solid in 65% of yield. M.p.: 116-118ºC. IR

(ATR/FTIR, cm^{-1}): 3300-2500, 1694, 1615.^{1}H-NMR (400 MHz, CDCl$_3$) δ: 1.17 (t, 3H, $J_{5\text{-}4}$ =7.4 Hz, H-5), 2.77 (qd, 2H, $J_{4\text{-}5}$ =7.4, $J_{4\text{-}2=}$1.0) Hz H-4), 6.41 (s, 1H, H-2). ^{13}C-NMR (100 MHz, CDCl$_3$) δ: 14.7 (C-5), 42.3 (C-4), 123.7 (C-2), 126.4 (C-3), 169.7 (C-1). HRMS (ESI-TOF) *m/z* [M+H]$^{+}$: Calculated for C$_5$H$_8$IO$_2$: 226.9563 found: 226.9656.

3.5.2.3. Synthesis of (Z)-3-iodohex-2-enoic acid (**36c**)
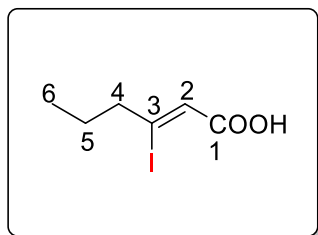
The same procedure mentioned above was used for the synthesis of **36c**, but using 2-hexynoic acidas starting material. In this case the desired product **36c** was obtained as a white solid in 55% of yield. M.p.: 82-83 ℃ (Arbarbi *et al*., 2002). IR (ATR/FTIR, cm^{-1}): 3200-3400, 1694, 1613.^{1}H-NMR (400 MHz, CDCl$_3$) δ: 0.92 (t, 3H, $J_{6\text{-}5}$ = 7.3 Hz, H-6), 1.62-1.64 (m, 2H, H-5), 2.71 (td, 2H, $J_{4\text{-}5}$ = 6.8 Hz, $J_{4\text{-}2}$ = 0.8 Hz, H-4), 6.40 (d, 1H, $J_{2\text{-}4}$ = 0.8 Hz, H-2). ^{13}C-NMR (100 MHz, CDCl$_3$) δ:12.9 (C-6), 22.8 (C-5), 50.5 (C-4), 124.7 (C-3), 125.2 (C-2), 169.8 (C-1). HRMS (ESI-TOF) *m/z* [M+H]$^{+}$: Calculated for C$_6$H$_{10}$IO$_2$: 240.9720; found; 240.9619.

3.5.3. Synthetic procedures: Preparation of butenolides (**32a – 32l**).

3.5.3.1. Synthesis of (Z)-4-methyl-5-(2-methylpropylidene)furan-2(5H)-one (**32a**)
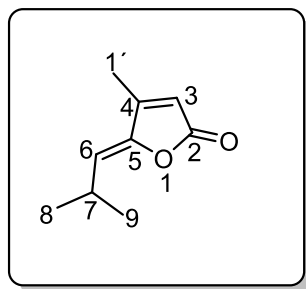
In a 10 mL round bottom flask with THF (1.50 mL) were combined (*Z*)-3-iodobut-2-enoic acid (**36a**) (50 mg, 0.23 mmol), Pd(PPh$_3$)$_2$Cl$_2$ (8.20 mg, 0.012 mmol), CuI (4.40 mg, 0.02 mmol) and Et$_3$N (0.72 mL, 0.71 mmol). Once all the reagents were dissolved, 3-methylbut-1-yne (**36a**) (0.12 ml, 1.18 mmol) was added to the reaction medium. The reaction was left stirring for 12 h at room temperature, and then diluted with EtOAc (5 mL) and filtered through Celite®. The filter cake was washed with EtOAc (20 mL), the combined filtrates were concentrated under reduced pressure. Purification of the compound was performed by silica gel flash chromatography using hexane/ethyl acetate (95:5 v/v) to afford **36a** as a yellow oil (21.00 mg, 67%) (Felluga *et al.*, 2007). IR (NaCl film, cm^{-1}): 2926, 1772, 1752, 1608. ^{1}H-NMR (400 MHz, CDCl$_3$) δ: 1.1 (d, 6H, $J_{8,7}$ = 6.8 Hz, H-8, H-9), 2.12 (s, 3H, H-1'), 2.96-3.02 (m,1H, H-7), 5.13 (d, 1H, $J_{6,7}$ = 9.6 Hz, H-6), 5.88 (s, 1H, H-3). ^{13}C-NMR (100 MHz, CDCl$_3$) δ: 11.7 (C-1`), 22.6 (C-9, C-8), 26.2 (C-7), 116.0 (C-6), 119.8 (C-3), 149.1 (C-4) 154.8 (C-5), 169.6 (C-2). HRMS (ESI-TOF) *m/z* [M+H]$^+$: Calculated for C$_9$H$_{13}$O$_2$:153.0910; found: 153.0905.

### 3.5.3.2. Synthesis of (Z)-5-benzylidene-4-methylfuran-2(5H)-one (32b)
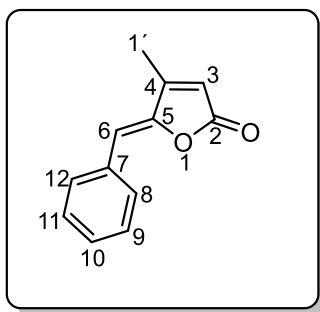
Compound **32b** was synthesized using a method similar to the one described to prepare compound **32a,** but in this case the alkyne added to the reaction medium wasphenylacetylene (**37b**) (0.13 mL, 1.18 mmol). The fractionation of the crude product by silica gel column chromatography, eluting with hexane/ethyl acetate (95:5 v/v) to afforded the required product **32b** as an orange solid (22.00 mg, 0.14 mmol, 62%) and 1,4-diphenylbuta1,3-diyne (10 mg) as side product.

*Data for **32b**.*M.p.: 100-102 ºC (Lit.[3] 102 ºC). IR (NaCl film, cm⁻¹): 2956, 2919, 2850, 1766, 1746, 1603.¹H-NMR (400 MHz, CDCl₃) δ: 2.26 (s, 3H, H-1´), 5.98 (s, 1H, H-6), 6.05 (s, 1H, H-3), 7.33-7.40 (m, 3H, H-9, H-10, H-11), 7.78-7.80 (m, 2H, H-8, H-12). ¹³C-NMR (100 MHz, CDCl₃) δ: 12.0 (C-1´), 109.9 (C-6), 115.5 (C-3), 128.8 (C-9, C-11), 129.0 (C-10), 130.5 (C-8, C-12), 132.7 (C-7), 149.4 (C-4), 156.0 (C-5), 169.5 (C-2). HRMS (ESI-TOF) *m/z* [M+H]⁺: Calculated for $C_{12}H_{11}O_2$:187.0754; found: 187.0755

*3.5.3.3. Synthesis of (Z)-5-benzylidene-4-ethylfuran-2(5H)-one (**32c**)*
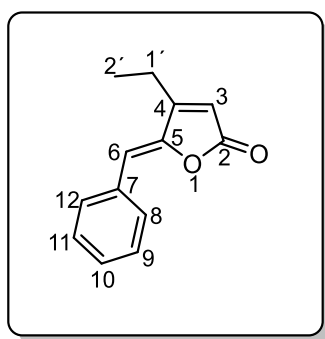
In a 10 mL round bottom flask with THF (1.50 mL) were combined *(Z)*-3-iodopent-2-enoic acid **(32b)** (50 mg, 0.22 mmol), Pd(PPh₃)₂Cl₂ (7.76 mg, 0.01 mmol), CuI (4.10 mg, 0.02 mmol) and Et₃N (0.10 mL, 0.66 mmol). Once all the reagents were completely dissolved, phenylacetylene (**37b**) (0.12 mL, 1.11 mmol) was added to the reaction medium. The reaction was left stirring for 12 h at room temperature, and then diluted with EtOAc (5.00 mL) and filtered through a Celite® pad. The filter cake was washed with EtOAc (20.00 mL), then the combined filtrates were concentrated under reduced pressure. Purification of the product was performed by silica gel flash chromatography using hexane/ethyl acetate (9:1 v/v) to afford **32c** as an orange solid (26.45 mg, 0.13 mmol, 60%) and of 1,4-diphenylbuta-1,3-diyne (8 mg) as side product. M.p. 155-157 ºC. IR (ATR/FTIR): 2972, 1766, 1598, 1446. ¹H-NMR (400 MHz, CDCl₃) δ: 1.30 (t, 3H, $J_{2´,1´}$ = 7.4 Hz, H-2´), 2.65 (qd, 2H, $J_{1´,2´}$ = 7.4 Hz, $J_{1´,3}$ = 1.4 Hz, H-1'), 5.98 (m, 1H, H-6), 6.07 (s, 1H,H-3), 7.28-7.42 (m, 3H, H-9, H-10, H-11), 7.70-7.82 (m, 2H, H-8, H-12). ¹³C-NMR (100 MHz, CDCl₃) δ: 12.4 (C-2`), 19.7 (C-1`), 109.8 (C-6), 113.9 (C-3), 128.9 (C-9, C-11),

129.2 (C-10), 130.8(C-8, C-12), 133.0 (C.7) 148.9 (C-4), 162.4 (C-5), 169.8 (C-2). HRMS (ESI-TOF) *m/z* [M+H] $^{+.}$ Calculated for $C_{13}H_{12}O_2$: 201.0910; found; 201.0920.

3.5.3.4. Synthesis of (Z)-5-benzylidene-4-propylfuran-2(5H)-one (**32d**)
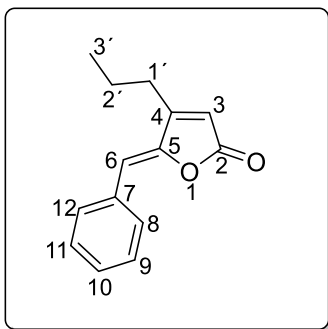
In a 10 mL round bottom flask with THF (1.50 mL) were combined *(Z)*-3-iodohex-2-enoic acid **(36c)** (50 mg, 0.21 mmol), Pd(PPh₃)₂Cl₂ (7.30 mg, 0.01 mmol), CuI (3.90 mg, 0.02 mmol) and Et₃N (0.10 mL, 0.64 mmol). Once all the reagents were completely dissolved, phenylacetylene (**37b**) (0.12 ml, 1.11 mmol) was added to the reaction medium. The reaction was stirred for 12 h at room temperature, and then quenched by addition of EtOAc (5.00 mL) and filtered through Celite®. The filter cake was washed with EtOAc (20.00 mL), then the combined filtrates were concentrated under reduced pressure. Purification of the compound was performed by silica gel flash chromatography using hexane/ ethyl acetate (9:1 v/v) to afford **32d** as an orange solid (18.40 mg, 0.09 mm0l, 41%) and the 22 mg of 1,4-diphenylbuta-1,3-diyneas side product. Mp:188-190 ºC. IR (ATR/FTIR, cm⁻¹): 3099, 2932, 1754.¹H-NMR (400 MHz, CDCl₃) *δ*:1.06 (t, 3H, $J_{3';2'}$ = 7.4 Hz, H-3´), 1.68-1.78 (m, 2H, H-2´), 2.55 (qd, 2H, $J_{1';2'}$ = 7.6 Hz, $J_{1';3}$ = 1.1 Hz, H-1'), 5.97 (s,1H, H-6), 6.07 (s, 1H,H-3), 7.33-7.42 (m, 3H, H-9, H-10, H-11), 7.81-7.82 (m, 2H, H-8, H-12). ¹³C-NMR (100 MHz, CDCl₃) *δ*: 14.0 (C-3`),21.6 (C-2´), 28.2 (C-1`), 109.9 (C-6), 114.4 (C-3), 128.9 (C-9, C-11), 129.1 (C-10), 130.7 (C-8, C-12), 133.0 (C-7). 149.1 (C-4), 160.8 (C-5), 169.8 (C-2). HRMS (ESI-TOF) *m/z* [M+H] $^{+}$: Calculated for $C_{14}H_{15}O_2$: 215.1067; found: 215.1077.

3.5.3.5. Synthesis of (Z)-5-hexylidene-4-methylfuran-2(5H)-one (**32e**)
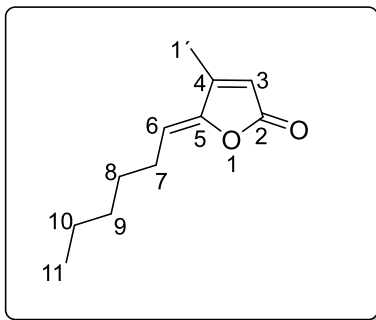
Compound **32e** was prepared using a similar method described to synthesize **32a,** but in this case using hept-1-yne (**37c**) (0.13 mL, 1.18 mmol). The desired compound was obtained as a yellow oil (21 mg, 0.12 mmol, 63%). IR (NaCl film, cm^{-1}): 2956, 2927, 2858, 1777, 1673. ^{1}H-NMR (400 MHz, CDCl$_3$) δ: 0.87-0.91 (m, 3H, H-11), 1.30-1.34 (m, 4H, H-10,H-9),1.45-1.47 (m, 2H, H-8), 2.13 (d, 3H, $J_{1'-3}$ = 1.6 Hz, H-1´), 2.36 (m 2H, H-7), 5.29 (t, 1H, $J_{6,7}$ = 7.6 Hz, H-6), 5.89 (s, 1H, H-3).^{13}C-NMR (100 MHz, CDCl$_3$) δ: (100 MHz, CDCl$_3$) δ: 11.7 (C-11), 14.0 (C-1´), 22.4 (C-10), 26.2 (C-9), 28.7 (C-8), 31.5 (C-7), 113.3 (C-6), 116.0 (C-3), 150.7 (C-4), 154.5 (C-5), 169.6 (C-2). HRMS (ESI-TOF) *m/z* [M+H] $^+$: Calculated for C$_{11}$H$_{17}$O$_2$: 181.1223; found: 181.1233.

3.5.3.6 Synthesis of (Z)-4-ethyl-5-hexylidenefuran-2(5H)-one (**32f**)
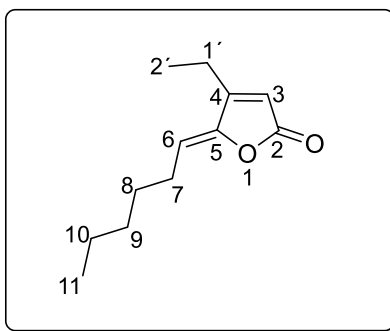
Compound **32f** was synthesized using a similar method described to prepare compound **32c,** but in this case hept-1-yne (**37c**) (0.14 mL, 1.10 mmol) was used. As result the desired compound **32f** was obtained as a yellow oil (16 mg, 0.09 mmol, 38%). IR (NaCl

film, cm[-1]): 2974, 2942, 2858, 1762, 1673.^{1}H-NMR (400 MHz, CDCl$_3$) δ: 0.86-0.89 (m, 3H, H-11), 0.96-1.10 (m, 3H, H-2´), 1.42-1.67 (m, 6H, H-8, H-9, H-10), 2.31-2.47 (m, 5H, H1', H-7), 5.31 (t, 1H, $J_{6,7}$ = 7.8 Hz, H-6), 5.88 (s, 1H, H-3). ^{13}C-NMR (100 MHz, CDCl$_3$) δ: 12.4 (C-11), 14.2(C-2), 19.6 (C-10), 22.7 (C-9), 26.4 (C-8), 29.0 (C1´), 31.7(C-7), 113.3 (C-3), 114.5 (C-6), 150.2 (C-4), 161 (C-5), 170 (C-2). HRMS (ESI-TOF) m/z [M+H] [+]: Calculated for C$_{12}$H$_{19}$O$_2$: 195.1380 found: 195.1381.

3.5.3.7. Synthesis of (Z)-5-hexylidene-4-propylfuran-2(5H)-one (32g)
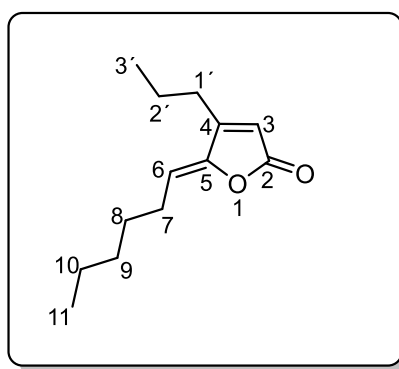
Compound **32g** was synthesized using a similar method described to prepare compound **32d,** but in this case the alkyne added to the reaction medium washept-1-yne (**37c**) (0.14 mL, 1.10 mmol). As result the desired compound was obtained as a yellow oil (16 mg, 0.08 mmol, 22%). IR (ATR, cm[-1]): 2981, 2934, 2855, 1772, 1769, 1653.^{1}H-NMR (400 MHz, CDCl$_3$) δ: 0.87 (t, 3H, $J_{11,10}$= 6.9 Hz, H-11), 0.98 (t, 3H, $J_{3´,2´}$= 7.4 Hz, H-3´),1.27-1.33 (m, 4H, H-9, H-10), 1.43-1.47 (m, 2H, H-8), 1.60- 1.66 (m, 2H, H-2´), 2.30-2.42 (m, 4H, H-1´, H-7), 5.20 (t, 1H, $J_{6,7}$ = 7.8 Hz, H-6), 5.86 (s, 1H, H-3). ^{13}C-NMR (100 MHz, CDCl$_3$) δ: 13.9 (C-11*), 14.1 (C-3´*), 21.6 (C-10), 22.6 (C-9), 26.3 (C-8), 28.1 (C-2´), 29.9 (C-7), 31.6 (C-1´), 113.4 (C-6), 114.9 (C-3), 150.3 (C-4), 159.4 (C-5), 169.9 (C-2). HRMS (ESI-TOF) m/z [M+H] [+]: Calculated for C$_{13}$H$_{21}$O$_2$: 209.1535 found: 209.1549.

3.5.3.8. Synthesis of (Z)-5-((1-hydroxycyclopentyl)methylene)-4-methylfuran-2(5H)-one (**32h**)
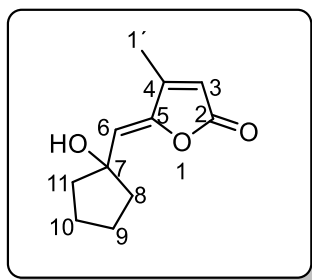
Compound **32h** was synthesized using a similar method described to prepare compound **32a,** employing 1-ethynylcyclopentan-1-ol (**32d**) (0.14 mL, 1.18 mmol). The required product was obtained as a yellow oil (31 mg, 0.16 mmol, 69%). IR (ATR/FTIR, cm^{-1}): 3600-3200, 2956, 1739. ^{1}H-NMR (400 MHz, CDCl$_3$) δ:1.74-1.96 (m, 8H, H-8, H-9, H-10, H-11), 2.13 (s, 3H, H-1´), 5.57 (s, 1H, H-6), 5.90 (s, 1H, H-3). ^{13}C-NMR (100 MHz, CDCl$_3$) δ: 12.0 (C-1´), 23.7 (C-9, C-10), 41.3 (C-8, C-11), 80.7 (C-7), 115.8 (C-3), 118.1 (C-6), 149.1 (C-4), 155.9 (C-5). 168.9 (C-2). HRMS (ESI-TOF) m/z [M-H$_2$O] $^+$: Calculated for C$_{11}$H$_{13}$O$_2$: 177.0910 found: 177.0906.

3.5.3.9. Synthesis of (Z)-4-ethyl-5-((1-hydroxycyclopentyl)methylene)furan-2(5H)-one (**32i**)
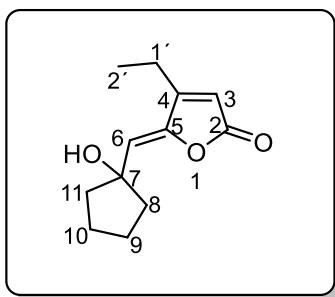
Compound **32i** was synthesized using a similar method described to prepare compound **32c,** but in this case the alkyne added to the reaction medium was1-ethynylcyclopentan-1-ol (**37d**) (0.13 mL, 1.10 mmol). As result the desired compound was obtained as a yellow oil (29 mg, 0.14 mmol, 64%). IR (NaCl film, cm^{-1}): 3600-3200, 2967,

2875, 1744. ^{1}H-NMR (400 MHz, CDCl$_3$) δ: 1.24 (t, 3H, $J_{2',1}$ = 7.4 Hz, H-2´) 1.76-1.96 (m, 8H, H-8,H-9,H-10, H-11), 2.45 (q, 2H, $J_{1',2}$ = 7.4 Hz, $J_{1',3}$ = 1.5 Hz H-1´), 5.55 (s, 1H, H-6), 5.90 (s, 1H, H-3).^{13}C-NMR (100 MHz, CDCl$_3$) δ: 12.2 (C-2´) 19.6 (C-1´), 23.8 (C-9, C-10), 41.5 (C-8, C-11),80.8 (C-7), 114.2 (C-3), 117.6 (C-6), 148.7 (C-4), 162.0 (C-5). 169.0 (C-2) HRMS (ESI-TOF) m/z [M-H$_2$O] $^{+}$: Calculated for C$_{12}$H$_{15}$O$_2$: 191.1100 found 191.1081.

3.5.3.10. Synthesis of (Z)-5-((1-hydroxycyclopentyl)methylene)-4-propylfuran-2(5H)-one (32j)
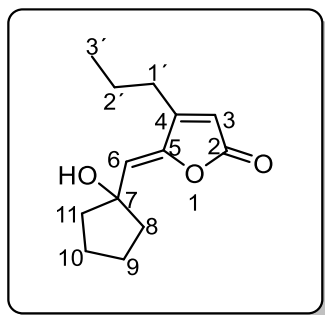
Compound **32j** was synthesized using a method similar described to prepare compound **32d,** using1-ethynylcyclopentan-1-ol (**37d**) (0.12 mL, 1.05 mmol) as a starting material. The desired compound was obtained as a yellow oil (27 mg, 0.12 mmol, 56%).IR (NaCl plate, cm^{-1}): 3600-3200, 2961, 2873, 1748, 1664. ^{1}H-NMR (400 MHz, CDCl$_3$) δ: 1.03 (t, 3H, $J_{3',2'}$ = 7.4 Hz, H-3´), 1.65-1.72 (m, H-2´), 1.75- 1.99 (m, 10H, H-8, H-9, H-10, H-11), 2.43 (td, 2H, $J_{1',2'}$ = 7.4 Hz, $J_{1',3'}$ = 1.2 Hz H-1´), 5.58 (s, 1H, H-6), 5.91 (s, 1H, H-3). ^{13}C-NMR (100 MHz, CDCl$_3$) δ: 14.1 (C-3´), 21.6 (C-2´), 23.8 (C-9, C-10), 28.2 (C-1´), 41.6 (C-8, C-11), 80.8 (C-7), 114.8 (C-3), 117.7 (C-6), 149.1 (C-4), 160.3 (C-5). 168.9 (C-2). HRMS (ESI-TOF) m/z [M-H$_2$O] $^{+}$ Calculated for C$_{13}$H$_{17}$O$_2$: 205.1223; found 205.1225.
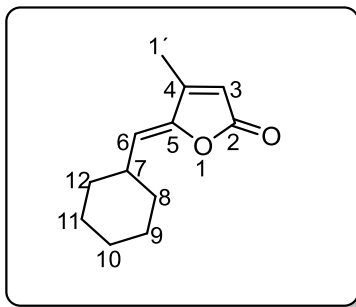
Compound **32k** was synthesized using a similar method described to prepare compound **32a,** usingcyclohexylacetylene (**37f**) (0.10 mL, 1.18 mmol) as a starting material, affording the desired product as a yellow oil (21 mg, 0.11 mmol, 63%). IR (NaCl film, cm^{-1}): 2927, 2852, 1774, 1668. ^{1}H-NMR (400 MHz, CDCl$_3$) δ: 1.14-1.75 (m, 10H, H-8, H-9, H10, H-11, H-12), 2.12 (1, 3H, H-1´), 2.68-2.71 (m, 1H, H-7), 5.15 (d, 1H, $J_{6,7}$=9.6 Hz, H-6), 5.88 (s, 1H, H-3). ^{13}C-NMR (100 MHz, CDCl$_3$) δ: 11.7 (C-1´), 25.5 (C-9, C11), 25.8 (C-10), 32.6 (C-8, C-12), 35.6 (C-7), 115.9 (C-6), 118.5 (C-3), 149.2 (C-4), 154.9 (C-5), 169.7 (C-2). HRMS (ESI-TOF) *m/z* [M+H] $^{+\cdot}$ Calculated for C$_{12}$H$_{16}$O$_2$ 193.1223; found 193.1223.

3.5.3.12. Synthesis of (Z)-5-(3-((tert-butyldimethylsilyl)oxy)propylidene)-4-methylfuran-2(5H)-one (**32l**)
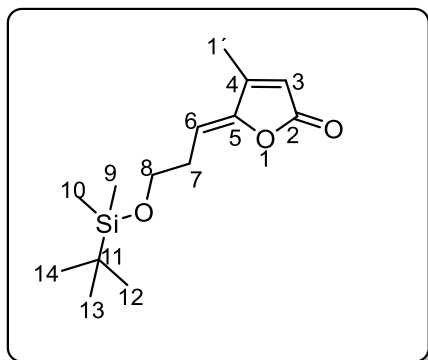
Compound **32l** was synthesized using a similar method described to prepare compound **32a**. For this reaction 4-(*tert*-butyldimethylsilyloxy)-1-butyne (**37g**) (0.25 mL,

1.18 mmol) was used and the desired compound was obtained as a yellow oil (31 mg, 0.12 mmol 48%). IR (NaCl film, cm^{-1}): 2955, 2929, 2857, 1777, 1609. ^{1}H-NMR (400 MHz, CDCl$_3$) δ: 0.05 (s, 6H, H-9, H-10),0.84 (s, 12H, H-12, H-13, H-14), 2.13 (s, 3H, H-1´), 2.60 (m, 2H, H-7),3.73 (t, 2H, $J_{8\text{-}7}$=6.3 Hz, H-8),5.41 (t, 1H, $J_{6\text{-}7}$=7.6 Hz, H-6),5.91 (s, 1H, H-3). ^{13}C-NMR (100 MHz, CDCl$_3$) δ: 5.1 (C-9, C-10), 12.0 (C-1´), 18.5 (C-11), 26.1 (C-12, C-13, C-14), 30.1 (C-7), 62.1 (C-8), 110.1 (C-3), 116.5 (C-6), 151.6 (C-5), 154.8 (C-4), 169.7 (C-2). HRMS (ESI-TOF) m/z [M+H]$^+$: Calculated for C$_{14}$H$_{25}$O$_3$Si 269,1567 found 269.1574.

3.5.4. Preparation of pulchellalactam (**5**)
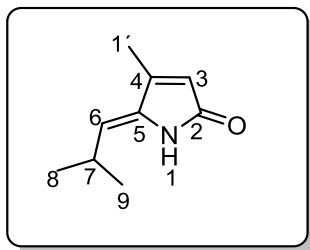
Compound **32a** (0.197 mmol, 30 mg) was added to a round bottom flask charged with stir bar. Next, an aqueous solution of NH$_3$ (30 % v/v) (0.58 ml) was added and the formation of a white suspension was observed. The reaction mixture was heated at 65 ºC for 6h, after that, the reaction was quenched with aqueous solution of HCl (10 % v/v) and stirred for 30 minutes. Then the reaction mixture was extracted with CH$_2$Cl$_2$ (3 x 5mL). The organic layers were combined and dried with anhydrous MgSO$_4$. The product was purified by flash chromatography eluting with hexane/ethyl acetate (70:30 v/v) to yield a clear oil (29 mg, 0.19 mmol, 95%). IR (NaCl plate, cm^{-1}): 3156, 3032, 2953, 2920 (Csp$_2$-H), 1707, 1673. ^{1}H-NMR (400 MHz, CDCl$_3$) δ: 1.11 (d, 6H, $J_{8\text{-}7}$ = $J_{9\text{-}7}$ = 6.0, H-8, H-9), 2.07 (s, 3H, $J_{1´\text{-}3}$= 1.4, H-1'), 2.63- 2.67 (m, 1H, H-7), 5.12 (d, 1H, $J_{6,7}$ =9.7 Hz, H-6), 5.86 (s, 1H, H-3), 8.39 (s, 1H, H-1). ^{13}C-NMR (100 MHz, CDCl$_3$) δ: 11.9 (C-1´), 22.9 (C-9, C8), 27.5 (C-7), 119.8 (C-6), 120.8 (C-4), 137.4 (C-3) 148.7 (C-5), 172.2 (C-2). HRMS (ESI-TOF) m/z [M+H]$^+$: Calculated for C$_9$H$_{13}$NO 153.0901; found 153.0905.

3.5.5. Biofilm inhibition bioassays

Bioassays of compounds **5** and **32a-32l** were carried out at University of Syracusse under the supervision of Professor Dachen Ren and PhD student Sweeta Roy.

3.5.5.1. Bacterial strains and culture conditions

Escherichia coli RP437 and *Pseudomonas aeruginosa* PAO1 were grown overnight in Luria-Bertani (LB) roth containing 10 g/L of tryptone, 5 g/L of yeast extract, and 10 g/L of sodium chloride at 37 °C with constant shaking at 200 rpm. *Vibrio harveyi*BB170 (AI-2) and *V. harveyi* BB886 (AI-1) reporter strains were grown at 30 °C in autoinducer bioassay medium (AB) containing 17.5 g/L NaCl, 12.3 g/L MgSO$_4$ and 2.0 g/L Casamino acids with pH adjusted to 7.5. Addition of 10 ml of 1 M KH$_2$PO$_4$ (pH 7.0), 10 ml of 0.1 mol/L L-arginine, 10 ml of glycerol, 1 mL of 10 µg/mL riboflavin and 1 mL of 1 mg/mL thiamine was added after sterilization. L-marine (LM) plates containing 10 g/L tryptone, 5 g/L yeast extract, 20 g/L NaCl, 15 g/L agar were used to count the number of colonies after growth overnight at 30 °C (Ren *et al*., 2004).

3.5.5.2. Biofilm assay

A microtiter plate-based crystal violet assay was used to evaluate biofilm formation. Briefly, *E. coli* RP437 and PAO1 biofilms were grown in sterile flat bottom 96 well plates. Each well was inoculated with an initial OD$_{600}$ of 0.05 in a total volume of 300 µL of LB medium. Each chemical compound was dissolved in DMSO and tested at a concentration of 50 µg/mL. The plates were incubated for 24 h at 37 °C without shaking. An initial reading was taken to record the total growth at OD$_{600}$. Afterwards the medium with planktonic cells was aspirated and washed three times with sterile DI water to remove any non-adherent cells. The plates were left to dry for 5 min. Then 300 µL of crystal violet solution (0.1% in water) was added to each well and incubated for 20 min at room temperature. The wells were then thoroughly washed three times with sterile DI water to remove any free crystal violet. A reading of OD$_{590}$ was taken to measure the liquid-solid interface biofilm at the bottom of each well. Then 95% ethanol was added to each well and shaken for 30 secs to

dissolve the bound crystal violet. A second reading was then taken at OD_{590} to quantify total biofilm including those at air-liquid interface. The readings were calibrated by subtracting the cell-free background signals, which included the media and the tested chemical compound.

3.5.5.3. Quorum sensing assay

The reporter strains, *V. harveyi* BB886 (AI-1 sensor +, AI-2 sensor -) and *V. harveyi* BB170 (AI-1 sensor -, AI-2 sensor +) were used to detect AI-1 and AI-2 activity respectively in the presence and absence of the chemical compounds. The assay is based on a previously described protocol (Bassler *et al.*, 1997). Briefly, cell-free supernatants of the reporter strains were collected by removing the cells from overnight cultures by centrifugation at 13,200 rpm for 10 mins at 4°C. The supernatant was then sterilized by filtering through a 0.22 µm membrane filter. The cell-free supernatants were stored at -20°C until use. To identify the optimal time, point to add the chemical compounds, relative bioluminescence/CFU of each reporter strain was followed over time. To do this, overnight cultures of *V. harveyi* BB170 and *V. harveyi* BB886 were grown in AB medium and diluted 1:5000 into fresh AB medium. Cell-free supernatant (10% v/v) were added to measure AI-1 or AI-2 activity and compare with samples without the added cell-free supernatant in a 96-well plate. Relative bioluminescence of *V. harveyi* reporters were measured every hour using a Turner Design 20/20 luminometer. Cell density was determined by diluting the same sample that was used for bioluminescence measurement and plating it on LM plates. The number of colonies was counted after growth overnight at 30°C. To identify which compounds can inhibit AI-1 or AI-2 quorum sensing, appropriate *V. harveyi* reporter with added supernatant was grown in a 96-well plate. At a predetermined time (3 h for BB886 and 5.5 h for BB170), each compound was added at a concentration of 10 µg/mL and the bioluminescence and cell density were measured after 1.5 hours of incubation. Each compound was tested in duplicate.

3.6.   REFERENCES

Anselmi, E., Cherry, K., Maaliki, C., Ngi, S.J. , Thibonnet, J., Abarbri, M., 2016. Two Novel and Simple Approaches to CD45 Protein Tyrosine Phosphatase Inhibitor (*Z*)-Pulchellalactam and Derivatives. Synthesis 48, 1407–1413.

Abarbri, A., Thibonnet, T., Parrain, J. L., Duchêne, A., 2002. Palladium-Catalysed Cross-Coupling of Iodovinylic Acids with Organometallic Reagents. Selective Synthesis of 3,3-Disubstituted Prop-2-enoic Acids. Synthesis 4, 544-550.

Barbosa, L. C. A., 2013 Espectroscopia no infravermelho na caracterização de compostos orgânicos. First ed. Editora UFV, Brasil.

Basak, A., Abouelhassan, Y., Huigens III, R., 2015. Halogenated quinolines discovered through reductive amination with potent eradication activities against MRSA, MRSE and VRE biofilms. Org. Biomol. Chem. 1, 1-5.

Bassler, B. L., Greenberg, P., Stevens A., 1997. Cross-Species Induction of Luminescence in the Quorum Sensing Bacterium *Vibrio harveyi.* Journal of Bacteriology, 179, 4043–4045.

Bessho, J.-I., Shimotsu, Y., Mizumoto, S., Mase, N., Yoda, H., Takabe, K., 2004. Convenient Synthesis of Pulchellalactan, a CD45 Protein Tyrosine Phosphatase Inhibitor from the Marine Fungus *Corollospora Pulchella*, and its Related Compounds. Heterocycles 63, 1013-1016

Bowden, K., Price, M. J., 1970. Addition to unsaturated carbonyl compounds. Part 1. The addition of hydrogen halides to propiolic acid. J. Chem. SOC. (B) 1466-1472.

Bryans, J. S., Chessum, N. E. A., Huther, N., Parsons, F., 2003. Metal-catalysed radical cyclizations leading to N-heterocycles: new approaches to gabapentin and Pulchellalactam. Tetrahedron59, 6221.

Chavan, S. P., Pathak, A., Dhawane, A. N., 2007. Total Synthesis of Pulchellalactam via an RCM Strategy.Synthesis 37, 1503–1510.

Chinchilla, R., Najera, C., 2011. Recent advances in Sonogashira reactions. Chem. Soc. Rev. 40, 5084–5121.

Clayden, J., Greevs, N., Warren, S., Wothers, P., Organic chemistry, 182-185, Second Edition,Oxford, 2005.

Fang, K., Jin, X., Hoon Hong, S., 2018. Probiotic *Escherichia coli* inhibits biofilm formation of pathogenic E. coli via extracellular activity of DegP. Scientific Reports 8, 1-11.

FAO, 2018. Report: Antimicrobial Resistance and Foods of Plant Origin.

Fauvarque J.F., Pulliger, F., 1981. Kinetics of Oxidative Addition of Zerovalent Palladium to Aromatic Iodides. Journal of Organometallic Chemistry 208, 419-427.

Felluga.G, Pagnoni, U. M., Parsons, A. F., Pattarozzi, M., Roncaglia, F., 2007. A novel short approach to (*Z*)-Pulchellalactam through transition-metal-catalyzed cyclization of 1-isopropylprop-2-enyl dihloroacetate. Synthesis 12, 1882-1886.

Fletcher, M., Jennings, M. C., Wuest, W., 2014. Draining the moat: disrupting bacterial biofilms with natural Products. Tetrahedron70, 6373-6383.

Galloway, W. R. J. D, Hodgkinson J. T., Bowden, S.D., Welch, M., Spring, D. R., 2011. Quorum Sensing in Gram-Negative Bacteria: Small-Molecule Modulation of AHL and AI-2 Quorum Sensing Pathways. Chem. Rev. 111, 28–6728.

Geske, G., O'Neill, J., Blackwell, H., 2008. Expanding dialogues: from natural autoinducers to non-natural analogues that modulate quorum sensing in Gram-negative bacteria. Chem Soc Rev. 37, 1432–1447.

He, C., Ke, J., Xu, H., Lei, A., 2013. Synergistic Catalysis in the Sonogashira Coupling Reaction: Quantitative Kinetic Investigation of Transmetalation. Angew. Chem. Int. Ed. 52, 1527–1530.

Hermet, J., Caubert, V., Langlois, N., 2006. Short Synthesis of Pulchellalactam. Synth. Commun. 36, 2253–2257.

Inack-Ngi, S., Rahmani, R., Commeiras, L., Chouraqui, G., Thibonnet, J., DuchÞne, A., Abarbri, M., Parrainb, J.L., 2009. Copper-Catalyzed Preparation of γ-Alkylidenebutenolides and Isocoumarins under Mild Palladium-Free Conditions. Adv. Synth. Catal. 351, 779–788.

Karak, M., Barbosa, L.C.A., Hargaden, G.D., 20014. Recent mechanistic developments and next generation catalysts for the Sonogashira coupling reaction. RSC Adv. 4, 53442–53466.

Kaura, A., Capalashb, N., Sharmaa, P., 2019. Communication mechanisms in extremophiles:Exploring their existence and industrial applications. Microbiological Research 221,15–27.

León, B., Jake, F.P., Haeckl, J., Linington, R., 2015. Optimized quinoline amino alcohols as disruptors and dispersal agents of *Vibrio cholerae* biofilms. Org. Biomol. Chem. 13, 8495-8499.

Li. W., Lin. S.T., Hsu. N., Chern. M, 2002. Efficient Total Synthesis of Pulchellalactam: a CD45 Protein Tyrosine Phosphatase Inhibitor. J. Org. Chem. 67, 4702–4706.

Lu, X., Huang X., Shengming, M., 1993. A convenient synthesis of (*Z*)-alkylidene butenolides. Tetrahedron Lett. 34, 5963-5966.

Lu, X., Li, Z., 1992. Novel Regio- and Stereospecific Hydrohalogenation Reaction of 2-Propynoic Acid and Its Derivatives. J. Org. Chem. 57, 709–713.

Ma, S., Lu, X., Li, Z., 1992. A Novel Regio- and Stereospecific Hydrohalogenation Reaction of 2-Propynoic Acid and Its Derivatives. J. Org. Chem. 57, 709-713.

Manefield, M., Rocky, N., Kumar, N., Read, R., Givskov, M., Steinberg, P., Kjelleberg, S., 1999. Evidence that halogenated furanones from *Delisea pulchra* inhibit acylated homoserine lactone (AHL)-mediated gene expression by displacing the AHL signal from its receptor protein. Microbiology 145, 283-29.

Mangaleswaran, S., Argade, N. P., 2004. A Facile Synthesis of CD45 Protein Tyrosine Phosphatase Inhibitor Marine Natural Product Pulchellalactam. Adv. Synth. Cat. 10, 1560-1562.

Mardjan, M. I. D., Parrain, J. L., 2016. Copper (I)-catalysed multicomponent reaction: straightforward access to hydroxy-1H-pyrrol-2(5*H)*-ones. Adv. Synt. Catal.358, 543-548.

Mayrink, S., Barbosa, L.C. A., Maltha C. R. A., Boukouvalas, J., Pedroso, S., Santos, S., Magalhães, P., Farias, L. M., Synthesis and evaluation of cadiolide analogues as inhibitors of bacterial biofilm formation. Medicinal Chemistry Research.

Mengal, S., Azam S., Kamran Taj, M., Rehman, U., Zafar, U., Mengal, A. N., Hussain, A., Taj, I., Samreen, Z., Shahzad, F., Wali, H., Ali, S. A., Hafsa Ali, S., 2019. *Pseudomonas aeruginosa* as a Pathogenic Organism. International Journal of Bacteriology 14, 286-291.

Nay, B., Riache, N., Evanno, L., 2009. Chemistry and biology of non-tetramic γ -hydroxy- γ -lactams and γ -alkylidene- γ -lactams from natural sources. Nat. Prod. Rep., 26, 1044–1062.

Negishi. E., 2002. Handbook of Organopalladium Chemistry for Organic Synthesis, second ed. Wiley-Blackwell, Oxford, UK.

Negishi, E., Alimardanov, A., Xu, C., 2000. An Efficient and Stereoselective Synthesis of Xerulin via Pd-Catalyzed Cross Coupling and Lactonization Featuring (*E*) -Iodobromoethylene as a Novel Two-Carbon Synthon. Org. Lett., 2, 65–67.

136

Negishi, E., Kotora, M., 1997. Regio- and Stereoselective Synthesis of y-Aikylidenebutenolides and Related Compounds. Tetrahedron, 53, 6707–6738.

Pan, J., Ren, D., 2009. Quorum sensing inhibitors: a patent overview. ExpertOpin. Ther. Patents 19, 1-21.

Pereira, U. A., Barbosa, L. C. A., Maltha, C. R. A., Demuner, A. J., Masood, M. A., Pimenta, A. L., 2014. γ-Alkylidene-γ-lactones and isobutylpyrrol-2(5*H*)-ones analogues to rubrolides as inhibitors of biofilm formation by Gram-positive and Gram-negative bacteria. Bioorg. Med. Chem. Lett. 24, 1052-1056.

Pereira, U. A., Barbosa, L. C. A., Maltha, C. R. A., Demuner, A. J., Masood, M. A., Pimenta, A. L., 2014. Inhibition of Enterococcus faecalis biofilm formation by highly active lactones and lactams analogues of rubrolides. Eur. J. Med. Chem. 82, 127-138.

Piers, E., Wong, T., Coish, P., Rogers, C., 1992. A convenient procedure for the efficient preparation of alkyl(2)-3-iodo-2-alkenoates. Can. J. Chem. 72, 1818-1819.

Qing, F., Zhang, Y., 1997. Ethyl 3-Iodo-4,4,4-Trifluoro-2(Z)-Butenoate: Regio- and Stereo-Specific Preparation and Palladium-Catalyzed Reaction with Terminal Alkynes Feng-Ling. Tetrahedron Lett. 38, 6729–6732.

Reichardt, C., Solvents and Solvent Effects in Organic Chemistry. 472-474 Third Edition, Weinheim, Wiley & Sons, 2003.

Ren, D., Sims, J.J., Wood. T.K., 2001. Inhibition of biofilm formation and swarming of *Escherichia coli* by (5*Z*)-4-bromo-5-(bromomethylene)-3-butyl-2(5H)-furanone. Environmental Microbiology3, 731-736.

Ren, D., Bedzyk, L. A., Setlow, P., England, D. F., Kjelleberg, S., Thomas, S.M., 2004 Differential gene expression to investigate the effect of (*5Z)*-4-bromo-5-(bromomethylene)-3-butyl-2 (*5H)*-furanone on *Bacillus subtilis*. Applied and environmental microbiology 70, 4941-4949

Ribaucourt, A., Hodgson, D. M., 2016.Total Synthesis and Structural Revision of the Cytotoxin Aruncin B. J. Org. Chem. 18, 18–21.

Sadekuzzaman, M., Yang, S., Mizan, M.F.R., Ha, S.D., 2015. Current and Recent Advanced Strategies for Combating Biofilms. Comprehensive Reviews in Food Science and Food Safety 14, 491-509.

Sharma, G., Sharma, S., Sharma, P., Chandola, D., Dang, S., Gupta, S., Gabrani, R., 2016. Escherichia coli biofilm: development and therapeutic strategies. Journal of Applied Microbiology 121, 309-319.

Sonogashira, K., 1975. A convenient synthesis of acetylenes: Catalytic substitution of acetylenic hydrgen with bromoalkenes, iodoarenes and bromopyridines. Tetrahedron 50, 4467–4470.

Sordi, M. B., Moreira, T. A., Montero, J. F. D., Barbosa, L. C. A., Benfatti, C. A. M., Magini, R. D. S., Pimenta, A. D. L., Souza, Matias J.C., 2018. Effect of γ-lactones and γ-lactams compounds on *Streptococcus mutans* biofilms. Journal of Applied Oral Science26,1-8.

Winterfeldt, E., 1967. Additions to the activated CC triple bond. Angew. Chem. internat. Edit. 6, 423-434.

Word Health Organization. 2019. Report We can not wait: Secure the future against pharmacoresistent diseases.

Wu1, H., Song, Z., Hentzer, M., Andersen, J. B., Molin S., Givskov, M., Høiby1, N., 2003. Synthetic furanones inhibit quorum-sensing and enhance bacterial clearance in *Pseudomonas aeruginosa* lung infection in mice. JAC, 53, 1054–1059

4. GENERAL CONCLUSION

The present work showed the synthesis and biological potential of two different types of heterocycles. The tetraoxanes synthesized in this work were obtained from a reliable materials and easy reactions; therefore, they are excellent candidates in order to develop either potential herbicides or drugs to treat leishmaniosis. With regard to the γ−alkyldienebutenolides obtained in this work, they probed to be promissory candidates in order two obtain new anti-quorum sensing agents. It is important to highlight that these compounds were stereoselectively synthesized in one step in good yields.

As is possible to conclude, the results obtained from this research revealed the importance of small molecules in the develop of new compound with the most diverse biological potential. We hope that the results presented in here will be useful and contribute to the development of further agrochemical or drugs.

DATA REFERRED TO CHAPTER 1
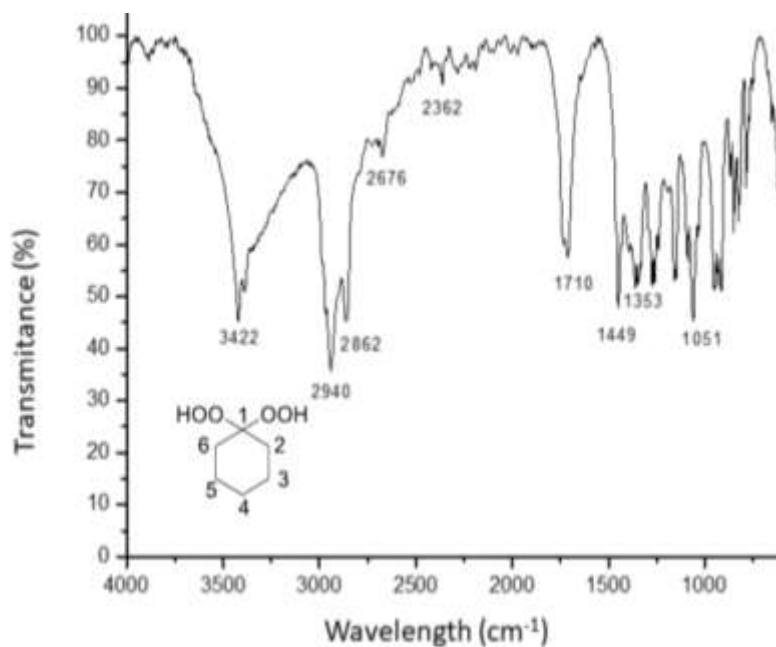
Figure 1.1A. IR (ATR/FTIR) of compound **36.**
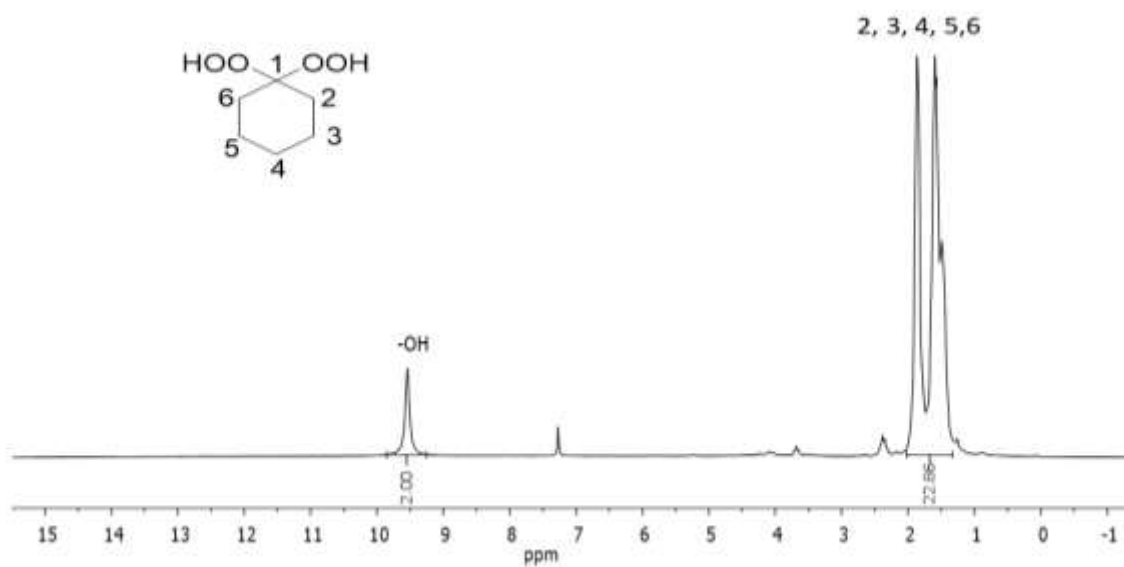
Figure 1.2A. ^{1}H-NMR of (400 MHz, CDCl$_3$) of compound **36.**
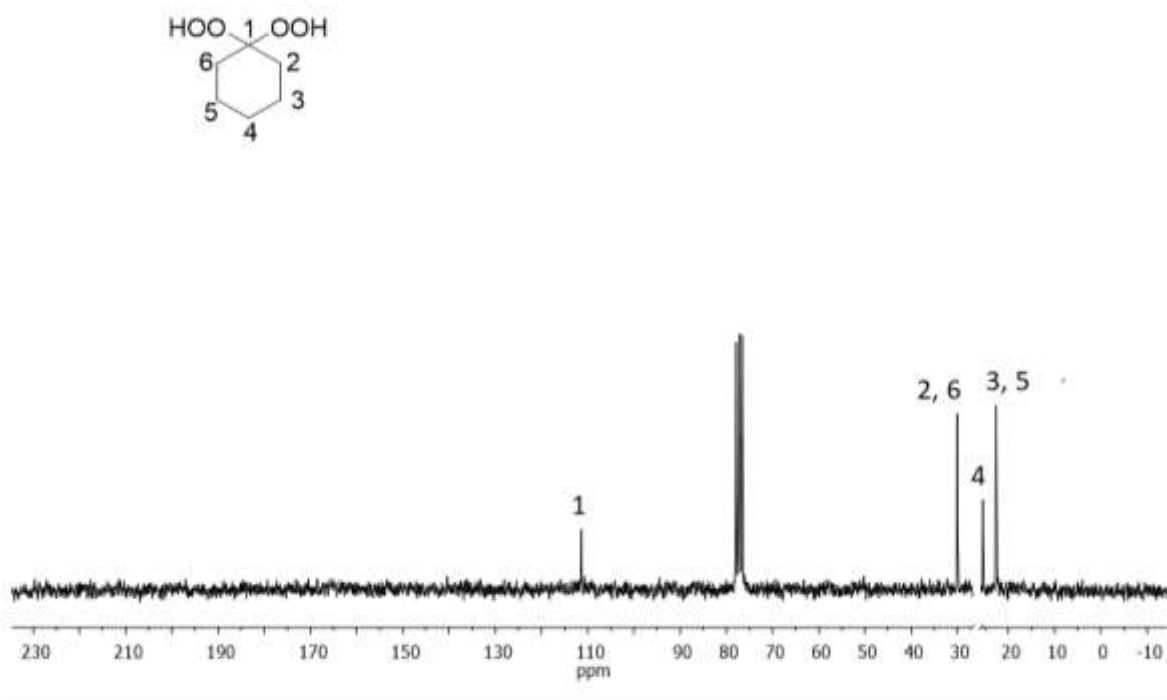
Figure 1.3A.^{13}C-NMR spectrum of (100 MHz, CDCl$_3$) of compound **36**.
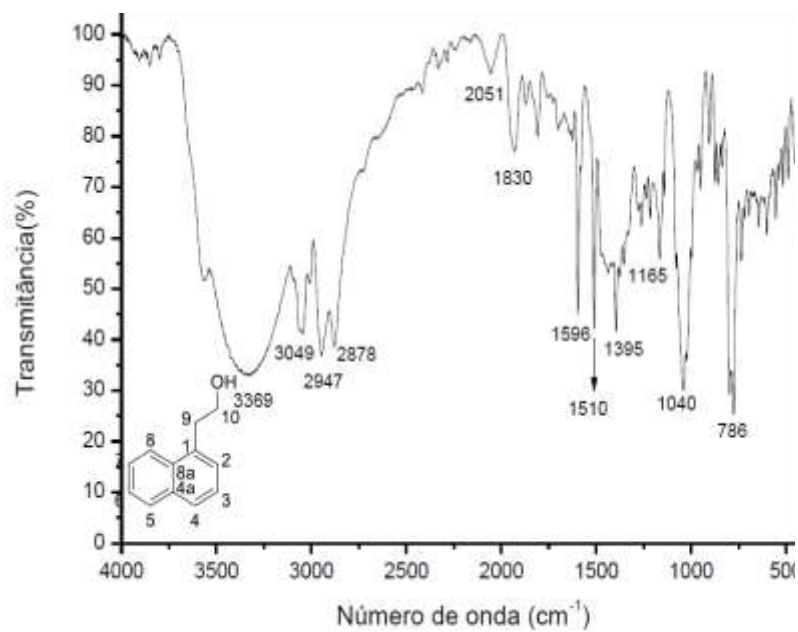
Figure 1.4A. IR (ATR/FTIR) of 2-(naphthalen-1-yl)ethan-1-ol.
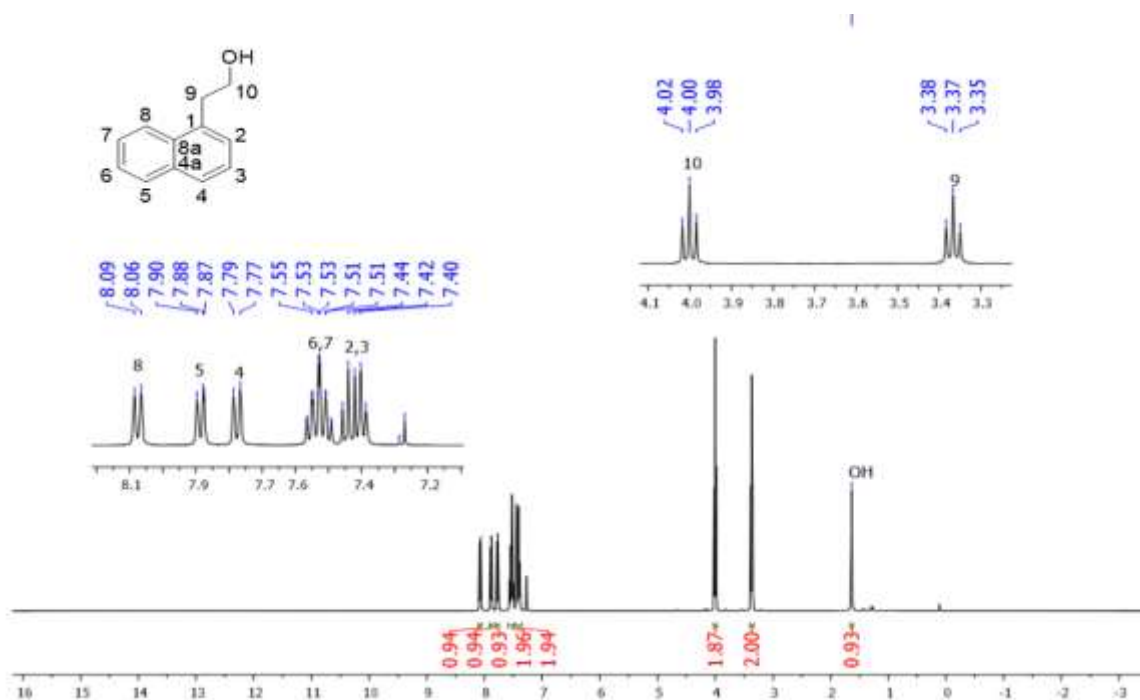
Figure 1.5A.^{1}H-NMR of (400 MHz, CDCl₃) of 2-(naphthalen-1-yl)ethan-1-ol.
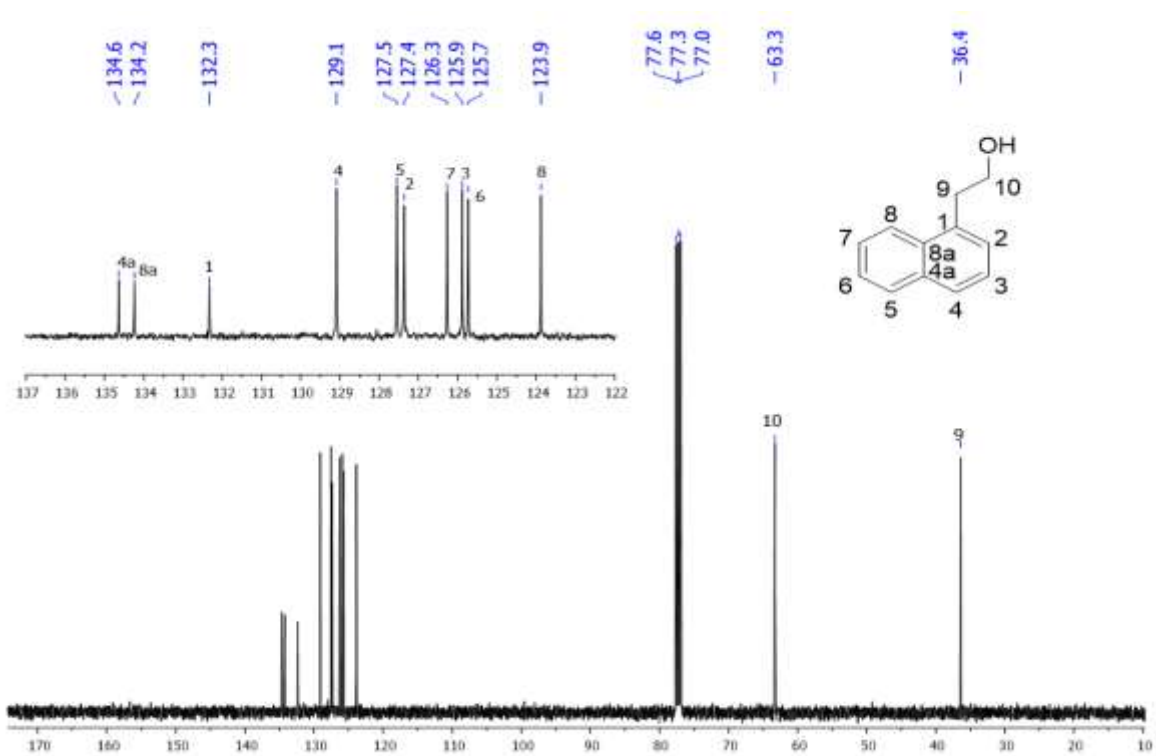
Figure 1.6A.^{13}C-NMR spectrum of (100 MHz, CDCl₃) of 2-(naphthalen-1-yl)ethan-1-ol
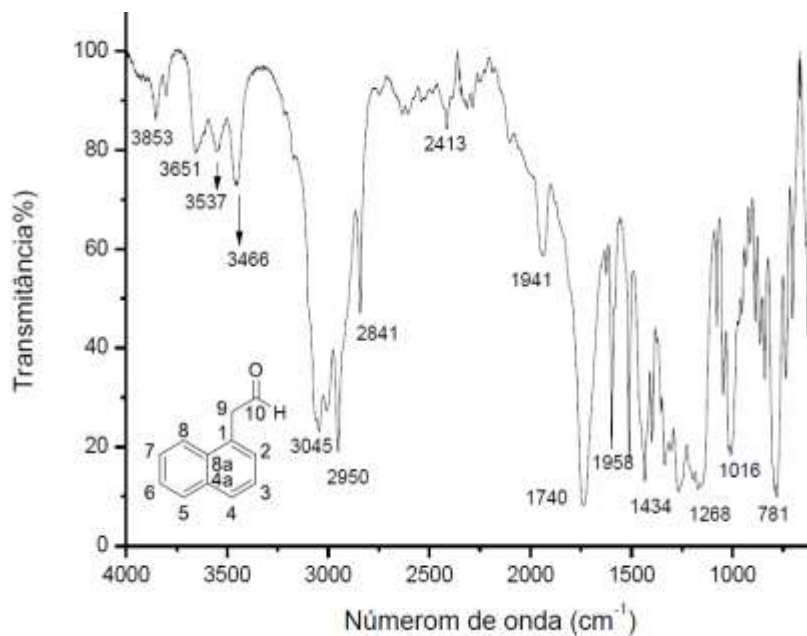
Figure 1.7A. IR (ATR/FTIR) of compound **35.**
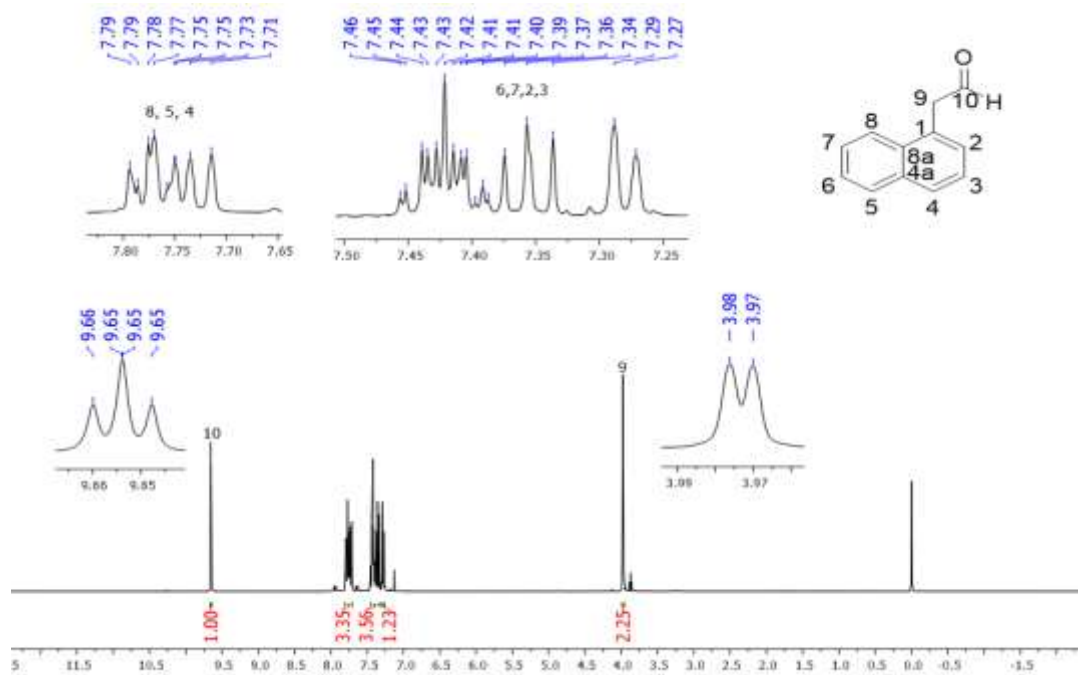
Figure 1.8A. ^{1}H-NMR of (400 MHz, CDCl₃) of compound **35**.
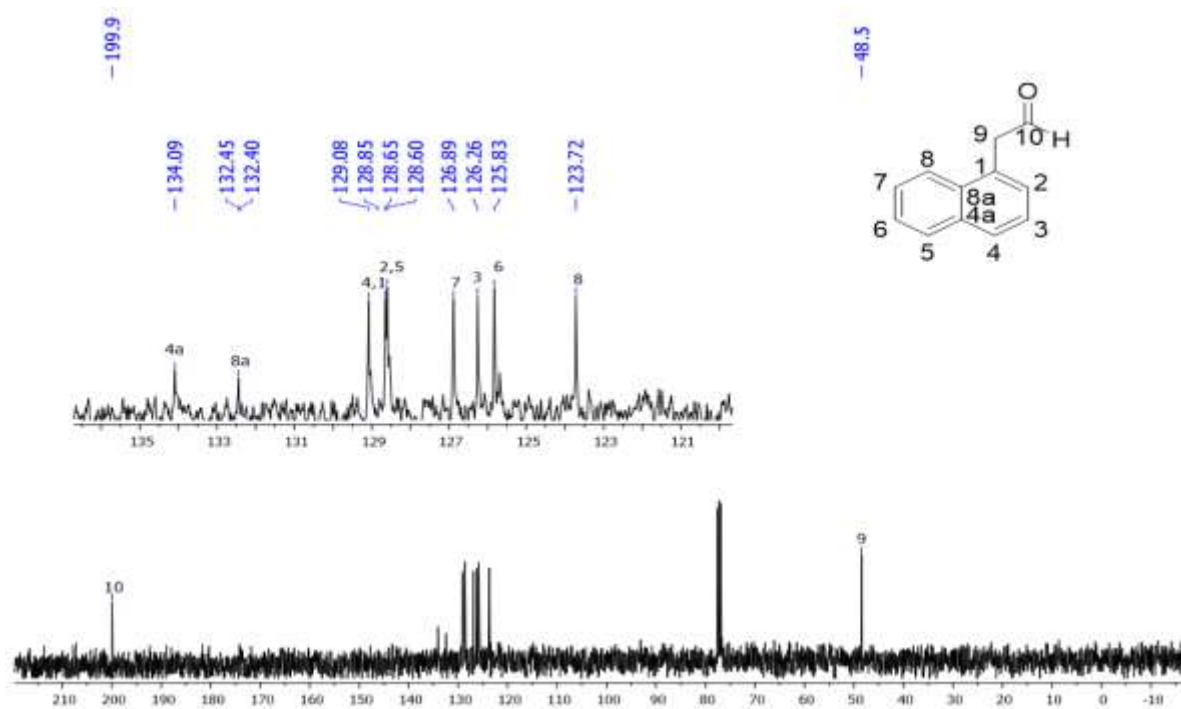
Figure 1. 9A. ^{13}C-NMR spectrum of (100 MHz, CDCl$_3$) of compound **35**.
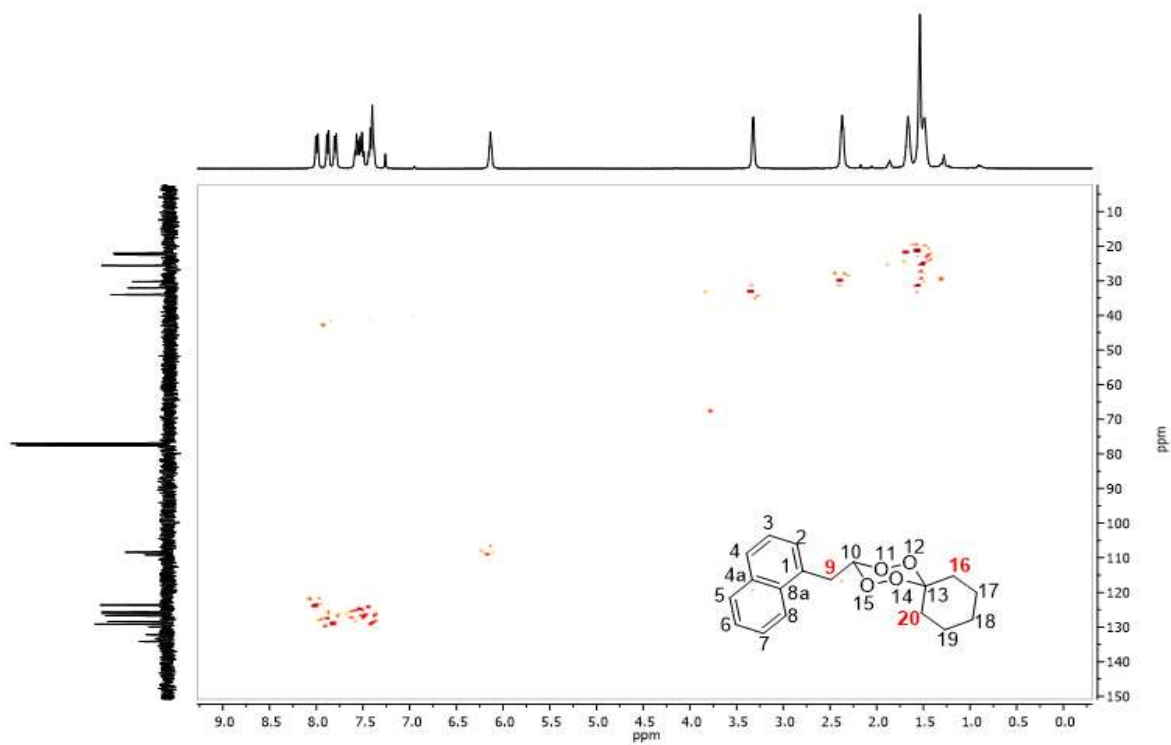
Figure 1. 10A. HSQC map of compound **37.**

144

Table 1.10. A Computed structures of tetraoxane **37**. Stabilization energy (**E**) is reported kJ mol^{-1}. B. D=Boltzmann Distribution.
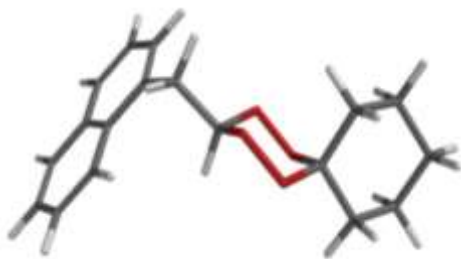
E (kJ mol^{-1}) = -2622097.74
B.D = 0.174
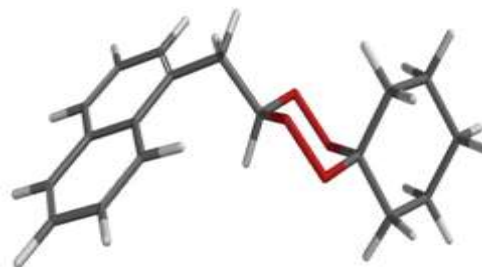
E (kJ mol^{-1}) = -2622097.23
B.D = 0.142
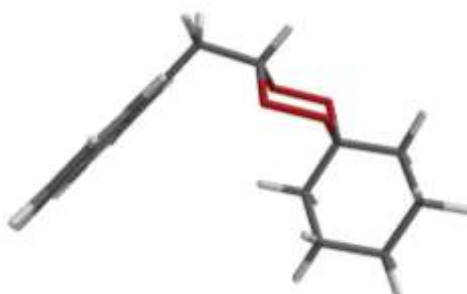
E (kJ mol^{-1}) = -2622094.17
B.D = 0.083
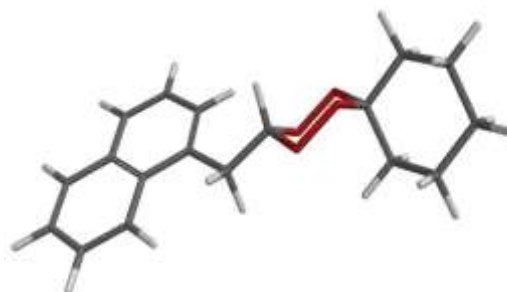
E (kJ mol^{-1}) = -2622094.07
B.D = 0.079
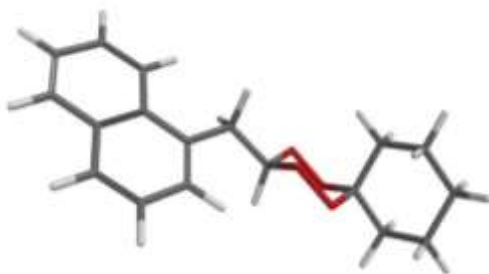
E (kJ mol^{-1}) = -2622093.94
B.D = 0.075
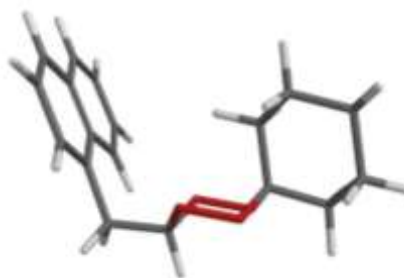
E (kJ mol^{-1}) = -2622093.35
B.D = 0.030
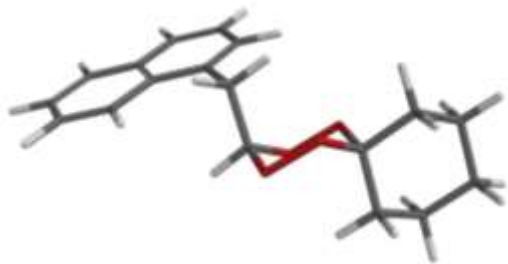
E (kJ mol^{-1}) = -2622089.43
B.D = 0.006
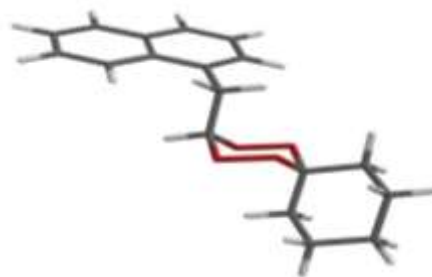
E (kJ mol^{-1}) = -2622088.62
B.D = 0.004
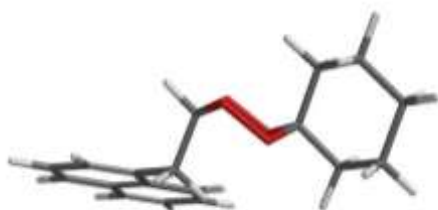
E (kJ mol^{-1}) =-2622087.75
B.D =0.003
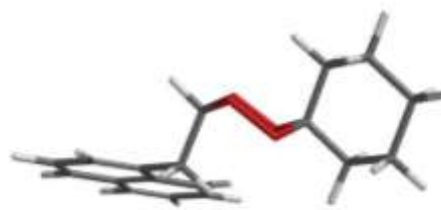
E (kJ mol^{-1}) = -2622088.44
B.D =0.004
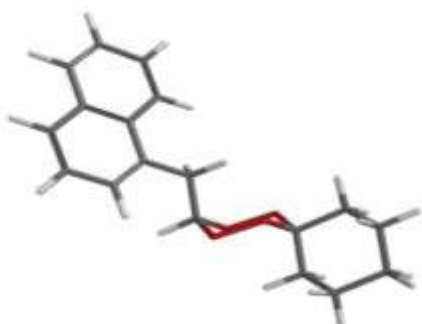
E (kJ mol^{-1}) =-2622082.25
B.D = 0.001
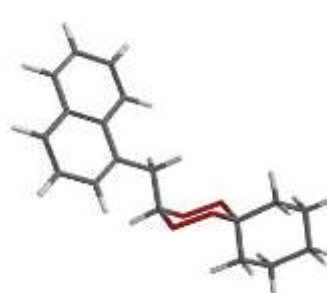
E (kJ mol^{-1}) = -2622082.43
B.D = 0.001
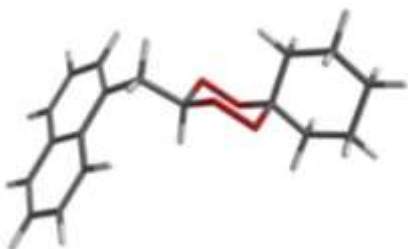
E (kJ mol^{-1}) = -2622098.03
B.D = 0.196

146

Table 1.1A. Effect of compounds **35,36** and **37** on the dry weight (roots and shoots) of *C. sativa* under greenhouse conditions after 21 days of growth. References 2-(naphtalen-1-yl)acetic acid (NAA), Glyphosate (GLY) and Imazethapyr (IMA). *Values are expressed aspercentage of the control.*

Cucumis Sativa		
Compound	*Shoot*	*Root*
37	44.2 ± 17.2	-15.3± 32.7
35	-15.0 ± 13.2	7.8±2.6
36	28.1 ± 14.4	67.3 ± 2.3
NAA	53.0 ± 6.3	53.8 ± 0.5
IMA	32.4 ± 17.2	3.7 ± 0.3
GLY	74.7 ± 29.6	97.9 ±3.6

Table 1.2A. Effect of compounds **35**, **36** and **37** on the dry weight (roots and shoots) of *S.bicolor* under greenhouse conditions after 21 days of growth. References 2-(naphtalen-1-yl)acetic acid (NAA), Glyphosate (GLY) and Imazethapyr (IMA). Values are expressed aspercentage of the control.

Sorghum bicolor		
Compound	*Shoot*	*Root*
37	61.1± 19.3	2.5± 1
35	5.7± 1.0	-3.8 ± 2.7
36	37.1 ± 14.0	22.7 ±11.71
NAA	41.1 ± 5.0	18.4 ± 7.2
IMA	84.4 ± 14.5	77.2 ± 19.8
GLY	31.5 ± 22.4	-63.0 ± 6.1

Table 1.3A. Effect of compounds **35**, **36** and **37** on the dry weight (roots and shoots) of *B. Pilosa* under greenhouse conditions after 21 days of growth. References 2-(naphtalen-1-yl)acetic acid (NAA), Glyphosate (GLY) and Imazethapyr (IMA). *Values are expressed as percentage of the control.*

Bidens Pilosa		
Compound	*Shoot*	*Root*
37	32.7± 8.5	46.3± 2.5
35	26.3± 7.3	36.7± 2.8
36	8.3 ± 11.8	20.4 ± 13.1
NAA	22.2 ± 7.1	49.6 ± 7.5
IMA	48.9 ± 3.6	66.3 ± 4.3
GLY	65.6 ± 6.3	73.0 ± 13.9

Table 1.4A. Effect of compounds **35**, **36** and **37** on the dry weight (roots and shoots) of *I. acuminate* under greenhouse conditions after 21 days of growth. References 2-(naphtalen-1-yl)acetic acid (NAA), Glyphosate (GLY) and Imazethapyr (IMA). *Values are expressed aspercentage of the control.*

Iponomea acuminate		
Compound	*Shoot*	*Root*
37	52.9± 6.9	15.3 ±0.1
35	40.0± 6.7	5.6 ± 3.1
36	6.4 ± 0.6	-53.6 ± 7.7
NAA	52.0 ± 8.0	61.9 ± 3.1
IMA	61.0 ± 6.8	43.9 ± 8.1
GLY	35.0 ± 18.3	12.7 ± 19.4

Table 1.5A. Effect of compounds **35**, **36** and **37** on the dry weight (roots and shoots) of *S. americaum* under greenhouse conditions after 21 days of growth. References 2-(naphtalen-1-yl)acetic acid (NAA), Glyphosate (GLY) and Imazethapyr (IMA). *Values are expressed aspercentage of the control.*

Compound	Shoot	Root
	Solanum americanum	
37	84.5 ± 3.1	91.6 ± 5.4
35	25.0 ± 13.2	-63 ± 7.5
36	76.4 ± 4.4	42.0 ± 3.1
NAA	-141.2 ± 22.1	31.1 ± 10.8
IMA	100 ± 0	100 ± 0
GLY	100 ± 0	100 ± 0

Table 1.6A. Effect of compounds **5** ,**6** and **8** on the dry weight (roots and shoots) of *A. ficoidea* under greenhouse conditions after 21 days of growth. References 2-(naphtalen-1-yl)acetic acid (NAA), Glyphosate (GLY) and Imazethapyr (IMA). *Values are expressed aspercentage of the control.*

Compound	Shoot	Root
	Amaranthus ficoidea	
37	87.6 ± 5.5	24.0 ± 6.8
35	72.9 ± 9.5	37.5 ± 4.9
37	79.8 ± 3.9	42.6 ± 9.1
NAA	95.4 ± 8.0	91.0 ± 2.3
IMA	95.0± 1.0	91.0 ± 2.3
GLY	93.0 ± 1.5	93.0 ± 5.2

Table 1.7A. Optimization conditions of the method for the separation of compound **35, 36, 37.**

Condition	Solvent A (%)	Solvent	Flux (mL/min)	Time (min)
1	(95)	B	1	40
2	(95) [*]	B	1	40
3	(20) [*]	B	1	40
4	(30) [*]	B	1	40
5	(70) [*]	B	1	40
6	(95) [*]	B	1	45
7	(95) [*]	B	1	50
8	(95) [*]	B	1	85
9	(90) [*]	B	1	95
10	(95) [*]	B	0.4	82
11	(95) [*]	B	1	82
12	(90) [*]	B	0.4	102
13	(95) [*]	B	0.4	95
15	(90) [*]	B	1	102
16	(90) [*]	C	0.4	102
17	(95) [*]	C	0.4	102

[*] In this cases 0.1 mL of trifluoracetic acid was added to the mobile phase. Solvent A: Water, B: Acetonitrile, C: Methanol
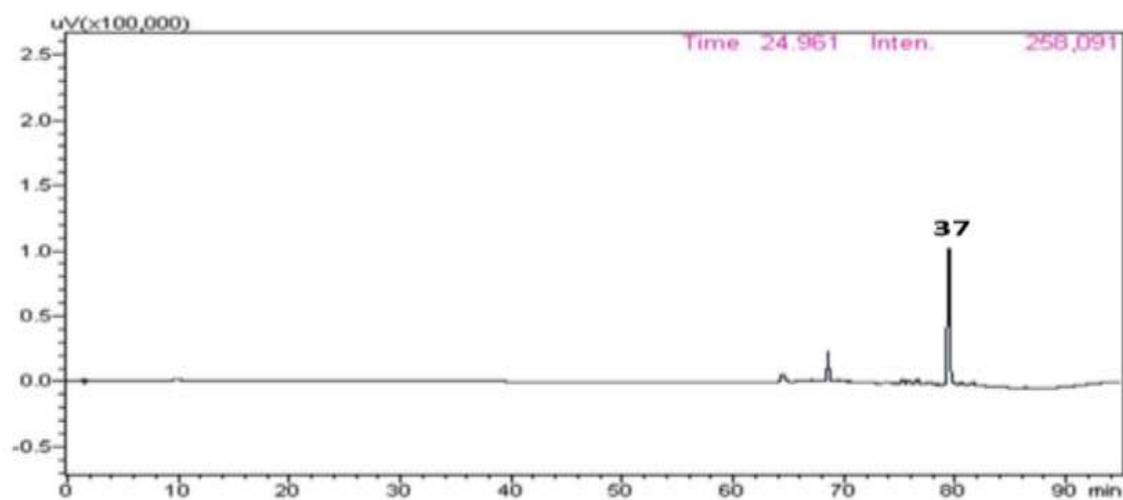
Figure 1.11A. HPLC chromatogram of compound **37** (81 min) at 2 mmol L^{-1}**.** The separations were carried out using a Phenomenex C18 column (2.6 μm size particles, length 100 mm, i.d. 3 mm) using a mixture ofacetonitrile/water 95:5 as eluent.
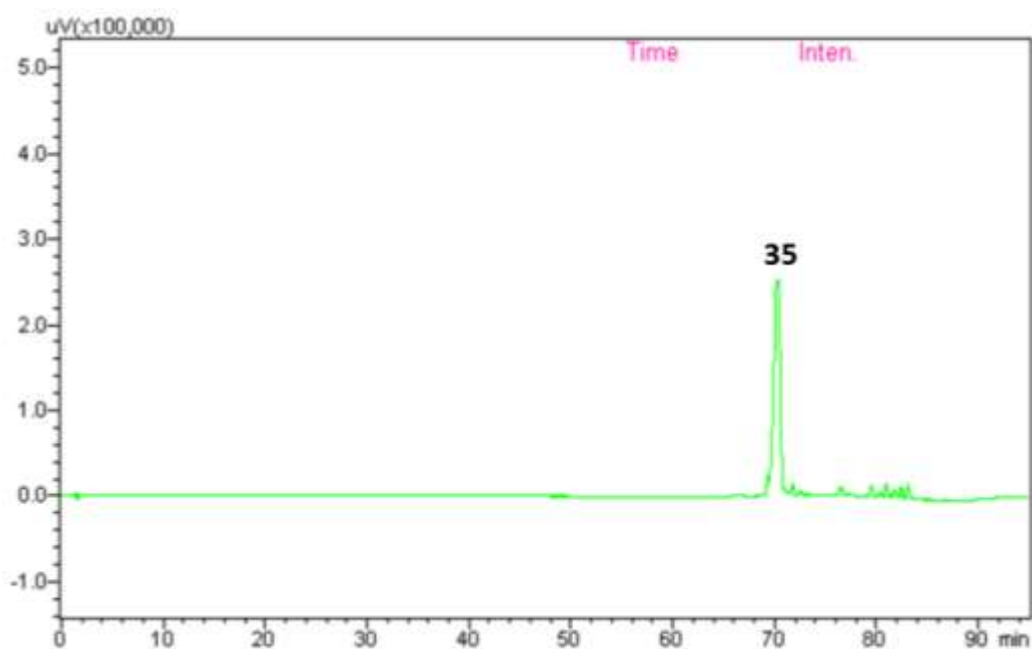
Figure 1.12A. HPLC chromatogram of compound 35 (70 min) at 2 mmol L^{-1}. The separations were carried out using a Phenomenex C18 column (2.6 μm size particles, length 100 mm, i.d. 3 mm) using a mixture of acetonitrile/water 95:5 as eluent
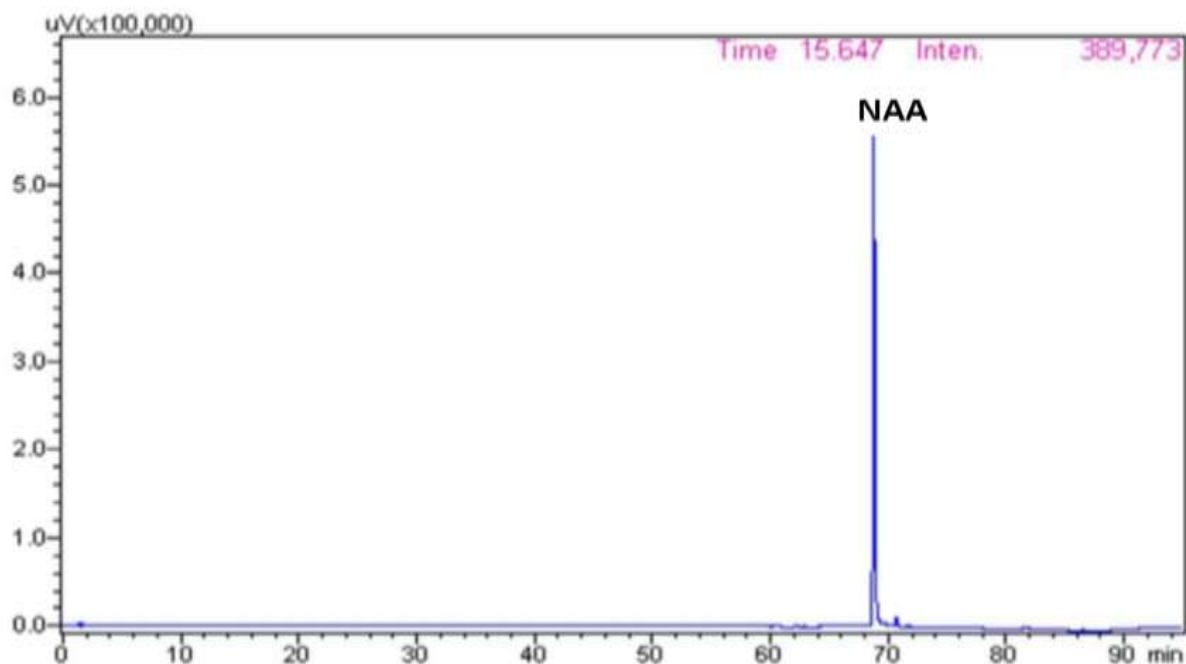
Figure 1.13A. HPLC chromatogram of NAA (71.1 min) at 2 mmol L^{-1}**.** The separations were carried out using a Phenomenex C18 column (2.6 μm size particles, length 100 mm, i.d. 3 mm) using a mixture ofacetonitrile/water 95:5 as eluent.

Table 1.8A. Concentration of compound **37** during the degradation experiment

Day	Conc (mmol/L)	Percentage (%)
1	1.6 ± 0.001	81.5 ± 0.05
3	1.1 ± 0.005	58.9 ± 9.8
5	1.2 ± 0.09	58.6 ± 3.9
7	1.1 ± 0.2	56.6 ± 6.3
9	1.2 ± 0.1	57.6 ± 6.1
11	1.3 ± 0.05	62.8 ± 2.4
13	0.5 ± 0.05	20.5 ± 1.3
15	0.07 ± 0.01	3.7 ± 0.5
19	0 ± 0	0 ± 0
22	0 ± 0	0 ± 0

DATA REFERRED TO CHAPTER 3
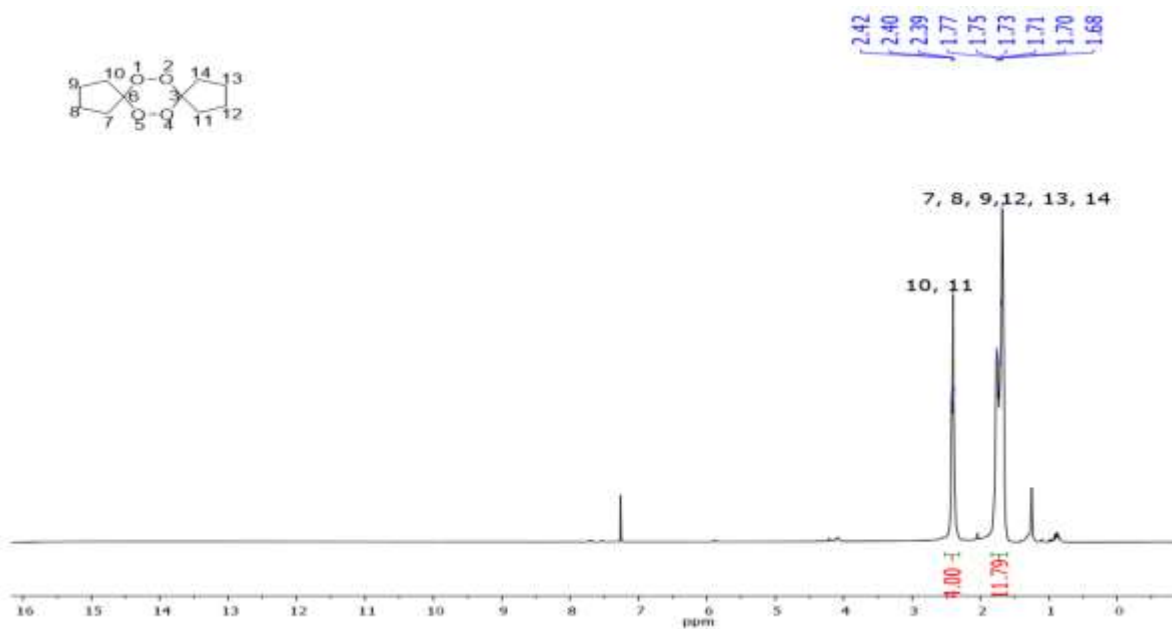
Figure 2.1A. ^{1}H-NMR of (400 MHz, CDCl$_3$) of compound **12a**.
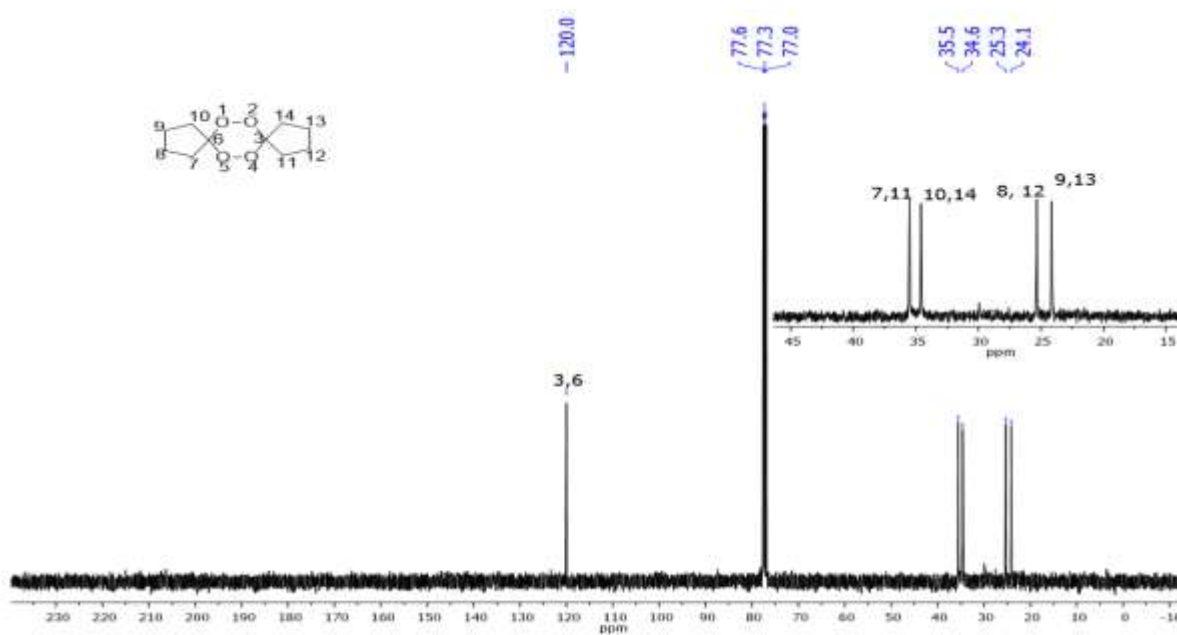
Figure 2.2A. ^{13}C-NMR spectrum of (100 MHz, CDCl$_3$) of compound **12a**.
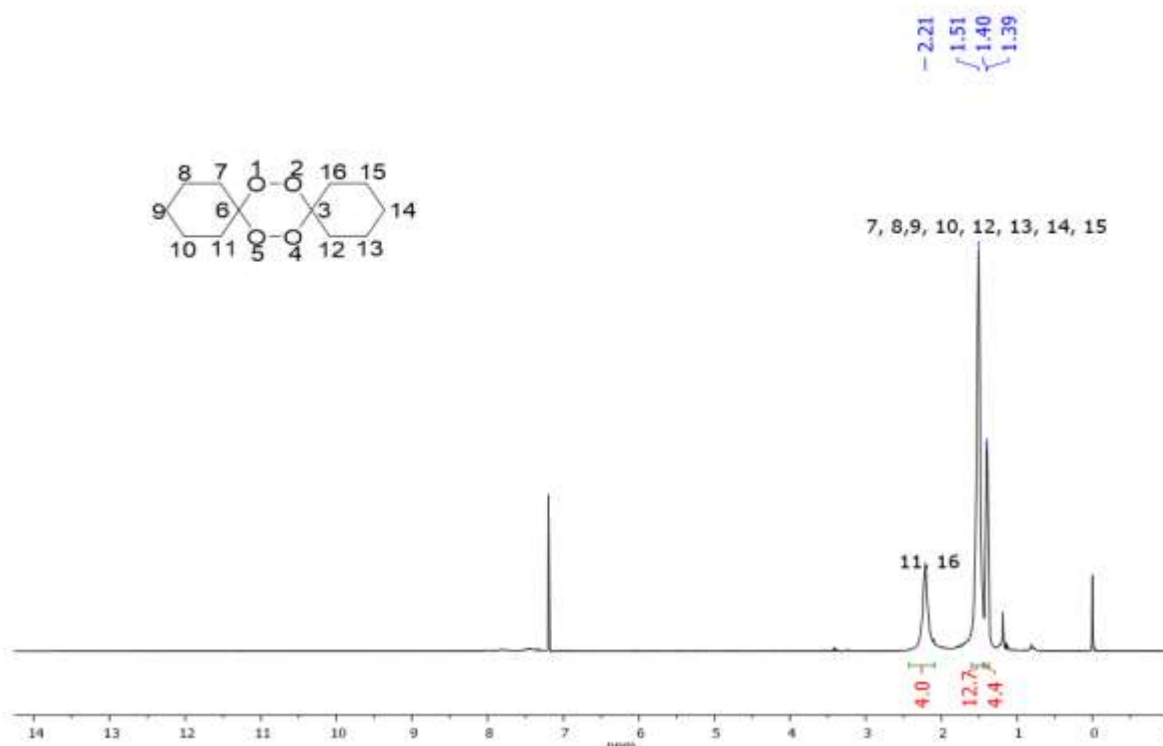
Figure 2.3A. ^{1}H-NMR of (400 MHz, CDCl$_3$) of compound **12b**.
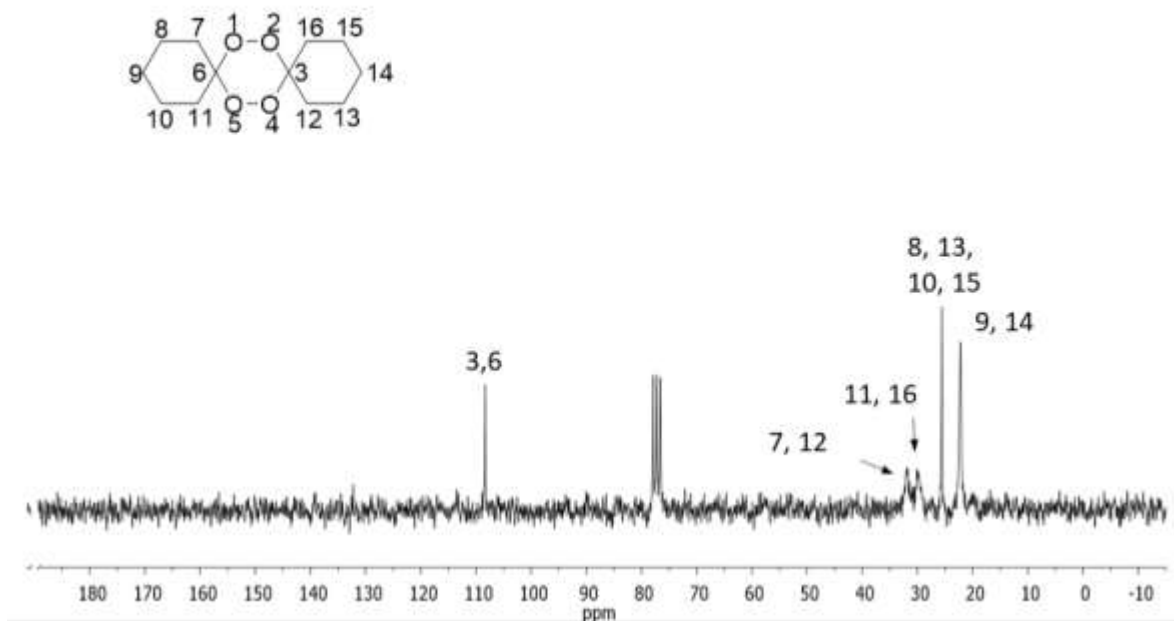
Figure 2.4A. ^{13}C-NMR spectrum of (100 MHz, CDCl$_3$) of compound **12b**.
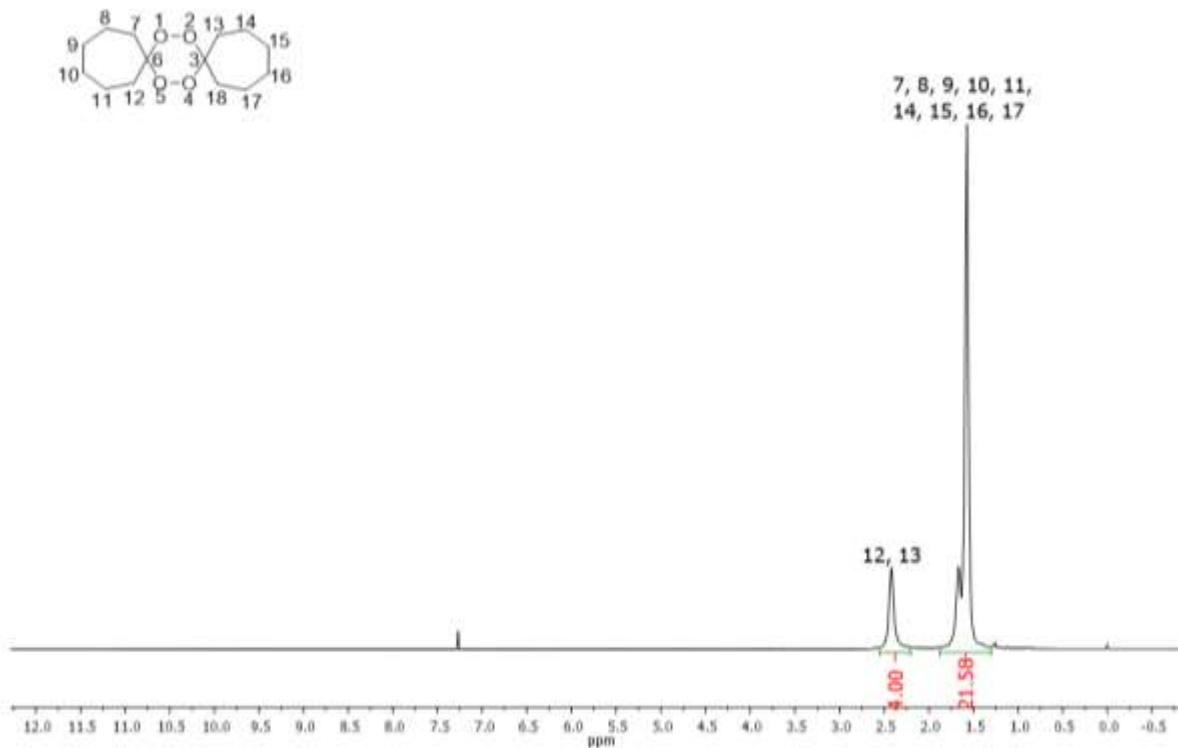
Figure 2.5A. ^{1}H-NMR of (400 MHz, CDCl$_3$) of compound (**12c**).
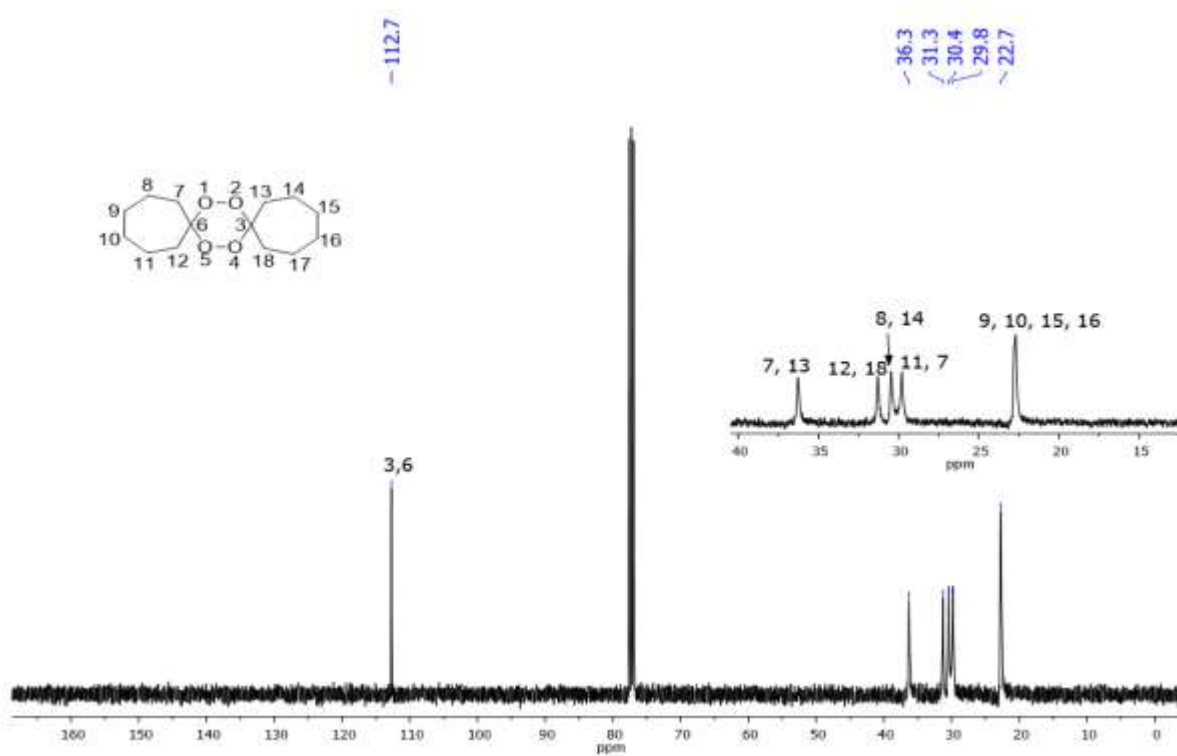
Figure 2.6A. ^{13}C-NMR spectrum of (100 MHz, CDCl$_3$) of compound (**12c**).

155
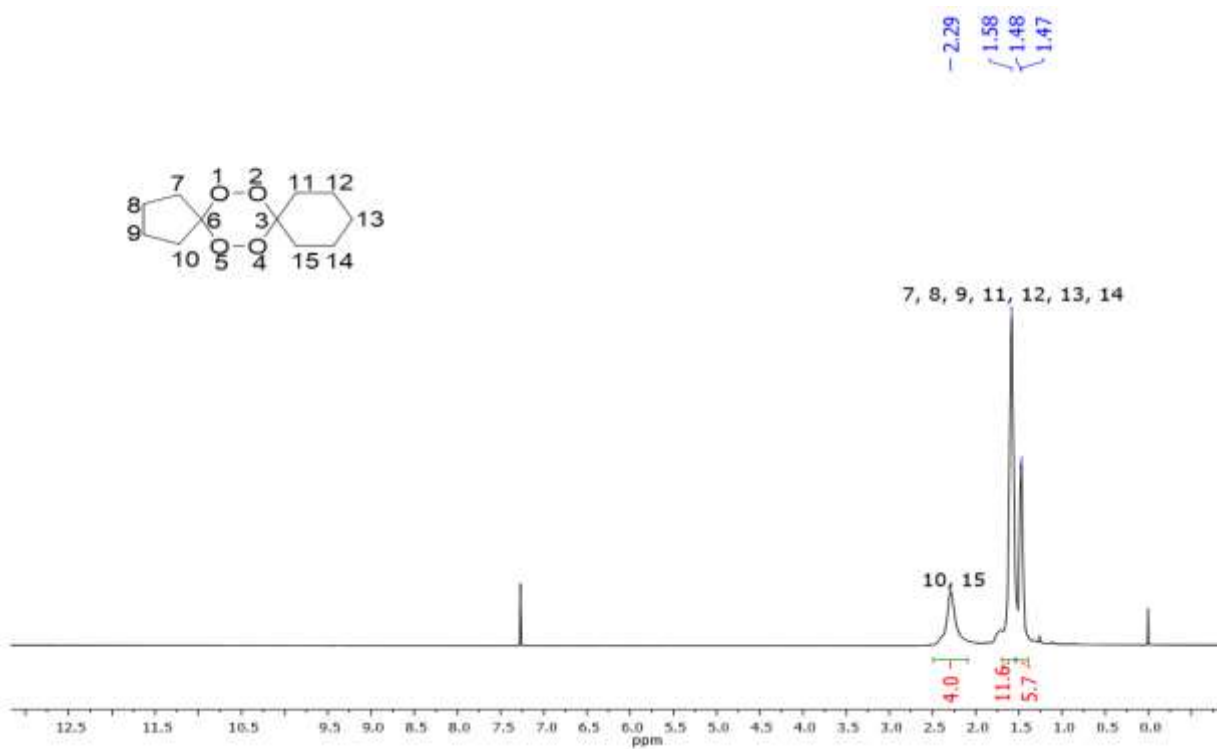
Figure 2.7A. ^{1}H-NMR of (400 MHz, CDCl$_3$) of compound **12d**.
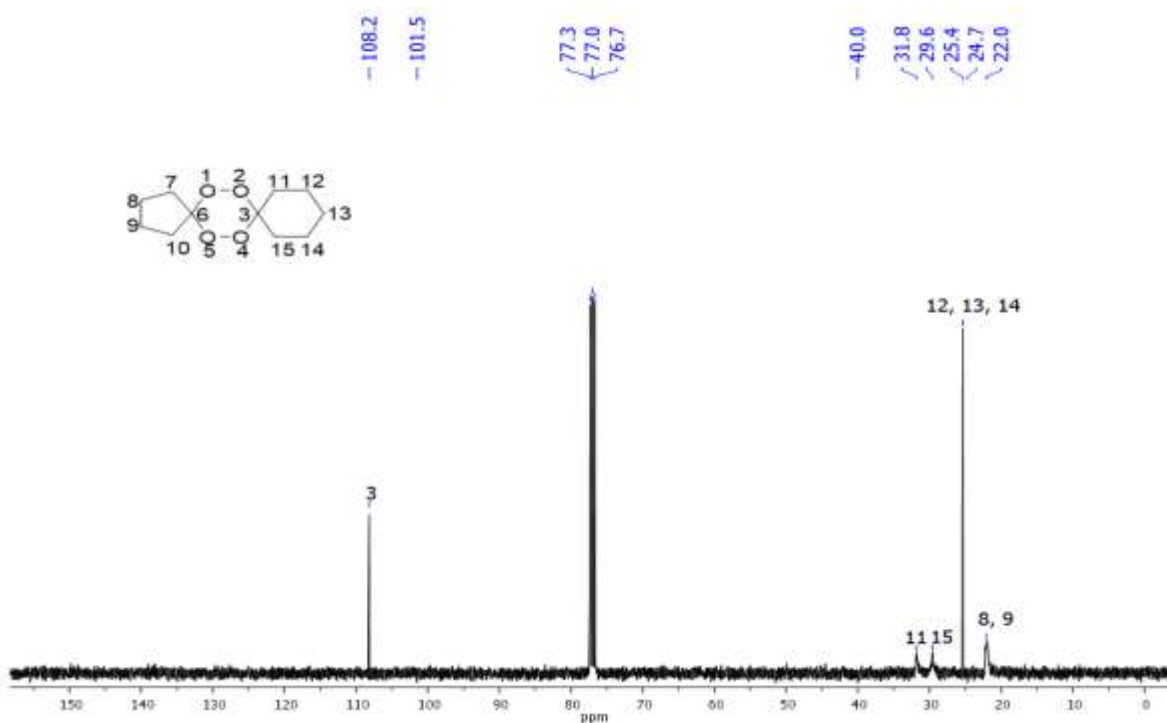
Figure 2.8A. ^{13}C-NMR spectrum of (100 MHz, CDCl$_3$) of compound **12d**.
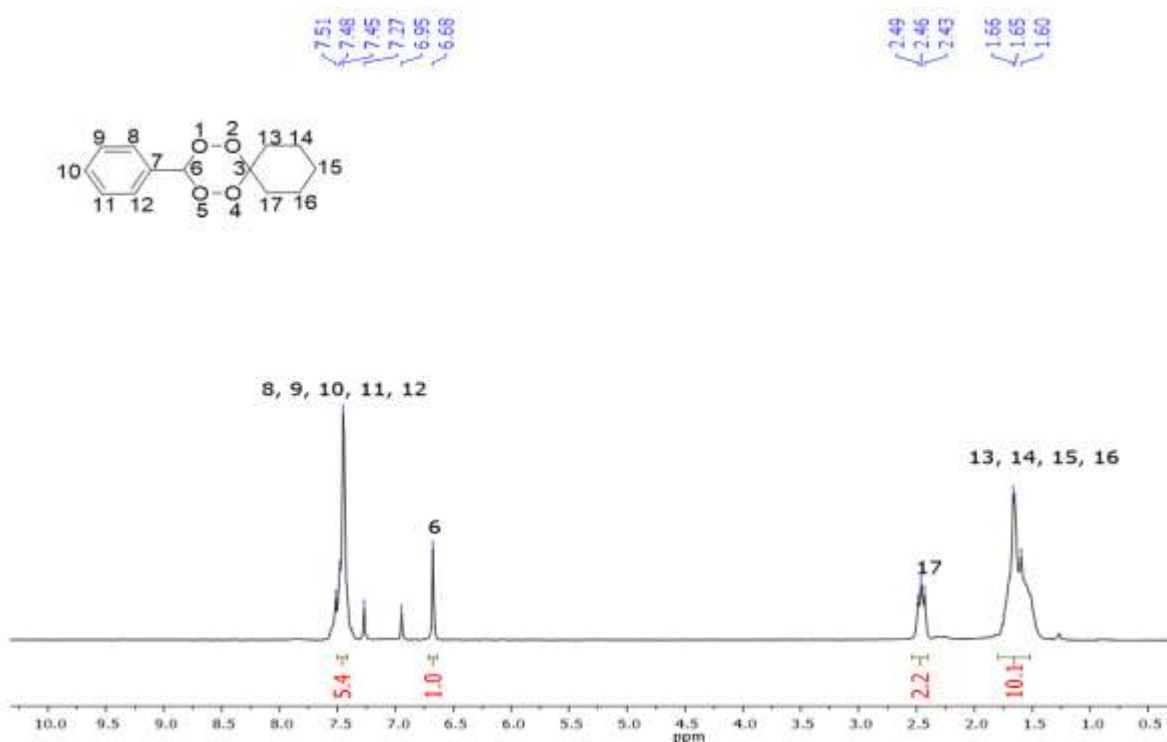
Figure 2.9A. ^{1}H-NMR of (400 MHz, CDCl$_3$) of compound **12f**.
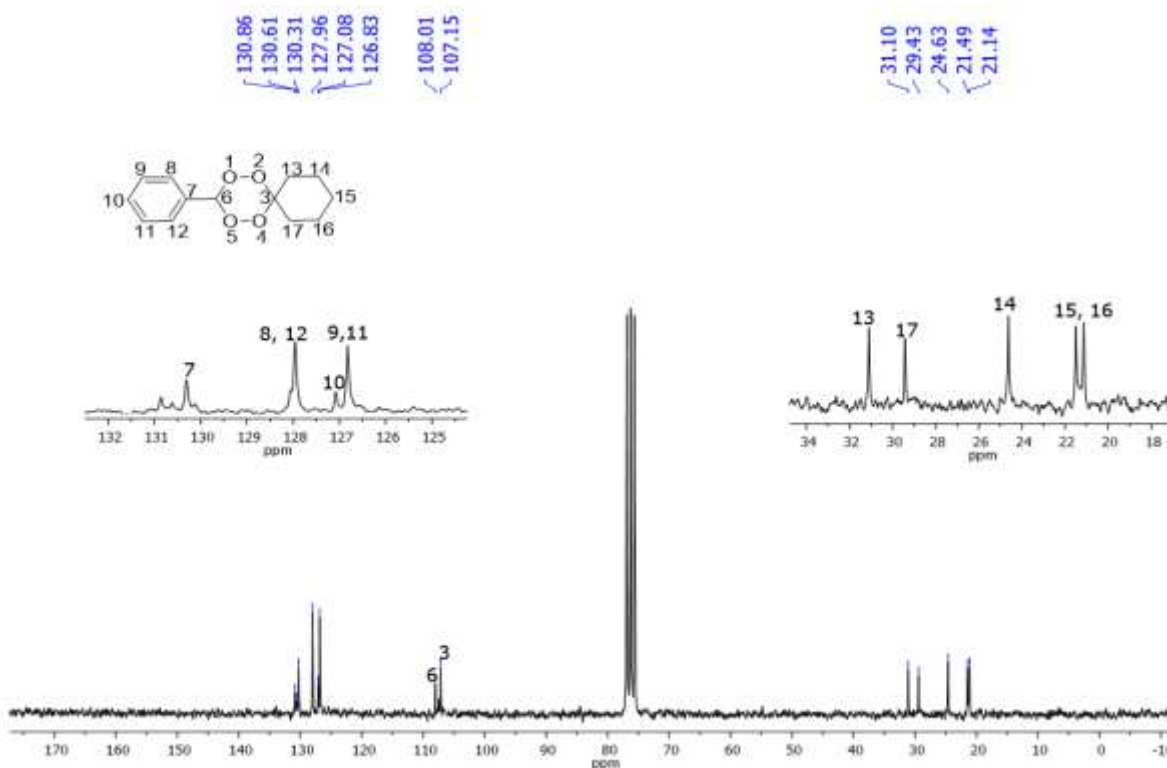
Figure 2.10A. ^{13}C-NMR spectrum of (100 MHz, CDCl$_3$) of compound **12f**.
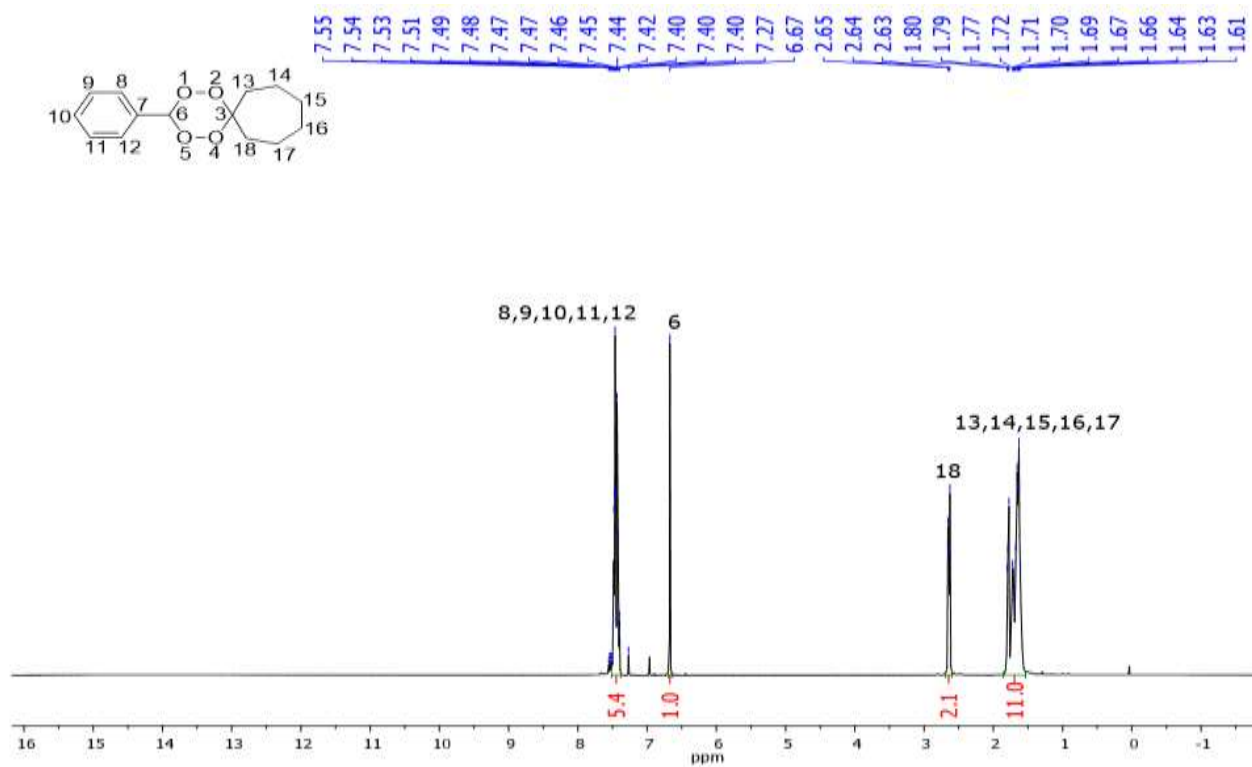
Figure 2.11A. ^{1}H-NMR of (400 MHz, CDCl$_3$) of compound **12g**.
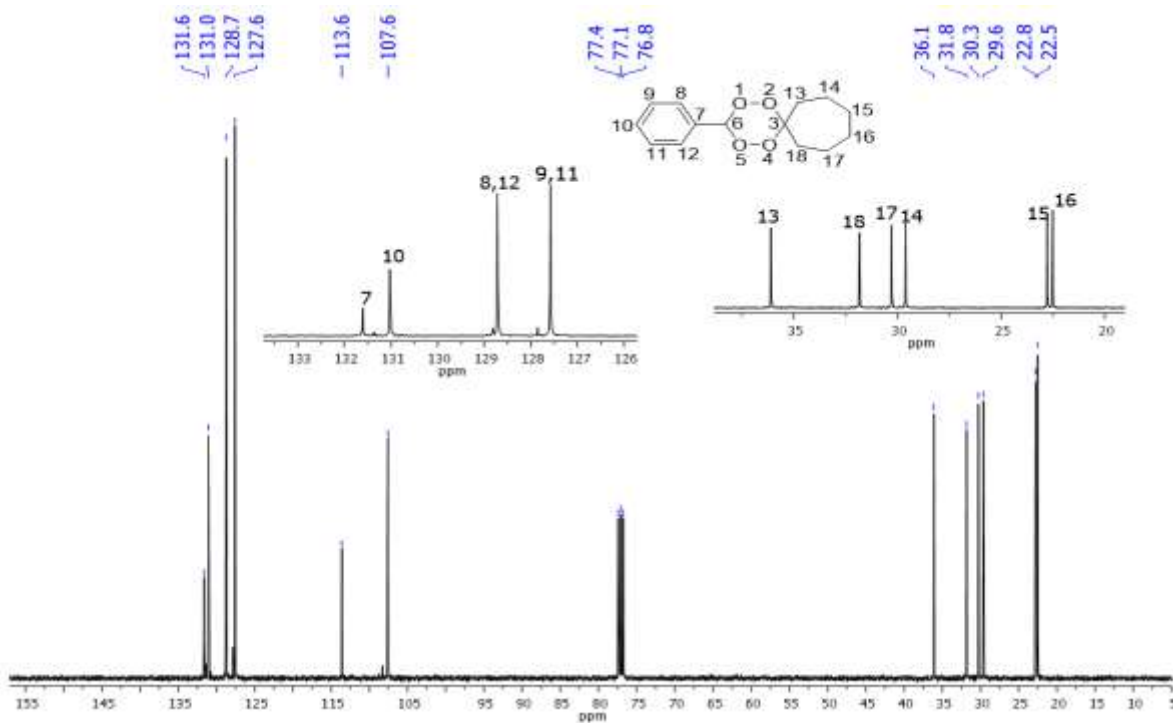
Figure 2.12A. ^{13}C-NMR spectrum of (100 MHz, CDCl$_3$) of compound **12g**.
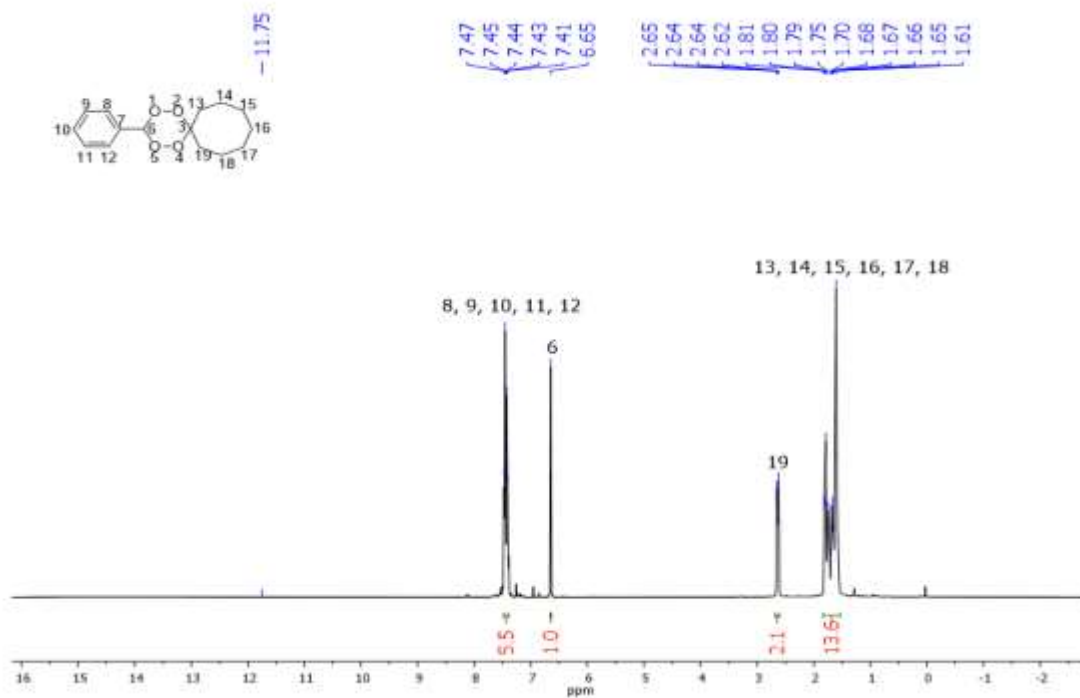
Figure 2.13A. ^{1}H-NMR of (400 MHz, CDCl$_3$) of compound **12h**.
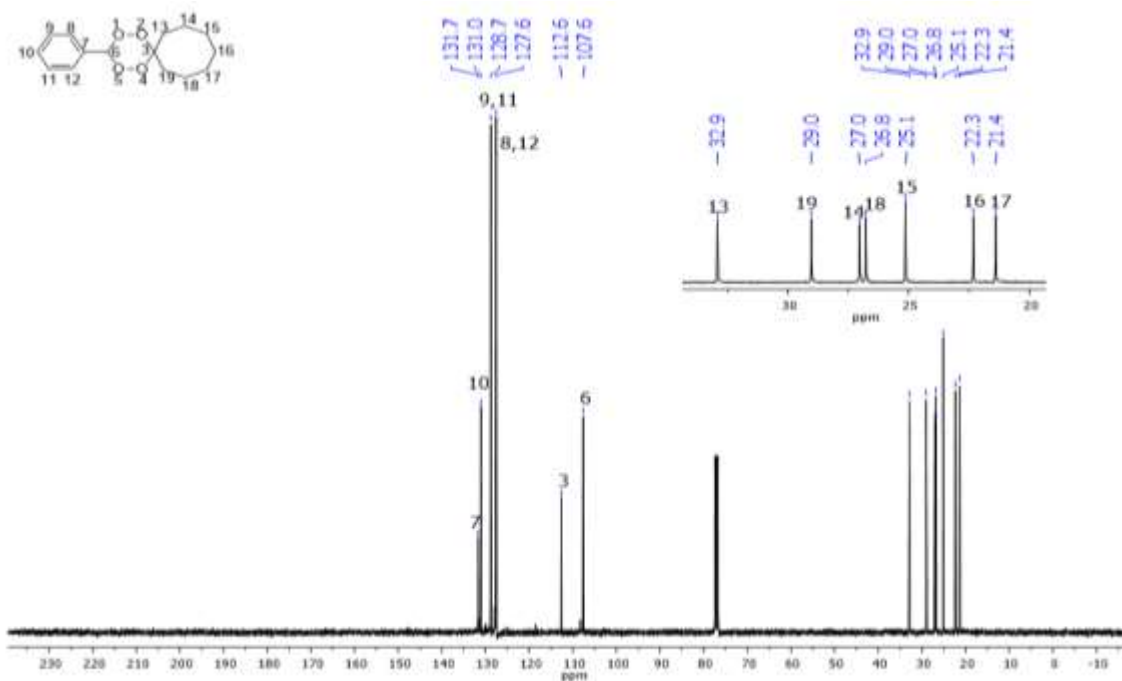
Figure 2.14A. ^{13}C-NMR spectrum of (100 MHz, CDCl$_3$) of compound **12h**.
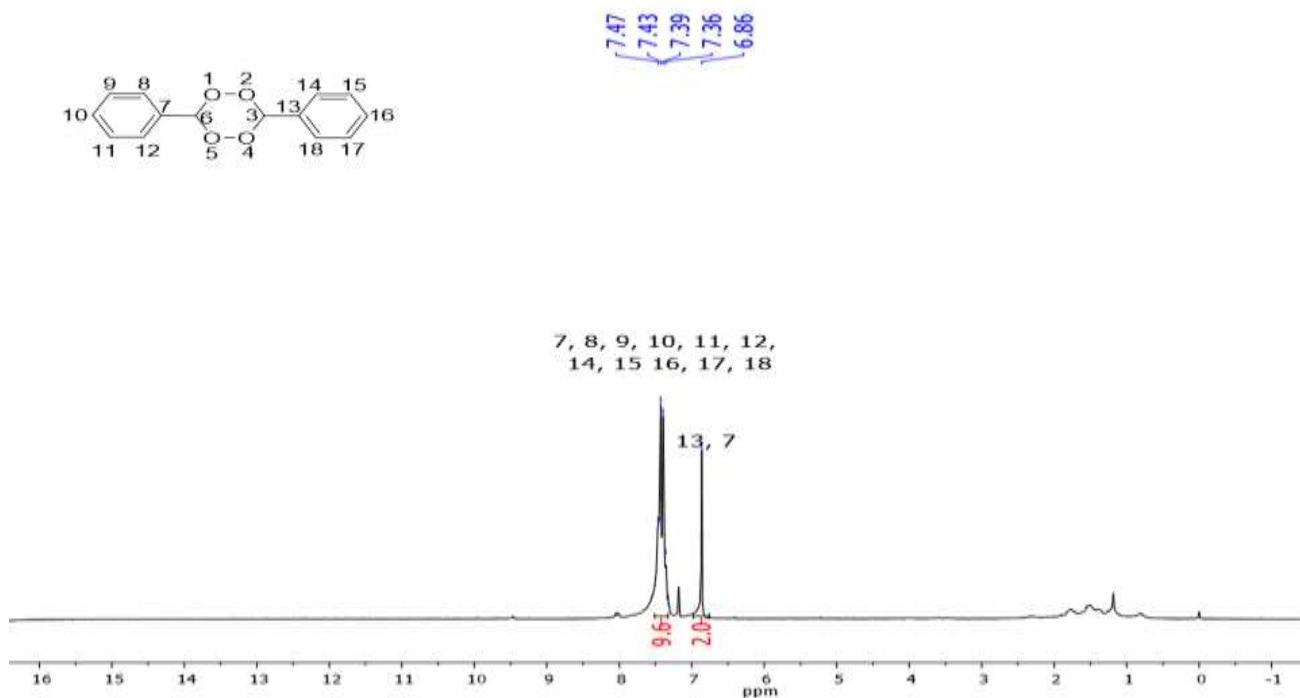
Figure 2.15A. ^{1}H-NMR of (400 MHz, CDCl$_3$) of compound **12i**.
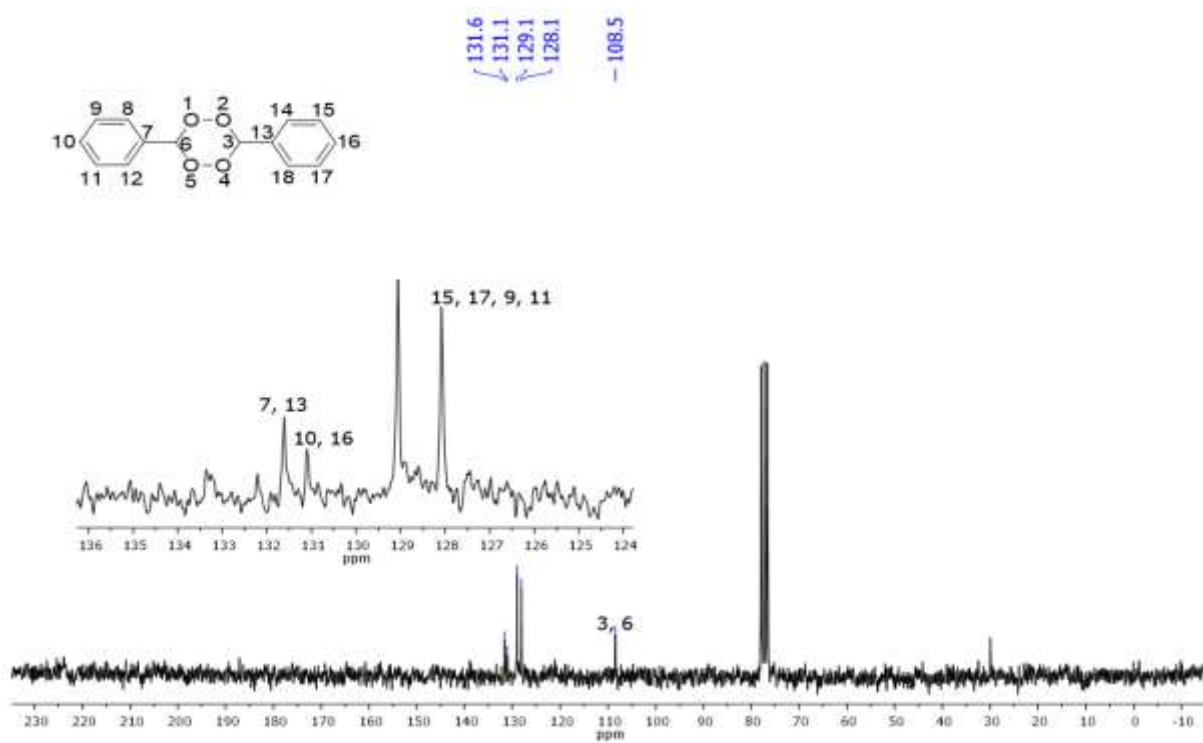
Figure 2.16A. ^{13}C-NMR spectrum of (100 MHz, CDCl$_3$) of compound **12i**.

160
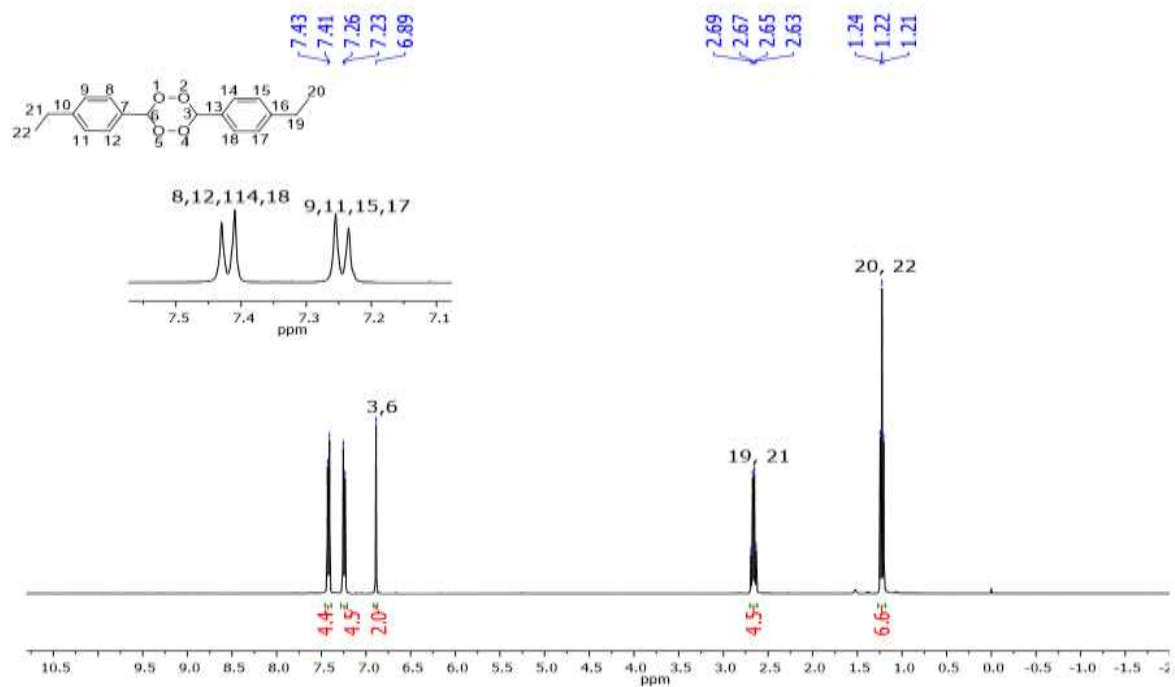
Figure 2.17A. ^{1}H-NMR of (400 MHz, CDCl$_3$) of compound **12j**,
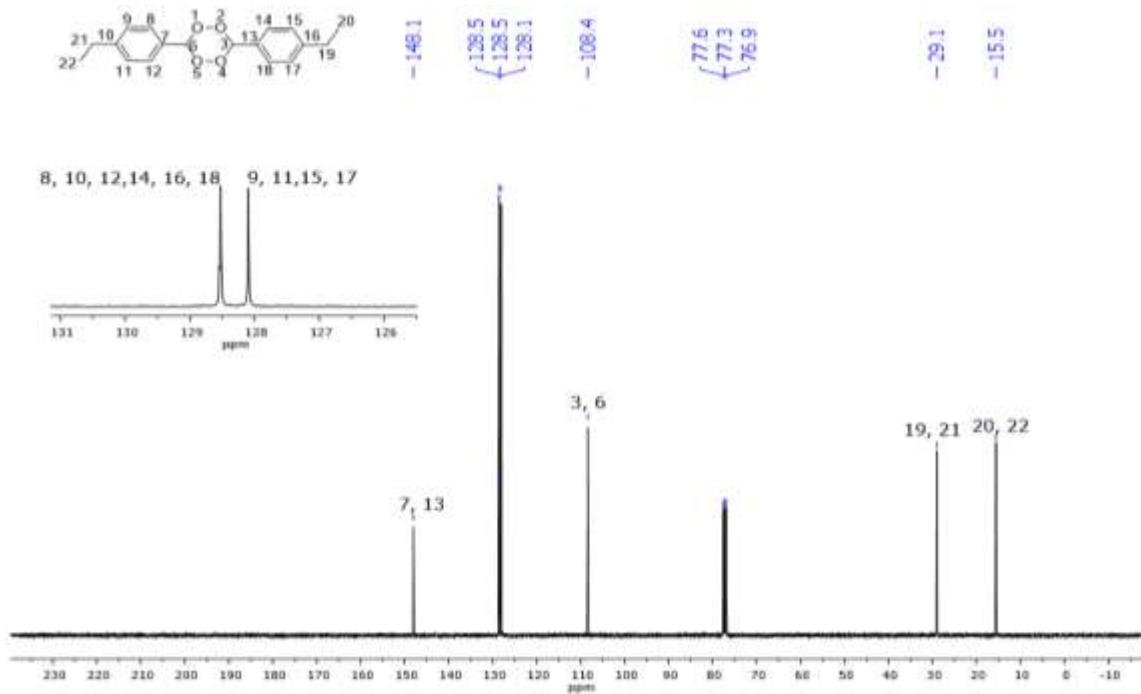
Figure 2.18A. ^{13}C-NMR spectrum of (100 MHz, CDCl$_3$) of compound **12j**.
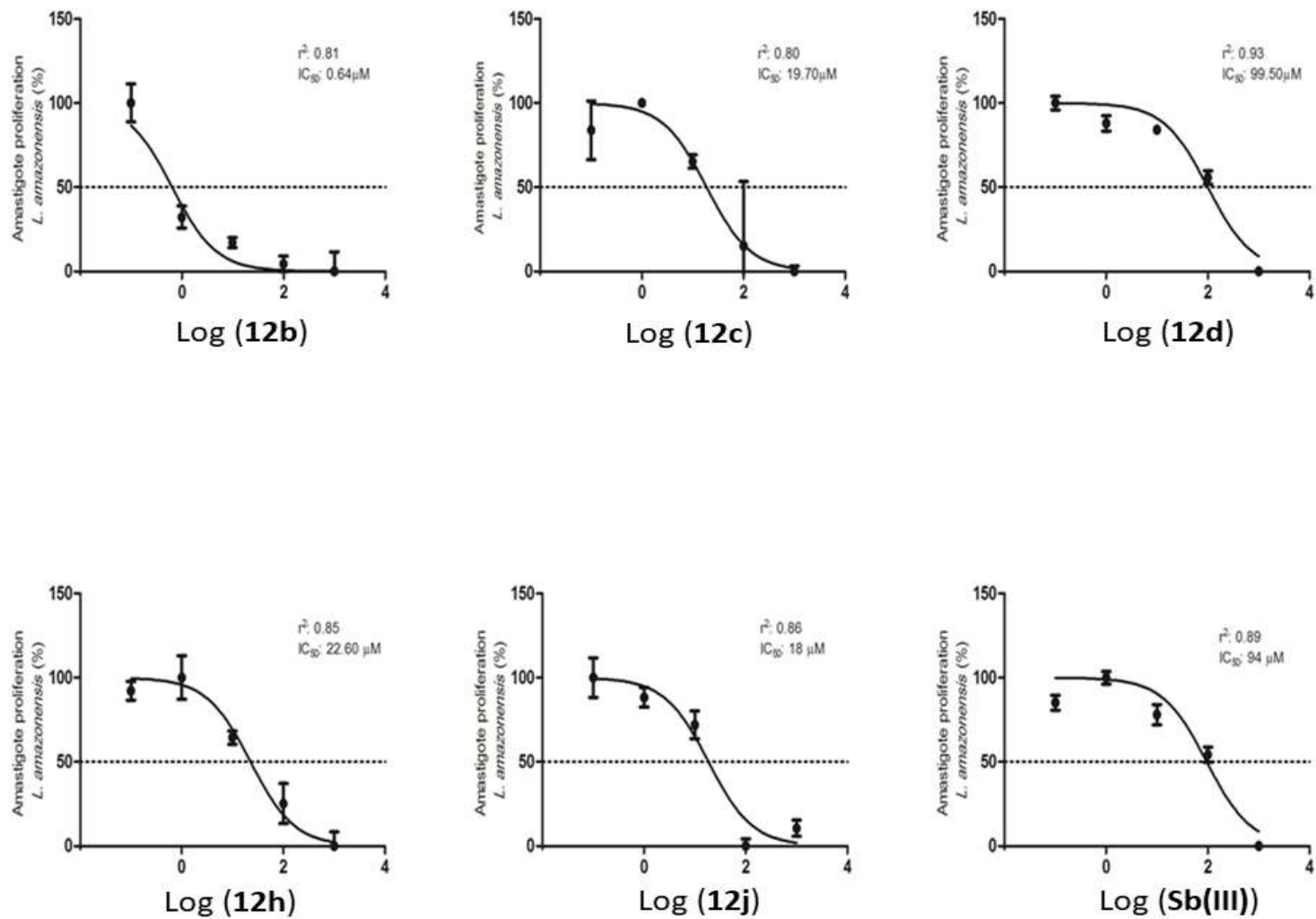
Figure 2.19A. Inhibition of intracellular amastigote forms of *L. amazonensis* caused by **12b**, **12c**, **12d**, **12h**, **12j** and Sb (III).
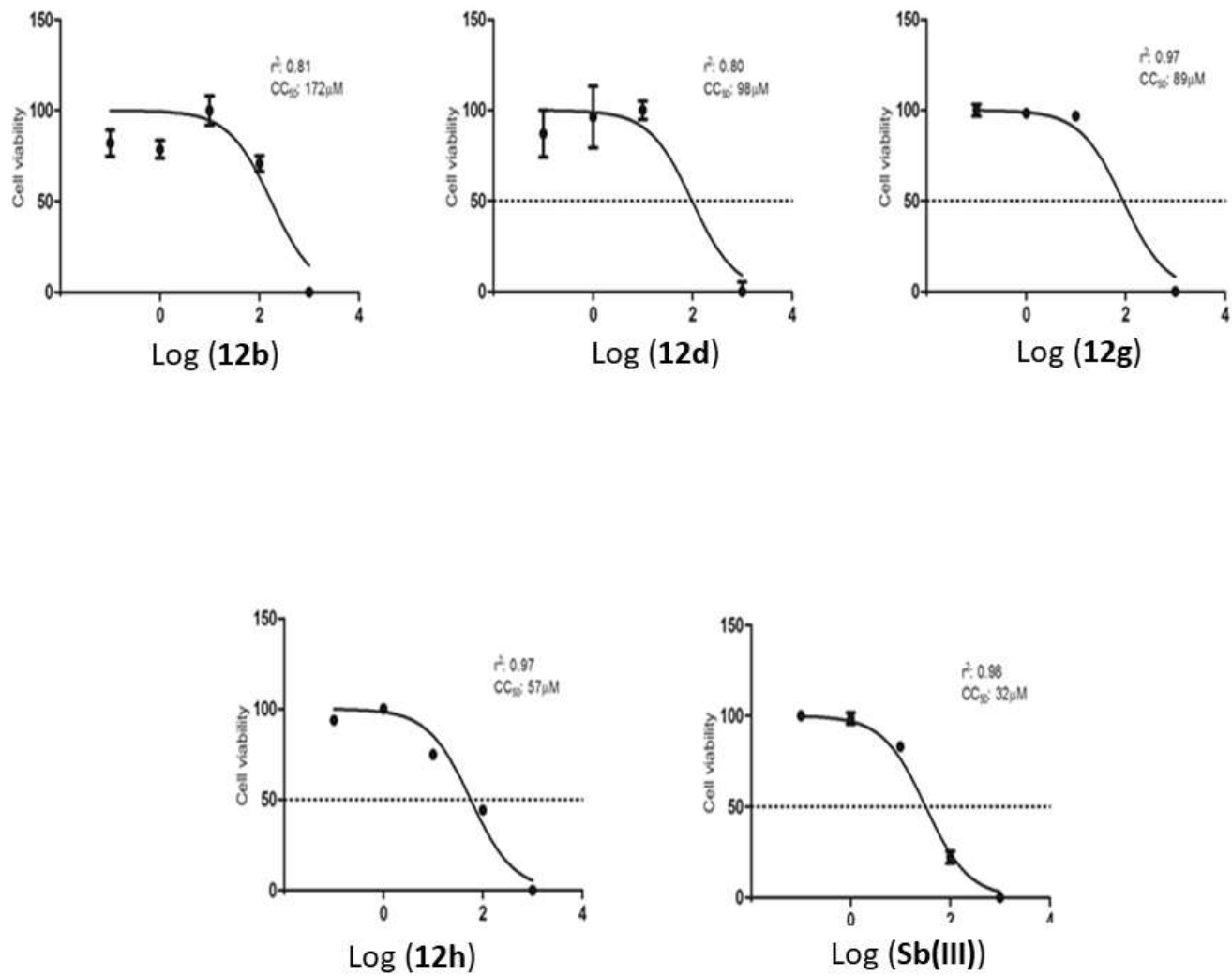
Figure 2.20A. Cytotoxicity of **12b**, **12d**, **12g**, **12j**, **12h** and Sb (III) against canine macrophages (DH82).
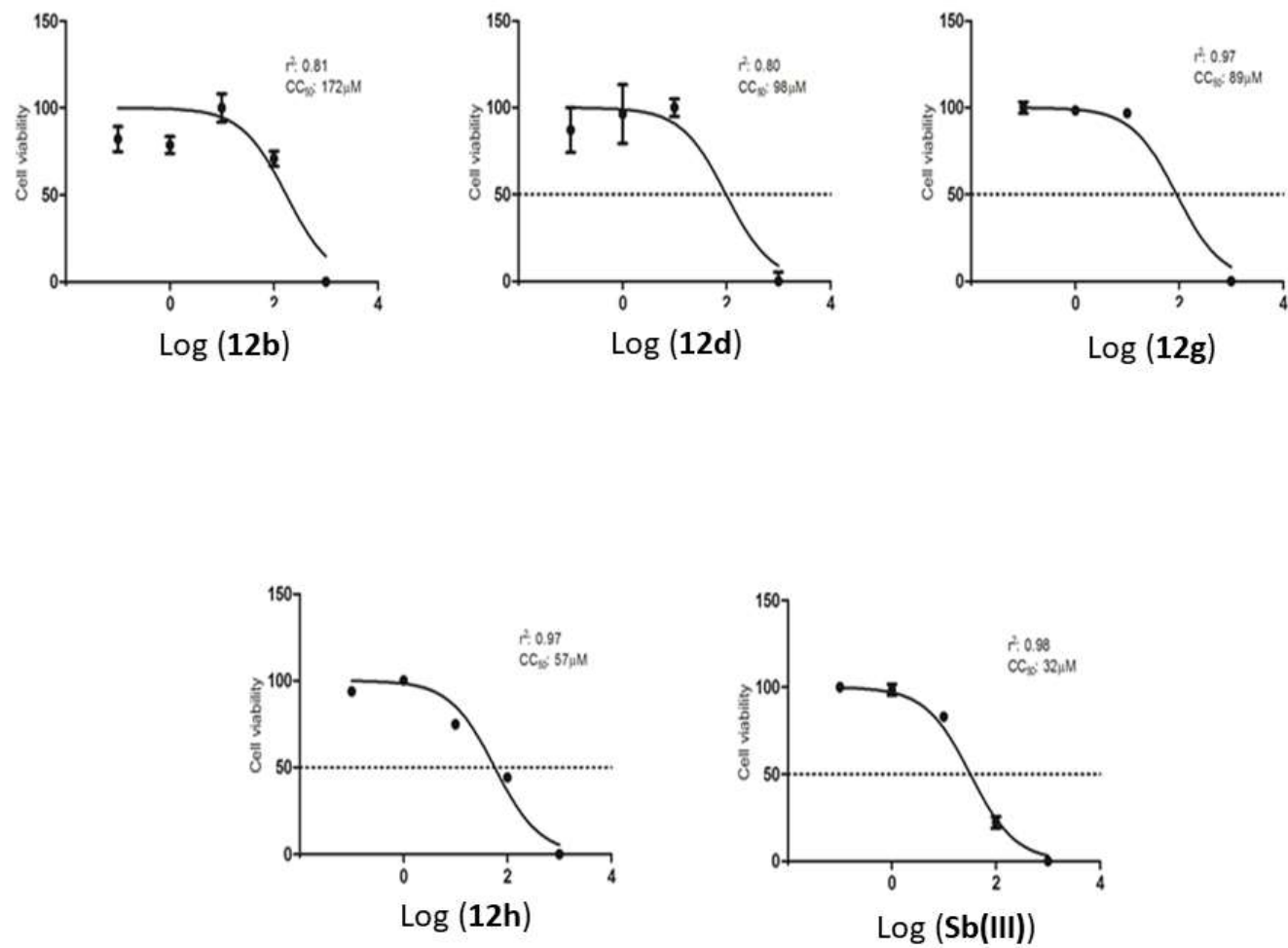
Figure 2.21.A. Cytotoxicity of **12b**, **12d**, **12g**, **12h** and Sb (III) against monkey renal cell (BG).

APPENDIX 3

DATA REFERRED TO CHAPTER 3
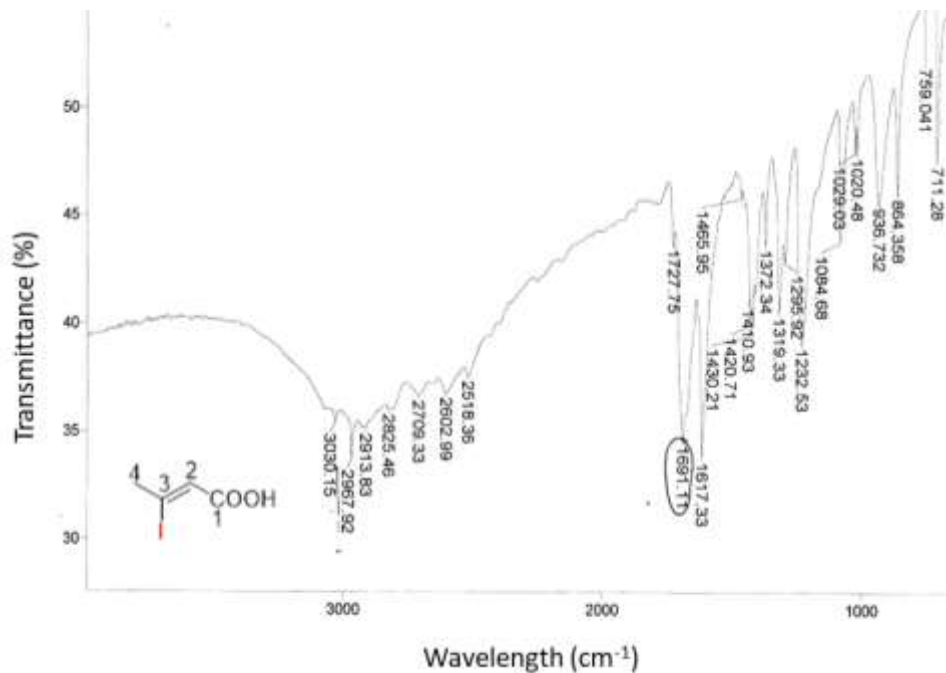
Figure 3.1A. IR ((NaCl film) of compound **36a.**
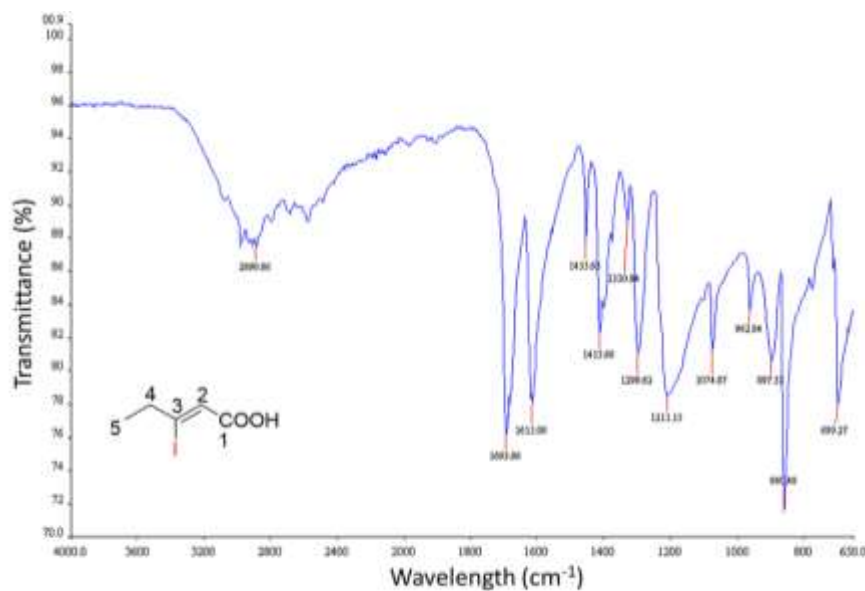
Figure 3.2A. IR (ATR/FTIR) of compound **36b.**
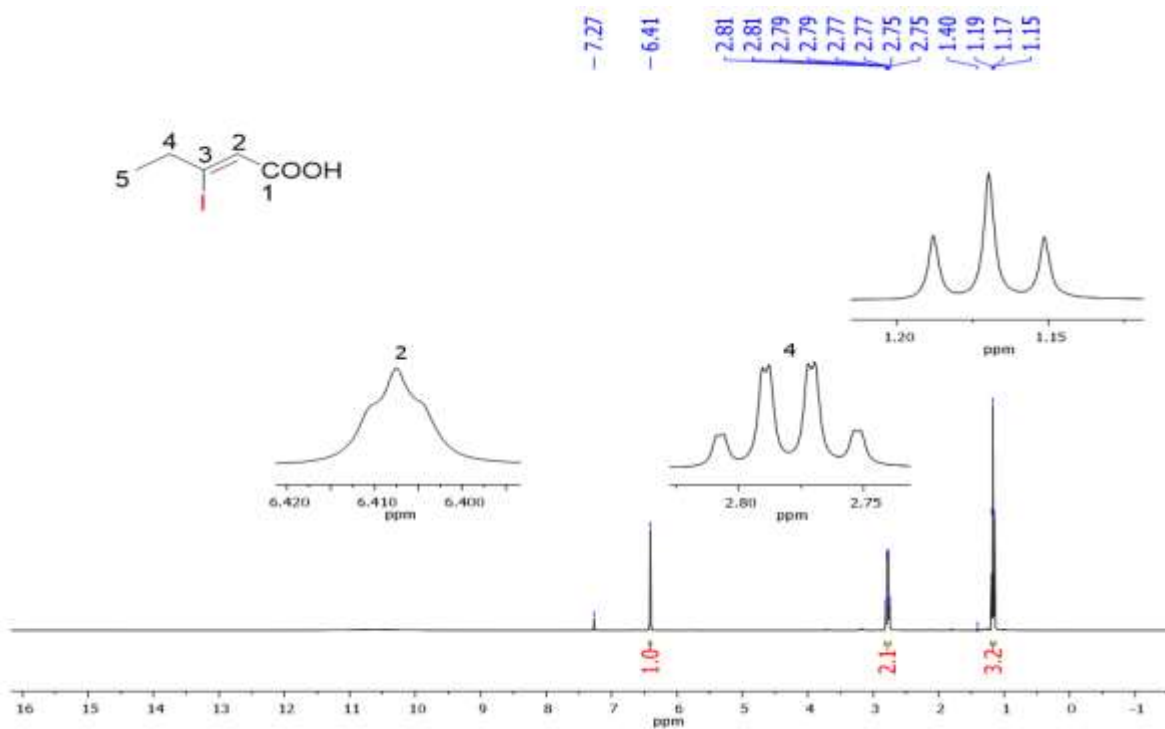
Figure 3.3A. ^{1}H-NMR of (400 MHz, CDCl$_3$) of compound **36b.**
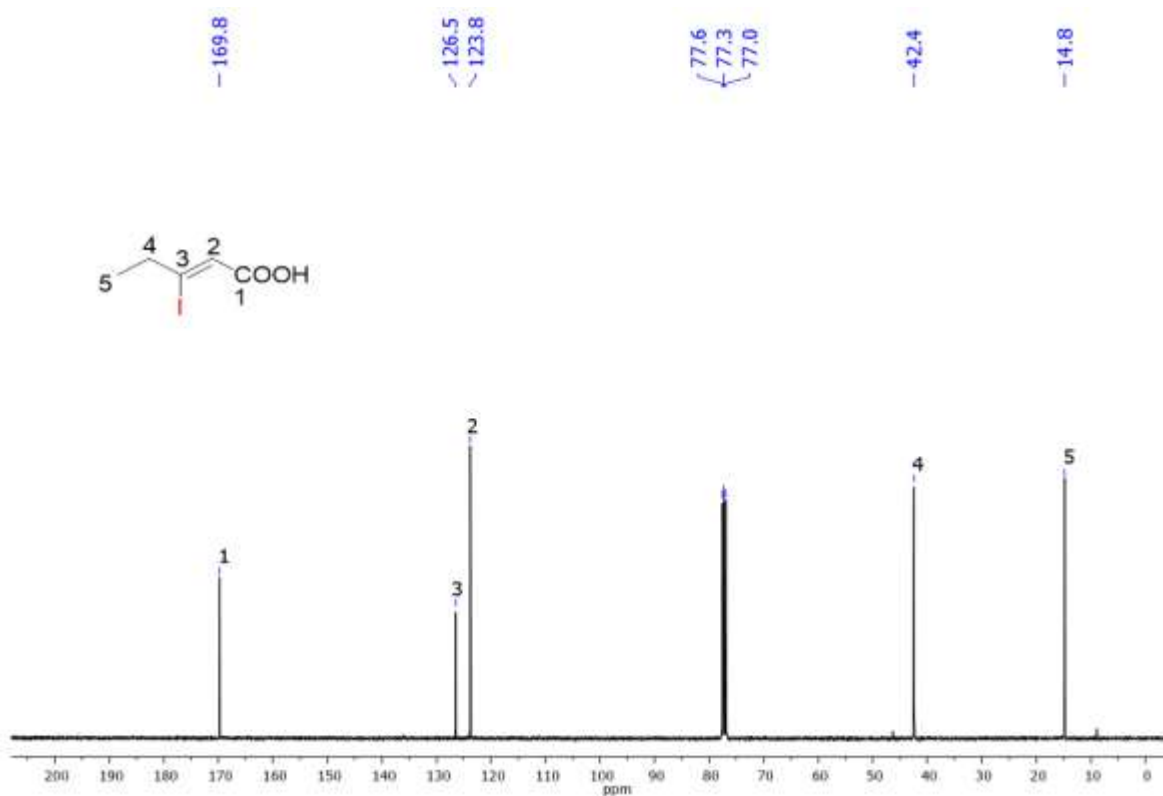
Figure 3.4A. ^{13}C-NMR spectrum of (100 MHz, CDCl$_3$) of compound **36b.**

166
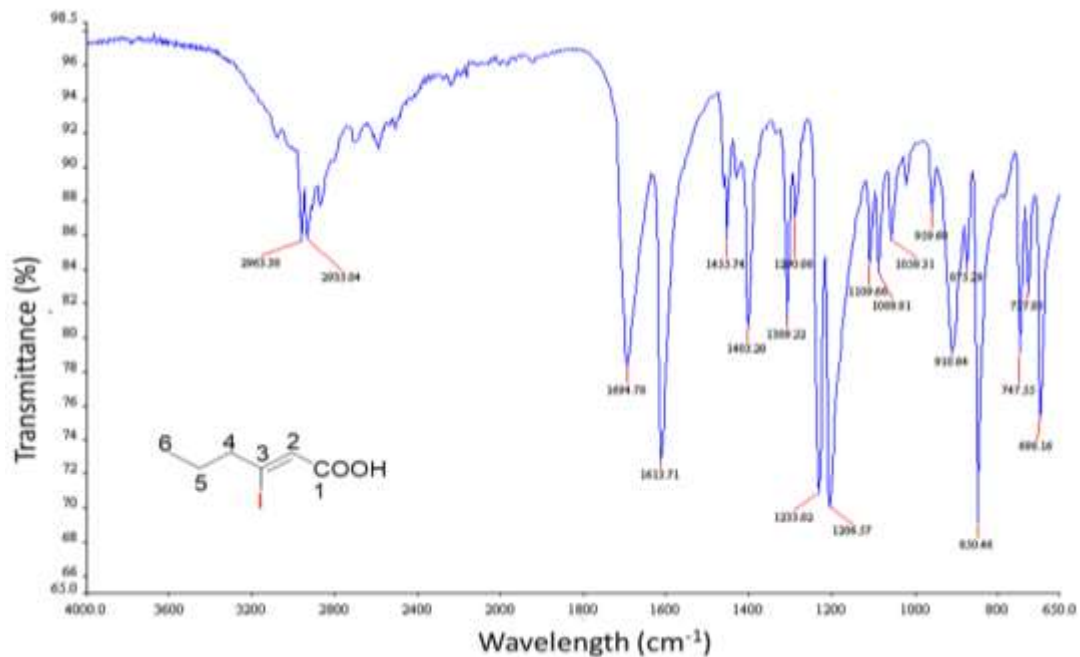
Figure 3.5A. IR (ATR/FTIR) of compound **36c.**
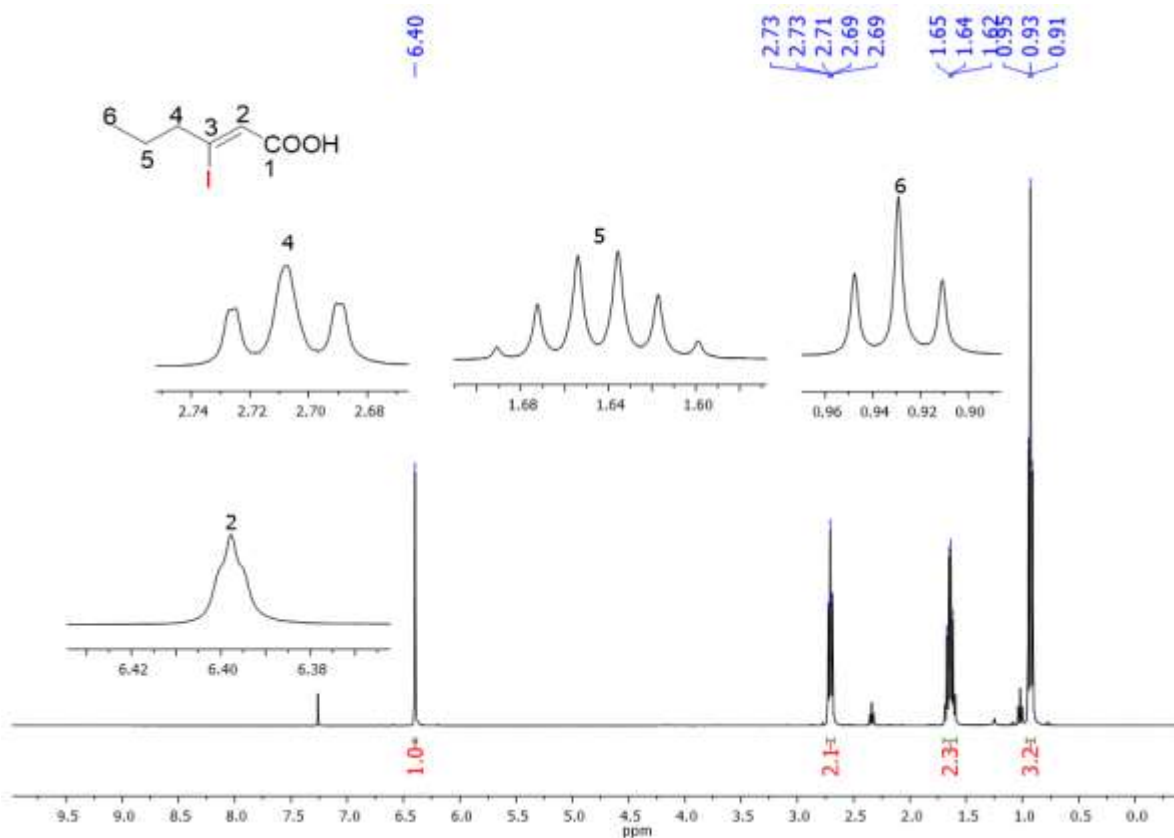
Figure 3.6A. ^{1}H-NMR of (400 MHz, CDCl$_3$) of compound **36c.**
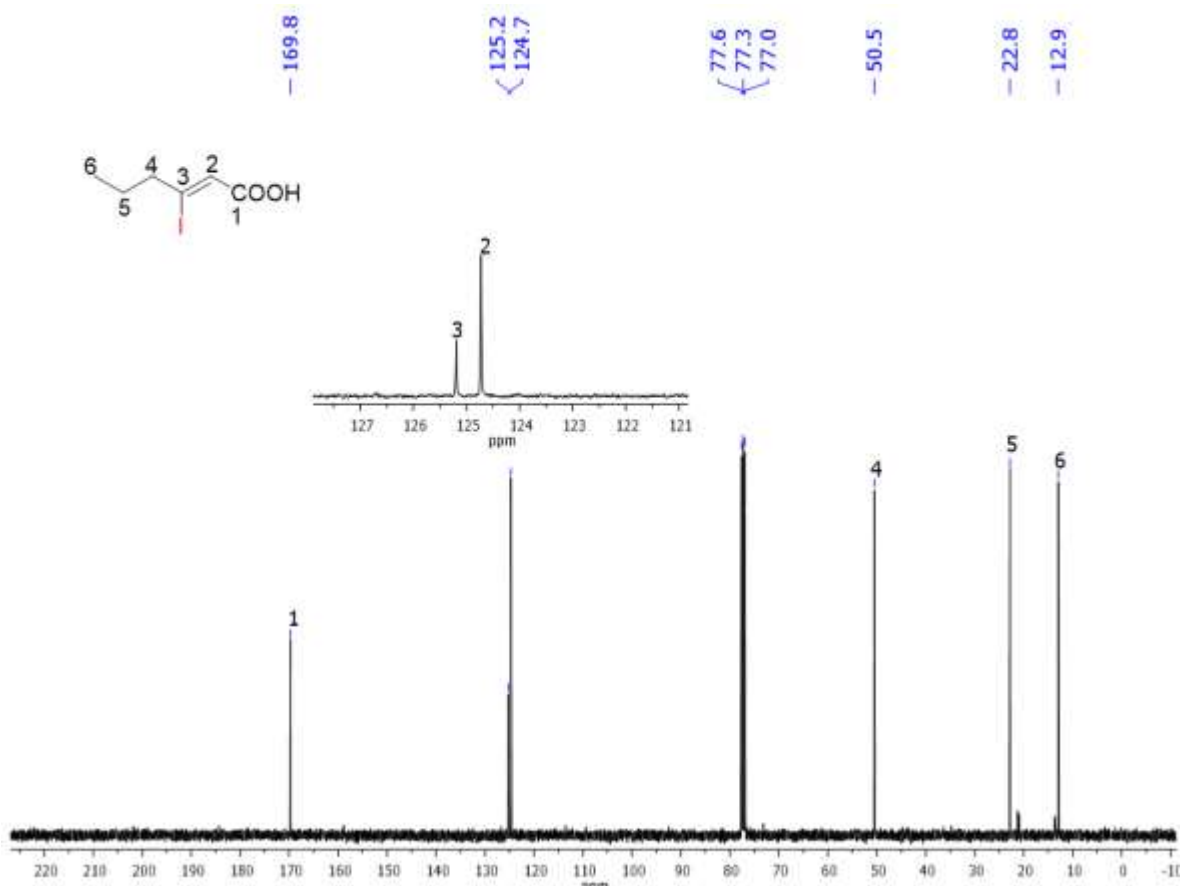
Figure 3.7A. ^{13}C-NMR spectrum of (100 MHz, CDCl$_3$) of compound **36c**.
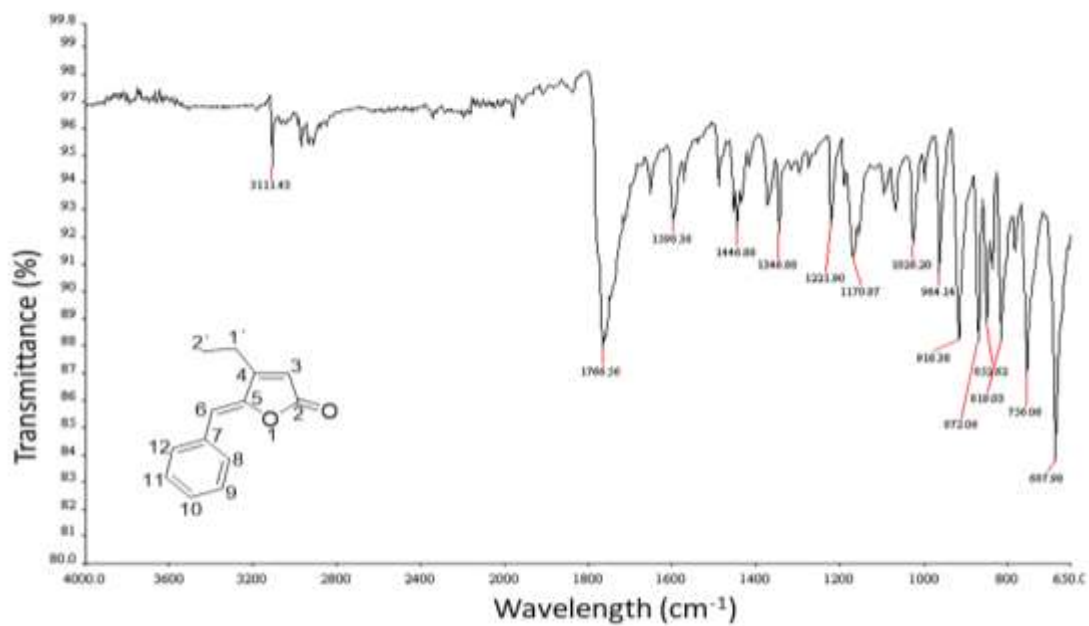
Figure 3.8A. IR (ATR/FTIR) of compound **32c**.

Figure 3.9A. ^{1}H-NMR of (400 MHz, CDCl$_3$) of compound (**32c**).

Figure 3.10. ^{13}C-NMR spectrum of (100 MHz, CDCl$_3$) of compound **32c.**

169
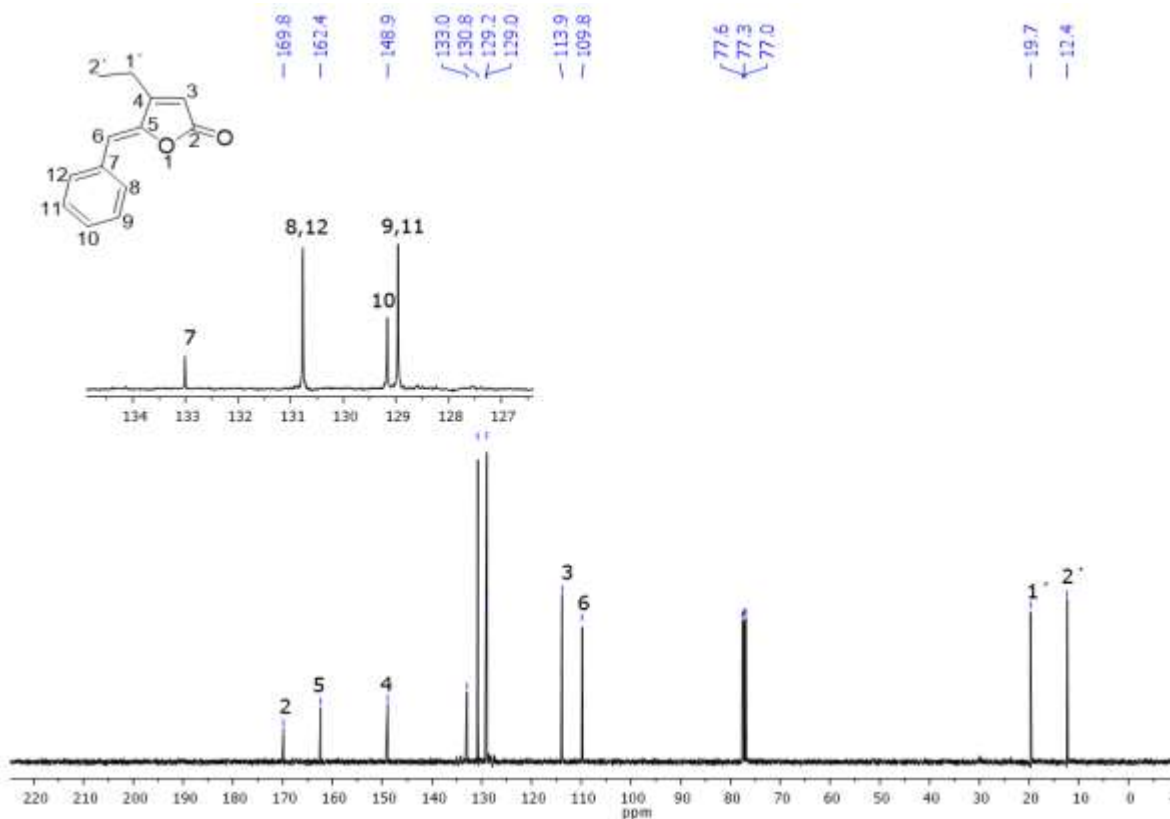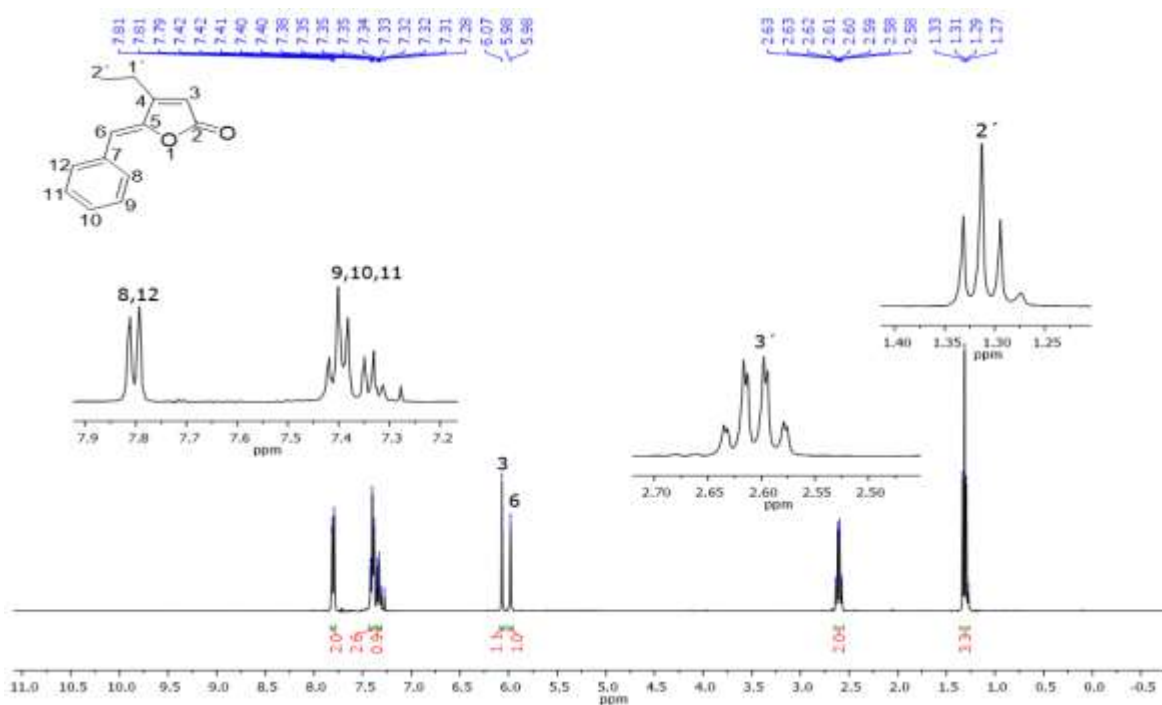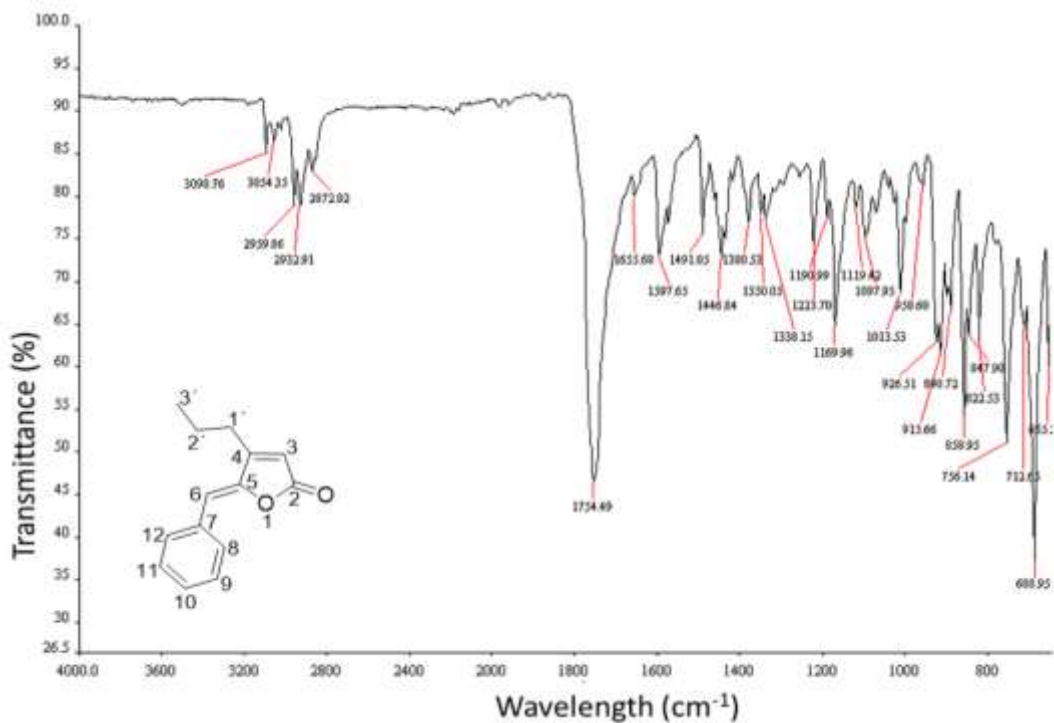
Figure 3.11A. IR (ATR/FTIR) of compound **32d.**
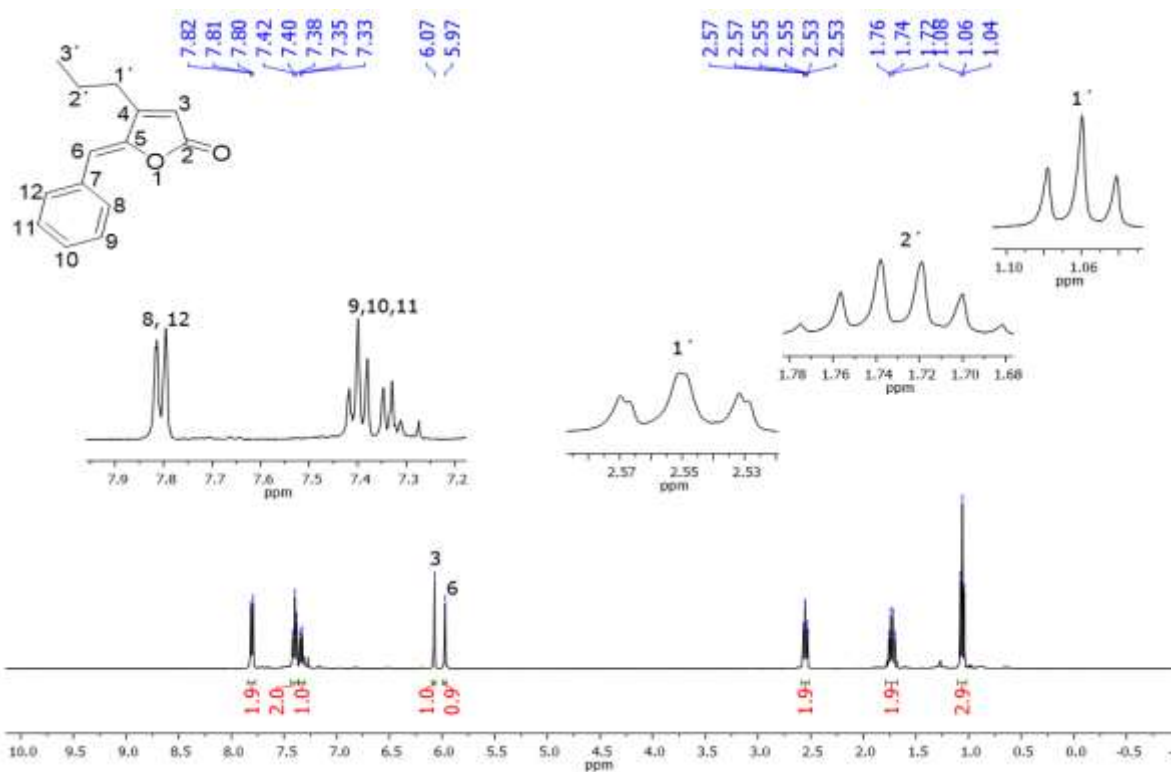
Figure 3.12A. ^{1}H-NMR of (400 MHz, CDCl$_3$) of compound **32d.**
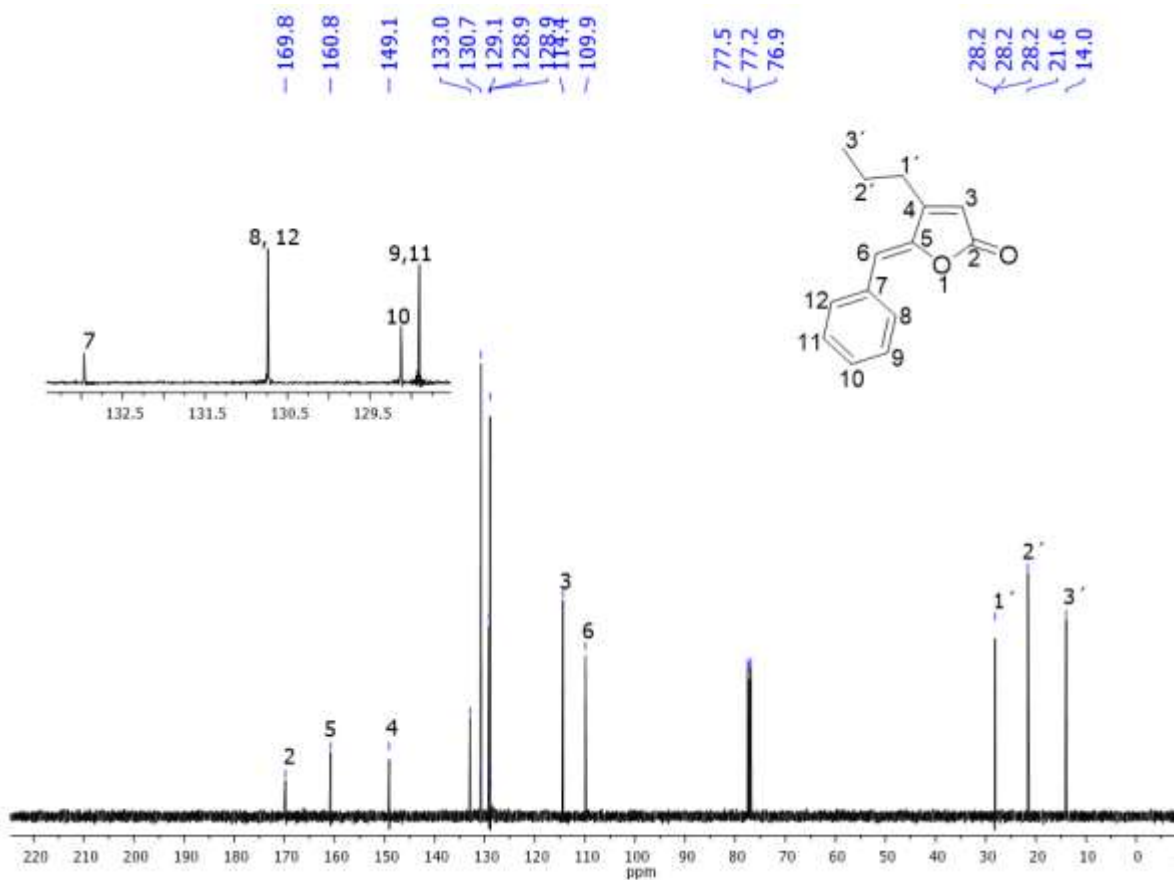
Figure 3.13A. ^{13}C-NMR spectrum of (100 MHz, CDCl$_3$) of compound **32d.**
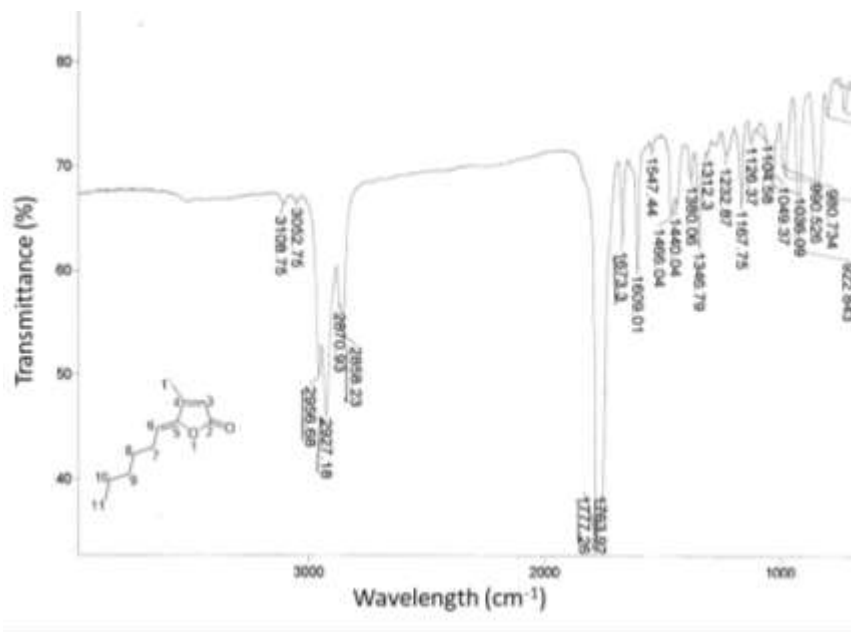
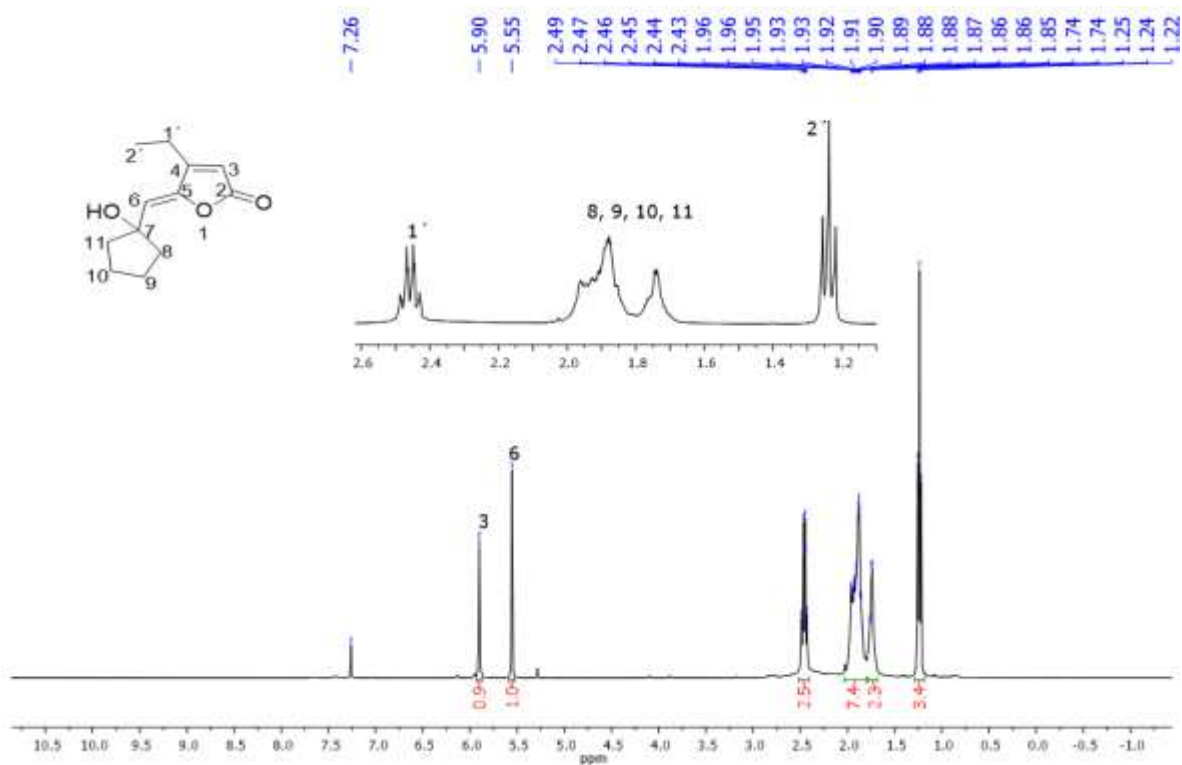**Figure 3.14A.** IR (NaCl film) of compound **32e.**
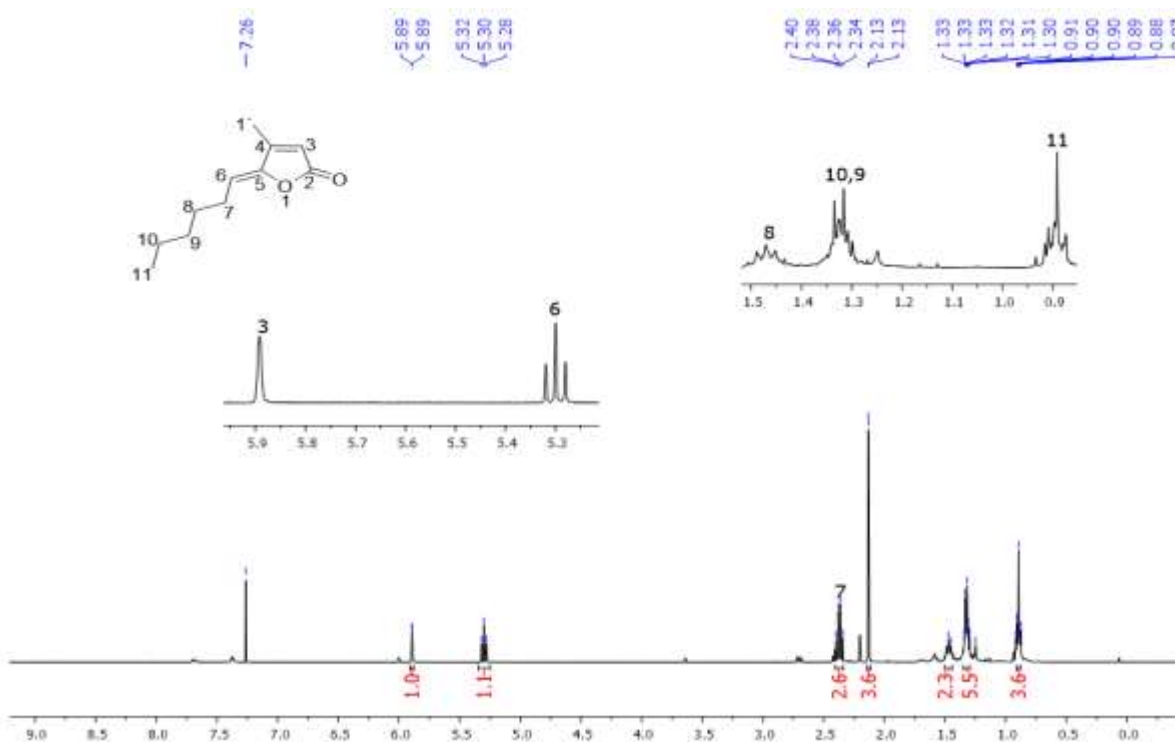
Figure 3.15A. ^{1}H-NMR of (400 MHz, CDCl$_3$) of compound **32e.**
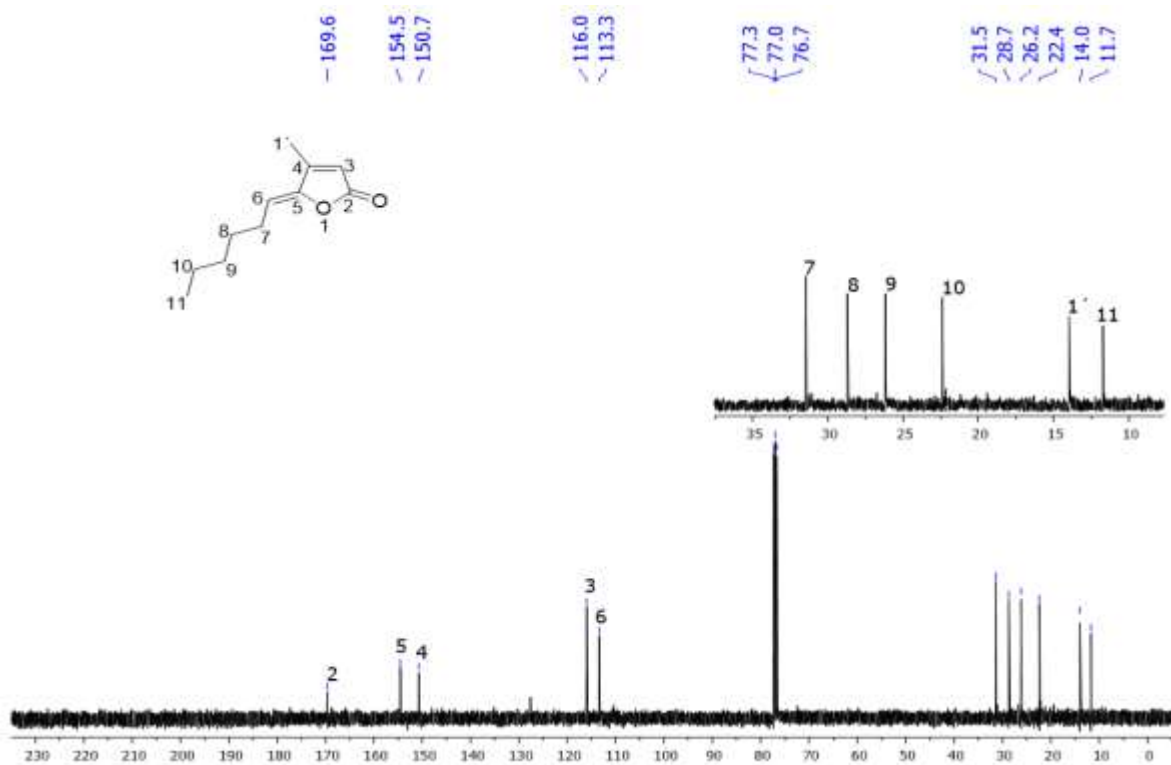
Figure 3.16A. ^{13}C-NMR spectrum of (100 MHz, CDCl$_3$) of compound **32e.**

172
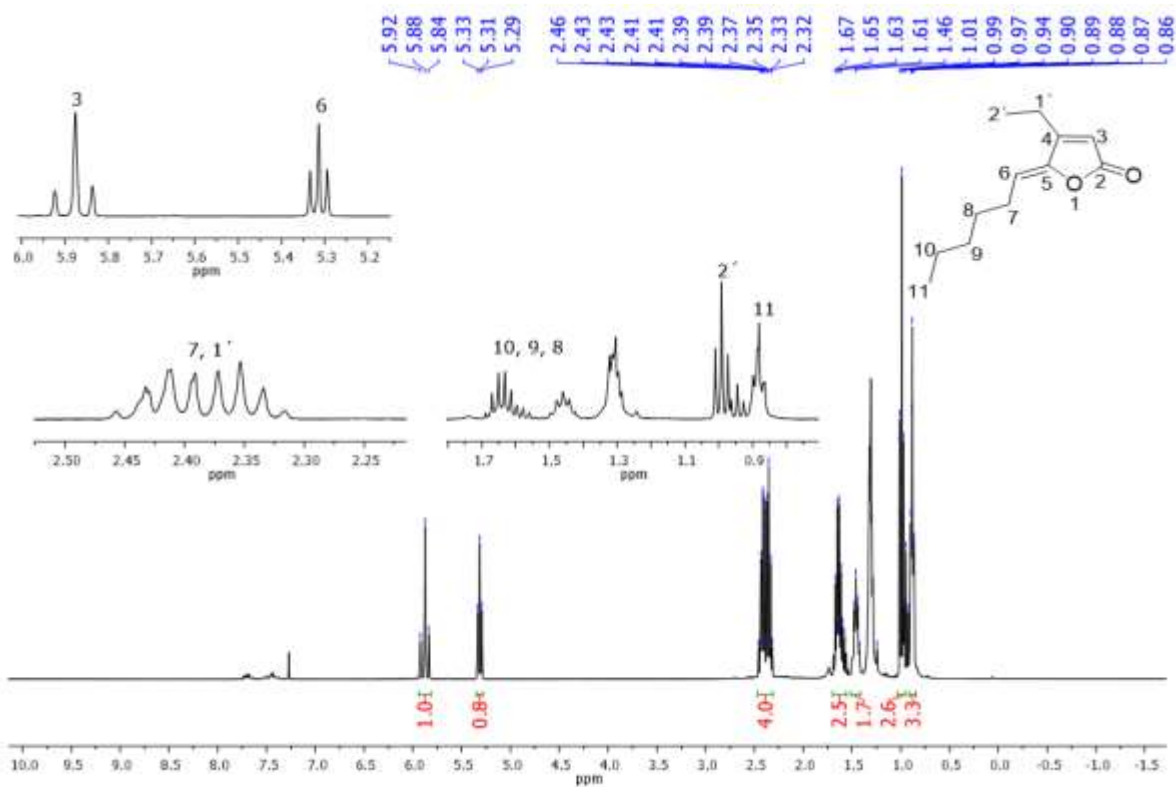
Figure 3.17A. ^{1}H-NMR of (400 MHz, CDCl$_3$) of compound **32f.**
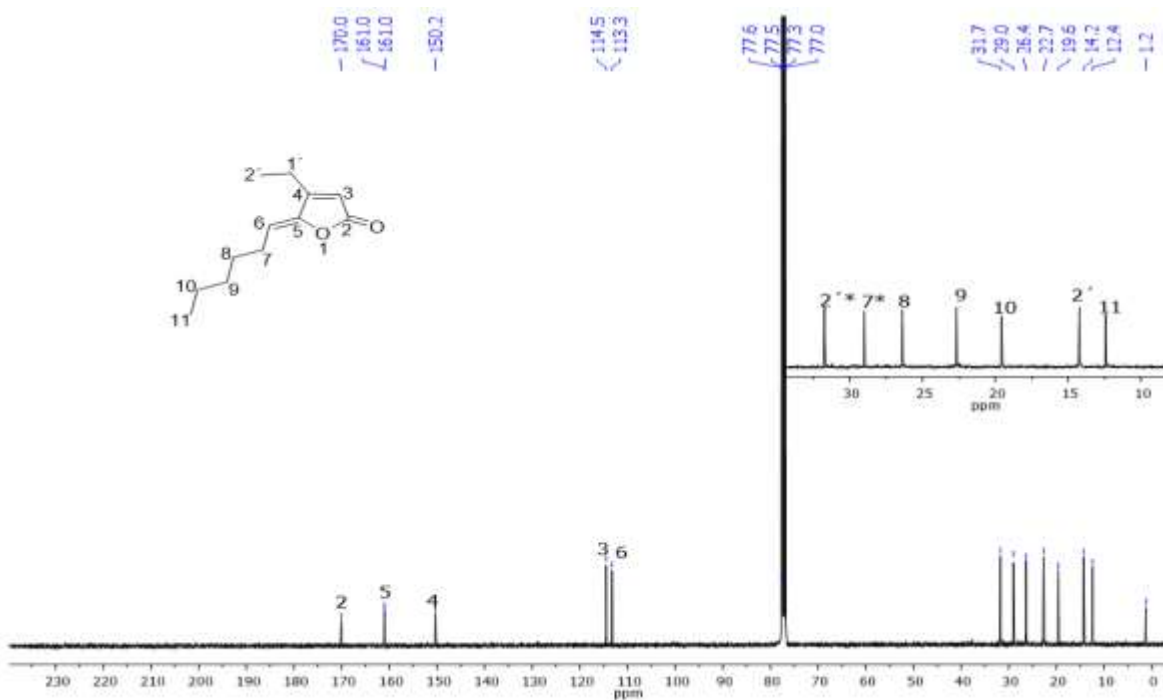
Figure 3.18A. ^{13}C-NMR spectrum of (100 MHz, CDCl$_3$) of compound **32f.**
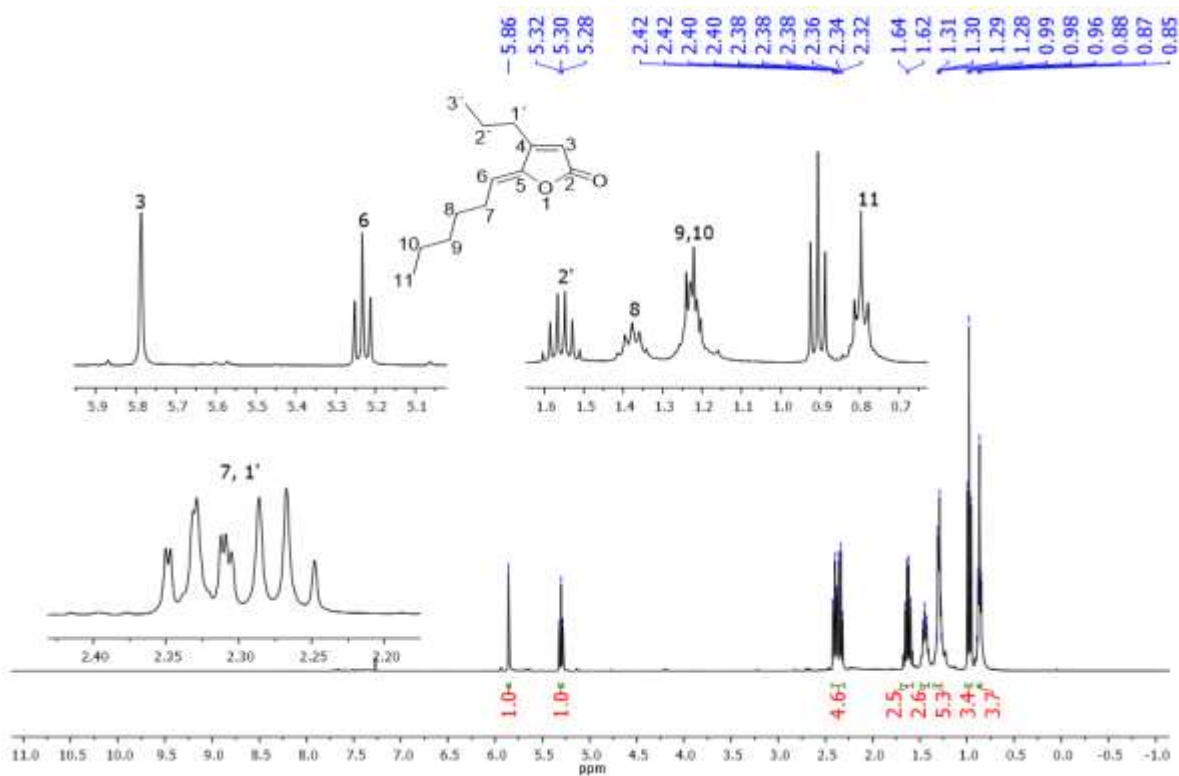
Figure 3.19A. ^{1}H-NMR of (400 MHz, CDCl$_3$) of compound **32g.**
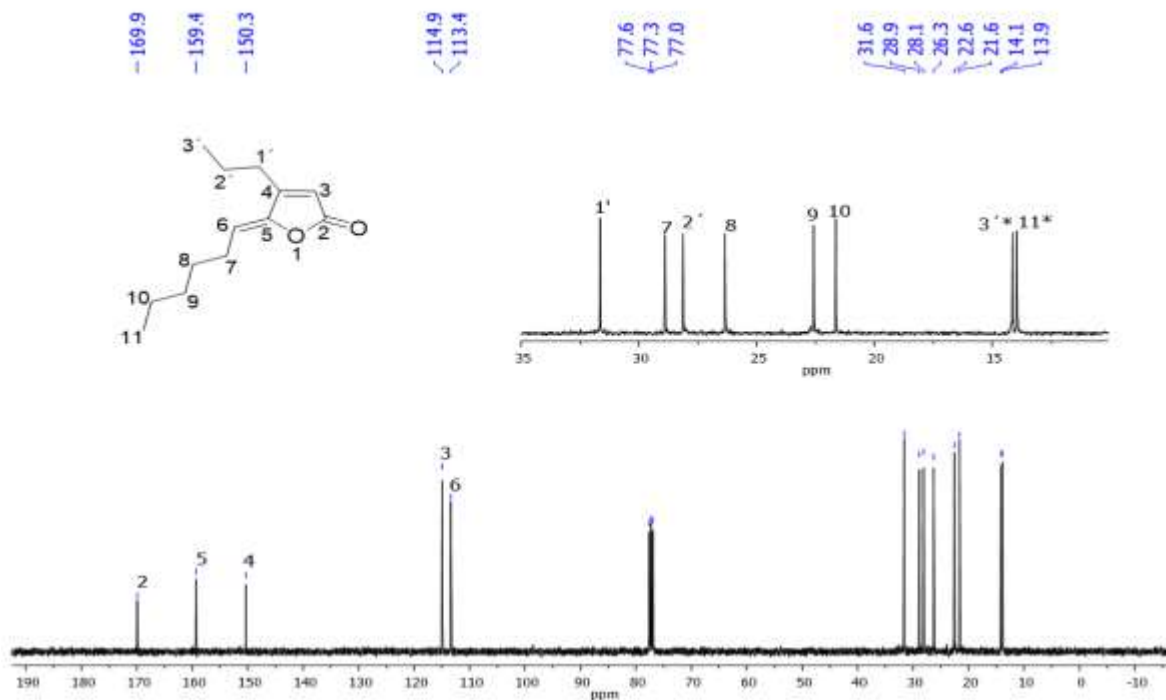
Figure 3.20A. ^{13}C-NMR spectrum of (100 MHz, CDCl$_3$) of compound **32g.**
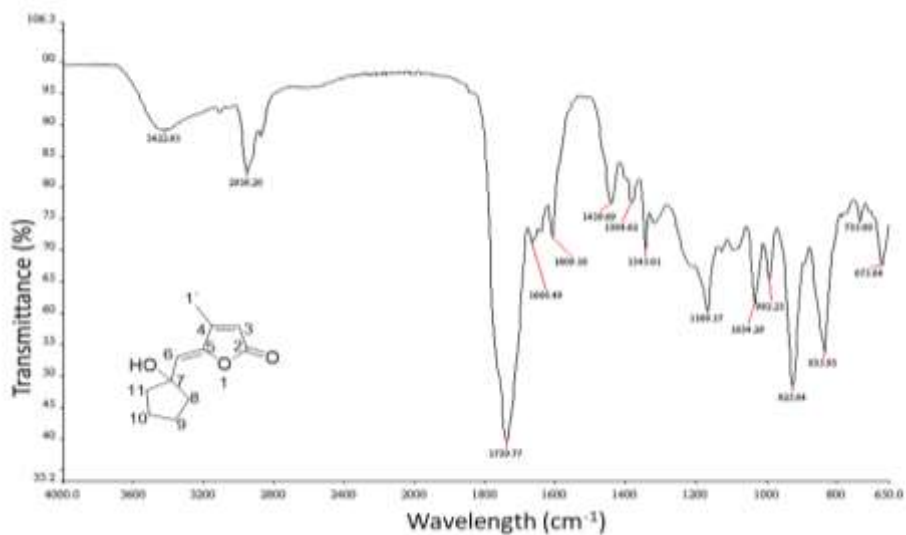
Figure 3.21A. IR (ATR/FTIR) of compound **32h.**
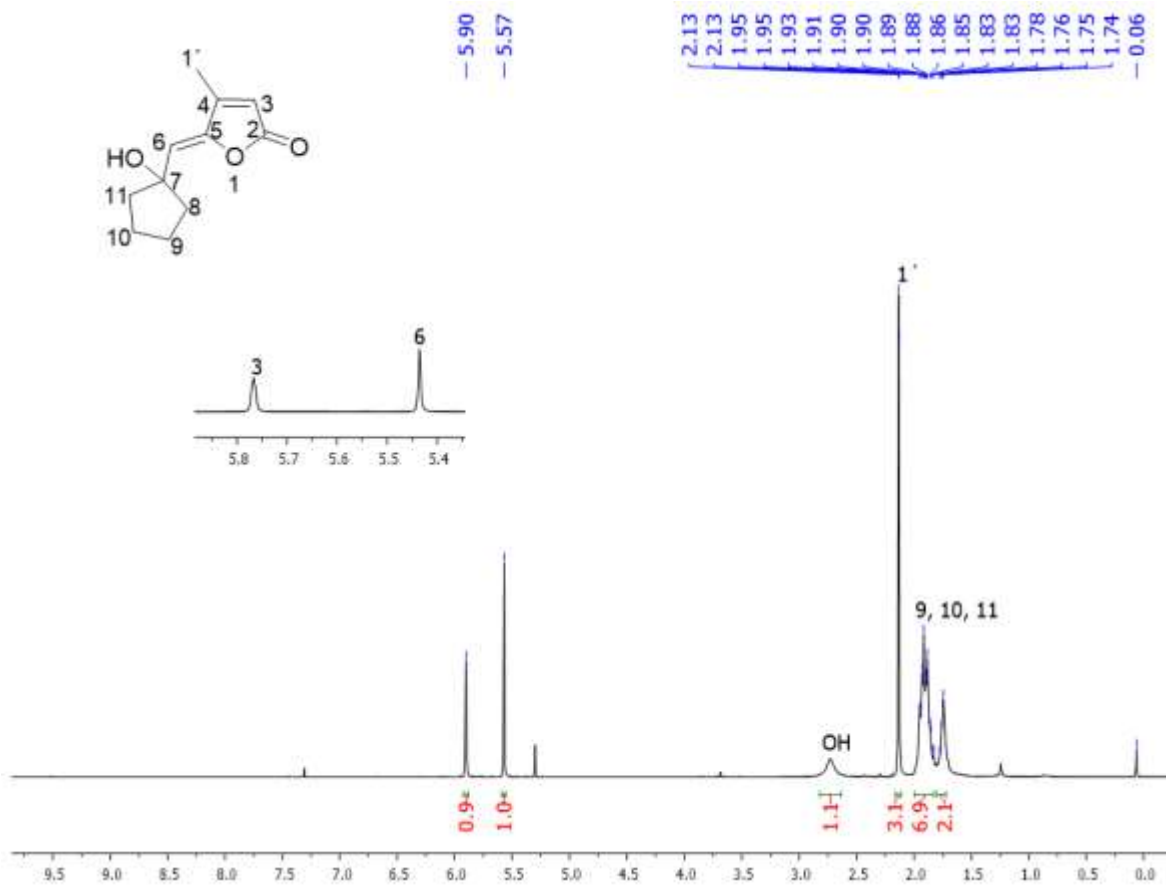
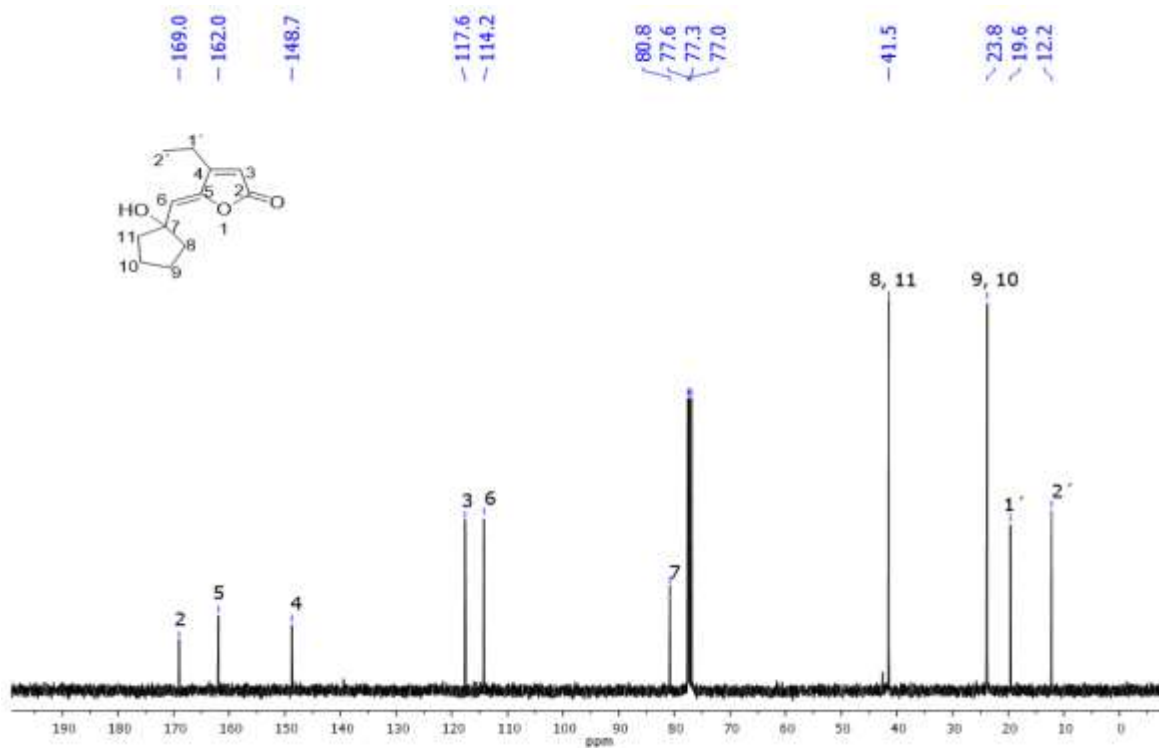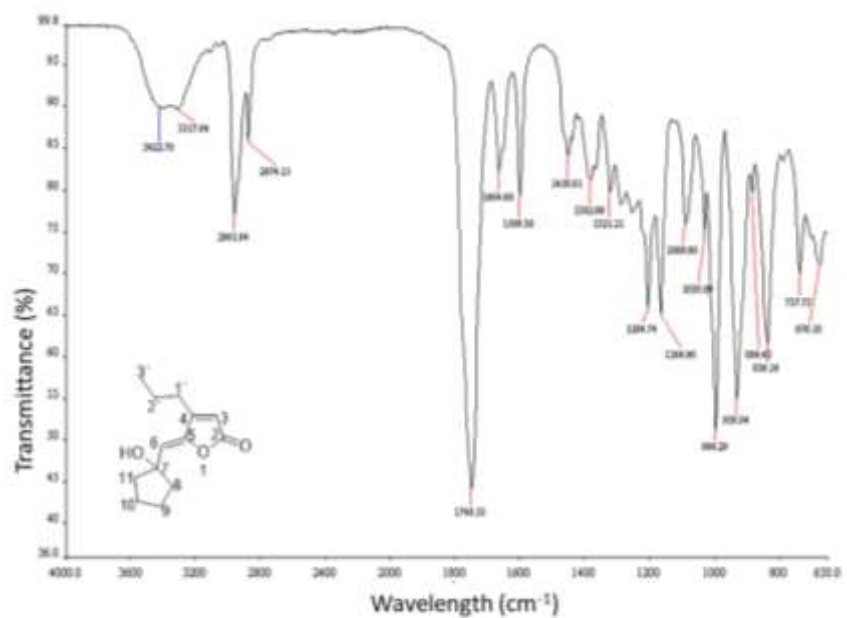**Figure 3.22A.** ¹H-NMR of (100 MHz, CDCl₃) of compound **32h.**
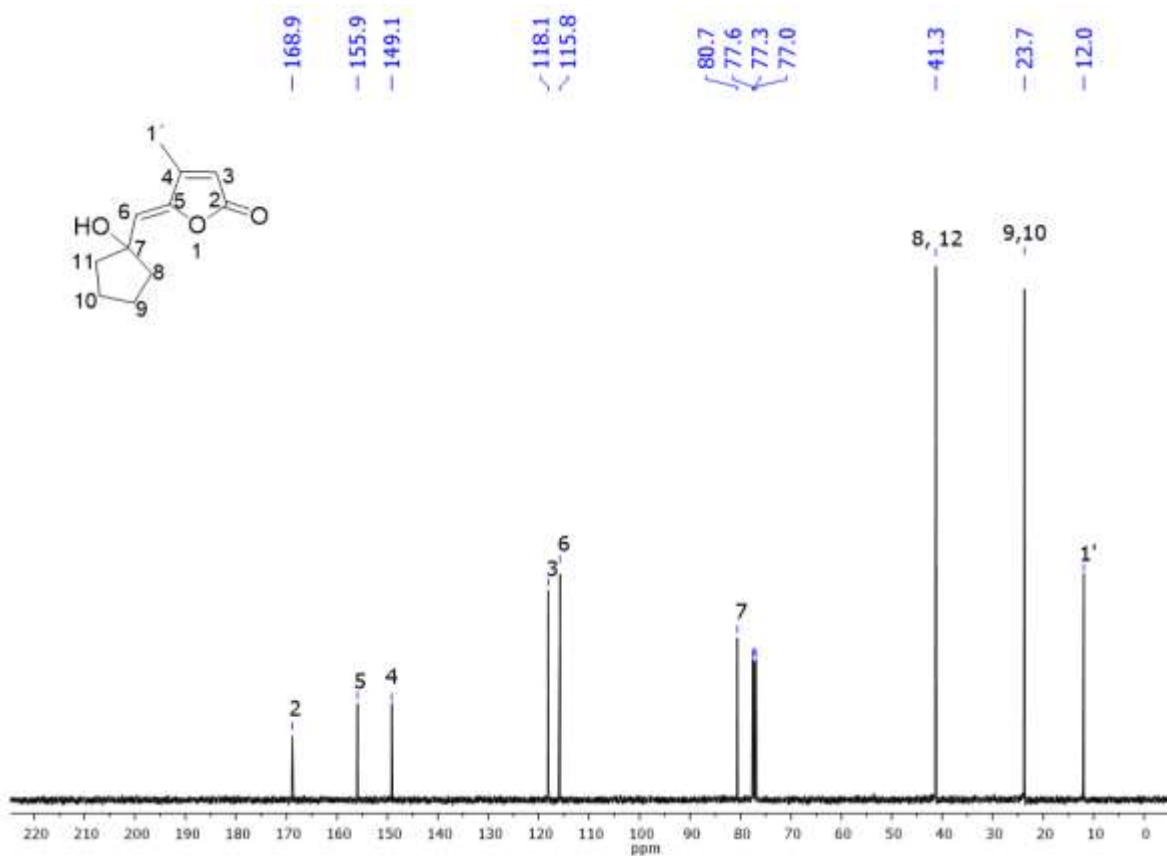
Figure 3.23A. ^{13}C-NMR spectrum of (100 MHz, CDCl$_3$) of compound **32h.**
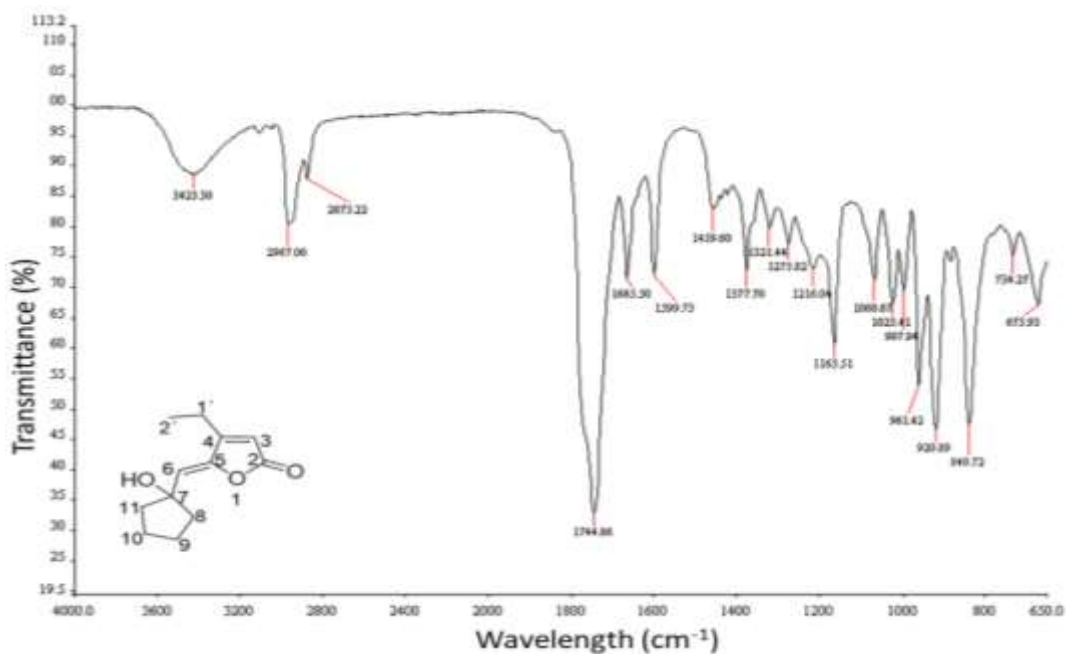
Figure 3.24. IR (ATR/FTIR) of compound **32i**

Figure 3.25A. ^{1}H-NMR of (400 MHz, CDCl$_3$) of compound **32i.**

Figure 3.26A. ^{13}C-NMR spectrum of (100 MHz, CDCl$_3$) of compound **32i.**

Figure 3.27A. IR (ATR/FTIR) of compound **32j.**
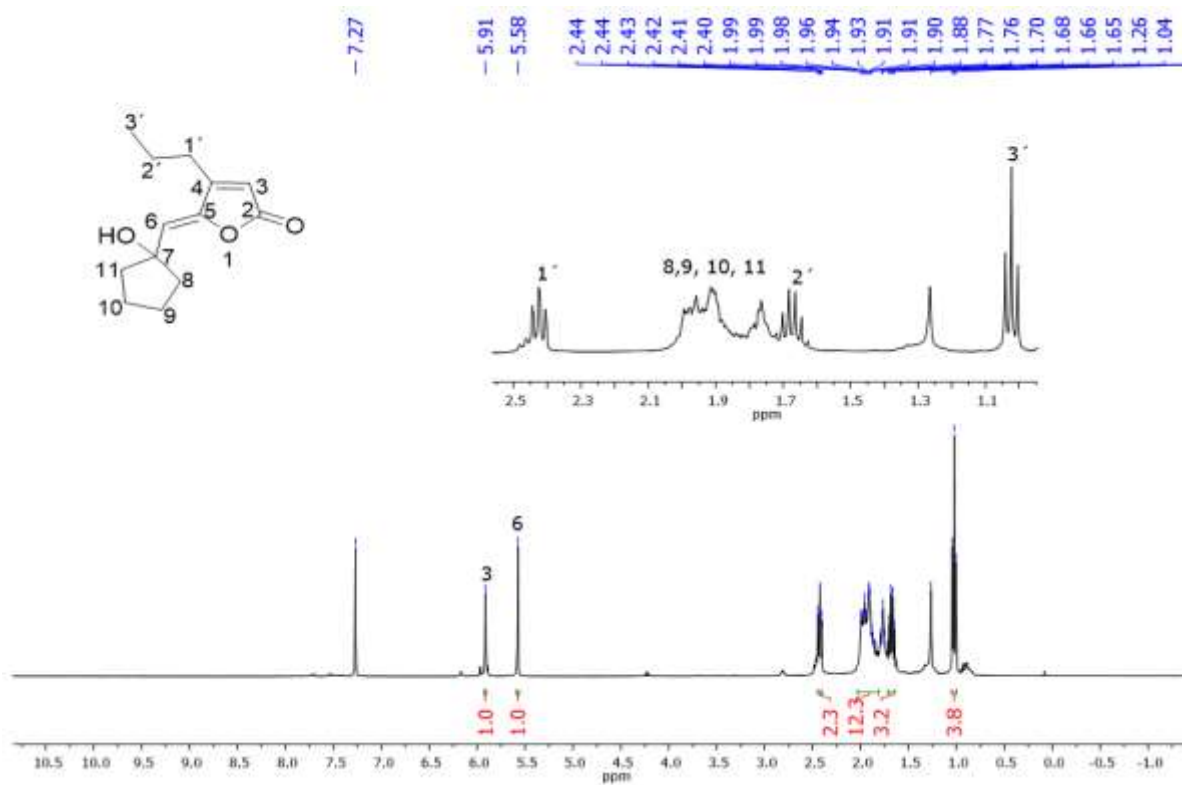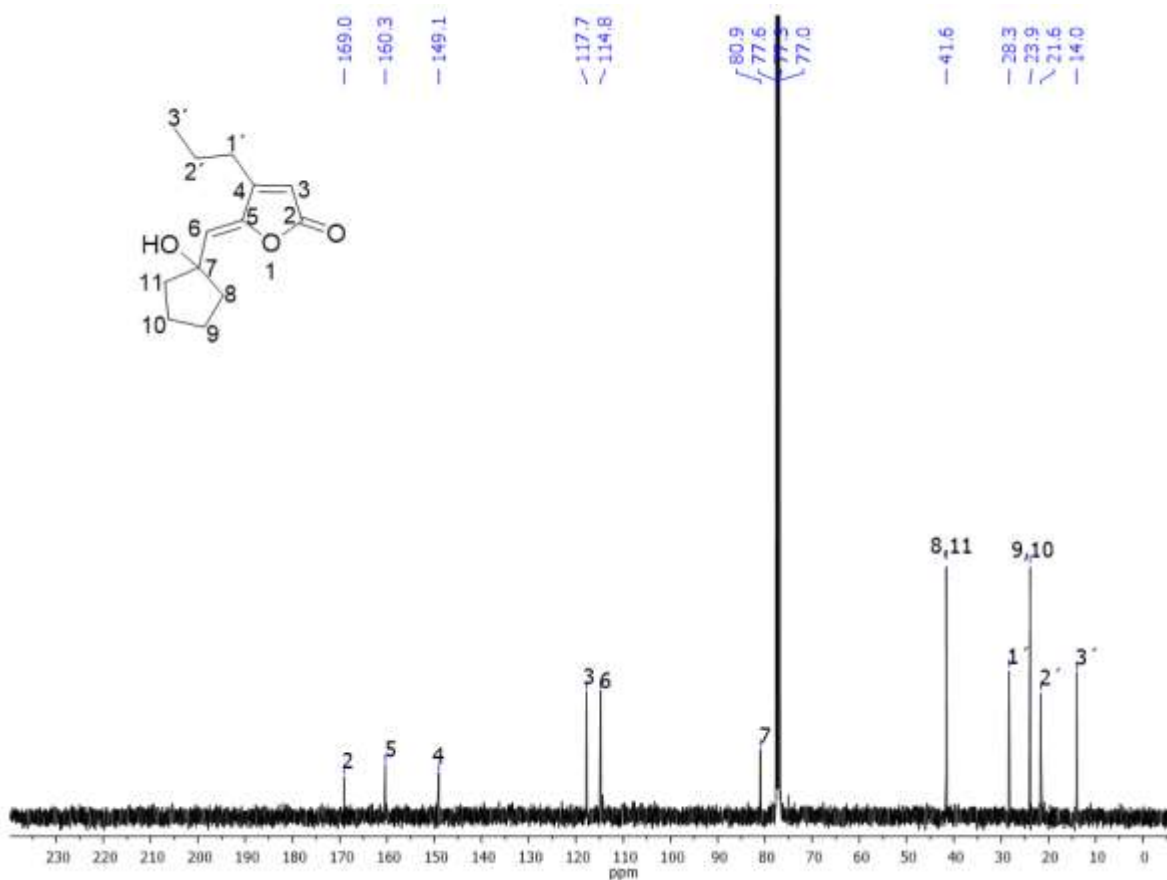

Figure 3.28A. ¹H-NMR of (400 MHz, CDCl₃) of compound **32j**

Figure 3.29A. ^{13}C-NMR spectrum of (100 MHz, CDCl$_3$) of 1compound **32j.**

Figure 3.30A. IR (NaCl film) of compound **32k.**
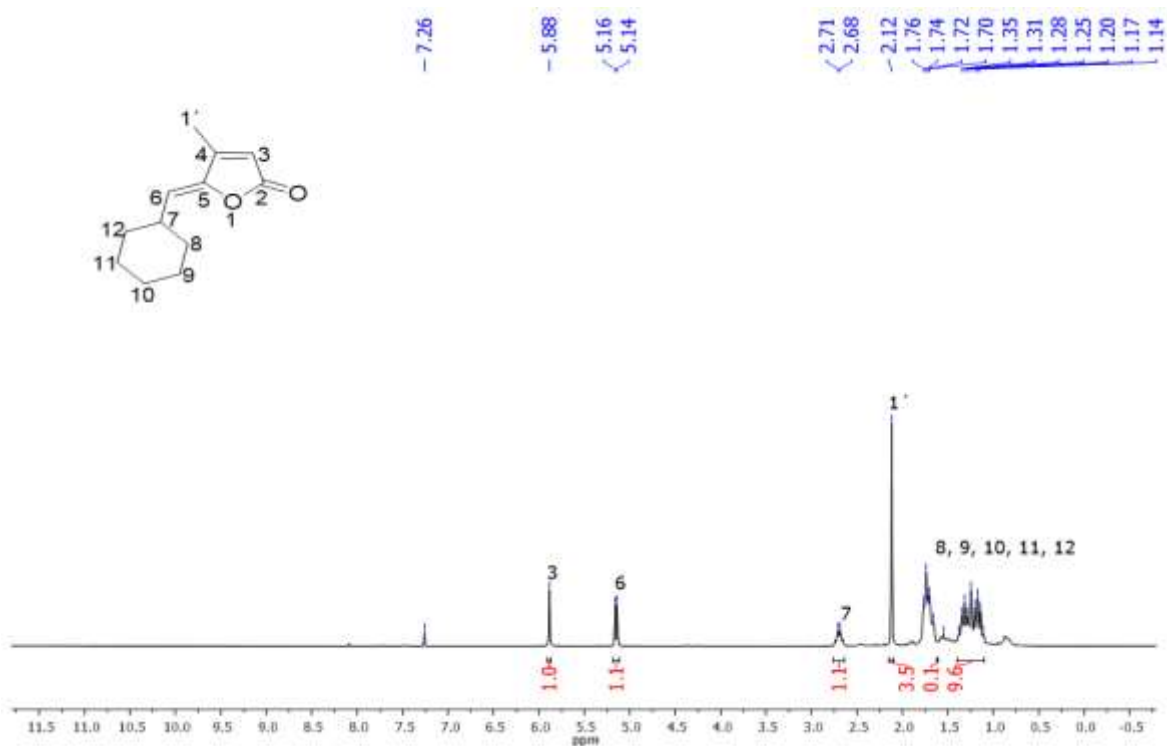
Figure 3.31A. ¹H-NMR of (400 MHz, CDCl₃) of compound **32k.**

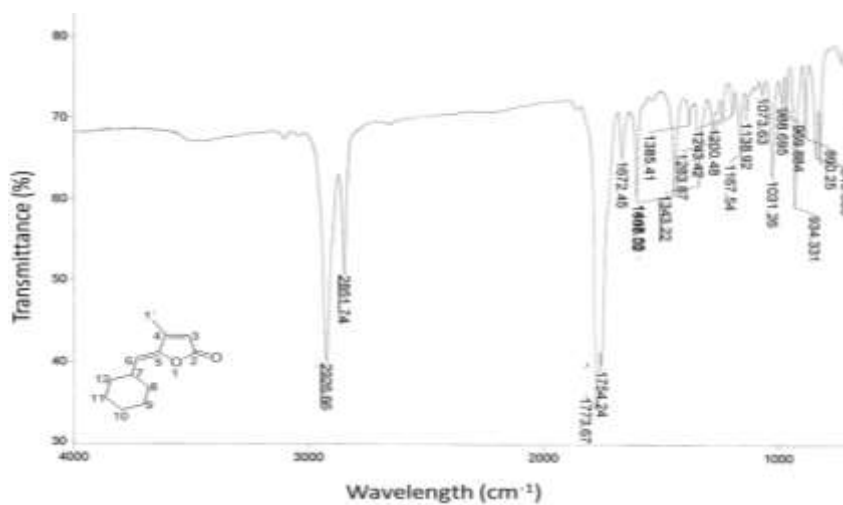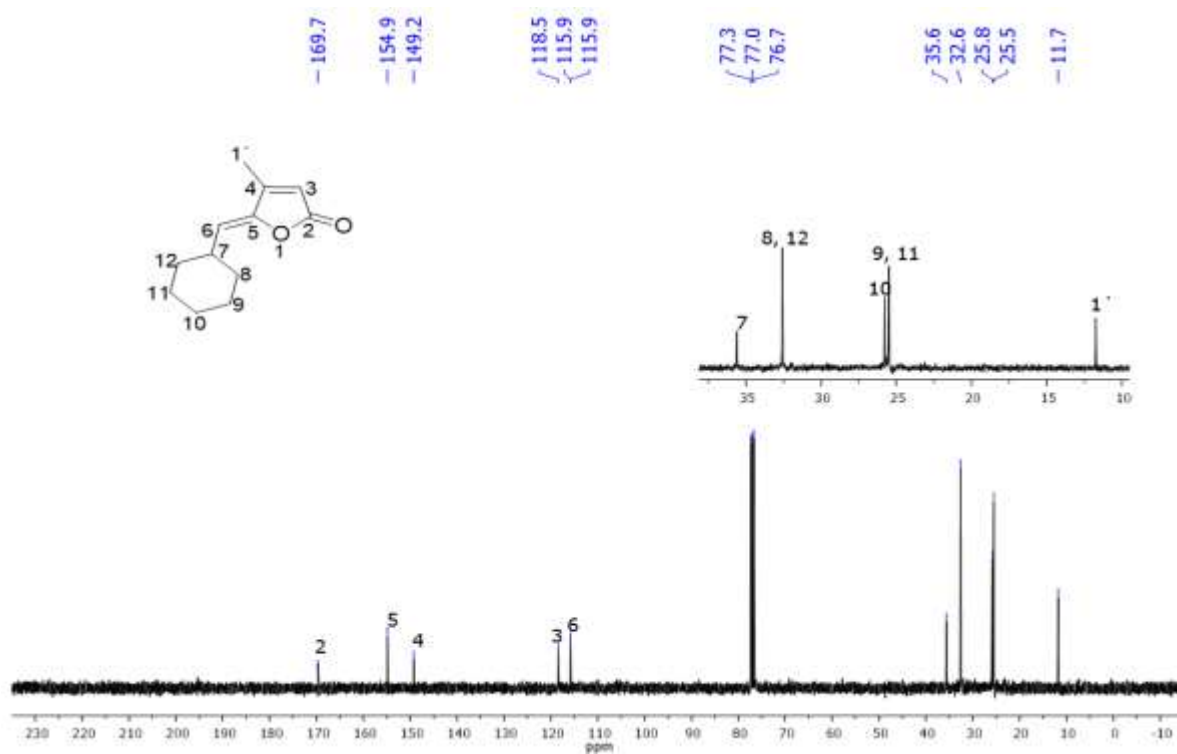**Figure 3.32A.** ¹³C-NMR spectrum of (100 MHz, CDCl₃) of compound **32k.**

180

Figure 3.33A. IR (NaCl film) of compound **32l.**

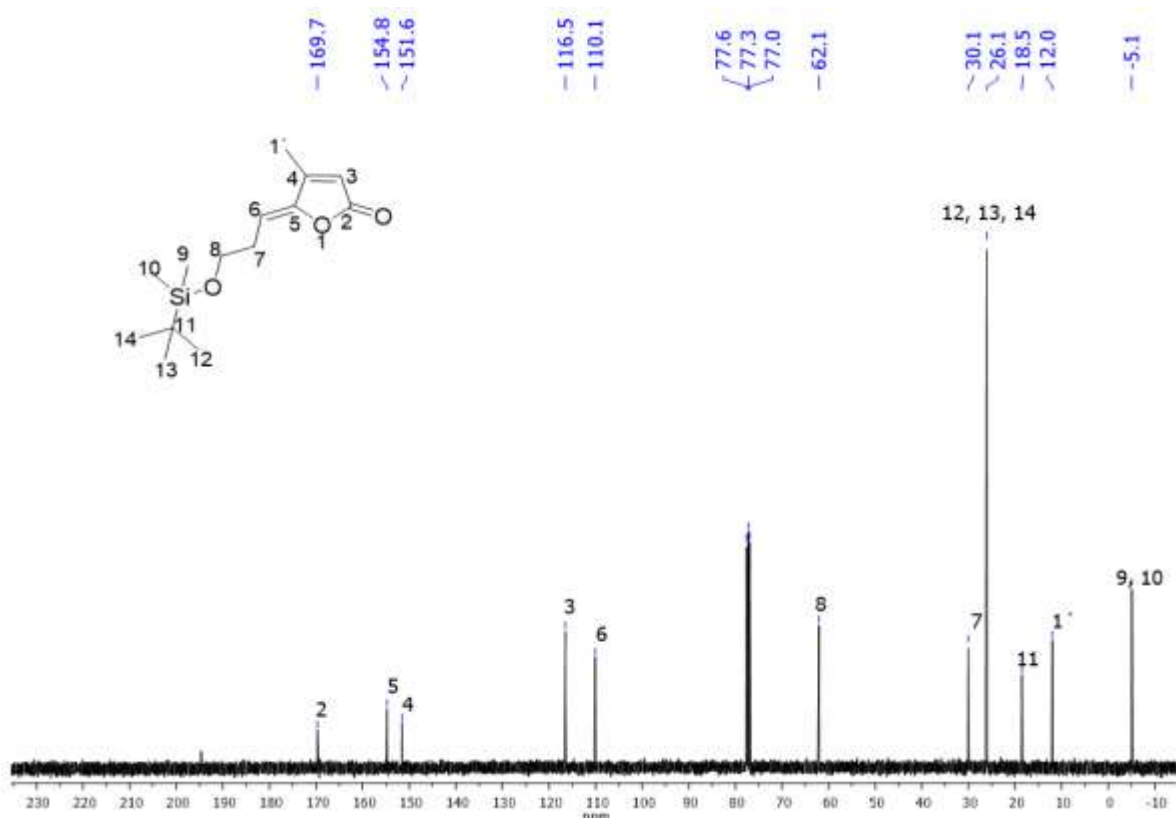**Figure 3.34A.** ¹H-NMR of (400 MHz, CDCl₃) of compound **32l**.

Figure 3.35A. ^{13}C-NMR spectrum of (100 MHz, CDCl$_3$) of compound **32l.**

Table 3.1A. NMR data reported by Sekine *et al.* and this work for butanolide **32a**
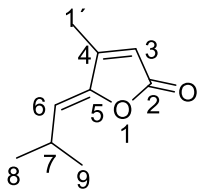
Position	δ_C		δ_H; multiplicity (J (Hz))	
	Felluga and co-workers (150 MHz)	**32a** (100 MHz)	Felluga and co-workers (500 MHz)	**32a** (400 MHz)
1			-	-
2	169.6	169.6	-	-
3	119.8	119.8	5.90, dq ($J_{3\text{-}1} = 1.4$; $J_{3\text{-}6} = 0.8$)	5.90, bs.
4	149.1	149.1		-
5	155.0	154.8		-
6	116.0	116.0	5.16, dd ($J_{6\text{-}1'} = 9.9$; $J_{6\text{-}3} = 0.8$)	5.16, d (9.7)
7	26.2	26.2	2.62 d of sept ($J = 6.6$; $J = 9.5$)	2.63, m
8	22.6	22.6	1.10 d (6.6).	1.11 d (6.8)
9	22.6	22.6	1.10 d (6.6).	1.11 d (6.8)
1´	11.8	11.7	2.14 d (1.5).	2.14, bs

Table 3.2A. NMR data reported by Felluga *et al.* and this work for butanolide **32b**
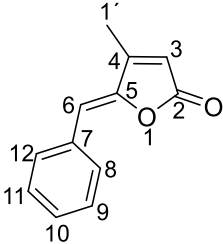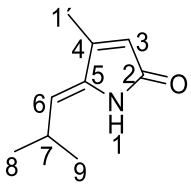
Position	δ_C		δ_H; multiplicity (*J* em *Hz*)	
	Sekine and co-workers (100 MHz)	**32b** (100 MHz)	LI and co-workers (400 MHz)	**32b** (400 MHz)
1				
2				
3	115.5	115.5	6.04 m	6.05 m
4				
5				
6	109.9	109.9	5.97 s	5.98 s
7	137.2	137.2		
8	130.5	130.5	7.78-7.22 m	7.78-7.82 m
9	128.8	128.8	7.37-7.42 m	7.37-7.42 m
10	129.0	129.0	7.30-7.36 m	7.30-7.36 m
11	128.8	128.7	7.37-7.42 m	7.30-7.36 m
12	130.5	130.5	7.78-7.42 m	7.37-7.82 m
1´	12.0	12.0	2.26 d (1.3)	2.26 d (1.3)

Table 3.3A. NMR data reported by Li *et al.* and this work for Pulchellalactam.

Position	δ_C		δ_H; multiplicity ($J(Hz)$)	
	Li and co-workers (150 MHz)	**5** (100 MHz)	Li and co-workers (300 MHz)	**5** (400 MHz)
1			8.41, s	8.39, s.
2	172.88	172.15		-
3	120.68	120.70	5.83, s.	5.86, s.
4	148.53	148.69		-
5	137.63	137.43		-
6	120.59	119.80	5.12, d (9.8)	5.12, d (9.7)
7	27.36	27.55	2.62 m.	2.63, m
8	22.84	22.85	1.1, d (6.6).	1.11 d
9	22.84	22.85	1.1, d (6.6).	1.11 d
1´	11.81	11.86	2.03, s.	2.07, s